Journal of Applied Mechanics

(Contributions of the ASME Applied Mechanics Division)

Ducted Fan Design Theory . . . . . *C. G. Van Nieuwl* 325
Effect of Spin on a Rolling Elastic Sphere . . . . . *K. L. Johnson* 332
Effect of Tangential Contact Force on a Rolling Elastic Sphere . . . *K. L. Johnson* 339
Vibration of a String Having Uniform Motion . . *F. R. Archibald and A. G. Emslie* 347
Synthesis of Four-Bar Mechanism . . . . . *J. Hirschhorn* 349
Binomial Forcing Functions in Nonlinear Systems . . . . . *T. J. Harvey* 352
Electrolytic Drift of Single-Axis Gyroscopes . . . . . *R. H. Cannon, Jr.* 357
Co-Ordinates Which Uncouple Equations of Motion . . . . . *K. A. Foss* 361
Sound Absorption Spectra Characteristics . . . . . *Y. C. Fung and M. V. Barton* 365
Coupled Vibrations of Thin-Walled Beams . . . . . *J. M. Gere and Y. K. Lin* 373
Timoshenko Beam Equation for Short Pulse-Type Loading . . . . *H. J. Plass, Jr.* 379
Nonaxial Bending of Ring Plates of Varying Thickness . . . . . *H. D. Conway* 386
Transverse Vibrations of Rectangular Orthotropic Plates . . . . . *N. J. Huffington, Jr., and W. H. Hoppmann II* 389
Contact Stresses Under Pressure and Twist . . *M. Hetenyi and P. H. McDonald, Jr.* 396
Stress-Strain Relations for Simple Model of Granular Medium . . . *H. Deresiewicz* 402
Plane Stress Solution of Elastic, Perfectly Plastic Wedge . . . . . *P. M. Naghdi* 407

Brief Notes

Effect of Tensile Plastic Deformation on Yield Condition . *L. W. Hu and J. P. Brust* 411
Frequencies of Uniform Beams With Additional Masses . . . . . *J. Hauser* 412
Equations for Toroidal Shells Subjected to Pressure . . . . . *G. D. Galletly* 412
Axisymmetric Bending Effects in Toroidal Shells . . . . . *G. D. Galletly* 415
Effect of Magnetic Field on Forced-Convection Heat Transfer . . . . . *R. Siegel* 419

Discussion on previously published papers by *J. L. Catchpole and H. S. Heaps; M. B. Landrith and R. D. Short, Jr.; P. Shulesbke; and J. P. Osterle, Y. T. Chou, and E. A. Saibel* 417

SEPTEMBER, 1958

VOL. 25, NO. 3

Transactions of The American Society of Mechanical Engineers

[illegible] of Applied Mechanics

[illegible] of the Transactions of the ASME, Applied Mechanics Division

[illegible]

W. [illegible], Jr., Secretary
S. C. [illegible] and J. [illegible], Technical Editors
P. A. [illegible], Contributing Technical Editor

[illegible]

Published quarterly by

[illegible] Society of Mechanical Engineers

[illegible]

[illegible] Office, 29th and Northampton Streets, Easton, Pa.
[illegible] of the Society, 29 West [illegible] Street, New York 18, N. Y.
[illegible] for Technical Papers, Journal of Applied Mechanics, ASME,
[illegible], Brown University, Providence 12, R. I.

[illegible]
J. W. [illegible], Jr., Publisher
[illegible], Secretary

[illegible]

[illegible]
J. J. [illegible], Jr., Editor
[illegible], Contributing Editor

[illegible]
R. C. [illegible], Production

[illegible] or opinions advanced in papers or [illegible] published in its publications (B13, Par. 4)

[illegible] Society, Box 70, [illegible] Street, New York 18, N. Y. [illegible] Society of Mechanical Engineers, [

Ducted Fan Design Theory

By C. G. VAN NIEKERK,[1] PRETORIA, UNION OF SOUTH AFRICA

A theory is outlined by means of which it is possible to design ducted fans directly and without having to choose any parameters in an arbitrary fashion. Optimum sizes and fan speeds are theoretically determined. The design of two fans, one having inlet guide vanes and the other of the low slip-stream-rotation type having NPL straighteners and often used in wind tunnels, are considered by way of example. While achieving a considerable degree of rationality, the theory introduces a concept of annulus efficiency that is still of an empirical nature. The empiricism is due to a present lack of knowledge about three-dimensional fan losses, and suggests further investigation.

Nomenclature

The following nomenclature is used in the paper:

A = area of fan annulus = $\pi(R^2 - r_0^2)$
C_L = lift coefficient
C_D = drag coefficient
c = chord
G = defined by Equation [7]
H = defined by Equation [8]
N = rotational speed
p = theoretical total pressure rise
p_e = effective total pressure rise
Q = torque
R = tip radius
r = radius
r_0 = hub radius
T = thrust
u = axial velocity
V = volumetric flow
α = incidence
γ = arc tan C_D/C_L
ϵ = swirl coefficient defined by Equation [42]
ϵ_g = swirl coefficient defined by Equation [23]
z = number of blades
η = fan efficiency
η_a = annulus efficiency
η_b = blade-element efficiency
θ = blade angle
λ = hub-tip ratio = r_0/R
ξ = pressure coefficient
ρ = air density
σ = characteristic number
ϕ = $\theta - \alpha$
ϕ_g = guide-vane air-exit angle
ψ = flow coefficient
Ω = angular velocity of fan
ω_g = angular velocity of swirl imparted by guide vanes
ω = angular velocity of swirl behind fan rotor

Subscripts

av = mean value
m = optimum value
0 = hub value

Introduction

A study of some existing fan design theories (1–5)[2] has indicated the need for further analytical development to achieve greater simplicity of the design procedure and to eliminate the usual necessity of having to assume several fan parameters without being able to assess their influence on fan efficiency in a rational way. Therefore a new theory has been evolved that will enable fans to be designed for optimum values of all parameters, without having to resort to laborious methods of calculation.

In its present form the theory is, in common with most other theories, limited to the case where the pressure rise and the axial air velocity are considered constant over the fan annulus. However, it seems possible to extend the analysis so as to make it applicable in instances where these quantities vary. The theory is further confined to the use of single airfoil data, but here again it is extensible. Of interest in this connection is the way in which Wallis (1) incorporates compressor-cascade data into a fan design theory.

Apart from these limitations, the theory enables optimum fan parameters to be established which otherwise would have to be chosen somewhat arbitrarily. This part of the analysis is not exact, but depends, for instance, on the degree of accuracy with which certain losses, here termed annulus losses, can be estimated. However, when deciding on fan sizes and fan speeds, even the results of a poor estimate are preferable to those obtained by ignoring the effect of these losses altogether. Other inaccuracies in this part of the analysis are introduced as a result of certain assumptions that have to be made, but, since their implications are best understood in proper context, these assumptions are only listed later in the paper.

Having served to establish the most suitable main parameters of a fan, the theory further enables the direct calculation of blade solidities and blade angles. This is accomplished by using a basic equation which is but slightly affected by large errors in the only estimated variable that it contains.

Fan With Inlet Guide Vanes

Performance Coefficients. A fan usually needs to be designed for specified conditions of pressure rise and volumetric flow, all other factors being governed by considerations of efficiency and economy.

The volumetric flow V and the effective total pressure rise p_e may be expressed conveniently in terms of the dimensionless coefficients

$$\psi = \frac{V}{A\Omega R} \quad \ldots\ldots [1]$$

$$\xi = \frac{p_e}{\frac{1}{2}\rho(\Omega R)^2} \quad \ldots\ldots [2]$$

---

[1] Senior Research Officer, National Mechanical Engineering Research Institute, South African Council for Scientific and Industrial Research, Pretoria, South Africa.

Contributed by the Applied Mechanics Division for presentation at the Annual Meeting, November 30–December 5, 1958, New York, N. Y., of The American Society of Mechanical Engineers.

Discussion of this paper should be addressed to the Secretary, ASME, 29 West 39th Street, New York, N. Y., and will be accepted until January 10, 1959, for publication at a later date. Discussion received after the closing date will be returned.

Note: Statements and opinions advanced in papers are to be understood as individual expressions of their authors and not those of the Society. Manuscript received by ASME Applied Mechanics Division, March 21, 1957. Paper No. 58—A-4.

[2] Numbers in parentheses refer to the Bibliography at the end of the paper.

where ψ is the flow coefficient, ξ the pressure coefficient, and where A is the area of the fan annulus, R the blade-tip radius, ρ the air density, and Ω the angular velocity of the fan.

By using the well-known fan laws (6) relating the flow, pressure and diameters of geometrically similar fans, it may be shown that

$$V^{1/2}\left(\frac{\rho}{p_s}\right)^{3/4} N = \text{const}$$

or, in terms of ψ and ξ, that

$$\frac{\psi^{1/2}}{\xi^{3/4}}(1 - \lambda^2)^{1/2} = \text{const}$$

where N is the rotational speed and λ the hub-tip ratio; i.e., $\lambda = r_0/R$, where r_0 is the hub radius.

The characteristic number σ of a fan is then defined as

$$\sigma = \frac{\psi^{1/2}}{\xi^{3/4}}(1 - \lambda^2)^{1/2} \quad [3]$$

or

$$\sigma = 0.035 V^{1/2}\left(\frac{\rho}{p_s}\right)^{3/4} N \quad [4]$$

where N is expressed in rpm, V in cu ft per sec, p_s in psf, and ρ in slugs per cu ft. Also, the theory assumes the fan to operate in a parallel annulus, so that the total pressure rise and the static pressure rise will be the same.

Strip Theory. The inlet guide vanes produce a swirl that is removed by the rotor, so that the exit flow from the fan is axial. This case is represented by the velocity diagram in Fig. 1.

Defining the lift coefficient of the rotor-blade element in terms of the mean relative velocity (1, 5), the strip-theory equations may be written as follows (2, 4)

$$\frac{dT}{dr} = \frac{1}{2}\rho z c u^2 G \cot\phi \quad [5]$$

$$\frac{dQ}{dr} = \frac{1}{2}\rho z c u^2 H r \cot\phi \quad [6]$$

$$G = \frac{C_L}{\sin\phi} - \frac{C_D}{\cos\phi} = \frac{C_L\cos(\phi+\gamma)}{\sin\phi\cos\phi\cos\gamma} \quad [7]$$

$$H = \frac{C_L}{\cos\phi} + \frac{C_D}{\sin\phi} = \frac{C_L\sin(\phi+\gamma)}{\sin\phi\cos\phi\cos\gamma} \quad [8]$$

$$\tan\gamma = \frac{C_D}{C_L} \quad [9]$$

$$\phi = \theta - \alpha \quad [10]$$

$$\frac{dT}{dr} = 2\pi r\left(\eta_h p + \frac{1}{2}\rho\omega_g^2 r^2\right) \quad [11]$$

where T, Q, r, z, c u, C_L, C_D, θ, α, p, η_h, and ω_g are, respectively, the thrust, torque, radius, number of blades, chord, axial velocity, lift coefficient, drag coefficient, blade angle, incidence, theoretical total pressure rise, blade-element efficiency, and angular velocity of swirl imparted by the guide vanes.

By momentum theory

$$\frac{dQ}{dr} = zr\rho u\omega_g r\frac{2\pi r}{z} \quad [12]$$

By equating work output and input

$$(2\pi r p u)dr = (2\pi r\rho u\omega_g r\Omega r)dr$$

i.e.

$$p = \rho\Omega r\omega_g r \quad [13]$$

Combining Equations [11], [12], and [13] with Equations [5] to [8] yields an equation for blade-element efficiency that also has been derived in different forms by Wallis (1), Patterson (3), and Keller (5); namely

$$\eta_h = \frac{u}{\Omega r}\cot(\phi+\gamma) - \frac{\omega_g}{2\Omega} \quad [14]$$

Also, from Fig. 1

$$\tan\phi = \frac{u}{\Omega r}\left[\frac{1}{1 + \frac{\omega_g}{2\Omega}}\right] \quad [15]$$

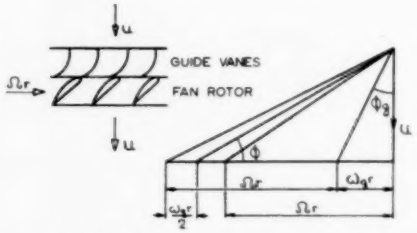

Fig. 1 Velocity diagram for fan with inlet guide vanes

Further, from Equations [5], [7], and [11], and using Equations [13] and [14]

$$\frac{zcC_L}{2\pi r} = \frac{2\omega_g r\sin\phi}{u(1 + \cot\phi\tan\gamma)} \quad [16]$$

Finally, by using Equation [15], Equation [14] may be written in the form

$$(1 - \eta_h) = \frac{\Omega r}{u}\tan\gamma\left[\frac{\left(1 + \frac{\omega_g}{2\Omega}\right)^2 + \frac{u^2}{\Omega^2 r^2}}{1 + \left(1 + \frac{\omega_g}{2\Omega}\right)\frac{\Omega r}{u}\tan\gamma}\right] \quad [17]$$

Fan Losses. By considering the fan losses it is possible to derive equations that may be used to obtain the most suitable fan design for any specified duty. For the purposes of this paper the analysis may be simplified by introducing the assumption of constant axial velocity and constant pressure rise over the fan annulus. Equation [1] may then be written

$$\psi = \frac{u}{\Omega R} \quad [18]$$

and, since the sum of all the fan losses reduces the theoretical total pressure rise p, introduced in Equation [11], to the effective total pressure rise p_s of Equation [2], we may also write

$$p_s = \eta p \quad [19]$$

where η is the over-all fan efficiency.

The total losses are mainly made up of blade profile drag losses, stator losses, and diffuser losses. Instead of lumping all these together, it is desirable to separate the group of losses that do not depend upon the direct action of the fan blades as such, but that occur as a result of friction and flow separation in the annular duct containing the fan. Writing then

$$p_s = p - \text{annulus losses} - \text{blade losses}$$

the term "blade losses" will, in the conventional way, involve the blade-element efficiency as given by Equation [14]. The term "annulus losses" will be associated with losses in the stator vanes, over the annular surfaces of the fan casing, and in the diffuser containing the tail fairing.

If the hub-tip ratio is not considered as a dependent variable, but held constant at different values, then the concept of an annulus efficiency η_a may be introduced in such a way that for any fan having a particular hub-tip ratio we may write

$$p_s = p - (1 - \eta_a)\frac{\rho}{2}u^2 - (1 - \eta_b)_{av}p \quad \ldots\ldots [20]$$

where $(1 - \eta_b)_{av}$ is the average blade-loss coefficient over the annulus.

The annulus losses are here defined in terms of axial velocity since for a fixed hub-tip ratio η_a is then constant and, neglecting scale effects, dependent only upon the shapes and surface finish of the stator vanes, fan casing, hub and tail fairing. The part of η_a which is associated with the stators is constant because, as will be seen further on, the design swirl coefficient $\omega_g r/u$ is limited in such a way that it will always be the same for any fan having a particular annulus geometry.

Since η_a refers only to losses that are associated with the velocity head through the annulus, Equation [20] does not allow for all such losses as those due to boundary-layer separation at the hub of the rotor, and other secondary losses not as yet properly understood. However, these losses, although relatively small (1), could be included as part of either the annulus or the blade losses. Rational evaluation of η_a, and adjustment of η_b to allow for secondary blade losses, may be accomplished by detailed examination of the various individual losses, but such a course is still rendered difficult by a lack of existing knowledge, as may be judged from work done by Wallis (1) in this connection. At present η_a has yet to be estimated roughly or its magnitude determined on a basis of experience.

By means of a simplifying assumption, which introduces errors that tend to cancel, and justification for which is indicated in a later section of this paper, it is now possible to use the theory so far outlined in order to derive information regarding conditions of minimum loss. This assumption implies that $(\omega_g/2\Omega)^2 \ll 1$ and $\tan\gamma \ll 1$, and involves writing Equation [17] in the form

$$(1 - \eta_b) = \frac{\Omega r}{u}\tan\gamma\left(1 + \frac{\omega_g}{\Omega} + \frac{u^2}{\Omega^2 r^2}\right) \quad \ldots\ldots [21]$$

For the usual type of airfoil section used in fans, $\tan\gamma$ is indeed small, and it may be shown that $(\omega_g/2\Omega)^2$ also will be small over the range of fan designs treated here. The average blade-loss coefficient over the annulus is then obtained from Equation [21] by integration between the limits r_0 and R

$$(1 - \eta_b)_{av} = \frac{2(1 - \lambda^2)(\tan\gamma)_{av}}{3(1 - \lambda^2)\psi} + \frac{2(\tan\gamma)_{av}(\lambda\epsilon_g + \psi)}{(1 + \lambda)} \quad \ldots [22]$$

where $(\tan\gamma)_{av}$ is the average value of $\tan\gamma$ along a blade, and

$$\epsilon_g = \frac{\omega_{g0}r_0}{u} \quad \ldots\ldots [23]$$

where ω_{g0} is the angular velocity of swirl at the hub.

Now, for p constant, Equation [13] shows that $\omega_g r^2 = \text{const}$, which is the condition for free-vortex flow. This condition, together with Equation [23], may be used to show that

$$\omega_g r^2 = \epsilon_g u r_0 \quad \ldots\ldots [24]$$

which, when substituted into Equation [13], leads to the important relationship

$$\eta = \frac{\xi}{2\epsilon_g\lambda\psi} \quad \ldots\ldots [25]$$

Then from Equation [20], by substituting from Equations [22] and [25]

$$(1 - \eta) = \frac{(1 - \eta_a)\psi}{2\epsilon_g\lambda} + \frac{2(1 - \lambda^2)(\tan\gamma)_{av}}{3(1 - \lambda^2)\psi} + \frac{2(\tan\gamma)_{av}(\lambda\epsilon_g + \psi)}{(1 + \lambda)} \quad \ldots [26]$$

Since λ as well as the values of η_a and ϵ_g are constant for a fan of a given annulus and stator geometry, and since $(\tan\gamma)_{av}$ will only vary slightly with changes in ψ over the range in which η is fairly high, this expression may be differentiated w.r.t. ψ in order to obtain the condition of minimum loss, i.e., the optimum value of ψ, which is thus found to be

$$\psi_m = \left[\frac{2\lambda(1 + \lambda + \lambda^2)(\tan\gamma)_{av}}{\frac{3}{2\epsilon_g}(1 - \eta_a)(1 + \lambda) + 6\lambda(\tan\gamma)_{av}}\right]^{1/2} \quad \ldots [27]$$

Higher values of ψ will lead to higher velocities and correspondingly greater losses in the stators and annulus, while lower values will cause reductions in η_b as may be seen from Equation [14].

Using Equations [3] and [25] we also obtain that, under optimum conditions

$$\sigma = \frac{(1 - \lambda^2)^{1/2}}{(2\epsilon_g\lambda\eta)^{3/4}\psi_m^{1/4}} \quad \ldots\ldots [28]$$

An expression for the optimum radius $R = R_m$ may finally be derived from Equations [2], [25], and [1] to yield

$$R_m = \frac{N\rho V}{p_s}\left[\frac{\epsilon_g\lambda\eta}{30(1 - \lambda^2)}\right] \quad \ldots\ldots [29]$$

It will be clear that, while Equations [28] and [29] refer to optimum conditions, this is only because of the substitution $\psi = \psi_m$. These expressions, together with Equation [26], are equally valid for other values of ψ.

Now, if η_a and ϵ_g are known for a particular λ, and a suitable value of $(\tan\gamma)_{av}$ adopted, then for this set of conditions, Equation [27] will yield the optimum flow coefficient ψ_m. Over a range of different λ, and corresponding η_a and ϵ_g, this equation may therefore be used to obtain a relationship between ψ_m and λ.

From Equation [26] follows a relationship between η and λ; from Equation [28] one between optimum σ and λ; and from Equation [29] one between $(R_m/N)(p_s/\rho V)$ and λ. For any particular value of λ a design will be optimum, provided the corresponding optimum σ is obtained, no matter how the variables V, p_s, and N are chosen. However, the fan radius will be determined by Equation [29].

For design purposes V and p_s will be given, and $(\tan\gamma)_{av}$ estimated, so that λ may be chosen to yield any desired N and R_m. For this chosen λ, and corresponding ϵ_g and η_a, the design will be optimum if $\psi = \psi_m$. The determination of ϵ_g and the estimation of η_a and $(\tan\gamma)_{av}$ is dealt with in the paragraphs that follow.

Thus far the analysis has involved making the assumptions that:

1 Free vortex flow conditions exist in the fan annulus, this being assumed for the sake of simplicity.

2 The term $(1 - \eta_a)\rho u^2/2$ in Equation [20] represents all the

fan losses apart from those due to blade-profile drag, η_a being considered constant for a fan of given annulus geometry, this implying that part of the losses due to boundary-layer effects at the blade tips and at the rotor hub are neglected in comparison with the sum of the blade losses, stator losses, and diffuser losses.

3 In Equation [17] both $(\omega_g/2\Omega)^2$ and $\tan\gamma$ are small, an assumption which has been discussed already, and which is later referred to again.

4 $(\tan\gamma)_{av}$ varies negligibly with changes in ψ over the range in which η approaches its maximum for any particular value of λ.

5 As implied by the second and fourth assumptions, scale effects may be ignored when deriving Equations [27] to [29]. This limits the range of fan sizes and speeds over which the theory is accurate, but only to the same extent as does the usual assumption that the fan laws are not subject to scale effects (6).

The only further assumptions that are made in the part of the treatment that follows involve a restriction of the theory to the use of free arifoil data, the imposition of empirical limitations on swirl coefficient, blade solidity, and lift coefficient, and the approximation that $(\cot\phi\tan\gamma)\ll 1$ at the hub of a fan.

Design Limitations. In order to obtain the maximum possible loading on the fan blades, it is desirable to use the largest permissible value of ω_g. Since, then, the maximum swirl that can be obtained without stalling in guide vanes is shown from work on accelerating cascades to be such that (1)

$$\frac{\omega_g r}{u} \leqslant 1.5$$

and since $\omega_g r/u$ is greatest at the hub, we may impose the limitation

$$\epsilon_g \leqslant 1.5 \qquad [30]$$

We may therefore always take $\epsilon_g = 1.5$, but this will sometimes lead to such high values of lift coefficient and blade solidity that the use of single airfoil characteristics will no longer be valid, so that design will have to be based on cascade data.

The theory may be adapted to the use of cascade data, but since existing data of this nature are usually only directly applicable to compressor design, and not necessarily to the design of fans, the theory, for the present, will be limited to the use of single airfoil data. As is usual (5), we therefore impose

$$\frac{zc_0 C_{L_0}}{2\pi r_0} \leqslant 1.1 \qquad [31]$$

where subscript 0 refers to conditions at the hub.

It is a reasonable approximation, especially in view of the empiricism already inherent in Equation [31], to assume that $(\cot\phi\tan\gamma)\ll 1$ at the hub. Equation [16] may then be written as

$$\frac{zc_0 C_{L_0}}{2\pi r_0} \simeq \frac{2\omega_{g_0} r_0 \sin\phi_0}{u}$$

so that by substituting from Equations [13], [15], [3], and [25] it may be shown that

$$\frac{4}{\epsilon_g^2\psi^2}(\psi^2 + \epsilon_g\lambda\psi + \lambda^2) \geqslant 12.2 \qquad [32]$$

where $\epsilon_g \leqslant 1.5$.

Taking $\psi = \psi_m$, and for chosen values of η_a and $(\tan\gamma)_{av}$, it is possible to determine, once for all, relationships between ϵ_g and λ from Equation [32] that will always yield either

$$\frac{zc_0 C_{L_0}}{2\pi r_0} = 1.1 \text{ or } \epsilon_g = 1.5$$

Such a set of curves is shown in Fig. 2.

Optimum Relationships. It is now possible to plot, for different values of $(\tan\gamma)_{av}$ and η_a, sets of permanently useful curves showing the optimum relationships between the various fan parameters.

Choosing, for instance, the fairly typical value of $(\tan\gamma)_{av} = 0.022$, we obtain, for different values of η_a, the relationships between η and λ from Equation [26], the relationships between σ and λ from Equation [28], and the relationships between (R_m/N) $(p_s/\rho V)$ and λ from Equation [29], as shown respectively in Figs. 3, 4, and 5.

The accuracy of these curves depends only upon the validity of the assumption introduced by writing Equation [17] as Equation [21]. This was investigated by obtaining some indication of the degree of error introduced. For this purpose, Equations [17] and [21] were expressed in terms of ϵ_g, ψ, and λ after successively substituting $r = r_0$, $r = (r_0 + R)/2$ and $r = R$. Curves of $(1 - \eta_h)$ against λ were then plotted, the given relationships between ϵ_g, ψ_m, and λ being used for the purposes of substitution in order to compare the exact and approximate forms of the equation. The error in $(1 - \eta_h)$ was generally found to amount to only a few per cent.

Values of $(\tan\gamma)_{av}$ may be taken to be typical of usual low drag airfoil sections, or else a specific profile may be chosen and an approximate mean $\tan\gamma$ estimated from the appropriate characteristic curves by considering a range of lift coefficients between roughly 0.7 and 1.0. The value 0.7 here corresponds to the highest [illegible]erally accepted to be attainable at a fan-blade tip (4), an[illegible]alue 1.0 to be the maximum allowable C_L at the hub (5).

When using the curves of Figs. 2 to 5 it also becomes necessary to choose a value of η_a. The estimation of η_a is, at present, still a somewhat empirical procedure in that it depends largely upon practical knowledge of the losses usually occurring in diffusers and different types of fans.

Design Procedure. Considering, by way of example, the design of a fan for which the delivery is to be 10,000 cfm at an effective total pressure rise of 20 psf, the first step would be to decide on a value for η_a. For this type of fan it could reasonably be assumed that $\eta_a = 0.8$ for all the values of λ that can possibly be expected to prove suitable, and Fig. 5 may then be used to derive the family of curves shown as solid lines in Fig. 6. Next, Equation [4] is used in conjunction with Fig. 4 to obtain the dashed curve in Fig. 6. This dashed curve now shows how R, λ, and N should be related in order to produce optimum conditions. As indicated by Fig. 3, it is preferable to choose λ fairly high, but this leads to the larger values of R and may therefore not be desirable.

Suppose it is decided to choose $\lambda = 0.5$, $R = 1.025$ ft, and $N = 1800$ rpm, as shown by the dotted lines in Fig. 6. The appropriate value of ϵ_g may then be read off in Fig. 2 and r_0, u, and Ω calculated. At each of a few radial stations from r_0 to R the value of ω_g is calculated from Equation [24], and Equation [15] used to determine ϕ at each station. This enables the product zcC_L at each station to be obtained from Equation [16].

When evaluating Equation [16] it is again necessary to assume $\tan\gamma$. The value $\tan\gamma = 0.022$ may be used throughout, or else $\tan\gamma$ may be individually estimated for each station. It will be clear, in any case, that even large errors in $\tan\gamma$ will have only little effect on zcC_L.

A suitable z is now chosen, and satisfactory hub and tip chords obtained by taking the lift coefficient at the hub near unity and that at the tip in the vicinity of 0.7. Chords at intermediate stations may be chosen to obtain any desired blade shape, and the corresponding values of C_L calculated. Finally, α follows from airfoil data, and θ is thus determined.

It may be desirable to calculate the Reynolds number at each station and thus to obtain accurate values of γ, these being in-

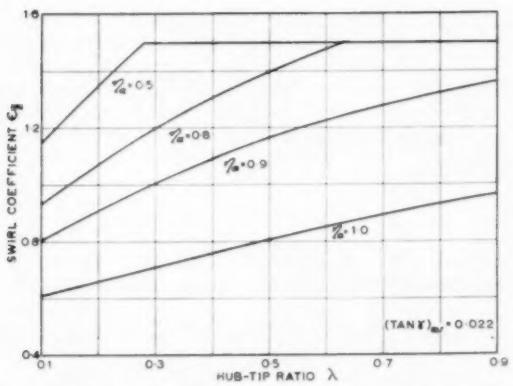

Fig. 2 Allowable swirl coefficients for fans with inlet guide vanes

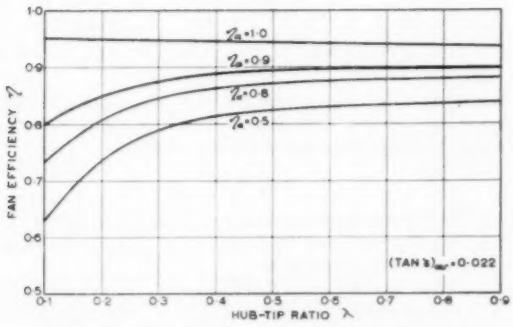

Fig. 3 Efficiency of fans with inlet guide vanes

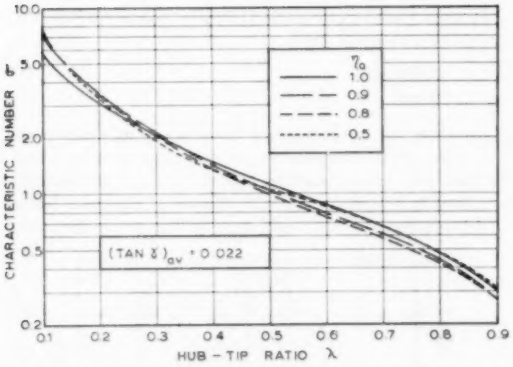

Fig. 4 Optimum characteristic number for fans with inlet guide vanes

serted in Equation [16] by way of a check on the accuracy of $zc\,C_L$. Usually, however, errors will be found negligible.

Fig. 1 shows that the inlet guide vanes are required to impart a swirl of circumferential velocity $\omega_g r$ to the inlet air. With ϕ, u, and Ω known, the required air deflection may be calculated at different radii. It then remains to design the guide vanes in such a way that they will produce this deflection of the incoming axial flow. When designing the usual type of high-solidity stator vanes it becomes necessary, in view of the present lack of more satisfactory cascade data, to resort to approximate methods (1) based on the results of work done on compressor cascades.

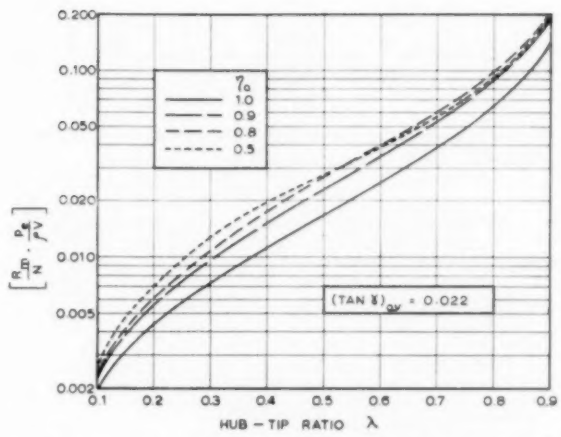

Fig. 5 Optimum radius-speed parameter for fans with inlet guide vanes

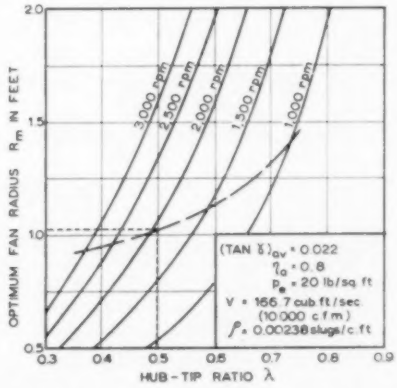

Fig. 6 Optimum relationship between λ, R, and N for a fan with inlet guide vanes

Fan Having Low Slipstream Rotation

This method of analysis is applicable to all types of ducted fan, the following procedure, for instance, being adopted when considering the design of fans that are equipped with NPL straighteners.

Equations [11] to [17] now become, respectively

$$\frac{dT}{dr} = 2\pi r\left(\eta_h p - \frac{1}{2}\rho\omega^2 r^2\right) \quad [33]$$

$$\frac{dQ}{dr} = \pi r\rho u\omega r\frac{2\pi r}{z} \quad [34]$$

$$p = \rho\Omega r\omega r \quad [35]$$

$$\eta_h = \frac{u}{\Omega r}\cot(\phi+\gamma) + \frac{\omega}{2\Omega} \quad [36]$$

$$\tan\phi = \frac{u}{\Omega r}\left[\frac{1}{1-\dfrac{\omega}{2\Omega}}\right] \quad [37]$$

$$\frac{ZcC_L}{2\pi r} = \frac{2\omega r\sin\phi}{u(1+\cot\phi\tan\gamma)} \quad [38]$$

$$(1 - \eta_h) = \frac{\Omega r}{u} \tan \gamma \left[\frac{\left(1 - \frac{\omega}{2\Omega}\right)^2 + \frac{u^2}{\Omega^2 r^2}}{1 + \left(1 - \frac{\omega}{2\Omega}\right) \frac{\Omega r}{u} \tan \gamma} \right] \quad [39]$$

where ω is the angular velocity of the swirl behind the fan.

Equation [39] is then written as

$$(1 - \eta_h) = \frac{\Omega r}{u} \tan \gamma \left(1 - \frac{\omega}{\Omega} + \frac{u^2}{\Omega^2 r^2}\right) \quad [40]$$

so that Equation [26] becomes

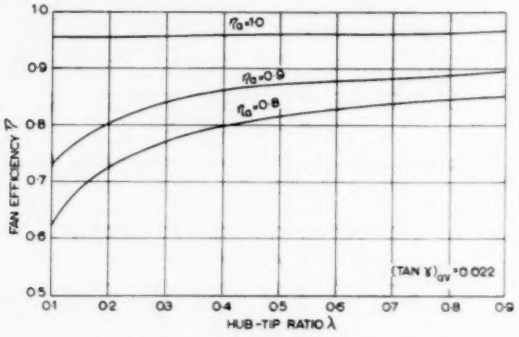

Fig. 7 Efficiency of fans having low slipstream rotation

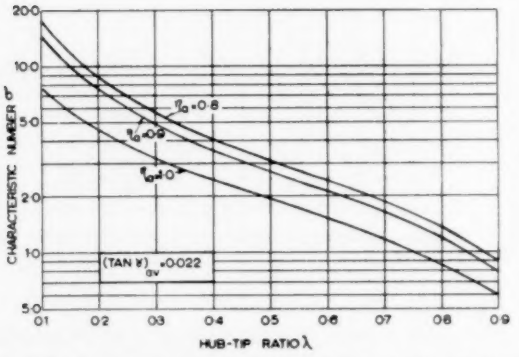

Fig. 8 Optimum characteristic number for fans having low slipstream rotation

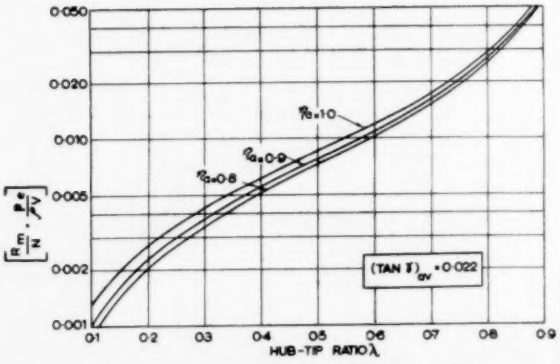

Fig. 9 Optimum radius-speed parameter for fans having low slipstream rotation

$$(1 - \eta) = \frac{(1 - \eta_a)\psi}{2\epsilon\lambda} + \frac{2(1 - \lambda^2)(\tan \gamma)_{av}}{3(1 - \lambda^2)\psi} + \frac{2(\tan \gamma)_{av}(\psi - \epsilon\lambda)}{(1 + \lambda)} \quad [41]$$

where, in the same way as before

$$\epsilon = \frac{\omega_0 r_0}{u} \quad [42]$$

and

$$\omega r^2 = \epsilon u r_0 \quad [43]$$

Equations [27], [28], and [29] become, respectively

$$\psi_m = \left[\frac{2\lambda(1 + \lambda + \lambda^2)(\tan \gamma)_{av}}{\frac{3}{2\epsilon}(1 - \eta_a)(1 + \lambda) + 6\lambda (\tan \gamma)_{av}} \right]^{1/2} \quad [44]$$

$$\sigma = \frac{(1 - \lambda^2)^{1/2}}{(2\epsilon\lambda\eta)^{3/4} \psi_m^{1/4}} \quad [45]$$

$$R_m = \frac{N\rho V}{p_s} \left[\frac{\epsilon\lambda\eta}{30(1 - \lambda^2)} \right] \quad [46]$$

As is usual in the case of wind-tunnel fans in which the swirl is removed by means of NPL straighteners, the limitation of low slipstream rotation gives rise to the condition (1)

$$\epsilon \leqslant 0.4$$

Under these circumstances the analysis of the paragraphs headed "Design Limitations" may be shown to be unnecessary, so that $\epsilon = 0.4$ always may be assumed.

In the same way as before, Equations [44], [41], [45], and [46] are then evaluated to yield Figs. 7, 8, and 9. Once again, these are permanently useful sets of curves.

Suppose then it is desired to design a fan for a wind tunnel having a 9-ft-diam working section in which the speed is to reach 250 fps, the wind-tunnel power factor being estimated as 0.27. A few simple calculations will yield

V = 16,000 cfs
p_s = 20 psf

Considering the magnitude of the losses that could occur in stators of the NPL straightener type, the range of suitable hub-tip ratios that may prove possible, and the type of tail fairing that can be used in a wind tunnel, it is reasonably assumed that η_a = 0.9. The curves shown as solid lines in Fig. 10 are then derived

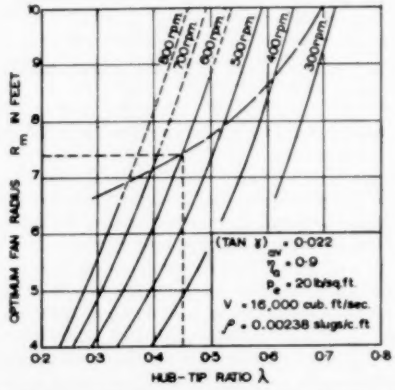

Fig. 10 Optimum relationship between λ, R_m and N for a fan having low slipstream rotation

from Fig. 9. Dotted portions of these curves indicate conditions where the tip speeds would exceed 550 fps, and should therefore be avoided. Again in the same way as before, Fig. 8 is used to derive the dashed curve in Fig. 10, and optimum relationships between λ, R, and N thus established. Dotted lines in Fig. 10 indicate a suitable choice of main fan parameters, namely, $\lambda = 0.45$, $R = 7.4$ ft, and $N = 600$ rpm. Detailed design of the fan blades follows in the way outlined previously, Equations [43], [37], and [38] being used.

Conclusion

More results of experimental investigations will have to become available if fans are to be more rationally and effectively designed. In particular, as pointed out in the present analysis, considerably more information is required about fan losses and also about such cascade-flow phenomena as are peculiar to fans.

In view of the increasing use of ducted fans, not only in the realm of aeronautics but also for ventilating work, further investigations may well be considered justified.

Acknowledgment

Permission granted by the South African Council for Scientific and Industrial Research to publish this paper is gratefully acknowledged.

Bibliography

1 "Design, Performance and Analysis of Ducted Axial Flow Fans," by R. A. Wallis, Report A.88, Aeronautical Research Laboratories (Australia), August, 1954.

2 "A Note on the Design of Ducted Fans," by B. Thwaites, *The Aeronautical Quarterly*, vol. 3, November, 1951, pp. 173–181.

3 "Ducted Fans: Design for High Efficiency," by G. N. Patterson, Report ACA-7, Australian Council for Aeronautics, July, 1944.

4 "The Design of Wind Tunnel Fans," by A. R. Collar, Reports and Memoranda No. 1889, Aeronautical Research Council (Great Britain), August, 1940.

5 "The Theory and Performance of Axial Flow Fans," by C. Keller, McGraw-Hill Book Company, Inc., New York, N. Y., 1937.

6 "Flow and Fan," by C. H. Berry, The Industrial Press, New York, N. Y., 1954, pp. 157–163.

The Effect of Spin Upon the Rolling Motion of an Elastic Sphere on a Plane

By K. L. JOHNSON,[1] CAMBRIDGE, ENGLAND

The motion and deformation of an elastic sphere rolling on an elastic plane are examined for the case when the sphere, in addition to its straight rolling motion, has an angular velocity of "spin" Ω about an axis normal to the plane. The action of spin is to twist the area of contact. Surface tractions resulting from this rotation are found, which demonstrate the necessity of partial slip in the area of contact. Previous investigations suggest that this slip cannot occur at the leading edge of the contact circle, so that a system of tractions is found which corresponds to zero stress at the leading point. It is shown that such a system of tractions gives rise to a transverse creep of the sphere in the direction of its rotation Ω. The magnitude of this creep is calculated for small values of Ω, when slip occurs to only a small extent. Experiments have been performed using a simple thrust bearing with plane parallel races. As the bearing rotates, the balls creep radially outward in the predicted manner. Quantitative measurements of this creep agree with the theoretical estimate over a wide range.

Introduction

THE motion of a sphere which rolls without sliding upon a plane has been analyzed in a companion paper (1)[2] into three categories: (*a*) Free rolling; (*b*) rolling under tangential forces; and (*c*) rolling with spin. The motion referred to as spin is defined as a relative angular velocity between the sphere and the plane about an axis through the point of contact normal to the plane.

Spin is a recognized feature of thrust and angular-contact ball bearings and is usually held responsible for the higher friction torque and considerably shorter life of these bearings in comparison with radial bearings in which free rolling occurs. In spite of its practical importance, few attempts seem to have been made to analyze the mechanism of the motion or to determine the surface stresses which are induced. Palmgren (2) and Poritsky, Hewlett, and Coleman (3) calculate the friction torque of angular-contact bearings assuming that the relative slip between the balls and the races consists of a rigid-body rotation with the spin velocity about a normal axis through the center of the contact area. The more recent work of Mindlin (4) and Lubkin (5) suggests that it is unjustifiable to ignore tangential displacements resulting from the elasticity of the surfaces and that, at least for small spin velocities, slip might occur over only a small portion of the area of contact, the remainder consisting of a locked region in which no relative motion occurs.

The author was interested to observe, partly by accident, that in a simple thrust bearing, made up of two flat concentrically rotating disks with evenly spaced balls rolling between them, the balls did not move around a perfectly circular path but exhibited a creeping motion radially outward. This occurred when the velocities were sufficiently small for the centrifugal forces to be negligible. The effect is mentioned casually by Palmgren (6) in connection with his rolling experiments with tangential forces, but is dismissed as insignificant, since he states in conclusion[3] that "the ball is always, while rolling, seeking surfaces which are exactly parallel, if such exist in the path of the ball." In the analysis of rolling with spin presented in this paper an attempt is made to assess the magnitude and to explain the mechanism of this radial creep.

Statement of the Problem

In this problem the sphere is taken to roll on the plane in a straight line parallel to the axis ox with a steady velocity U. Contact is maintained by a force N acting in a direction normal to the plane, which gives rise of a circular area of contact of radius a given by

$$a^3 = \frac{3(1-\nu)ND}{8G} \qquad [1]$$

At the same time a steady angular velocity of spin Ω about the normal axis oz is maintained by an applied twisting couple M_z. In view of the observations mentioned in the introduction, tangential creep velocities ΔU and ΔV might be expected as shown in Fig. 1.

Clearly the action of the spin rotation, as the sphere rolls for-

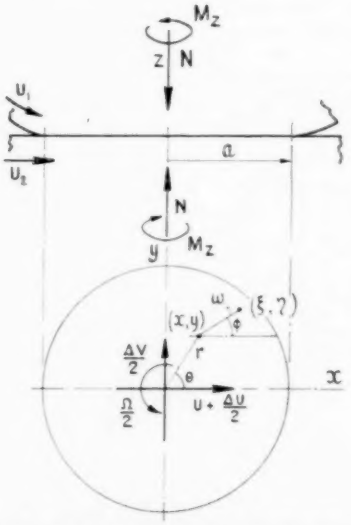

Fig. 1 Area of contact under action of an angular velocity of spin Ω

[1] Engineering Laboratory, Department of Engineering, University of Cambridge, Cambridge, England.

[2] Numbers in parentheses refer to the Bibliography at the end of the paper.

Contributed by the Applied Mechanics Division for presentation at the Annual Meeting, New York, N. Y., November 30–December 5, 1958, of THE AMERICAN SOCIETY OF MECHANICAL ENGINEERS.

Discussion of this paper should be addressed to the Secretary, ASME, 29 West 39th Street, New York, N. Y., and will be accepted until January 10, 1959, for publication at a later date. Discussion received after the closing date will be returned.

NOTE: Statements and opinions advanced in papers are to be understood as individual expressions of their authors and not those of the Society. Manuscript received by ASME Applied Mechanics Division, September 17, 1956. Paper No. 58—A-5.

[3] Reference (7), p. 35.

ward, is to twist the area of contact, thereby inducing tangential components of traction X and Y. It is required to find X, Y, ΔU. and ΔV and the moment M_z arising from a given angular velocity of spin.

The method of analysis follows closely that applied to the problem of rolling under tangential forces given in (1), to which reference should be made for notation, and so on. It was shown there that considerable simplification could be secured by assuming the sphere and plane to have similar elastic constants and by ignoring the warping of the contact surface, whereupon the problem reduced to one of two identical spheres rolling upon each other. The same expedient is applied to the present problem, thereby introducing several important conditions which now arise from the geometrical and elastic symmetry of the system.

Conditions From Symmetry

Reducing the problem to the contact of equal spheres with like elastic constants permits Ω to be divided equally between the surfaces, and reference to Fig. 1 indicates symmetry about the axis Ox. Therefore the equality of action and reaction gives

$$X(x, y) = -X(x, -y) \quad [2]$$

and

$$Y(x, y) = Y(x, -y) \quad [3]$$

$$M_z = \int_0^a \int_0^{2\pi} (Yx - Xy) r dr d\theta \quad [4]$$

and since there is no resultant tangential force

$$\int_0^a \int_0^{2\pi} X r dr d\theta = \int_0^a \int_0^{2\pi} Y r dr d\theta = 0 \quad [5]$$

The particle velocities at point $P(x, y)$ are now given by

$$q_x(x, y, U) = U + \frac{\Delta U}{2} - \frac{\Omega}{2} y + U \frac{\partial u}{\partial x} (x, y, \text{sgn } U) \quad [6]$$

$$q_y(x, y, U) = \frac{\Delta V}{2} + \frac{\Omega}{2} x + U \frac{\partial v}{\partial x} (x, y, \text{sgn } U) \quad [7]$$

Symmetry of the system about Ox gives

$$q_{x1}(x, -y, U) = q_{x2}(x, y, U)$$

and

$$q_{y1}(x, -y, U) = -q_{y2}(x, y, U)$$

where (x_1, y_1) and (x_2, y_2) are contacting points. The relative velocity between such points is therefore given by

$$s_x = q_x(x, y, U) - q_x(x, -y, U)$$

and

$$s_y = q_y(x, y, U) + q_y(x, -y, U)$$

which, from Expressions [6] and [7], give

$$s_x = \Delta U - \Omega y + U \frac{\partial u}{\partial x} (x, y, U) - U \frac{\partial u}{\partial x} (x, -y, U) \quad [8]$$

$$s_y = \Delta V + \Omega x + U \frac{\partial v}{\partial x} (x, y, U) + U \frac{\partial v}{\partial x} (x, -y, U) \quad [9]$$

As in the previous problem, we might expect the area of contact to be divided into a locked region and a region in which slip occurs. In the locked region the relative velocity between contacting points is zero, whence

$$\frac{\partial u}{\partial x} (x, -y, U) - \frac{\partial u}{\partial x} (x, y, U) = \xi_x - p \frac{y}{a} \quad [10]$$

and

$$-\frac{\partial v}{\partial x} (x, -y, U) - \frac{\partial v}{\partial x} (x, y, U) = \xi_y + p \frac{x}{a} \quad [11]$$

where p is a nondimensional spin factor, $\Omega a/U$.

It has not been found possible in this problem to make a simple and physically reasonable supposition for the shape of the locked region once slip has developed to any appreciable extent. The investigations are confined therefore to the assumption that negligible slip occurs over the whole circle of contact.

The method of solution follows that given in reference (1); tangential tractions are specified over the whole area of contact ($r < a$) and the "problem of the plane" solved to obtain the surface displacements, which must satisfy the no-slip conditions of Equations [10] and [11] over the area $r < a$. The boundary conditions in this case reduce to:

$$\left.\begin{array}{l} X \text{ and } Y, \text{ to be specified, consistent} \\ \text{with Conditions [2], [3], and [5]} \\ \text{and} \qquad Z' = 0 \end{array}\right\} \quad r \lessgtr a$$

$$X = Y = Z = 0, \qquad r > a$$

Solution for No Slip

The method employed by Mindlin (4)[4] has been used here to find the tangential surface displacements u and v due to a number of distributions of tangential tractions of similar form acting over the circle $r < a$. The surface integrals obtained by substituting these tractions into Equation [32] of reference (4), although tedious, present no real difficulties. The results of these calculations are summarized for convenience in Table 1.

Considering the data of Table 1 in the light of conditions [2], [3], [5], [10], and [11], it is apparent that the required tractions will be those giving rise to expressions for $\partial u/\partial x$ containing terms proportional to y, and for $\partial v/\partial x$ containing terms proportional to x, such tractions are

$$X_b = \bar{X}_b \frac{xy}{a(a^2 - r^2)^{1/2}} \quad [12]$$

$$Y_1 = \bar{Y}_1 \frac{1}{a} (a^2 - r^2)^{1/2} \quad [13]$$

and

$$Y_b = \bar{Y}_b \frac{x^2}{a(a^2 - r^2)^{1/2}} \quad [14]$$

Each satisfies conditions [2] and [3] and, in order that there should be no resultant tangential force, it follows immediately that Y_1 and Y_b must be added together such that

$$\bar{Y}_b = -\bar{Y}_1 \quad [15]$$

The displacements due to the superposition of tractions [12], [13], and [14] give

$$\frac{\partial u}{\partial x} = \frac{\bar{X}_1 \pi 3(2 - \nu)}{32Ga} y + \frac{\bar{Y}_1 \pi 2\nu}{32Ga} y - \frac{(-\bar{Y}_1)\pi\nu}{32Ga} y$$

$$\frac{\partial v}{\partial x} = \frac{\bar{X}_1 \pi 3\nu}{32Ga} x - \frac{\bar{Y}_1 \pi 2(4 - \nu)}{32Ga} x + \frac{(-\bar{Y}_1)\pi(10 - \nu)}{32Ga} x$$

which satisfy the conditions of no slip, conditions [10] and [11], provided that

$$\xi_x = \xi_y = 0 \quad [16]$$

---

[4] See also "Theory of Elasticity," by A. E. H. Love, p. 242, where a solution to the problem of the plane with given surface tractions is expressed in terms of the potential functions of Boussinesq and Cerruti.

Table 1 Tangential surface displacements within the circle of contact $r < a$

Suffix	Tangential traction, $\frac{X}{\bar{X}}$	Tangential force, $\frac{T_x}{\pi a^2 \bar{X}}$	Twisting couple, $\frac{M_z}{\pi a^3 \bar{X}}$	$\frac{32Gu}{\pi a \bar{X}}$	$\frac{32G}{\pi \bar{X}}\left(\frac{\partial u}{\partial x}\right)$	$\frac{32Gv}{\pi a \bar{X}}$	$\frac{32G}{\pi \bar{X}}\left(\frac{\partial v}{\partial x}\right)$
(1)	$(a^2 - r^2)^{1/2}/a$	$^2/_3$	0	$\{2(2-\nu)(2a^2 - x^2 - y^2) + \nu(x^2 - y^2)\}/a^2$	$2(4-3\nu)x/a$	$2\nu xy/a^2$	$2\nu y/a$
(2)	$a/(a^2 - r^2)^{1/2}$	2	0	$8(2-\nu)$	0	0	0
(3)	$x/(a^2 - r^2)^{1/2}$	0	0	$2(4-3\nu)x/a$	$2(4-3\nu)$	$2\nu y/a$	0
(4)	$y/(a^2 - r^2)^{1/2}$	0	$-^2/_3$	$2(4-\nu)y/a$	0	$-2\nu x/a$	-2ν
(5)	$xy/a(a^2 - r^2)^{1/2}$	0	0	$3(2-\nu)xy/a^2$	$3(2-\nu)y/a$	$\nu\{2a^2 - 3(x^2 + y^2)\}/2a^2$	$-3\nu x/a$
	$\frac{Y}{\bar{Y}}$	$\frac{T_y}{\pi a^2 \bar{Y}}$	$\frac{M_x}{\pi a^3 \bar{Y}}$	$\frac{32Gu}{\pi a \bar{Y}}$	$\frac{32G}{\pi \bar{Y}}\left(\frac{\partial u}{\partial x}\right)$	$\frac{32Gv}{\pi a \bar{Y}}$	$\frac{32G}{\pi \bar{Y}}\left(\frac{\partial v}{\partial x}\right)$
(1)	$(a^2 - r^2)^{1/2}/a$	$^2/_3$	0	$2\nu xy/a^2$	$2\nu y/a$	$\{2(2-\nu)(2a^2 - x^2 - y^2) - \nu(x^2 - y^2)\}/a^2$	$-2(4-\nu)x/a$
(2)	$a/(a^2 - r^2)^{1/2}$	2	0	0	0	$8(2-\nu)$	0
(3)	$x/(a^2 - r^2)^{1/2}$	0	$^2/_3$	$-2\nu y/a$	0	$2(4-\nu)x/a$	$2(4-\nu)$
(4)	$y/(a^2 - r^2)^{1/2}$	0	0	$-2\nu x/a$	-2ν	$2(4-3\nu)y/a$	0
(5)	$x^2/a(a^2 - r^2)^{1/2}$	$^2/_3$	0	$-\nu xy/a^2$	$-\nu y/a$	$\{2(4-3\nu)a^2 + (10-\nu)x^2 + (10-9\nu)y^2\}/2a^2$	$(10-\nu)x/a$

$$\bar{X}_1 = \frac{8G}{\pi}\frac{(3-\nu)}{3(3-2\nu)}p \quad \ldots\ldots [17]$$

and

$$\bar{Y}_1 = \frac{8G}{\pi}\frac{(1-\nu)}{3(3-2\nu)}p \quad \ldots\ldots [18]$$

The resultant tractions are therefore

$$X = \frac{8G(3-\nu)}{\pi 3(3-2\nu)}\frac{p}{a}\frac{xy}{(a^2 - r^2)^{1/2}} \quad \ldots\ldots [19]$$

and

$$Y = \frac{8G(1-\nu)}{\pi 3(3-2\nu)}\frac{p}{a}\frac{a^2 - 2x^2 - y^2}{(a^2 - r^2)^{1/2}} \quad \ldots\ldots [20]$$

The distribution is symmetrical about the y-axis and provides no resultant couple about the axis of spin. This is to be expected, since the stipulation of a perfectly elastic solution with no slip permits no energy dissipation as rolling proceeds.

In common with the no-slip solution for rolling under a tangential force the tractions [19] and [20] exhibit a singularity at $r = a$ which will be relieved in practice by slip.

Solution for Vanishingly Small Slip

It has been shown previously that the application of tangential tractions in both the x and y-directions to the contact surface of a rolling sphere causes slip to initiate at the trailing edge of the contact circle. In each of the cases examined, any assumption of slip between contacting points before they have passed through the locked region has been shown to contradict the law of friction. It will now be assumed that this state of affairs applies to the present problem of tangential tractions due to spin, and any tendency to slip at the point $(-a, 0)$ will be eliminated by making the tangential traction there equal to zero. This device already has been shown to give reasonable results in the case of rolling under tangential forces ($T \ll \mu N$), where a more complete solution is available for comparison [see Appendix to reference (1)].

It is possible to make the resultant traction at the point $(-a, 0)$ have zero value and still satisfy the conditions for no slip over the area of contact by adding to the no-slip solution the tractions

$$X_4 = \bar{X}_4 \frac{y}{(a^2 - r^2)^{1/2}} \quad \ldots\ldots [21]$$

and

$$Y_3 = \bar{Y}_3 \frac{x}{(a^2 - r^2)^{1/2}} \quad \ldots\ldots [22]$$

where

$$\bar{X}_4 = \frac{8G(3-\nu)}{\pi 3(3-2\nu)}p \quad \text{and} \quad \bar{Y}_3 = -\frac{8G(1-\nu)}{\pi 3(3-2\nu)}p$$

are chosen so that the resultant values of X and Y are zero at $(-a, 0)$. The final tractions then become

$$X = \frac{8G(3-\nu)}{\pi 3(3-2\nu)}\frac{p}{a}\frac{(a+x)y}{(a^2 - r^2)^{1/2}} \quad \ldots\ldots [23]$$

and

$$Y = \frac{8G(1-\nu)}{\pi 3(3-2\nu)}\frac{p}{a}\frac{a^2 - 2x^2 - ax - y^2}{(a^2 - r^2)^{1/2}} \quad \ldots\ldots [24]$$

The combined traction $|Q| = (X^2 + Y^2)^{1/2}$, which is no longer symmetrical about the y-axis, is shown in Fig. 2.

The additional tractions X_4 and Y_3 produce displacements (see Table 1) for which

$$\frac{\partial u}{\partial x} = 0$$

$$\frac{\partial v}{\partial x} = \frac{\bar{X}_4\pi(-2\nu)}{32G} + \frac{\bar{Y}_3\pi}{32G}2(4-\nu) = \frac{2-\nu}{3(3-2\nu)} \quad \ldots [25]$$

This constant term, when included in the no-slip condition [11], gives rise to a transverse creep

$$\xi_y = \frac{2(2-\nu)}{3(3-2\nu)}p = \frac{2(2-\nu)}{3(3-2\nu)}\frac{\Omega a}{U} \quad \ldots\ldots [26]$$

Hence a mechanism has been found to explain the transverse creep which is observed to accompany rolling with spin.

A second feature of the nonsymmetrical distribution of tractions [23] and [24] is that the resultant moment about the spin axis is no longer zero

$$M_z = \frac{2\pi a^3}{3}(-\bar{X}_4 + \bar{Y}_3) = -\frac{32(2-\nu)}{9(3-2\nu)}Ga^3p \quad \ldots [27]$$

The results of this section are not exact, either for the case of no slip or when slip occurs, but may be taken to represent the limit to which the creep ξ_y and the resisting moment M_z tend when the

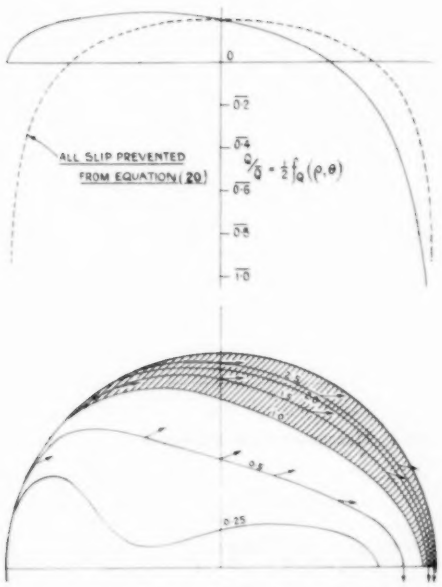

Fig. 2 Contours of resultant surface traction under action of a small angular velocity of spin (vanishingly small slip). Slip might be expected to extend over the shaded area when $pD/\mu a \simeq 1.0$.

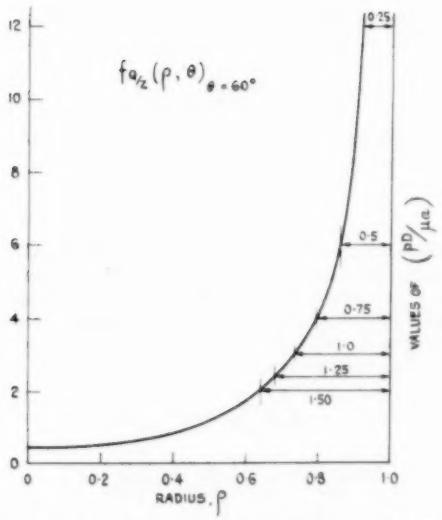

Fig. 3 Estimated progress of slip with increasing spin

degree of slip is small; i.e., for small values of p. The range of values of p for which Equations [26] and [27] might be expected to be valid may be deduced from the contours of traction shown in Fig. 2. It will be seen that the resultant traction

$$|Q| = \frac{8G(2-\nu)}{\pi 3(3-2\nu)} p\mathbf{F}_q\left(\frac{r}{a}, \theta\right) \quad [28]$$

reaches its maximum value, for any given radius, at $\theta \simeq \pm 60$ deg. Slip will progress radially inward from the trailing edge over the region in which $|Q| \geq \mu Z$; i.e.

$$\frac{8G(2-\nu)}{\pi 3(3-2\nu)} p\mathbf{F}_q(\rho, \theta) \geq \mu \frac{3N}{2\pi a^2}(1-\rho^2)^{1/2}$$

where $\rho = r/a$.

Substituting for a from [1] and writing $\mathbf{F}_q(\rho, \theta)/(1-\rho^2)^{1/2}$ as $\mathbf{F}_{q/z}(\rho, \theta)$, the penetration of slip is given by the condition

$$\mathbf{F}_{q/z}(\rho, \theta) \geq \frac{3(3-2\nu)}{2(2-\nu)(1-\nu)}\left(\frac{\mu a}{pD}\right) \quad [29]$$

Apparently, the degree of slip is governed by the nondimensional parameter $(pD/\mu a)$. The function $\mathbf{F}_{q/z}$ is sketched in Fig. 3 for $\theta = 60$ deg. Using Equation [29], the values of $(pD/\mu a)$ to produce increasing penetration of slip are deduced.[5] For example, slip penetrates to $\rho = 0.8$ at $\theta = 60$ deg when $(pD/\mu a)$ reaches the value 0.77, and to $\rho = 0.7$ when $(pD/\mu a)$ is 1.19.

We are now able to estimate, tentatively, the conditions under which the theoretically deduced transverse creep and resisting moment given by Equations [26] and [27] might be expected to apply. The results represent limiting solutions for small slip, but might be expected to provide a reasonable approximation for values of $(pD/\mu a)$ less than 1.0. Slip would then nowhere extend within $\rho = 0.75$ and would roughly cover the shaded area in Fig. 2.

Equations [26] and [27] may be rewritten in terms of the slip parameter $(pD/\mu a)$

$$\frac{\xi_x D}{\mu a} = \frac{2(2-\nu)}{3(3-2\nu)}\left(\frac{pD}{\mu a}\right) \quad [30]$$

$$\frac{M_s D}{\mu G a^4} = -\frac{32(2-\nu)}{9(3-2\nu)}\left(\frac{pD}{\mu a}\right) \quad [31]$$

or, more generally, to cover the values of $(pD/\mu a)$ for which slip is significant

$$\frac{\xi_x D}{\mu a} = f_1\left(\frac{pD}{\mu a}\right) \quad [32]$$

and

$$\frac{M_s D}{\mu G a^4} = f_2\left(\frac{pD}{\mu a}\right) \quad [33]$$

In the absence of a complete solution these functions may be determined by experiment.

Experimental

Experimental observations have been made of the transverse creep which accompanies rolling with spin. Also, with less success, an attempt has been made to measure the resisting moment about the spin axis.

A convenient arrangement in which spin occurs is provided by a simple thrust bearing. The bearing used possessed flat horizontal races, the load being transmitted through three symmetrically spaced balls. The lower race was fixed, while the upper race turned about a vertical central spindle and carried a dead load. If the upper race turns with angular velocity 2Ω the ball centers move round their track of radius R with a velocity $U = \Omega R$. It is clear that there is a relative angular velocity of 2Ω between the two races so that spin must occur between the ball and the races at one or both points of contact. If the surface conditions at both points of contact are identical, in order for the spin moments M_s acting on the ball to be equal and opposite, the ball will turn about a vertical (spin) axis with angular velocity Ω. The angular velocity of spin of the ball relative to the race at

[5] This calculation can only be approximate and apply to a relatively small degree of slip, since the action of slip modifies the traction within the locked region.

each contact is thereby $\pm\Omega$, and the rolling velocity at each contact $\pm U = \pm\Omega R$. Thus the spin factor becomes

$$p = \frac{\Omega a}{\Omega R} = \frac{a}{R} \quad \text{[34]}$$

having the same sign at each point of contact, so that the slip parameter reduces to

$$\frac{pD}{\mu a} = \frac{D}{\mu R} \quad \text{[35]}$$

As the bearing rotates the creep, transverse to the rolling direction, causes the balls to move radially outward, so that the track radius R gradually increases. This movement was measured by micrometer for one circulation of the balls around the track, and is denoted by δ. Thus for the experimental arrangement, Equations [32] and [33] become

$$\frac{\delta}{2\pi R}\frac{D}{\mu a} = f_1\left(\frac{D}{\mu R}\right) \quad \text{[36]}$$

$$\frac{M_s}{\mu N a} = \frac{3(1-\nu)}{8} f_2\left(\frac{D}{\mu R}\right) \quad \text{[37]}$$

For a given value of $(D/\mu R)$, corresponding to a given pattern of slip, Equation [36] suggests that δ is proportional to a. Variations in a were obtained by increasing the normal load. A typical set of creep measurements is shown in Fig. 4 for a series of ball diameters, which adequately demonstrate the linearity of δ with a. If the slopes of these lines are plotted in the form of Equation [36] then we should expect the results to follow a unique function of $(D/\mu R)$.

Difficulty arises in the choice of suitable values for μ. Reference to the legend accompanying Fig. 5 shows that creep measurements were made under a variety of surface conditions. Both hard and soft races were used in the "as-ground" and polished state (the balls were at all times hard and polished). The majority of the experiments were performed with lubricant present, but some measurements were made dry. To correlate these results the coefficient of sliding friction was measured in each case (see legend to Fig. 5). As would be expected, the measured coefficient of friction depended little upon surface finish and hardness. The creep measurements, on the other hand, showed a marked change as a result of polishing the races. To correlate the results into a unique function of $D/\mu R$, the effective value of μ for the polished races requires to be about half of the value for the rougher races. Even assuming that microslip over part of the area of contact is governed by Amonton's law so that we may write $Q = \mu Z$, the experiments suggest that the constant μ cannot be compared with the value associated with steady sliding.

This phenomenon had been observed by the author previously (8) during experiments on the static contact of spherical surfaces under tangential forces. It was suggested then that the infinite tractions associated with no slip might be relieved, in part, by distortion of the surface asperities rather than by microslip as assumed in the analysis. In this way a rough surface, with its more flexible asperities, would accommodate higher tractions before the onset of appreciable slip.

To avoid the difficulty of the indeterminate nature of the constant μ, the results of the creep experiments have been plotted in the form $[\delta/(2\pi a)](D/R)$ against D/R in Fig. 5. At small values of D/R the experimental results compare very favorably with the analytical solution of Equation [30]. Taking the effective value of μ to be no greater than 0.2, Equation [30] is seen to be a close fit over the range $D/(\mu R) < 1$. For large values of $D/(\mu R)$, the creep approaches a constant value whose magnitude is dependent upon the nature of the surface. When slip has progressed over a large proportion of the contact area, the magnitude

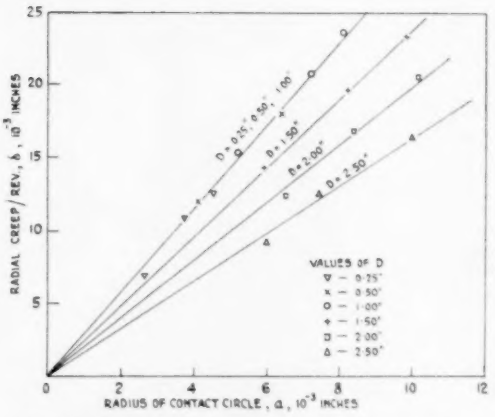

Fig. 4 Measurements of transverse creep due to spin

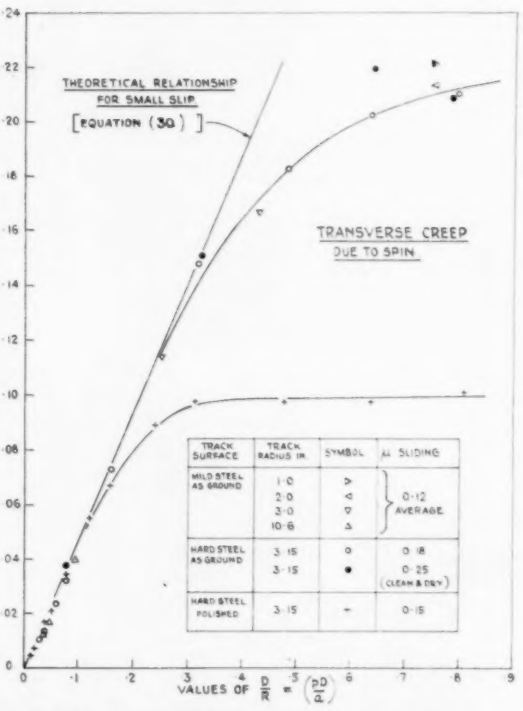

Fig. 5 Correlated results of measurements of transverse creep due to spin, compared with linear theoretical relationship

of the surface tractions, and hence the resulting creep, are no longer dependent upon the amount of spin.

An attempt was made to obtain the twisting moment function of Equation [37] experimentally by measurement of the torque-resisting rotation of the bearing. The over-all resistance was obtained by measuring the retardation of the bearing when rotating freely and slowly. In addition to the resistance due to spin, the over-all torque includes the resistance to straight free rolling—the usual rolling friction. Assuming the elastic-hysteresis theory presented by Tabor (9) to be correct, the rolling-friction force is given by

$$F = \alpha\Phi \quad \text{[38]}$$

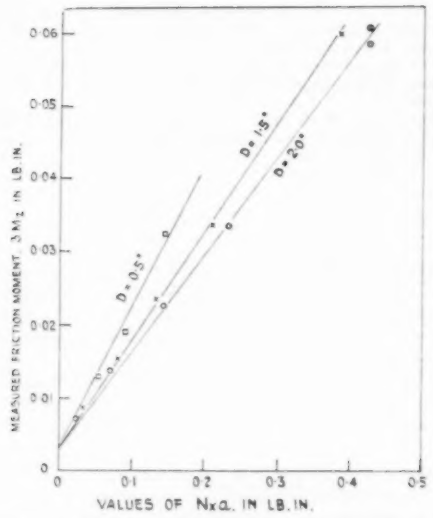

Fig. 6 Measured resisting moment during rolling with spin. This moment is made up of a component due to spin and a component due to elastic hysteresis.

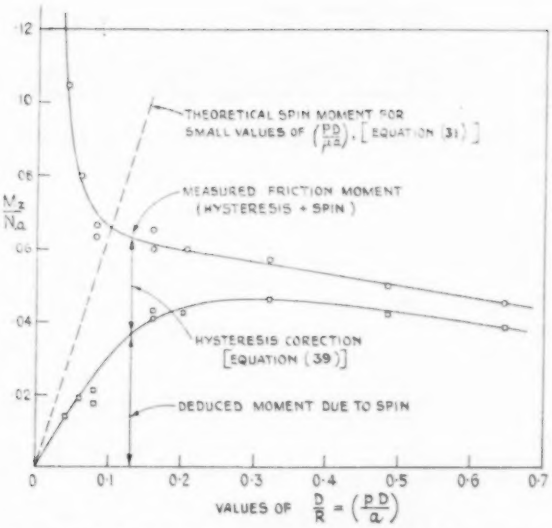
THEORETICAL SPIN MOMENT FOR SMALL VALUES OF (PD/μ²a), [EQUATION (31)]
MEASURED FRICTION MOMENT (HYSTERESIS + SPIN)
HYSTERESIS CORECTION [EQUATION (39)]
DEDUCED MOMENT DUE TO SPIN
M₂/Na
VALUES OF D/R = (PD/a)

Fig. 7 Analysis of resisting moment measurements into spin and hysteresis components

where $$\Phi = 0.00105 \left(\frac{N^2}{D}\right)^{2/3} \text{ lb in.}$$

is the elastic work done per unit distance rolled for a steel ball rolling on a plane, and α is the fraction of this work dissipated by hysteresis.[6] Hence the friction moment per ball due to hysteresis is

$$(M_s)_h = FR = 0.00105 \left(\frac{N^2}{D}\right)^{2/3} \alpha R$$

Using Equation [1] this may be rewritten

$$(M_s)_h = 0.36\alpha \left(\frac{R}{D}\right) Na \quad \ldots\ldots\ldots\ldots [39]$$

Tabor quotes a figure of 2 per cent for the value of α for hard-steel rolling surfaces. Measurements by the author (unpublished) of the hysteresis loss at the stationary contact of a hard-steel sphere and plane gave an approximately constant value of 0.4 per cent for normal loading within the elastic range. We may write therefore

$$(M_s)_h = k \left(\frac{R}{D}\right) Na$$

where k is a constant of magnitude 0.0015 to 0.0072. To the hysteresis moment must be added the moment due to spin given by Equation [37] so that (taking μ as a constant) the total resisting moment is

$$\frac{M_s}{Na} = \left(\frac{M_s}{Na}\right)_h + \left(\frac{M_s}{Na}\right)_s = k \left(\frac{R}{D}\right) + f\left(\frac{D}{R}\right) \ldots [40]$$

It may be seen that both components are functions of the ratio (D/R) and, for a constant value of this ratio, are proportional to the product $N \times a$. Typical measurements of friction torque at varying loads are shown in Fig. 6. They are approximately proportional to Na. The small, fairly constant, intercept at $Na = 0$ represents the friction of the bearing spindle.

Reference to Equation [40] shows that the hysteresis component becomes large and predominates at small values of (D/R). The slopes of Fig. 6, M/Na, are plotted against (D/R) in Fig. 7. Multiplying through by (D/R) and extrapolating back to $D/R = 0$ yields a value of $k = 0.0037$ which is consistent with the values estimated from independent measurements. Thus the hysteresis component can be subtracted from the total to leave the spin component.

It is immediately apparent that in the region of small slip (D/R small) the hysteresis component is much larger than the spin component so that no reliable comparison with the linear relationship of Equation [31] is possible. For larger values of D/R the hysteresis component becomes small and the experiments should give a reasonable measure of the resisting moment due to spin. With increasing spin velocities, slip relieves the high stresses at the trailing edge of the contact area, causing the resisting moment to depart from the linear relationship of Equation [31], and to approach a limiting value. A tendency for the moment to decrease at large values of D/R was observed.

Acknowledgments

The author gratefully acknowledges the help given by Prof. J. N. Goodier in discussion of the problem in elasticity, and by Mr. J. Walden in carefully performing many of the experiments.

Bibliography

1 "The Effect of a Tangential Contact Force Upon the Rolling Motion of an Elastic Sphere on a Plane," by K. L. Johnson, see following paper in this issue of the JOURNAL OF APPLIED MECHANICS, pp. 339–346.

2 "Sliding Friction in Ball Bearings," by A. Palmgren, *Ball Bearing Journal*, No. 4, 1928, S.K.F. Co., Philadelphia, Pa.

3 "Sliding Friction of Ball Bearings of the Pivot Type," by H. Poritsky, C. W. Hewlett, Jr., and R. E. Coleman, Jr., JOURNAL OF APPLIED MECHANICS, TRANS. ASME, vol. 69, 1947, p. A-261.

4 "Compliance of Elastic Bodies in Contact," by R. D. Mindlin, JOURNAL OF APPLIED MECHANICS, TRANS. ASME, vol. 71, 1949, pp. 259–268.

[6] Dr. Tabor has drawn the author's attention to a mistaken assumption in his original paper (10) which caused the expression for Φ quoted in (9) to be too large by a factor of 2. His values of α deduced from rolling experiments are therefore too small by the same factor. A more exact treatment by Greenwood and Tabor is in the course of publication. Corrected values of Φ and α are given above.

5 "The Torsion of Elastic Spheres in Contact," by J. L. Lubkin, JOURNAL OF APPLIED MECHANICS, TRANS. ASME, vol. 73, 1951, pp. 183–187.

6 "Investigations With Regard to Rolling Under Tangential Pressure," by A. Palmgren, *Ball Bearing Journal*, No. 3, 1928, S.K.F. Co.

7 "Ball and Roller Bearing Engineering," by A. Palmgren, S.K.F. Co.

8 "Surface Interaction Between Elastically Loaded Bodies Under Tangential Forces," by K. L. Johnson, *Proceedings of the Royal Society*, series A, vol. 230, 1955, pp. 531–548.

9 "The Mechanism of Rolling Friction—II. The Elastic Range," by D. Tabor, *Proceedings of the Royal Society*, series A, vol. 229, 1955, pp. 198–220.

10 "The Elastic Work in Rolling a Sphere on Another Surface," by D. Tabor, *British Journal of Applied Physics*, vol. 6, 1955, pp. 79–81.

The Effect of a Tangential Contact Force Upon the Rolling Motion of an Elastic Sphere on a Plane

By K. L. JOHNSON,[1] CAMBRIDGE, ENGLAND

The motion and deformation of an elastic sphere rolling on an elastic plane under a normal contact pressure N have been studied for the case where a tangential force T is also sustained at the point of contact. Provided that $T < \mu N$ (μ = coefficient of friction), the sphere rolls without sliding but exhibits a small velocity relative to the plane, termed "creep." Following the work of Mindlin and Poritsky, it is shown that creep arises from slip over part of the area of contact, and further, that this slip takes place toward the trailing edge of the contact area. On the assumption of a locked region in which no slip occurs, of circular shape, tangential to the circle of contact at its leading point, surface tractions are found which satisfy the condition of no slip within the locked region and are approximately consistent with the laws of friction in the slip region. The variation of creep velocity with tangential force is thereby determined. Experimental measurements of the creep of a steel ball rolling on a flat steel surface are in reasonable agreement with the theoretical results.

Introduction

This paper and its sequel[2] examine the motion of an elastic sphere which rolls without sliding on an elastic plane, taking into account the deformation of the two surfaces under the action of the contact force exerted between them.

A pressure between the surfaces, acting normal to the plane, has the effect of enlarging the "point of contact" into a small circular area. In addition, the surfaces may sustain a tangential component of force without sliding, provided that the limiting friction force is not exceeded. Thus as rolling proceeds, the line of action of the resultant force transmitted between the sphere and plane may be inclined to the normal at an angle not exceeding the angle of friction for the two surfaces.

To define the kinematic aspects of the problem, it has been found convenient to regard the motion relative to the point of contact, which remains stationary in space. The origin O of rectangular co-ordinate axes is taken to be at the center of the circle of contact. Axes Ox and Oy lie in the undistorted plane, with Ox in the direction of rolling; Oz is therefore normal to the plane, Fig. 1. In this view a steady rolling motion of the sphere on the plane appears as a stationary pattern of elastic distortion around the contact region through which the material of both bodies flows at a steady rate. This will be recognized to be the Eulerian co-ordinate system, familiar in the field of hydrodynamics, but which has been applied to problems in elasticity by Bishop and Goodier (1).[3]

Focusing attention on a particular point lying within the contact area, slip is said to be taking place at that point if the velocities with which the two surfaces pass through that point are unequal. If there is no point in the contact area at which the velocities of the two surfaces are identical, then complete slip or sliding[4] is taking place.

The particle velocities at any point are made up of two components; the first due to the rigid-body motions of the sphere or plane, and the second arising from the pattern of strain through which the material is flowing. The rigid-body motions corresponding to steady rolling are shown in Fig. 1. The plane has a linear velocity U (the rolling velocity) parallel to Ox. The sphere has an angular velocity ω about a diametral axis parallel to Oy, and in addition may have an angular velocity Ω relative to the plane about the normal axis Oz. This latter motion is referred to as "spin," and is usually associated with rolling along a curved path.

From the previous discussion there emerge three distinct categories into which the rolling problem may be classified:

Free rolling, in which the resultant force transmitted between the contact surfaces is perpendicular to the plane, and further

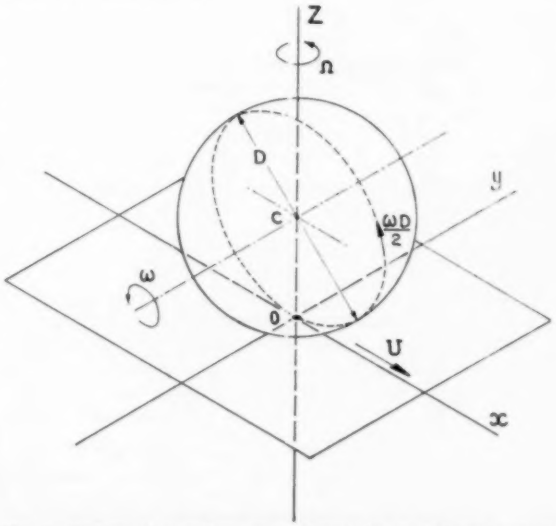

Fig. 1 Rolling of a sphere on a plane; the co-ordinate system

[1] Engineering Laboratory, Department of Engineering, University of Cambridge.

[2] "The Effect of Spin Upon the Rolling Motion of an Elastic Sphere on a Plane," by K. L. Johnson, see preceding paper in this issue of the JOURNAL OF APPLIED MECHANICS, pp. 332–338.

Contributed by the Applied Mechanics Division for presentation at the Annual Meeting, New York, N. Y., November 30–December 5, 1958, of THE AMERICAN SOCIETY OF MECHANICAL ENGINEERS.

Discussion of this paper should be addressed to the Secretary, ASME, 29 West 39th Street, New York, N. Y., and will be accepted until January 10, 1959, for publication at a later date. Discussion received after the closing date will be returned.

NOTE: Statements and opinions advanced in papers are to be understood as individual expressions of their authors and not those of the Society. Manuscript received by ASME Applied Mechanics Division, September 17, 1956. Paper No. 58—A-7.

[3] Numbers in parentheses refer to the Bibliography at the end of the paper.

[4] The term "sliding" is used to denote the condition of complete bodily slip, while "slip" refers to the condition at a specified point, or points, in the contact area.

there is no angular velocity of spin between the sphere and the plane.

Rolling under tangential forces, which takes place when the transmitted force is not normal to the plane, but contains a tangential component. The tangential component may be resolved into the direction of rolling (longitudinal) and at right angles to that direction (transverse).

Rolling with spin, which occurs when the sphere and the plane move with an angular velocity relative to each other, about an axis normal to the plane.

The small resistance to motion in free rolling has been attributed by some, notably Osborne Reynolds (2), Heathcote (3), and Eldredge (4), to slip over the area of contact arising from the geometry of the indentation of the surface on which the ball rolls. In developing this theory, tangential displacements of the contact surfaces produced by frictional tractions are ignored, even though their magnitude is of the same order as the displacements due to normal pressure which define the shape of the indentation.

An alternative explanation of the energy dissipated in free rolling lies in the influence of the (so-called) elastic hysteresis of the material of the two surfaces. Palmgren (5) favors this view and, more recently, Tabor (6) has shown that careful rolling-friction measurements are consistent with the elastic hysteresis hypothesis.

This paper is not concerned with the resistance in free rolling except for the fact it is unavoidably present in experiments which are described.

It has long been appreciated that the effect of a tangential component of force between two bodies rolling together gives rise to a slow velocity of one surface relative to the other in a direction opposed to the tangential force acting upon it. The phenomenon, usually referred to as creep, is well understood in relation to the motion of a belt over a pulley, clearly described by Swift (7). A significant feature, common to all examples of creep during rolling, is the fact that the area of contact is divided into two distinct regions; one in which the surfaces move together without relative velocity and the other over which slip occurs. The creep velocity arises from the difference in state of strain between the two surfaces over that part of the area of contact where they remain locked together.

Identical solutions have been found by Carter (8) and Poritsky (9) for the two-dimensional problem of two cylinders rolling together with a normal force N' and a tangential force T' per unit length acting between them. Owing to the normal pressure the cylinders are in contact over a strip of width $2b$ given by the Hertz theory. If μ is the coefficient of friction between the surfaces, Poritsky shows that the cylinders remain locked together with no slip over a strip of width

$$2d = 2b\,(1 - T'/\mu N')^{1/2} \qquad [1]$$

from which it follows that when $T' = 0$ no slip occurs, and when $T' = \mu N'$ slip has penetrated over the entire contact surface. In the discussion Cain (10) demonstrates that the locked region must have one boundary coincident with the leading edge of the area of contact, and that slip occurs after contacting points have rolled through the locked region, if the direction of slip is to be consistent with the laws of friction and to oppose the tangential force acting between the surfaces.

An approximate numerical solution for the rolling of a ball on a curved surface under tangential force has been obtained by Palmgren (11) which involves approximating the elliptical area of contact to a rectangle. For the case evaluated, the analysis compares favorably with experimental results, but it is an unfortunate feature of his experiments that spin is present in addition to tangential forces.

Statement of the Problem

The ball is pressed onto the plane by a normal force N resulting in a circular area of contact of radius a over which, by the Hertz theory, the pressure is distributed according to

$$Z = \frac{3N}{2\pi a^2}\left(1 - \frac{r^2}{a^2}\right)^{1/2} \qquad [2]$$

where

$$a^3 = \frac{3(1-\nu)ND}{8G} \qquad [3]$$

for a ball of diameter D rolling on a flat surface of similar elasticity, where G = modulus of rigidity and ν = Poisson's ratio.

The area of contact is shown in Fig. 2. The path of rolling is parallel to the x-axis so that material is flowing through the area of contact in the positive direction with a mean rolling velocity U. A tangential force T, having components T_x and T_y, is transmitted across the surface ($T < \mu N$). As a result of this force the sphere has component velocities of creep relative to the plane denoted by ΔU and ΔV. It is required to find the distribution of tangential tractions X and Y over the surface of contact resulting from these tangential forces, and the corresponding values of the creep velocities ΔU and ΔV.

As in the Hertz theory, it is proposed to neglect the slight warping of the contact surface, so that it may be taken to be a plane area having a circular boundary of radius given by Equation [3]. Further, if the sphere and plane are assumed to have the same elastic properties, the problem is equivalent to that of two identical spheres rolling together with their circular area of contact lying centrally in the x-y plane.

The theoretical problem for which a solution is sought concerns, therefore, a system of two bodies rolling together which are geometrically and elastically symmetrical with respect to the three co-ordinate axes. Several important conditions follow from this symmetry.[5] A further simplification is secured by considering separately the cases where T_x and T_y act alone.

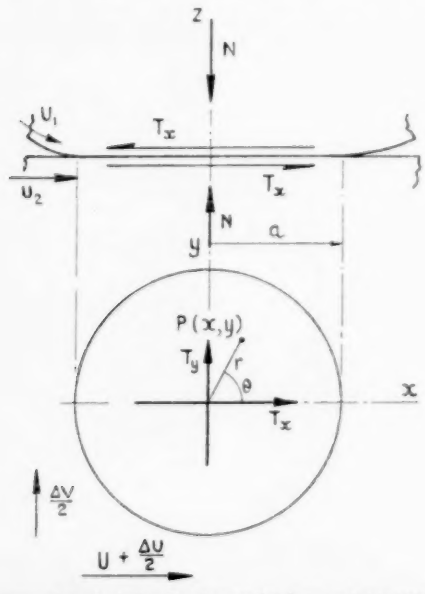

Fig. 2 Area of contact showing tangential-force components T_x and T_y. Creep velocities are denoted by ΔU and ΔV.

[5] The effect of the warping of the contact surface and unequal elastic constants upon the results so obtained is discussed subsequently.

Conditions Arising From Symmetry

With T_x acting alone, reference to Fig. 2 shows that if the lower sphere is rotated through 180 deg about Oy it becomes identical with the upper sphere, provided the direction of U is reversed. If (x_1, y_1) and (x_2, y_2) are two points in contact, after rotation about Oy, $x_2 = -x_1$ and $y_2 = y_1$. Equal and opposite tractions $X_2 = -X_1$ and $Y_2 = -Y_1$ are transmitted between the two surfaces at this point. The tractions themselves may be expressed

$$X = f(x, y, \text{sgn } U) \text{ and } Y = f(x, y, \text{sgn } U) \quad [4]$$

Remembering that rotation about Oy causes a change in sign of X but not in Y, the symmetry of the two bodies about Oy gives

$$X(-x, y, -U) = X(x, y, U) \quad [5]$$

and

$$Y(-x, y, -U) = -Y(x, y, U) \quad [6]$$

The over-all magnitude of the tractions X and Y is governed by the conditions of equilibrium

$$T_x = \int\int X\, dx\, dy, \quad T_y = \int\int Y\, dx\, dy \quad [7]$$

These conditions apply over the whole area of contact whether slip occurs or not.

Conditions which must be satisfied by the tangential surface displacements if no slip is to occur also follow from symmetry. The components of surface velocity at the point $P(x, y)$, denoted by q_x and q_y, may be expressed

$$q_x = f(x, y, U) \text{ and } q_y = f(x, y, U)$$

If (x_1, y_1) and (x_2, y_2) are two points instantaneously in contact, the components of relative velocity of slip between them are denoted by

$$s_x = q_{x1} - q_{x2} \quad \text{and} \quad s_y = q_{y1} - q_{y2}$$

With T_x acting alone, symmetry about Oy gives

$$q_{x1}(-x, y, -U) = -q_{x2}(x, y, U)$$

and

$$q_{y1}(-x, y, -U) = q_{y2}(x, y, U)$$

whereupon

$$s_x = q_x(x, y, U) + q_x(-x, y, -U) \quad [8]$$

and

$$s_y = q_y(x, y, U) - q_y(-x, y, -U) \quad [9]$$

It is now necessary to express the velocities q_x and q_y in terms of the rigid-body motions, and the local velocity components arising from the pattern of strain through which the material is flowing. In the Eulerian co-ordinate system the particle velocities are given by (1)

$$q_x = U + \left(U\frac{\partial}{\partial x} + V\frac{\partial}{\partial y} + \frac{\partial}{\partial t}\right)u$$

$$q_y = V + \left(U\frac{\partial}{\partial x} + V\frac{\partial}{\partial y} + \frac{\partial}{\partial t}\right)v$$

where U and V are the rigid-body velocities, and where u and v are the tangential elastic displacement at P.

In view of the symmetry, the creep velocities ΔU and ΔV may be divided equally between the two bodies, so that

$$U_1 = U + \frac{\Delta U}{2}, \qquad U_2 = U - \frac{\Delta U}{2}$$

$$V_1 = \frac{\Delta V}{2}, \qquad V_2 = -\frac{\Delta V}{2}$$

Now ΔU and ΔV are small compared with U, furthermore, for steady rolling u and v do not vary with time, so that the expressions for q_x and q_y reduce to

$$q_x = U + \frac{\Delta U}{2} + U\frac{\partial u}{\partial x}(x, y, \text{sgn } U) \quad [10]$$

$$q_y = \frac{\Delta V}{2} + U\frac{\partial v}{\partial x}(x, y, \text{sgn } U) \quad [11]$$

Expressions [8] and [9] for the relative velocity components become

$$s_x = \Delta U + U\frac{\partial u}{\partial x}(x, y, U) - U\frac{\partial u}{\partial x}(-x, y, -U) \quad [12]$$

and

$$s_y = \Delta V + U\frac{\partial v}{\partial x}(x, y, U) + U\frac{\partial v}{\partial x}(-x, y, -U) \quad [13]$$

Over any region in which there is no slip taking place the relative velocities s_x and s_y must of necessity be zero whence

$$\frac{\partial u}{\partial x}(-x, y, -U) - \frac{\partial u}{\partial x}(x, y, U) = \frac{\Delta U}{U} \equiv \xi_x = \text{const} \quad [14]$$

and

$$-\frac{\partial v}{\partial x}(-x, y, -U) - \frac{\partial v}{\partial x}(x, y, U) = \frac{\Delta V}{U} \equiv \xi_y = \text{const} \quad [15]$$

Equations [14] and [15], therefore, provide conditions which must be satisfied by the strain components $\partial u/\partial x$ and $\partial v/\partial x$ over that part of the surface of contact in which no slip takes place, and at the same time enable the magnitude of the creep-velocity ratios ξ_x and ξ_y to be calculated.

It is to be expected, however, that over part, at least, of the contact area slip will in fact take place. In this region Equations [14] and [15] will not be satisfied but alternative conditions may be obtained by an appeal to the simple laws of friction. It is assumed that the resultant tangential traction Q can nowhere exceed the normal traction Z multiplied by a constant coefficient of friction, and that in the region where slip has occurred Q is taken to have its limiting value μZ; i.e., within the locked region

$$|Q| \equiv (X^2 + Y^2)^{1/2} < \frac{3\mu N}{2\pi a^2}\left(1 - \frac{r^2}{a^2}\right)^{1/2} \quad [16]$$

while on the boundary of the locked region and within the slip region

$$|Q| = \frac{3\mu N}{2\pi a^2}\left(1 - \frac{r^2}{a^2}\right)^{1/2} \quad [17]$$

The direction of Q at any point in the slip region is determined in fact by the direction of the relative velocity between the surfaces at that point, which it must oppose. Since this direction is not known in advance, the expedient will be used of choosing the direction of Q a priori to coincide with the direction of the tangential force; i.e.,

$$\left.\begin{array}{ll} \text{when } T_x \text{ acts alone} & Y = 0 \\ \text{and when } T_y \text{ acts alone} & X = 0 \end{array}\right\} \quad [18]$$

The direction of relative sliding at any point associated with this assumed traction may be calculated subsequently by the use

of Equations [12] and [13] in order to confirm that the chosen direction of Q does not contradict the physical law of friction that it should oppose the direction of relative slip.

A further difficulty is that the shape of the boundary which divides the locked region from the slip region is not known in advance. In consequence, it has been found necessary to follow a "trial-and-error" approach. A shape for the locked region is assumed at the outset which, together with specified tractions over the area of contact, enables the tangential surface displacements to be found. For the assumed solution to be correct, the displacements must satisfy the no-slip conditions [14] and [15] within the locked region and the laws of friction in the slip region.

To complete the boundary conditions it is necessary to specify the normal traction (or displacement) in the contact area. Physically, it is required that the bodies should remain in contact and in equilibrium across the contact surface, for which w and Z' must be continuous across that surface. Z' denotes the normal traction resulting from the tangential force only, and is given by

$$Z' = -\frac{2G}{1-2\nu}\left[(1-\nu)\left(\frac{\partial w}{\partial z}\right)_{z=0} + \nu\left(\frac{\partial u}{\partial x}+\frac{\partial v}{\partial y}\right)_{z=0}\right] \quad [19]$$

In obtaining a solution to the problem of static contact between spheres Mindlin (13) makes the assumption that $Z' = 0$, while showing that this is only exactly true for no slip (whence $\partial u/\partial x = \partial v/\partial y = 0$) and for bodies of equal elastic constants (where continuity of w and $\partial w/\partial z$ across the contact surface gives $\partial w/\partial z = 0$). The assumption that $Z' = 0$ will be maintained here, whether slip occurs or not.

In consequence of the symmetry one sphere only need be considered which, following Hertz, is taken to be a semi-infinite solid. The problem in elasticity therefore reduces to the "problem of the plane" in which the surface tractions are given over the whole boundary. To summarize the boundary conditions:

1 In the locked region, X and Y to be specified, consistent with Equations [5], [6], and [16]; $Z' = 0$.

2 In the slip region, X and Y given by Equations [17] and [18]; $Z' = 0$.

3 Outside the area of contact ($r > a$); $X = Y = Z' = 0$.

The solution to the boundary-value problem in elasticity defined in the foregoing is obtained by the methods employed by Cattaneo (12) and Mindlin (13) in studying the effects of a tangential force acting between two spheres in static (as opposed to rolling) contact. Reference should also be made to Love (14) (page 242).

Static Contact

Mindlin shows first that the tractions

$$X = \frac{T_x}{2\pi a}\frac{1}{(a^2-r^2)^{1/2}}, \quad Y = 0 \quad [20]$$

produce displacements[6] over the circle of contact

$$u = \text{constant} = \frac{(2-\nu)T_x}{4Ga}, \quad v = 0 \quad [21]$$

which correspond to no slip over the whole of the contact area, under the action of a static force T_x.

Examining this solution for the case of rolling contact we see that the tractions of Equations [20] satisfy the symmetry conditions [5] and [6], and since $\partial u/\partial x = \partial v/\partial x = 0$, the displacements satisfy the no-slip conditions [14] and [15] with the result $\xi_x = \xi_y = 0$; i.e., no creep occurs. It would appear therefore that the tractions [20] and the displacements [21] also provide a solution to the rolling problem, for materials of perfect elasticity and with all slip prevented. It is interesting to note that the exclusion of a region of slip leads to zero creep velocities. This result might be expected from energy considerations, since slip provides the only mechanism in an elastic solid to account for the external work done by the tangential force when creep occurs.

It is obvious that only an academic solution has been found, since the infinite traction at the boundary of the contact area ($r = a$) insures that some slip will in fact take place. If slip occurs in a direction parallel to the x-axis over the whole contact area, then the tractions are taken to be

$$X = \frac{3\mu N}{2\pi a^3}(a^2-r^2)^{1/2}, \quad Y = 0 \quad [22]$$

which are shown to give rise to surface displacements

$$u = \frac{3\mu N}{64Ga^3}[2(2-\nu)(2a^2-x^2-y^2)+\nu(x^2-y^2)], \qquad v = \frac{3\mu N}{64Ga^3}2\nu xy \quad [23]$$

Cattaneo's device of adding tractions

$$X' = -\left(\frac{a'}{a}\right)^3\frac{3\mu N}{2\pi a'^3}(a'^2-r^2)^{1/2}, \quad Y' = 0 \quad [24]$$

over the circle $0 < r < a'$ results in total displacements

$$u + u' = \frac{3\mu N(2-\nu)}{16Ga}\left(1-\frac{a'^2}{a^2}\right) = \text{const}, \qquad v + v' = 0, \quad 0 < r < a' \quad [25]$$

Thus the combination of tractions [22] and [24] results in no slip over the circle $0 < r < a'$. This result defines the locked region as a circle concentric with the circle of contact and the slip region as an annulus whose width increases with tangential force. Experimental evidence of an annular region of slip in static contact has been obtained by Mindlin, Mason, et al. (15), and Johnson (16).

Rolling Contact

(a) *Longitudinal Force.* At first sight it would appear that the combined tractions [22] and [24], together with the corresponding displacements, provide a solution to the case of rolling contact. Both tractions are even in x, satisfying condition [5], and nowhere exceed μZ, satisfying [16].

In the locked region $\partial u/\partial x = \partial v/\partial x = 0$ which satisfy conditions [14] and [15] with zero creep. It will be shown, however, that the remaining condition is not satisfied; the direction of relative motion does not oppose the frictional traction throughout the annulus of slip.

The displacements outside the contact area ($r > a$) due to the traction of Equation [22] acting alone have been evaluated previously (17) with the result[7]

$$\frac{\partial u}{\partial x} \doteq -\frac{3\mu N(2-\nu)}{16Ga^2}\frac{x}{a}\frac{2}{\pi}\left[\sin^{-1}\frac{a}{r} - \frac{a}{r}\left(1-\frac{a^2}{r^2}\right)^{1/2}\right], \qquad \frac{\partial v}{\partial x} \doteq 0 \quad [26]$$

[6] In what follows, u and v, without subscript, denote displacements in the plane $z = 0$.

[7] The approximation involves neglecting terms whose order of magnitude is $\nu/2(2-\nu)$, i.e., 0.09, compared with unity.

Within the contact area ($r < a$), from Equations [23][8]

$$\frac{\partial u}{\partial x} = -\frac{3\mu N}{32Ga^3}(4 - 3\nu)x, \quad \frac{\partial v}{\partial x} = -\frac{3\mu N}{32Ga^3}\nu y \ldots [27]$$

Replacing a by a' in Equations [26] and [27] and multiplying by the factor $-(a'/a)^3$ gives the values of $\partial u'/x$ and $\partial v'/\partial x$, resulting from the traction X'. These expressions, together with the resultant value of $\partial u/\partial x$ due to $X + X'$, are sketched, for $y = 0$, in Fig. 3(*a*). It will be seen that in the annulus of slip $\partial u/\partial x$ is $+ve$ for $x < 0$, and $-ve$ for $x > 0$. Over the locked region $\partial u/\partial x = \partial v/\partial x = 0$, from which it follows (see Equations [14] and [15]) that the creep velocities ΔU and ΔV are zero.

The relative velocity components between the two surfaces at any point are given by Equations [12] and [13]. Noting from Equation [26] that $\partial u/\partial x$ is an odd function of x, and that $\partial v/\partial x = 0$, it follows that

$$s_x = 2U\frac{\partial u}{\partial x}(x, y, U), \quad s_y = 0 \ldots [28]$$

The traction X is positive over the whole of the annulus of slip, while the relative velocity of slip is also positive over the region $x < 0$, a result which entirely contradicts the physical law of friction.

In order to obtain a more correct solution to the problem of rolling contact it is necessary to redefine the locked region. Following the two-dimensional solution of Poritsky, the example of creeping belts and also the foregoing results, we are led to expect slip to take place after the contacting points have passed through the locked region. As a tentative solution, let it be assumed that the locked region remains a circle of radius a' but is moved in a position so as to be tangential to the contact circle at the leading point $(-a, 0)$, Fig. 3(*b*). Its center would then be at the point $(-c, 0)$ where

$$c = a - a' \ldots [29]$$

The traction X and the accompanying displacements of Equations [23] remain as before, but the added traction becomes

$$X' = -\left(\frac{a'}{a}\right)^3 \frac{3\mu N}{2\pi a'^3}(a'^2 - r'^2)^{1/2} \ldots [30]$$

where

$$r'^2 = (x + c)^2 + y^2 \ldots [31]$$

This traction results in

$$\frac{\partial u'}{\partial x} = \frac{3\mu N}{32Ga^3}(4 - 3\nu)(x + c), \quad \frac{\partial v'}{\partial x} = \frac{3\mu N}{32Ga^3}\nu y \ldots [32]$$

which, when added to Equations [27], give over-all values

$$\frac{\partial u}{\partial x} = \frac{3\mu N(4 - 3\nu)c}{32Ga^3}, \quad \frac{\partial v}{\partial x} = 0 \ldots [33]$$

Noting that for negative values of U the locked region should be tangential to the circle of contact at $(a, 0)$, so that c becomes negative, Equations [33] satisfy the no-slip conditions [14] and [15] in the assumed locked region, with the result

$$\xi_x = \frac{\Delta U}{U} = -\frac{3\mu N(4 - 3\nu)c}{16Ga^3}, \quad \xi_y = 0 \ldots [34]$$

The creep ratio in the x-direction is in this case no longer zero. The value of a' can be obtained from the equilibrium condition [7], which gives

$$\frac{T_x}{\mu N} = 1 - \left(\frac{a'}{a}\right)^3 \ldots [35]$$

[8] Making the same approximation as in Equation [26] would give

$$\frac{\partial u}{\partial x} \doteq -\frac{3\mu N(2 - \nu)x}{16Ga^3} \quad \text{and} \quad \frac{\partial v}{\partial x} \doteq 0$$

which are consistent with Equation [26] at $r = a$.

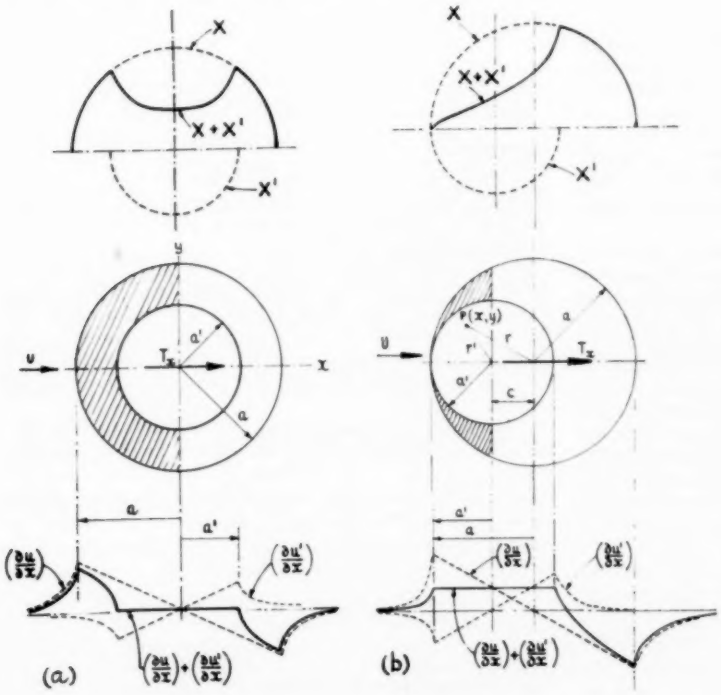

Fig. 3 (*a*) Mindlin's solution for static contact under tangential force. Slip takes place in the annulus $a' < r < a$. Relative slip velocity is proportional to $(\partial u/\partial x + \partial u'/\partial x)$ which is positive in shaded area. (*b*) Modified solution for rolling contact. Locked region is taken to be circle radius a'. $(\partial u/\partial x + \partial u'/\partial x)$ is constant, corresponding to no slip, over this circle. Slip velocity remains positive in shaded area.

whence

$$\frac{c}{a} = 1 - \frac{a'}{a} = 1 - \left(1 - \frac{T_x}{\mu N}\right)^{1/3} \quad \ldots\ldots [36]$$

Substituting in [34] gives an expression for the creep ratio in terms of the tangential force; viz.

$$\xi_x = -\frac{3\mu N(4 - 3\nu)}{16Ga^2}\left[1 - \left(1 - \frac{T_x}{\mu N}\right)^{1/3}\right] \quad \ldots\ldots [37]$$

It will be seen that the combined tractions X over the slip region and $X + X'$ over the locked region satisfy the required conditions of Equations [5] and [16].

It remains to examine the direction of relative slip outside the locked region. In this case, because of the traction X'

$$\left.\begin{aligned} \frac{\partial u'}{\partial x} &= \frac{3\mu N(2 - \nu)}{16Ga^2}\,\frac{x + c}{a}\,\frac{2}{\pi} \\ &\quad \left[\sin^{-1}\frac{a'}{r'} - \frac{a'}{r'}\left(1 - \frac{a'^2}{r'^2}\right)^{1/3}\right] \\ \frac{\partial v'}{\partial x} &= 0 \end{aligned}\right\} \quad \ldots [38]$$

in the region $r' > a'$. Thus the net value of $\partial u/\partial x$ in the region of slip is given by adding Equations [27] and [38], and is drawn for $y = 0$ in Fig. 3(*b*). The relative velocity between the two surfaces in this region is found from Equations [12] and [13], which give

$$\left.\begin{aligned} s_x &= -\frac{3\mu N(2 - \nu)}{8Ga^2}\,\frac{x + c}{a} \\ &\quad \left[1 - \frac{2}{\pi}\sin^{-1}\frac{a'}{r'} + \frac{2}{\pi}\,\frac{a'}{r'}\left(1 - \frac{a'^2}{r'^2}\right)^{1/3}\right] \\ s_y &= 0 \end{aligned}\right\} \quad \ldots [39]$$

The value of s_x given by this expression is found to be positive and hence in the same direction as the traction in the shaded area of Fig. 3(*b*). The existence of an area in which the law of friction is contravened implies that the assumed circular shape of the locked region cannot be correct. The shaded "area of error" is, however, in no event large compared with the total area of applied traction (< 8 per cent) and becomes small both when $T_x \to 0$ and when $T_x \to \mu N$, so that the foregoing solution should represent a reasonable approximation.

(*b*) *Transverse Force.* The transverse creep ξ_y associated with a transverse tangential force T_y may be obtained without difficulty by the same method. Mindlin's solution for static contact gives a concentric circular locked region, with tangential tractions which are everywhere positive and parallel to the tangential force T_y. Applying this solution to the rolling problem and investigating the direction of slip in the annulus $a' < r < a$, again results in slip velocities which are approximately parallel to the tangential traction (i.e., parallel to oy) and positive in the shaded region of Fig. 3(*a*), where $z < 0$. We were led, therefore, to expect that in the case of a transverse force also, slip will take place at the trailing edge and not at the leading edge of the circle of contact. As before, the locked region is taken to be a circle tangential to the leading edge at the point $(-a, 0)$.

With T_y acting alone, the system is symmetrical about oz, which leads to conditions similar to [5] and [6] which must be satisfied by the surface tractions, and to conditions similar to [14] and [15] which must be satisfied by the surface displacements in the region of no slip.

It may be shown that the tractions

$$\left.\begin{aligned} X + X' &= 0 \\ Y + Y' &= \frac{3\mu N}{2\pi a^3}(a^2 - r^2)^{1/2} \\ &\quad - \left(\frac{a'}{a}\right)^3 \frac{3\mu N}{2\pi a^3}(a'^2 - r'^2)^{1/2} \end{aligned}\right\} \quad \ldots [40]$$

satisfy the necessary conditions and result in strains

$$\frac{\partial u}{\partial x} = 0, \quad \frac{\partial v}{\partial x} = \frac{3\mu N(4 - \nu)c}{32Ga^2}$$

over the circle of no slip $r' < a'$. These values correspond to zero longitudinal creep ($\xi_x = 0$) and a transverse creep given by

$$\xi_y = -\frac{3\mu N(4 - \nu)}{16Ga^2}\left[1 - \left(1 - \frac{T_y}{\mu N}\right)^{1/3}\right] \quad \ldots\ldots [41]$$

This result compares with Equation [37] for the longitudinal creep. The distribution of surface tractions is the same in each case and is everywhere parallel to the applied force.

It is still necessary to confirm that the direction of slip opposes the frictional traction. The relative velocity in the slip region has been calculated and, as before, turns out to be approximately parallel to the traction (in this case Y) and of negative sign everywhere except in the shaded portion of Fig. 3(*b*).

The theoretical results just derived have all been obtained for a system comprising identical spheres. The slight warping of the contact surface which occurs when a sphere rolls on a plane or when the two bodies have unequal elastic constants is ignored, but the experience of Tabor (6) suggests that its influence is small. Dissimilar elastic constants make the distribution of equal creep velocities to each surface in Equations [10] and [11] untenable. However, by distributing creep velocities ΔU_1 and $-\Delta U_2$, ΔV_1 and $-\Delta V_2$ to the sphere and plane, respectively, where $\Delta U_1 + \Delta U_2 = \Delta U$ and $\Delta V_1 + \Delta V_2 = \Delta V$, it may be shown that for bodies having elastic constants ν_1, G_1, and ν_2, G_2 the net creep is given by

$$\xi = \frac{1}{2}\left[\xi(\nu_1, G_1) + \xi(\nu_2, G_2)\right] \quad \ldots\ldots [42]$$

in which the results of Equations [37] and [41] apply

Experimental

To check the validity of the theoretical results, particularly in view of the approximations involved, simple experiments were designed to measure the creep due to both longitudinal and transverse tangential forces.

The apparatus is shown in Fig. 4. Two hard steel balls of 1-in. diam were mounted on a spindle by soldered joints. When placed in contact with a plane, in fact, a hard steel parallel strip, the balls were free to roll with equal velocity in a direction perpendicular to the axis of the spindle. The balls were loaded by two hangers mounted on small ball races at each end of the spindle.

A longitudinal tangential component of force at the contact between each ball and the plane was obtained by tilting the plane through an angle β in the direction of rolling. The system was restrained from free rolling down the incline by strings, parallel to the plane, passing over pulleys mounted at the ends of the spindle. Reference to Fig. 4(*a*) shows that the contact force is now inclined at an angle α to the plane, given by

$$\frac{T_x}{N} = \tan\alpha = \frac{R}{R + \frac{1}{2}D}\tan\beta$$

where R is the radius of the pulley.

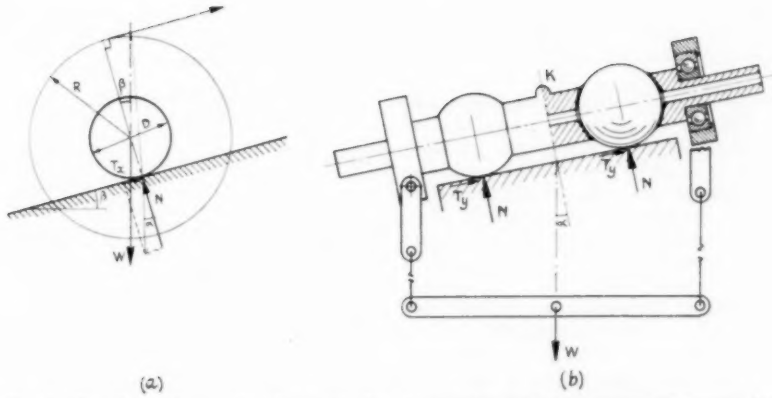

Fig. 4 Experimental apparatus for measuring creep under action of tangential forces. (*a*) Application of a longitudinal tangential force. (*b*) Application of a transverse tangential force.

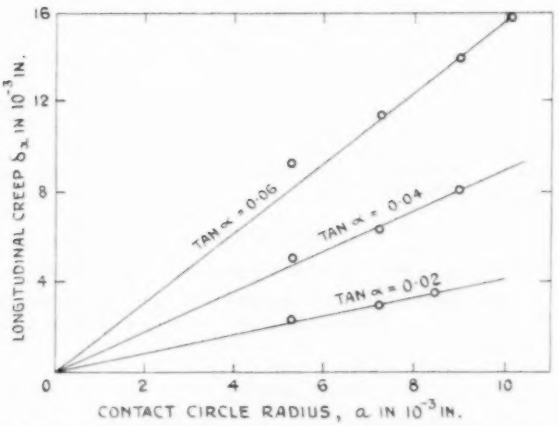

Fig. 5 Experimental variation of creep with increasing area of contact, obtained by increasing normal load

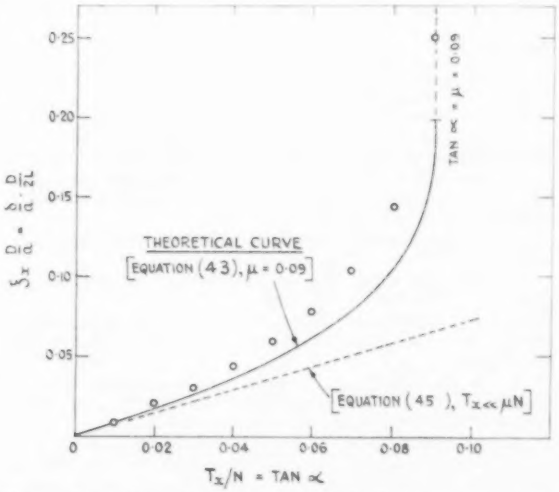

Fig. 6 Comparison of experimental longitudinal creep measurements with theoretical analysis

The system was rolled slowly up the plane for a distance $L = 10$ in. by pulling on the two strings, and then allowed to roll slowly back by gradually releasing the strings. The spindle returned to its initial angular position relative to the plane with the spherical knob K resting in contact with a parallel slip placed on the plane. The longitudinal creep of the system down the plane (denoted by δ) resulting from a traversal up and down the plane was measured by micrometer or, in cases where greater sensitivity was required, by observing a line scratched on the spindle by a microscope mounted above.

Both the balls and the plane possessed a good surface finish. Before each experiment they were cleaned, washed in benzene and ether, and wiped dry.

By use of Equation [3], the Expression [37] for the longitudinal creep may be written

$$\frac{\delta}{2L} = -\xi_x = \frac{\mu(4-3\nu)}{2(1-\nu)}\,\frac{a}{D}\left[1-\left(1-\frac{\tan\alpha}{\mu}\right)^{1/3}\right] \quad [43]$$

Thus for a constant value of tan α, the creep should be proportional to a/D. The ball diameter D remained unchanged, but a was varied by increasing the load. The direct proportionality of δ with a is shown by the experimental results plotted in Fig. 5. Macroscopic sliding began on the downward run at tan α = 0.09, compared with values of $\mu = 0.12$–0.14 measured in steady rectilinear sliding. Fig. 6 is plotted from the slopes of the straight lines of Fig. 5 and compared with Equation [43], drawn for $\mu = 0.09$.

The application of a transverse tangential force was obtained by tilting the plane through an angle perpendicular to the direction of rolling as shown in Fig. 4(*b*). The plane was maintained horizontal in the direction of rolling so that the pulley strings could be dispensed with. The rolling motion was produced by hand so that the velocities of rolling, as in the previous experiment, were very small, certainly less than 10 fpm. The transverse creep displacements across the plane due to a double traversal were measured by micrometer. The procedure was the same as before and the results are shown in Fig. 7. In this case intermittent sliding began at tan $\alpha = 0.11$. Transforming Equation [41] gives

$$\frac{\delta}{2L} = -\xi_y = \frac{\mu(4-\nu)}{2(1-\nu)}\,\frac{a}{D}\left[1-\left(1-\frac{\tan\alpha}{\mu}\right)^{1/3}\right] \quad [44]$$

which is plotted for comparison, putting $\mu = 0.11$.

The experiment was repeated with the surface flooded with a normal lubricating oil. It will be seen from Fig. 7 that the coefficient of limiting friction has been reduced by the lubricant, but only from 0.11 to 0.09, although it is evident, from the low value

obtained dry, that grease films were still present. Thus the addition of a lubricating oil at rolling velocities too small to introduce any hydrodynamic action, has little effect upon the creep process.

Comparing the experimental results with the theoretical relationships of Equations [43] and [44], reasonably good agreement is found, particularly for small values of $T(T \ll \mu N)$ and again just before sliding begins $(T \to \mu N)$. The discrepancy is most marked in the intermediate range and is greatest at $T \doteq 0.75\mu N$ when the theoretical creep is about 25 per cent less than the measured value. The principal assumption underlying the theoretical treatment is that the locked region is circular and tangential to the circle of contact at the leading point $(-a, 0)$. It has been pointed out already that this assumption cannot be exact since it leads to slip velocities which are inconsistent with the direction of the assumed traction over the shaded area shown in Fig. 3(*b*). This area of error, although never large, reaches its maximum value when $a' \doteq 0.6\ a$; i.e., when $T \doteq 0.72\mu N$. It would seem reasonable to conclude that the departure of the true locked region from its assumed circular shape is the principal reason for the discrepancy between the experimental and theoretical results.

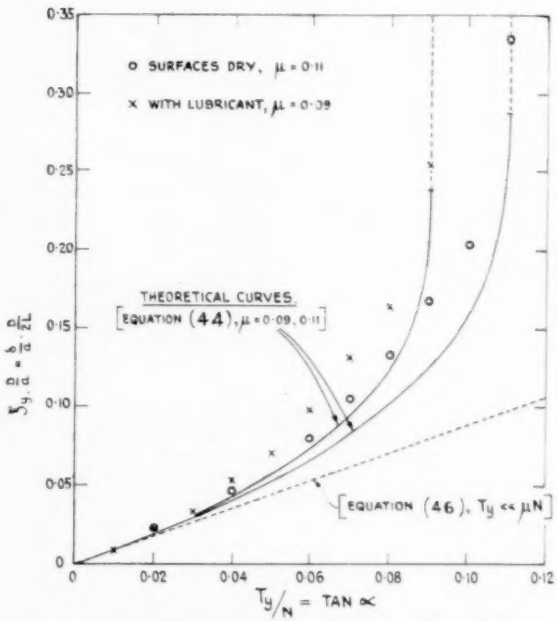

Fig. 7 Comparison of experimental transverse creep measurements with theoretical analysis

Bibliography

1 "On Eulerian Co-ordinates in Elastic Wave Propagation," by R. E. D. Bishop and J. N. Goodier, *Journal of the Mechanics and Physics of Solids*, vol. 2, 1954, pp. 103–109.

2 "On Rolling Friction," by Osborne Reynolds, *Philosophica Transactions of the Royal Society*, vol. 166, part 1, 1875, p. 155.

3 "The Ball Bearing: In the Making, Under Test and on Service," by H. L. Heathcote, *Proceedings of the Institute of Automobile Engineers*, vol. 15, 1921, p. 569.

4 "Rolling Friction," by K. R. Eldredge, PhD dissertation, Cambridge, 1952.

5 "Ball and Roller Bearing Engineering," by A. Palmgren, S.K.F. Co., Philadelphia, Pa., 1945.

6 "The Mechanism of Rolling Friction—II, The Elastic Range," by D. Tabor, *Proceedings of the Royal Society*, series A, vol. 229, 1955, pp. 198–220.

7 "Power Transmission by Belts: An Investigation of Fundamentals," by H. W. Swift, *Proceedings of The Institution of Mechanical Engineers*, 1928, vol. II, pp. 659–745.

8 "On the Action of a Locomotive Driving Wheel," by F. W. Carter, *Proceedings of the Royal Society*, series A, vol. 112, 1926, pp. 151–157.

9 "Stresses and Deflections of Cylindrical Bodies in Contact With Application to Contact of Gears and of Locomotive Wheels," by H. Poritsky, JOURNAL OF APPLIED MECHANICS, TRANS. ASME, vol. 72, 1950, pp. 191–201.

10 Discussion to reference (9) by B. S. Cain, JOURNAL OF APPLIED MECHANICS, TRANS. ASME, vol. 72, 1950, pp. 465–466.

11 "Investigations With Regard to Rolling Under Tangential Pressure," by A. Palmgren, *Ball Bearing Journal*, No. 3, 1928, S.K.F. Co.

12 "Sul Contatto di due Corpi Elastici," by C. Cattaneo, *Accademia de Lincei, Rendiconti*, series 6, vol. xxvii, 1938, pp. 342–348, 434–436, 474–478.

13 "Compliance of Elastic Bodies in Contact," by R. D. Mindlin, JOURNAL OF APPLIED MECHANICS, TRANS. ASME, vol. 71, 1949, pp. 259–268.

14 "Treatise on the Mathematical Theory of Elasticity," by A. E. H. Love, Cambridge University Press, fourth edition, 1927.

15 "Effects of Oscillating Forces on the Contact Surfaces of Elastic Spheres," by R. D. Mindlin, W. P. Mason, T. F. Osmer, and H. Deresiewicz, Proceedings of the First U. S. National Congress of Applied Mechanics, pp. 203–208.

16 "Surface Interaction Between Elastically Loaded Bodies Under Tangential Forces," by K. L. Johnson, *Proceedings of the Royal Society*, series A, vol. 230, 1955, pp. 531–548.

17 "The Effects of an Oscillating Tangential Force at the Interface Between Elastic Bodies in Contact," by K. L. Johnson, PhD thesis, University of Manchester, 1954, p. 58.

APPENDIX

Limiting Solution for Small Tangential Forces $(T \ll \mu N)$

If the tangential force is small compared with the limiting friction force, the expressions for the creep, Equations [37] and [41], reduce to

$$\xi_x = -\frac{(4 - 3\nu)}{16Ga^2} T_x \quad \ldots\ldots [45]$$

$$\xi_y = -\frac{(4 - \nu)}{16Ga^2} T_y \quad \ldots\ldots [46]$$

Under these circumstances the slip is confined to a thin "new moon" at the trailing edge of the circle of contact.

It is of interest to examine the limit to which the corresponding tractions tend when $T \ll \mu N$. With the aid of Equation [35] the tractions $X + X'$ of Equations [22] and [30] may be written in the form

$$X + X' = \frac{3T_x}{2\pi} \frac{(a^2 - r^2)^{1/2} - (a'^2 - r'^2)^{1/2}}{a^3 - a'^3} \quad \ldots\ldots [47]$$

Now the limit of this distribution of traction as a' is made to approach a (i.e., $T_x \to 0$) may be shown without difficulty to be the traction

$$X = \frac{T_x}{2\pi a^2} \frac{a + x}{(a^2 - r^2)^{1/2}} \quad \ldots\ldots [48]$$

Similarly, in the case of a transverse force the traction becomes

$$Y = \frac{T_y}{2\pi a^2} \frac{a + x}{(a^2 - r^2)^{1/2}} \quad \ldots\ldots [49]$$

Rather surprisingly, the magnitude of these limiting tractions rises to infinity on the boundary of the circle of contact except for the point $(-a, 0)$ where it is zero. Physically, this zero value corresponds to the imposed condition that there should be no slip at this point.

The Vibration of a String Having a Uniform Motion Along Its Length

By F. R. ARCHIBALD[1] and A. G. EMSLIE,[2] CAMBRIDGE, MASS.

In calculating the natural frequencies of a power chain or belt it is usual to use the theory of vibrating strings. However, the speed of the chain or belt may be a considerable fraction of the wave velocity as given by $(T/\rho)^{1/2}$. It might be expected hat this would have a marked effect on the natural frequencies. This is shown to be so and the formula for the natural frequencies of a moving string is obtained. The problem of the forced vibration of the string is also considered.

In calculating the natural frequencies of a strand of power chain or a belt, it is customary to use the usual formula for a vibrating string, viz.

$$f_n = \frac{n}{2l}\left(\frac{T}{\rho}\right)^{1/2} \quad [1]$$

$n = 1, 2, 3, \ldots$, T is the string tension, and ρ is the mass per unit length of the string.

The differential equation which must be satisfied by points on the string is

$$\frac{\partial^2 y}{\partial t^2} = \frac{T}{\rho}\frac{\partial^2 y}{\partial x^2} \quad [2]$$

It is well known that $(T/\rho)^{1/2}$ is the velocity with which a wave will travel along the string. In a power chain the values of T and ρ are such as to give values of the wave velocity not far different, in some cases, from the velocity of the chain itself. It is therefore not unnatural to think that this circumstance might have some influence on the natural frequencies of the strand. It turns out to have a most important influence if the chain speed is a significant fraction of the wave speed.

The similar, but more difficult, problem of the lateral vibration of a pipe carrying a flowing fluid has been solved by G. W. Housner.[3] In that problem the differential equation was obtained by the application of Hamilton's principle. This method will be used here. Later it will be shown how the differential equation can be obtained in a much simpler way, and in fact it is not at all difficult to obtain it by the usual Newtonian method. But by this latter method it would be easy to overlook at least one of the force components on an element of the string if the result from the more powerful methods were not available.

For small displacements (Fig. 1) the velocity of the string in the x-direction is v and in the y-direction is:

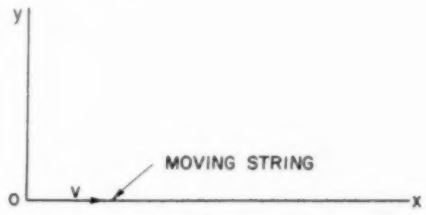

Fig. 1

$$\dot{y} + vy' = \frac{\partial y}{\partial t} + v\frac{\partial y}{\partial x} \quad [3]$$

According to Hamilton's principle the variation of

$$\int_{t_1}^{t_2}(T - V)dt$$

is zero where T and V are, respectively, the kinetic and potential energies of the system, i.e.

$$\delta\int_{t_1}^{t_2}(T - V) = 0 \quad [4]$$

It is easily seen that T is given as follows

$$T = \int_{x_1}^{x_2}\frac{1}{2}\rho[v^2 + (\dot{y} + vy')^2]dx \quad [5]$$

The potential energy V is obtained in the following way

$$dV = T(ds - dx)$$

Hence and by making the usual approximations

$$V \cong \int_{x_1}^{x_2}\frac{1}{2}T\left(\frac{\partial y}{\partial x}\right)^2 dx \quad [6]$$

Substituting the values of T and V from Equations [5] and [6] into Equation [4]

$$\delta\int_{t_1}^{t_2}\int_{x_1}^{x_2}\left\{\frac{1}{2}\rho[v^2 + (\dot{y} + vy')^2] - \frac{1}{2}T(y')^2\right\}dx\,dt = 0$$

Performing the variation gives

$$\int_{t_1}^{t_2}\int_{x_1}^{x_2}[\rho(\dot{y} + vy')(\delta\dot{y} + v\delta y') - Ty'\delta y']dx\,dt = 0 \quad [7]$$

The products here are expanded and making use of the relations

$$\delta\dot{y} = \frac{\partial}{\partial t}(\delta y) \quad \text{and} \quad \delta y' = \frac{\partial}{\partial x}(\delta y)$$

Equation [7] can be written

$$\int_{t_1}^{t_2}\int_{x_1}^{x_2}\left\{\rho\left[\dot{y}\frac{\partial}{\partial t}(\delta y) + v\dot{y}\frac{\partial}{\partial x}(\delta y) + vy'\frac{\partial}{\partial t}(\delta y) + v^2y'\frac{\partial}{\partial x}(\delta y)\right] - Ty'\frac{\partial}{\partial x}(\delta y)\right\}dx\,dt = 0$$

When each term is integrated by parts, the following differential equation is obtained

---

[1] Head of Applied Mechanics Group, Arthur D. Little, Inc., Cambridge, Mass. Mem. ASME.

[2] Head of Physics Group, Arthur D. Little, Inc.

[3] "Bending Vibrations of a Pipe Line Containing Flowing Fluid," by G. W. Housner, JOURNAL OF APPLIED MECHANICS, TRANS. ASME, vol. 74, 1952, pp. 205–208.

Presented at the West Coast Conference of the Applied Mechanics Division, Los Angeles, Calif., September 8–10, 1958, of THE AMERICAN SOCIETY OF MECHANICAL ENGINEERS.

Discussion of this paper should be addressed to the Secretary, ASME, 29 West 39th Street, New York, N. Y., and will be accepted until October 10, 1958, for publication at a later date. Discussion received after the closing date will be returned.

NOTE: Statements and opinions advanced in papers are to be understood as individual expressions of their authors and not those of the Society. Manuscript received by ASME Applied Mechanics Division, March 21, 1957. Paper No. 58—APM-7.

$$\frac{\partial^2 y}{\partial t^2} + 2v\frac{\partial^2 v}{\partial l \partial x} - \left(\frac{T - \rho v^2}{\rho}\right)\frac{\partial^2 y}{\partial x^2} = 0 \quad \ldots\ldots [8]$$

As may be verified, the solution of the differential equation is

$$y = C_1 \cos\omega\left[t + \left(\frac{v\rho + (\rho T)^{1/2}}{T - \rho v^2}\right)x\right] + C_2 \cos\omega\left[t + \left(\frac{v\rho - (\rho T)^{1/2}}{T - \rho v^2}\right)x\right] \quad \ldots\ldots [9]$$

or

$$y = C_1 \sin\omega\left[t + \left(\frac{v\rho + (\rho T)^{1/2}}{T - \rho v^2}\right)x\right] + C_2 \sin\omega\left[t + \left(\frac{v\rho - (\rho T)^{1/2}}{T - \rho v^2}\right)x\right] \quad \ldots\ldots [10]$$

Choosing Equation [9] and the boundary conditions $x = 0$, $y = 0$, and $x = l$, $y = 0$ the following equations are obtained

$$C_1 + C_2 = 0$$

$$\cos\omega\left[t + \left(\frac{v\rho + (\rho T)^{1/2}}{T - \rho v^2}\right)l\right] - \cos\omega\left[t + \left(\frac{v\rho - (\rho T)^{1/2}}{T - \rho v^2}\right)l\right] = 0$$

It is therefore concluded that

$$\omega\left[t + \left(\frac{v\rho + (\rho T)^{1/2}}{T - \rho v^2}\right)l\right] = \omega\left[t + \left(\frac{v\rho - (\rho T)^{1/2}}{T - \rho v^2}\right)l\right] + 2\pi n$$

And hence

$$f_n = \frac{n(T - \rho v^2)}{2l(\rho T)^{1/2}} \quad \ldots\ldots [11]$$

If v is zero, Equation [11] reduces to the usual form for the natural frequencies of a vibrating string as given in Equation [1]. If the tension T is composed wholly of centrifugal tension the natural frequency is zero. The relation between f_n and the dimensionless ratio $\rho v^2/T$ is shown graphically in Fig. 2.

It is seen that a lightly loaded high-speed chain or belt could be excited to resonance by periodic forces of quite low frequency.

It is interesting to note that Equation [8] can be derived in a quite different way. Consider a co-ordinate system x' moving with the string. Relative to this co-ordinate system the wave equation is

$$\frac{\partial^2 y}{\partial t^2} = c^2\frac{\partial^2 y}{\partial x'^2} \quad \ldots\ldots [12]$$

where $c = (T/\rho)^{1/2}$ is the wave velocity. The general solution of Equation [12] is

$$y = F_1(x' - ct) + F_2(x' + ct) \quad \ldots\ldots [13]$$

where F_1 and F_2 are arbitrary functions which represent progressive waves moving in opposite directions along the x'-axis.

The transformation equation relating the moving frame x' to the fixed frame x is

$$x' = x - vt \quad \ldots\ldots [14]$$

The result of applying this transformation to Equations [12] and [13] is

$$\frac{\partial^2 y}{\partial t^2} + 2v\frac{\partial^2 y}{\partial x \partial t} = (c^2 - v^2)\frac{\partial^2 y}{\partial x^2} \quad \ldots\ldots [15]$$

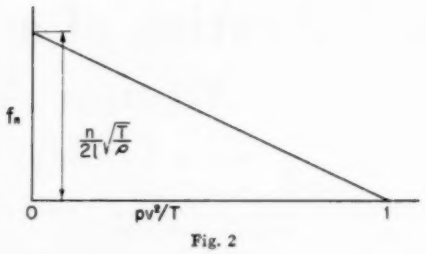

Fig. 2

and

$$y = F_1[x - (c + v)t] + F_2[x + (c - v)t] \quad \ldots\ldots [16]$$

Equation [16] is the general solution of Equation [15], which is seen to be identical with Equation [8]. The solution now corresponds to waves moving in opposite directions with speeds $(c + v)$ and $(c - v)$, respectively.

If the waves on the string are excited by a periodic source of angular frequency ω, Equation [16] takes the form

$$y = Ae^{i\left(\omega t - \frac{x}{c+v}\right)} + Be^{i\left(\omega t + \frac{x}{c-v}\right)} \quad \ldots\ldots [17]$$

where A and B are the (complex) amplitudes of the two waves. A simple example is the case of a belt passing over two pulleys, one of which is mounted eccentrically, so that a displacement

$$y = ae^{i\omega t} \quad \ldots\ldots [18]$$

is applied to the belt at $x = 0$, while $y = 0$ at $x = l$. For these two boundary conditions, the amplitudes A and B are easily calculated

$$A = \frac{a}{1 - e^{-i\omega l\left(\frac{1}{c+v} + \frac{1}{c-v}\right)}} \quad \ldots\ldots [19]$$

$$B = \frac{a}{1 - e^{i\omega l\left(\frac{1}{c+v} + \frac{1}{c-v}\right)}} \quad \ldots\ldots [20]$$

The absolute values of the amplitudes are the same

$$|A| = |B| = \frac{a}{2\left|\sin\frac{\omega l}{2}\left(\frac{1}{c+v} + \frac{1}{c-v}\right)\right|} \quad \ldots\ldots [21]$$

Resonance occurs when the denominator of Equation [21] becomes zero, corresponding to infinite amplitude. The condition for this is

$$\frac{\omega l}{2}\left(\frac{1}{c+v} + \frac{1}{c-v}\right) = n\pi \quad \ldots\ldots [22]$$

This result can be written in the form

$$\frac{l}{c+v} + \frac{l}{c-v} = n\tau \quad \ldots\ldots [23]$$

where $\tau = 2\pi/\omega$ is the period of the excitation. Equation [23] shows that resonance takes place when the time for the wave to travel from the eccentric pulley to the smooth pulley and back is an integral multiple of the number of revolutions of the eccentric pulley. The resonance condition is identical to Equation [11].

The foregoing work also should apply to the vibration of a gas column when the gas is in motion along its containing cylinder.

The Synthesis of a Four-Bar Mechanism for Prescribed Extreme Values of the Angular Velocity of the Driven Link

By J. HIRSCHHORN,[1] SYDNEY, AUSTRALIA

The "component method" of synthesis of four-bar mechanisms was discussed in detail in a previous publication.[2] The present paper shows the application of this method to the synthesis of four-bar linkages with prescribed extremes of the angular velocity of the driven or output link.

In the four-bar mechanism, Fig. 1, the driving crank q which revolves with a constant angular velocity ω_q causes the driven link s to oscillate. Thus ω_s is variable both in magnitude and sense.

It is desired to design a linkage which would give prescribed values of maximum ω_s and minimum ω_s with a specified constant ω_q and a given length p of the fixed link.

The configuration, velocity, and acceleration diagrams of this mechanism are defined by the following equations

$$\text{Configuration diagram} \begin{cases} q_x + r_x = s_x + p \dots\dots [1] \\ q_y + r_y = s_y \dots\dots [2] \end{cases}$$

$$\text{Velocity diagram} \begin{cases} \omega_q q_y + \omega_r r_y = \omega_s s_y \dots\dots [3] \\ \omega_q q_x + \omega_r r_x = \omega_s s_x \dots\dots [4] \end{cases}$$

$$\text{Acceleration diagram} \begin{cases} \omega_q^2 q_x + \omega_r^2 r_x + \alpha_r r_y = \omega_s^2 s_x + \alpha_s s_y \dots [5] \\ \omega_q^2 q_y + \omega_r^2 r_y - \alpha_r r_x = \omega_s^2 s_y - \alpha_s s_x \dots [6] \end{cases}$$

In the present case, because ω_s is either a maximum or a minimum

$$\alpha_s = \frac{d\omega_s}{dt} = 0$$

and Equations [5] and [6] reduce to

$$\text{Acceleration diagram for extremes of } \omega_s \begin{cases} \omega_q^2 q_x + \omega_r^2 r_x + \alpha_r r_y = \omega_s^2 s_x \dots [5a] \\ \omega_q^2 q_y + \omega_r^2 r_y - \alpha_r r_x = \omega_s^2 s_y \dots [6a] \end{cases}$$

From Equations [1] to [4], [5a], and [6a], the x and y projections of the links may be expressed in terms of the other quantities as follows

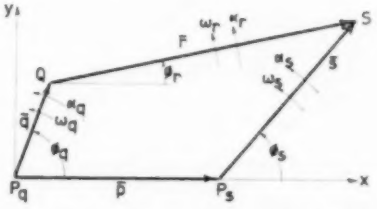

Fig. 1 Configuration diagram. Angular velocities ω; angular accelerations α.

$$\frac{q_x}{p} = \frac{(\omega_q - \omega_r)(\omega_s - \omega_r)^2\omega_q\omega_s - \omega_s[(\omega_q - \omega_r)^2(\omega_s - \omega_r)^2 + \alpha_r^2]}{(\omega_q - \omega_s)[(\omega_q - \omega_r)^2(\omega_s - \omega_r)^2 + \alpha_r^2]} \dots\dots [7]$$

$$\frac{q_y}{p} = \frac{(\omega_s - \omega_r)\omega_q\omega_s\alpha_r}{(\omega_q - \omega_s)[(\omega_q - \omega_r)^2(\omega_s - \omega_r)^2 + \alpha_r^2]} \dots\dots [8]$$

$$\frac{s_x}{p} = \frac{(\omega_q - \omega_r)^2(\omega_s - \omega_r)\omega_q\omega_s - \omega_q[(\omega_q - \omega_r)^2(\omega_s - \omega_r)^2 + \alpha_r^2]}{(\omega_q - \omega_s)[(\omega_q - \omega_r)^2(\omega_s - \omega_r)^2 + \alpha_r^2]} \dots\dots [9]$$

$$\frac{s_y}{p} = \frac{(\omega_q - \omega_r)\omega_q\omega_s\alpha_r}{(\omega_q - \omega_s)[(\omega_q - \omega_r)^2(\omega_s - \omega_r)^2 + \alpha_r^2]} \dots\dots [10]$$

$$\frac{r_x}{p} = \frac{\omega_q\omega_s(\omega_q - \omega_r)(\omega_s - \omega_r)}{(\omega_q - \omega_r)^2(\omega_s - \omega_r)^2 + \alpha_r^2} \dots\dots [11]$$

$$\frac{r_y}{p} = \frac{\omega_q\omega_s\alpha_r}{(\omega_q - \omega_r)^2(\omega_s - \omega_r)^2 + \alpha_r^2} \dots\dots [12]$$

By combining these equations in pairs, the lengths of the links may be calculated

$$\frac{q^2}{p^2} = \frac{q_x^2 + q_y^2}{p^2} = \frac{\omega_s^2\alpha_r^2 + (\omega_s - \omega_r)^2\omega_s^2\omega_r^2}{(\omega_q - \omega_s)^2[(\omega_q - \omega_r)^2(\omega_s - \omega_r)^2 + \alpha_r^2]} \dots\dots [13]$$

$$\frac{s^2}{p^2} = \frac{s_x^2 + s_y^2}{p^2} = \frac{\omega_q^2\alpha_r^2 + (\omega_q - \omega_r)^2\omega_q^2\omega_r^2}{(\omega_q - \omega_s)^2[(\omega_q - \omega_r)^2(\omega_s - \omega_r)^2 + \alpha_r^2]} \dots\dots [14]$$

$$\frac{r^2}{p^2} = \frac{r_x^2 + r_y^2}{p^2} = \frac{\omega_q^2\omega_s^2}{(\omega_q - \omega_r)^2(\omega_s - \omega_r)^2 + \alpha_r^2} \dots\dots [15]$$

Denoting by the suffix 1 all variable quantities corresponding to maximum ω_s, and by the suffix 2 those referring to minimum ω_s, the following system of three equations is obtained

[1] Senior Lecturer in Mechanical Engineering. New South Wales University of Technology.

[2] "The Synthesis of Four-Bar Mechanisms by the Method of Components," by J. Hirschhorn, Journal of Applied Mechanics, Trans. ASME, vol. 79, 1957, pp. 22–24.

"Synthesis of Four-Bar Linkages With Prescribed Reduction Ratio Limits," by N. Rosenauer, *Australia Journal of Applied Science*, vol. 7, 1956, pp. 1–9.

Contributed by the Applied Mechanics Division for presentation at the Annual Meeting, New York, N. Y., November 30–December 5, 1958, of The American Society of Mechanical Engineers.

Discussion of this paper should be addressed to the Secretary, ASME, 29 West 39th Street, New York, N. Y., and will be accepted until January 10, 1959, for publication at a later date. Discussion received after the closing date will be returned.

Note: Statements and opinions advanced in papers are to be understood as individual expressions of their authors and not those of the Society. Manuscript received by ASME Applied Mechanics Division, July 26, 1956. Paper No. 58—A-2.

From [13]

$$\frac{\omega_{s1}^2\alpha_{r1}^2 + (\omega_{s1} - \omega_{r1})^2\omega_{s1}^2\omega_{r1}^2}{(\omega_q - \omega_{s1})^2[(\omega_q - \omega_{r1})^2(\omega_{s1} - \omega_{r1})^2 + \alpha_{r1}^2]} = \frac{\omega_{s2}^2\alpha_{r2}^2 + (\omega_{s2} - \omega_{r2})^2\omega_{s2}^2\omega_{r2}^2}{(\omega_q - \omega_{s2})^2[(\omega_q - \omega_{r2})^2(\omega_{s2} - \omega_{r2})^2 + \alpha_{r2}^2]} \quad [16]$$

From [14]

$$\frac{\alpha_{r1}^2 + (\omega_q - \omega_{r1})^2\omega_{r1}^2}{(\omega_q - \omega_{s1})^2[(\omega_q - \omega_{r1})^2(\omega_{s1} - \omega_{r1})^2 + \alpha_{r1}^2]} = \frac{\alpha_{r2}^2 + (\omega_q - \omega_{r2})^2\omega_{r2}^2}{(\omega_q - \omega_{s2})^2[(\omega_q - \omega_{r2})^2(\omega_{s2} - \omega_{r2})^2 + \alpha_{r2}^2]} \quad [17]$$

From [15]

$$\frac{\omega_{s1}^2}{(\omega_q - \omega_{r1})^2(\omega_{s1} - \omega_{r1})^2 + \alpha_{r1}^2} = \frac{\omega_{s2}^2}{(\omega_q - \omega_{r2})^2(\omega_{s2} - \omega_{r2})^2 + \alpha_{r2}^2} \quad [18]$$

Elimination of α_{r2}^2 from Equations [16] and [18] yields

$$\left\{\frac{(\omega_q - \omega_{s2})^2}{(\omega_q - \omega_{s1})^2} - \frac{\omega_{s2}^2}{\omega_{s1}^2}\right\}\alpha_{r1}^2 = (\omega_{s2} - \omega_{r2})^2\omega_{r2}^2 - (\omega_q - \omega_{r2})^2(\omega_{s2} - \omega_{r2})^2 + \frac{(\omega_q - \omega_{r1})^2(\omega_{s1} - \omega_{r1})^2\omega_{s2}^2}{\omega_{s1}^2} - \frac{(\omega_q - \omega_{r2})^2(\omega_{s1} - \omega_{r1})^2\omega_{r1}^2}{(\omega_q - \omega_{s1})^2} \quad [19]$$

Elimination of α_{r1}^2 from Equation [19] leads to

$$\omega_{s2}^2(\omega_q - \omega_{s2})^2\{\omega_{s1}^2(\omega_q - \omega_{s2})^2[(\omega_{s1} - \omega_{r1})^2 - (\omega_q - \omega_{r1})^2]\omega_{r1}^2 - \omega_{s1}^2(\omega_q - \omega_{s1})^2(\omega_{s1} - \omega_{r1})^2[\omega_{r1}^2 - (\omega_q - \omega_{r1})^2] + \omega_{s2}^2(\omega_q - \omega_{s1})^2(\omega_q - \omega_{r1})^2[\omega_{r1}^2 - (\omega_{s1} - \omega_{r1})^2]\} = -T \quad [20]$$

The term T on the right-hand side of Equation [20] is similar to the left-hand side, except that the suffixes 1 and 2 are interchanged. Equation [20] is a cubic equation in ω_{r1} and ω_{r2}. Since it contains two unknown quantities it is obvious that the problem has an infinite number of possible solutions.

The best method of obtaining a definite result is to assume a value for either ω_{r1} or ω_{r2}, within limits set by the following criteria

$$\omega_{s1}[\omega_q(3\omega_{r1} - \omega_q) - \omega_{s1}(3\omega_{r1} - \omega_{s1})] < 0 \quad [21]$$

$$\omega_{s2}[\omega_q(3\omega_{r2} - \omega_q) - \omega_{s2}(3\omega_{r2} - \omega_{s2})] > 0 \quad [22]$$

The foregoing expressions represent the second time derivative

$$\dot{\alpha}_s = \frac{d^2\omega_s}{dt^2}$$

of the angular velocity of the driven link at the instant when the latter assumes its extreme values (see Appendix for derivation).

After selecting a suitable value for ω_{r1} in accordance with Expression [21] the cubic equation is solved. Of the three roots of this equation, the one which satisfies Expression [22] and yields positive values for α_{r1}^2 and α_{r2}^2 has physical meaning.

It is worth while to note that, if either ω_{r1} or ω_{r2} be taken as zero, the cubic equation will reduce to a quadratic one, simplifying calculations considerably.

The following also should be borne in mind: In the case of an oscillating-lever mechanism, i.e., a mechanism in which the driven link performs an oscillatory motion, ω_{s1} and ω_{s2} have opposite sense

$$\omega_{s1} > 0, \qquad \omega_{s2} < 0$$

In the case of a double-crank mechanism, i.e., a mechanism in which the driven link revolves in the same sense throughout its motion, ω_{s1} and ω_{s2} are both positive

$$\omega_{s1} > \omega_q \quad \text{and} \quad \omega_{s2} < \omega_q$$

Example 1. Oscillating-Lever Mechanism

Design a linkage to satisfy the following conditions:

Angular velocity of driving link ..... ω_q = 10 rad/sec
Maximum angular velocity of driven link .... ω_{s1} = 6 rad/sec
Minimum angular velocity of driven link .... ω_{s2} = −8 rad/sec
Length of fixed link ..... p = 10 in.

In this case ω_{r1} may be taken as zero since this value agrees with Condition [21].

With the foregoing values Equation [20] reduces to

$$21\omega_{r2}^2 - 60\omega_{r2} - 108 = 0$$

The two roots of this equation are

$$\omega_{r2} = 1.25 \text{ rad/sec}$$

$$\omega_{r2} = -4.11 \text{ rad/sec}$$

The first root does not satisfy Condition [22] and is discarded. The second root agrees with Condition [22] and yields positive values for α_{r1}^2 and α_{r2}^2

$$(\alpha_{r1}^2 = 197,\ \alpha_{r2}^2 = 3740)$$

These results are substituted into Equations [7] to [12] and the link projections are calculated:

Position 1 (corresponding to max ω_s)

q_x = −0.78 in.	q_y = 3.32 in.	q = 3.41 in.
s_x = −1.30 in.	s_y = 5.53 in.	s = 5.69 in
r_x = 9.48 in.	r_y = 2.21 in.	r = 9.74 in.

Position 2 (corresponding to min ω_s)

q_x = 3.03 in	q_y = −1.56 in.
s_x = −0.46 in.	s_y = 5.67 in.
r_x = 6.51 in.	r_y = 7.23 in.

The mechanism is shown in Fig. 2.

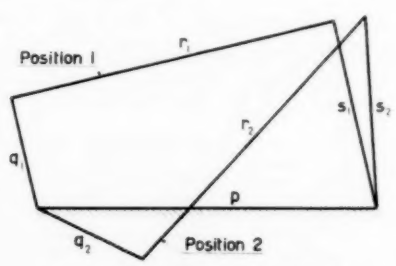

Fig. 2 Oscillating-lever mechanism

Example 2. Double-Crank Mechanism

Design a linkage to satisfy the following conditions:

Angular velocity of driving link ..... ω_q = 10 rad/sec
Maximum angular velocity of driven link .... ω_{s1} = 15 rad/sec
Minimum angular velocity of driven link .... ω_{s2} = 5 rad/sec
Length of fixed link ..... p = 10 in.

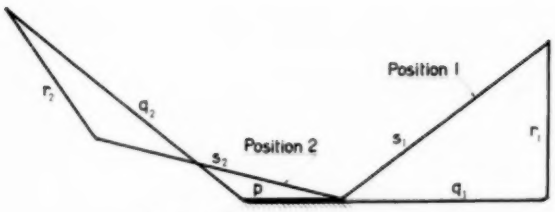

Fig. 3 Double-crank mechanism

In this case, in order to satisfy Condition [21], $\omega_{r1} > 8.33$ rad/sec. However, further calculations reveal that, if only integer numbers are considered, the choice of suitable values of ω_{r1} is limited to the range 11 to 18 rad/sec, as values outside this range give negative α_{r1}^2 and α_{r2}^2.

With a selected value of $\omega_{r1} = 15$ rad/sec, Equation [20] reduces to

$$10\omega_{r2}^3 - 225\omega_{r2}^2 + 1500\omega_{r2} - 3125 = 0$$

This equation has only one real solution of $\omega_{r2} = 12.5$ rad/sec, which satisfies Condition [22] and yields

$$\alpha_{r1}^2 = 9490 \text{ and } \alpha_{r2}^2 = 703$$

The link projections are as follows:
Position 1 (corresponding to max ω_s)

$q_x = 30.00$ in.	$q_y = 0.00$ in.	$q = 30.00$ in.
$s_x = 20.00$ in.	$s_y = 15.40$ in.	$s = 25.24$ in.
$r_x = 0.00$ in.	$r_y = 15.40$ in.	$r = 15.40$ in.

Position 2 (corresponding to min ω_s)

$q_x = -23.32$ in.	$q_y = 18.85$ in.
$s_x = -24.42$ in.	$s_y = 6.30$ in.
$r_x = 8.90$ in.	$r_y = -12.55$ in.

The mechanism is shown in Fig. 3.

APPENDIX

Derivation of Equation

$$\dot{\alpha}_s = \omega_s[\omega_q(3\omega_r - \omega_q) - \omega_s(3\omega_r - \omega_s)]$$

Equation [5] is multiplied by r_x, Equation [6] is multiplied by r_y, and the two resulting equations are added together, thus eliminating α_r,

$$\omega_q^2(q_x r_x + q_y r_y) + \omega_r^2(r_x^2 + r_y^2) = \omega_s^2(r_x s_x + r_y s_y) + \alpha_s(r_x s_y - r_y s_x) \quad [23]$$

Since the terms

$$(q_x r_x + q_y r_y) \quad \text{and} \quad (r_x s_x + r_y s_y)$$

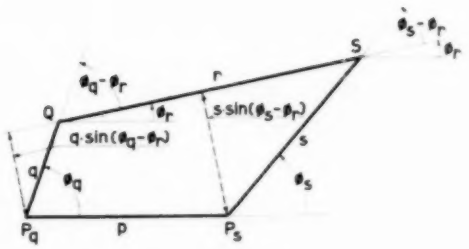

Fig. 4

are recognized, respectively, as the scalar products $\bar{q}\cdot\bar{r}$ and $\bar{r}\cdot\bar{s}$, and the term $(r_x s_y - r_y s_x)$ as the vector product $\bar{r} \times \bar{s}$, Equation [23] may be written in the following form

$$\omega_q^2 qr\cos(\phi_q - \phi_r) + \omega_r^2 r^2 = \omega_s^2 rs\cos(\phi_s - \phi_r) + \alpha_s rs\sin(\phi_s - \phi_r) \quad [24]$$

Equation [24] is now differentiated with respect to time and, with $\alpha_q = 0$ and $\alpha_r = 0$, the following relation is obtained

$$-\omega_q^2 q(\omega_q - \omega_r)\sin(\phi_q - \phi_r) + 2\omega_r\alpha_r r = -\omega_s^2 s(\omega_s - \omega_r)\sin(\phi_s - \phi_r) + \dot{\alpha}_s s\sin(\phi_s - \phi_r) \quad [25]$$

Next, $\alpha_r r$ is expressed in terms of the other quantities, thus: Equation [5a] is multiplied by $-r_y$, Equation [6a] is multiplied by r_x, and the resulting equations are added together, giving

$$-\omega_q^2(q_x r_y - q_y r_x) - \alpha_r(r_x^2 + r_y^2) = \omega_s^2(r_x s_y - r_y s_x) \quad [26]$$

or

$$\omega_q^2 rq\sin(\phi_q - \phi_r) - \alpha_r r^2 = \omega_s^2 rs\sin(\phi_s - \phi_r) \quad [27]$$

from which

$$\alpha_r r = \omega_q^2 q\sin(\phi_q - \phi_r) - \omega_s^2 s\sin(\phi_s - \phi_r) \quad [28]$$

Substituting Equation [28] into Equation [25] yields the following expression for $\dot{\alpha}_s$

$$\dot{\alpha}_s = \frac{\omega_q^2 q(3\omega_r - \omega_q)\sin(\phi_q - \phi_r)}{s\sin(\phi_s - \phi_r)} - \omega_s^2(3\omega_r - \omega_s) \quad [29]$$

Since the velocity of the point Q in the direction Q–S is equal to the velocity of the point S in the same direction, Fig. 4

$$\omega_q q\sin(\phi_q - \phi_r) = \omega_s s\sin(\phi_s - \phi_r) \quad [30]$$

and Equation [29] becomes

$$\dot{\alpha}_s = \omega_s[\omega_q(3\omega_r - \omega_q) - \omega_s(3\omega_r - \omega_s)]$$

NOTE: This is not a general expression for $\dot{\alpha}_s$, but one which is valid only if ω_q is constant and ω_s is either a maximum or a minimum.

Natural Forcing Functions in Nonlinear Systems[1]

By T. J. HARVEY,[2] PALO ALTO, CALIF.

The response of nonlinear, second-order systems is examined from a new point of view which greatly simplifies presentation of the usual frequency-response diagrams. The use of "natural" forcing functions results in a general equation relating the maximum amplitude of the applied force to the maximum amplitude of the restoring force. The relationship is found to be a function of the ratio of the period of free oscillation to the period of the forcing function. The results apply for any second-order system without damping and with a nonlinear (or linear) restoring force. The special cases of a linear system and of Duffing's equation are considered to illustrate similarities as well as differences between treatment of linear and nonlinear frequency-response problems.

Nomenclature

THE following nomenclature is used in the paper:

- $y(t)$ = dependent variable
- ω_n = natural circular frequency of single-degree-of-freedom linear system
- ω = circular frequency of forcing function in Equation [1]
- t = independent variable
- $f(y)$ = restoring function defined in Equation [2]
- K = quantity defined in Equation [4]
- y_0, v_0 = y and first derivative of y evaluated at $t = 0$
- $y_{1,2}$ = dummy variables of integration
- T = period of oscillation
- $I(a^2)$ = integral defined in Equation [9]
- T_n = period of free oscillation
- δ = ratio of forcing function to restoring function defined in Equation [13]
- T_0 = period of free oscillation for infinitesimal amplitude
- m = amplitude (max) of restoring function
- p = amplitude (max) of forcing function
- η = variable introduced in Equation [21]
- C_2 = constant multiplier of y^3 in Duffing's equation
- α, β = quantities defined in Equations [27] and [28]
- C = ratio, α/β
- ϕ = variable introduced in Equation [33]
- $\lambda = \dfrac{m\sqrt{C_2}}{\omega_n^2}$

Introduction

Interest in the frequency response of nonlinear systems has been generated by the behavior of linear systems—in particular, the resonance phenomena which they exhibit. The equation used to study the frequency response of linear single-degree-of-freedom systems is

$$\ddot{y}(t) + \omega_n^2 y(t) = A \sin \omega t \quad [1]$$

A natural extension of Equation [1] for study of nonlinear systems is

$$\ddot{y} + \omega_n^2 f(y) = A \sin \omega t \quad [2]$$

where $f(y)$ is a nonlinear function of y, as in $f(y) = (y + y^3)$, for example. Many investigators have studied Equation [2] in detail and obtained solutions which indicate the effects of parameter ω upon solution y. It is the point of this paper that Equation [2] is not necessarily the most profitable one to study. There are two major reasons for taking this point of view: (*a*) In all but the most elementary cases, the solution is very difficult to obtain. (*b*) Little use is made of the extensive knowledge already acquired in cases where the right-hand side of Equation [2] is zero. The approach taken here, then, is one which attempts to find a simple method of studying the forced oscillations of nonlinear systems by making use of the properties of the free oscillations.

Basic Equations

To arrive at a simple method for handling the forced oscillations of nonlinear systems, we choose a more general relation than that expressed in Equation [2]. Instead of letting the right-hand side equal to $A \sin \omega t$, an arbitrary periodic function $f(t)$ is chosen

$$\ddot{y} + \omega_n^2 f(y) = f(t) \quad [3]$$

Since investigation into the free response of nonlinear systems indicates that such response is usually periodic rather than harmonic, $f(t)$ is arbitrarily designated periodic, rather than harmonic, in this equation. Now, how can $f(t)$ be further defined so that a simple, meaningful solution to Equation [3] can be found?

Because the free oscillations of Equation [3] have been studied extensively, it is proposed here that a forcing function which will produce oscillations of the same form as the free oscillations will lead to a simple solution. Such a forcing function will be called a natural forcing function. Furthermore, only those oscillations having the same period as the forcing function will be considered. Regardless of the form of $f(y)$, it is true that $f(y)$ has the same period as y. Thus a function having the same period as $f(y)$ also has the same period as y. If $f(t)$ is chosen such that

$$f(t) = Kf(y) \quad [4]$$

then Equation [3] can be written

$$\ddot{y} + (\omega_n^2 - K)f(y) = 0 \quad [5]$$

which is identical in form to the equation for the free oscillations, with the only difference being that constant ω_n^2 is replaced by $(\omega_n^2 - K)$. For this reason, the forcing function defined by Equation [4] will produce periodic oscillations having the same period as the forcing function, and having the same form as the free oscillations of the system.

---

[1] This paper was originally prepared as a thesis for the MS degree in Engineering at the University of California at Los Angeles.

[2] Group Engineer, Structures Department, Lockheed Missile Systems Division, Palo Alto, Calif.

Contributed by the Applied Mechanics Division for presentation at the Annual Meeting, New York, N. Y., November 30–December 5, 1958, of THE AMERICAN SOCIETY OF MECHANICAL ENGINEERS.

Discussion of this paper should be addressed to the Secretary, ASME, 29 West 39th Street, New York, N. Y., and will be accepted until January 10, 1959, for publication at a later date. Discussion received after the closing date will be returned.

NOTE: Statements and opinions advanced in papers are to be understood as individual expressions of their authors and not those of the Society. Manuscript received by ASME Applied Mechanics Division, April 29, 1957. Paper No. 58—A-6.

The solution to Equation [5] can be obtained by the method of quadratures[3]

$$t = \int_{y_0}^{y} \frac{dy_2}{\left[v_0^2 - 2(\omega_n^2 - K)\int_{y_0}^{y_1} f(y_1)dy_1\right]^{1/2}} \quad [6]$$

The period can be found by appropriate adjustment of the limit y

$$T = \frac{1}{(\omega_n^2 - K)^{1/2}} \int_{y_0}^{y_T} \frac{dy_2}{\left[a^2 - 2\int_{y_0}^{y_1} f(y_1)dy_1\right]^{1/2}} \quad [7]$$

where

$$a^2 = \frac{v_0^2}{\omega_n^2 - K} \quad [8]$$

and the limit y_T is chosen such that y has executed one complete oscillation from the initial position y_0. If a^2 is fixed, then the value of the integral in Equation [7] is set. Defining

$$I(a^2) = \int_{y_0}^{y_T} \frac{dy_2}{\left[a^2 - 2\int_{y_0}^{y_2} f(y_1)dy_1\right]^{1/2}} \quad [9]$$

Equation [7] can be written

$$T = \frac{I(a^2)}{(\omega_n^2 - K)^{1/2}} \quad [10]$$

Squaring both sides and solving for K

$$K = \omega_n^2\left(1 - \frac{I^2}{\omega_n^2 T^2}\right) \quad [11]$$

Inspection of Equation [10] shows that I/ω_n is the value of the period when $K = 0$, which is the period of free oscillation, then defining

$$T_n = \frac{I(a^2)}{\omega_n} \quad [12]$$

and defining

$$\delta = \frac{K}{\omega_n^2} \quad [13]$$

Equation [11] becomes

$$\delta = 1 - \frac{T_n^2}{T^2} \quad [14]$$

By inspection of Equation [4], the quantity $\delta = K/\omega_n^2$ can be seen to be the ratio of forcing function $f(t)$ to restoring function $\omega_n^2 f(y)$. Equation [14] then allows calculation of the ratio of the forcing function to the restoring function for any second-order nonlinear system in terms of the period of the free oscillations of the system and the period of the forcing function. This holds true, of course, only if the forcing function and the response have the same period and if the forcing function is a "natural" one. It should be noted that T_n is a function of the parameter a^2 which is in turn related to the amplitude of the response. Therefore for constant a^2, the parabola defined by Equation [14] shows how the input amplitude must vary with the period T to maintain a constant output amplitude. Nevertheless, Equation [14] does show that use of natural forcing functions allows great use to be made of the more readily obtained results for the free-oscillation case.

[3] "Mathematical Methods in Engineering," by T. von Karman and M. A. Biot, McGraw Hill Book Company, Inc., New York, N. Y., 1940, p. 113.

In engineering problems, greater interest seems to be in the ratio of restoring function to forcing function for fixed forcing-function amplitude.

There are many cases where the frequency response can be obtained in a straightforward manner. Equation [14] can be written in the form

$$\delta = 1 - \left(\frac{T_n}{T_0}\right)^2\left(\frac{T_0}{T}\right)^2 \quad [15]$$

The quantity T_n/T_0 relates the way the period of free oscillation is affected by the output amplitude. For a system which becomes stiffer as the amplitude increases (a hard system), T_n/T_0 will decrease as the amplitude increases. The converse applies for a "soft" system. If T_n/T_0 can be expressed analytically as a function of the restoring-function amplitude, then the ratio of restoring function to forcing function can be found as a function of T_0/T by evaluating the roots of a polynomial. If T_n/T_0 cannot be approximated analytically, then the most straightforward method for obtaining this would seem to be to plot δ versus T for several values of response amplitude. Then the input amplitude could be calculated by multiplying the response amplitude by δ, and the input amplitudes listed as points in the $\delta - T$ plane. Once a sufficient number of points have been obtained, curves can be drawn through points of equal input amplitude to give the desired result.

Application of Equation [15] to a Hard System

To study the behavior of a hard system, a convenient choice is made for the effect of amplitude upon natural period. Accordingly, the ratio T_n/T_0 is assumed to be

$$\frac{T_n}{T_0} = \frac{1}{(1 + m^2)^{1/2}} \quad [16]$$

It can be seen that this expression behaves in the manner of a hard system since the ratio T_n/T_0 decreases as the amplitude m increases. Substituting in Equation [15]

$$\delta = 1 - \frac{1}{1 + m^2}\left(\frac{T_0}{T}\right)^2 \quad [17]$$

since $m\delta = p$, then Equation [17] becomes

$$p = m - \frac{m}{1 + m^2}\left(\frac{T_0}{T}\right)^2$$

rearranging in descending powers of m

$$m^3 - m^2 + m\left[1 - \left(\frac{T_0}{T}\right)^2\right] - p = 0 \quad [18]$$

The roots of Equation [18] have been found for various values of p, and their absolute values are plotted versus T_0/T in Fig. 1. The real part of the complex conjugate roots is also plotted. The complex roots, however, do not represent physically realizable equilibrium positions. The plot shown in Fig. 1 is in qualitative agreement with the results obtained by other methods.[4]

The investigation thus far indicates that the use of natural forcing functions allows a simple and meaningful solution to be obtained for the fundamental frequency response of nonlinear systems. Furthermore, the generality of the method indicates possible areas of future study (such as the case where Equation [18] is a quintic or higher) which can be handled in a similar manner.

[4] "Non-Linear Vibrations," by J. J. Stoker, Interscience Publishers, Ltd., London, 1950, p. 86.

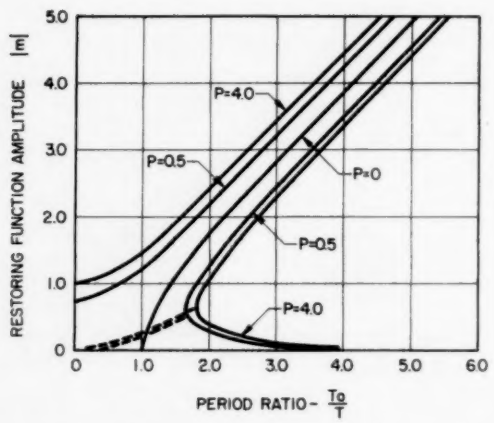

Fig. 1 Restoring function versus period ratio for $\frac{T_n}{T_0} = \frac{1}{(1+m^2)^{1/2}}$

Application to a Linear System

To illustrate the nature of the so-called natural forcing functions, it is useful to treat two special cases in detail. The linear system and Duffing's equation are of greatest interest, and their study provides considerable useful information.

To study the linear system, the restoring function is defined by

$$f(y) = y \quad [19]$$

assuming $y_0 = 0$ Equation [6] becomes

$$t = \frac{1}{(\omega_n^2 - K)^{1/2}} \int_0^b \frac{dy_1}{(a^2 - y_1^2)^{1/2}} \quad [20]$$

letting $y_1 = a\eta$

$$t = \frac{1}{(\omega_n^2 - K)^{1/2}} \int_0^{y/a} \frac{d\eta}{(1 - \eta^2)^{1/2}} \quad [21]$$

The period is given by

$$T = \frac{4}{(\omega_n^2 - K)^{1/2}} \int_0^1 \frac{d\eta}{(1 - \eta^2)^{1/2}} = \frac{2\pi}{(\omega_n^2 - K)^{1/2}} \quad [22]$$

which can be solved for K

$$K = \omega_n^2 - \left(\frac{2\pi}{T}\right)^2 \quad [23]$$

Equation [21] defines a function[3] $y(t)$

$$y(t) = a \sin (\omega_n^2 - K)^{1/2} t$$

or

$$y(t) = a \sin \left(\frac{2\pi}{T}\right) t \quad [24]$$

and

$$f(t) = Ka \sin \left(\frac{2\pi}{T}\right) t \quad [25]$$

The foregoing derivation indicates the method of determining the natural response when the restoring function is given by a polynomial in y. Equations [24] and [25] show that the choice of $f(t)$ as a constant times a harmonic function of time is the natural one for a linear system, and they indicate the reason for simplicity of the usual solution for frequency response of a linear system. With this in mind, the attempts to apply harmonic excitations in the study of nonlinear systems would seem to place unnecessary restrictions and difficulties in the path of the investigator.

Duffing's Equation

One of the most frequently studied nonlinear equations is Duffing's, in which the restoring function is

$$f(y) = y + C_2 y^3 \, y(t)$$

For the sake of generality, C_2 is not fixed here. Again assuming $y_0 = 0$, Equation [6] becomes

$$t = \frac{1}{(\omega_n^2 - K)^{1/2}} \int_0^y \frac{dy_2}{\left(a^2 - y_2^2 - \frac{C_2}{2} y_2^4\right)^{1/2}} \quad [26]$$

This can be rewritten as

$$t = \frac{1}{(\omega_n^2 - K)^{1/2}} \int_0^y \frac{dy_2}{\left[\frac{C_2}{2}(\alpha^2 - y_2^2)(\beta^2 + y_2^2)\right]^{1/2}} \quad [27]$$

where

$$\alpha^2 = \frac{-1 + (1 + 2a^2C_2)^{1/2}}{C_2} \quad [28]$$

$$\beta^2 = \frac{+1 + (1 + 2a^2C_2)^{1/2}}{C_2}$$

letting $\eta = y_2/\alpha$, Equation [27] becomes

$$t = \frac{1}{(\omega_n^2 - K)^{1/2}} \int_0^{y/\alpha} \frac{d\eta}{\beta\left[\frac{C_2}{2}(1 - \eta^2)(1 + C^2\eta^2)\right]^{1/2}} \quad [29]$$

where

$$C^2 = \frac{\alpha^2}{\beta^2} \quad [30]$$

using Equations [28] and [30], it can be shown that

$$\left.\begin{aligned} \beta^2 &= \frac{2}{C_2(1 - C^2)} \\ \text{and} \\ \alpha^2 &= \frac{2C^2}{C_2(1 - C^2)} \end{aligned}\right\} \quad [31]$$

which allows Equation [29] to be written

$$t = \frac{1}{(\omega_n^2 - K)^{1/2}} \int_0^{y/\alpha} \frac{d\eta}{\frac{1}{(1 - C^2)^{1/2}}[(1 - \eta^2)(1 + C^2\eta^2)]^{1/2}} \quad [32]$$

letting[3] $y/\alpha = \cos\phi$

$$t = \frac{(1 - C^2)^{1/2}}{[(\omega_n^2 - K)(1 + C^2)]^{1/2}} \int_0^{\phi} \frac{d\phi_1}{\left(1 - \frac{C^2}{1 + C^2}\sin^2\phi_1\right)^{1/2}} \quad [33]$$

Equations [32] and [33] define the function $y(t)$

$$y(t) = \left[\frac{2C^2}{C_2(1 - C^2)}\right]^{1/2} Cn\left[\frac{(\omega_n^2 - K)(1 + C^2)}{1 - C^2}\right]^{1/2} t \quad [34]$$

which is an elliptic function; the well-known natural response for Duffing's equation. The restoring function now can be calculated, and from it, the forcing function

$$f(t) = K\omega_n^2 \left\{ \left[\frac{2C^2}{C_2(1-C^2)} \right]^{1/2} Cn \left[\frac{(\omega_n^2 - K)(1+C^2)}{1-C^2} \right] t + C_2 \left[\frac{2C^2}{C_2(1-C^2)} \right]^{3/2} Cn^3 \left[\frac{(\omega_n^2 - K)(1+C^2)}{1-C^2} \right]^{1/2} t \right\} \quad \ldots\ldots [35]$$

indicating that the natural forcing function in the case of Duffing's equation is a combination of elliptic functions. This raises the question: "Will not the unusual wave form of these forcing functions render them useless in practical engineering problems?" The answer can only be found by comparing results obtained in this manner with those obtained experimentally and by other analytical means.

To accomplish the calculation of the frequency response for Duffing's equation, the quantity T_n/T_0 must be found as a function of restoring function maximum amplitude, m. From Equation [34]

$$m = \omega_n^2 \left\{ \left[\frac{2C^2}{C_2(1-C^2)} \right]^{1/2} + C_2 \left[\frac{2C^2}{C_2(1-C^2)} \right]^{3/2} \right\} = \omega_n^2 \left(\frac{1+C^2}{1-C^2} \right) \left[\frac{2C^2}{C_2(1-C^2)} \right]^{1/2} \quad \ldots\ldots [36]$$

while Equation [33] can be used to calculate T_n and T_0

$$\frac{T_n}{T_0} = \frac{2(1-C^2)^{1/2}}{\pi(1+C^2)^{1/2}} \int_0^{\pi/2} \frac{d\phi_1}{\left(1 - \frac{C^2}{1+C^2}\sin^2\phi_1\right)^{1/2}} \quad \ldots [37]$$

Using Equations [36] and [37], the quantities

$$\lambda = \frac{m\sqrt{C_2}}{\omega_n^2} \quad \text{and} \quad T_n/T_0$$

were calculated for various values of C. T_n/T_0 was then plotted versus λ in Fig. 2. It was not possible to find a simple analytical expression which would fit the curve in Fig. 2 in all regions. However, the expression

$$\frac{T_n}{T_0} = \frac{1}{(1 + 0.461\,|\lambda| - 0.0103\lambda^2)^{1/2}} \quad \ldots\ldots [38]$$

provided a good fit in the region $\lambda < 12.0$.

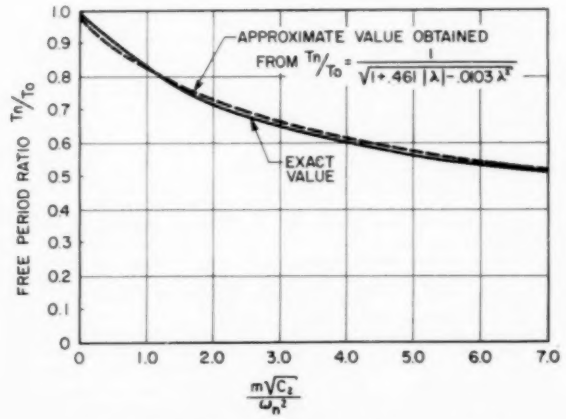
APPROXIMATE VALUE OBTAINED FROM $T_n/T_0 = \frac{1}{\sqrt{1+.461\,|\lambda| - .0103\lambda^2}}$
EXACT VALUE
FREE PERIOD RATIO T_n/T_0
$\frac{m\sqrt{C_2}}{\omega_n^2}$

Fig. 2 Free-period ratio versus λ for $f(y) = y + C_2y^3$

In a manner similar to that used for the linear system, the following equality was obtained

$$p = m - \frac{m}{[1 + 0.461\,|\lambda| - 0.0103\lambda^2]} \left(\frac{T_0}{T} \right)^2 \quad \ldots\ldots [39]$$

solving for $(T_0/T)^2$

$$\left(\frac{T_0}{T} \right)^2 = \left(1 - \frac{p}{m} \right) (1 + 0.461\,|\lambda| - 0.0103\lambda^2) \quad \ldots [40]$$

Using this equation, and knowing that only real values of m are of interest, the solutions can be found easily by setting p, and calculating T_0/T for many values of m. This was done and the results are shown in Fig. 3, for $\omega_n^2 = C_2 = 1.0$. Results obtained using Duffing's solution[4] are also shown in Fig. 3 as dotted lines. Inspection of Fig. 3 shows that the values are not in particularly close agreement. The reason is that Duffing's solution is only valid where C_2 is small. This procedure was repeated for $\omega_n^2 = 1.0$, $C_2 = 0.1$, and the results are shown in Fig. 4. The agreement obtained here is somewhat better, as might be expected.

Figs. 3 and 4 indicate that the method of Duffing, and the methods presented here, give essentially the same results in cases where Duffing's method is applicable. Duffing's solution gives slightly lower values of T_0/T in all cases, which may be due either to the differences in wave form (Duffing used the sinusoidal

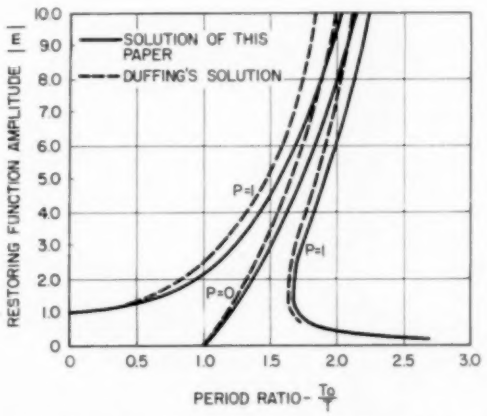

Fig. 3 Restoring function versus period ratio for $f(y) = y + y^3$

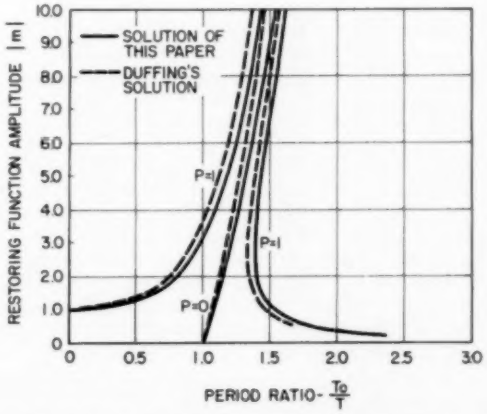

Fig. 4 Restoring function versus period ratio for $f(y) = y + 0.1y^3$

forcing function, while the elliptic forcing function is used in this paper), or the approximate character of Duffing's solution. This idea is supported by the results for $p = 0$, which correspond to the free oscillations of the system. The methods used in this paper yield the exact solution in this case. Duffing's solution is approximate in the case of the free oscillations, and it is significant that the period ratio predicted by Duffing's solution is lower than that predicted by Equation [40] by essentially the same magnitudes for the case $p = 1.0$ as it is for the case $p = 0$. It may be inferred then that, since Duffing's result for the period ratio is low in the case of the free oscillations, the same trend could be expected in the case of forced oscillations.

Conclusions

The use of natural forcing functions as presented in this paper provides a useful, exact solution for the fundamental frequency response of second-order systems with nonlinear restoring forces. The basic equations are applicable to any second-order system regardless of the form of the restoring force. These equations are in such a form that knowledge of the manner in which the natural period varies with restoring-force amplitude is sufficient to describe completely the fundamental frequency response. This method then provides a link between the extensive knowledge of the free oscillations of nonlinear systems and the limited knowledge of their forced oscillations. Certain questions remain to be answered concerning the usefulness of the method in engineering problems. These arise mainly from the fact that the wave form of natural forcing functions may be quite different from the sinusoidal forcing functions which are of interest to engineers. The author feels that these differences are not a major consideration in most problems, as was illustrated by the study of Duffing's equation, but an experimental investigation of the results presented in this paper would be a worth-while project.

Acknowledgment

The author wishes to express his thanks for the guidance and encouragement given him by Prof. Louis A. Pipes of the University of California at Los Angeles.

Kinematic Drift of Single-Axis Gyroscopes[1]

By R. H. CANNON, JR.,[2] CAMBRIDGE, MASS.

A gyroscope can incur steady drift by kinematically rectifying angular vibrations of the platform on which it is mounted. The phenomenon, for an unrestrained single-degree-of-freedom gyro, results from oscillatory precession of the gyro momentum vector from its nominal spatial orientation, so that it senses platform motions about axes other than the one it is controlling. The magnitude of the drift can be accurately predicted and the vibration climate of the platform restricted accordingly. Quantitative experimental verification is presented.

Nomenclature

The following is used in the paper (refer to Fig. 1):

H = spin angular momentum of gyro wheel
$\mathbf{H}$ = total angular momentum of gyro (wheel plus frame)
I = moment of inertia of gyro (wheel plus frame)
ϕ = angular displacement of gimbal
$\frac{d}{dt}$ or $\dot{}$ = derivative with respect to time
$\dot{\theta}$ = component of gyro-frame angular velocity (in space) about gyro output z-axis
σ = rotation of gyro frame relative to platform
$\bar{\Omega}$ = total angular velocity of gyro frame; has components $\Omega_x, \Omega_y, \Omega_z$
$\bar{1}$ = unit vector

Subscripts

X, Y, Z = axes defined by gimbal system (not orthogonal, in general); X-axis is fixed, Fig. 1

x, y, z = axes fixed in gyro frame;

- x is "input" axis
- y is spin axis
- z is "output" axis

(orthogonal)

x_p, y_p, z_p = axes fixed in platform; (Z, z, and z_p always coincide)

Stable platforms such as are used to provide a fixed angular reference for inertial navigators,[3] depend on low-drift gyros for fixity. When a gyro drifts, the platform follows with resulting performance errors of the system being controlled.

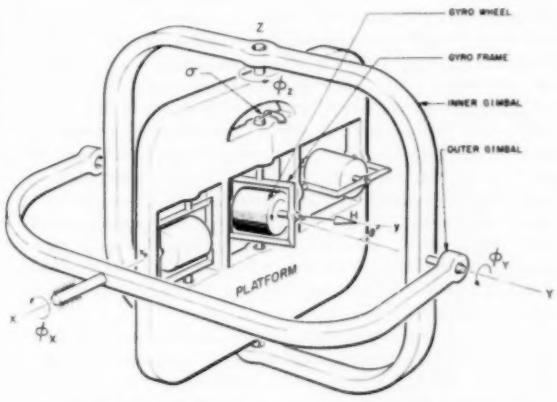

Fig. 1 Stable platform using single-axis gyroscopes

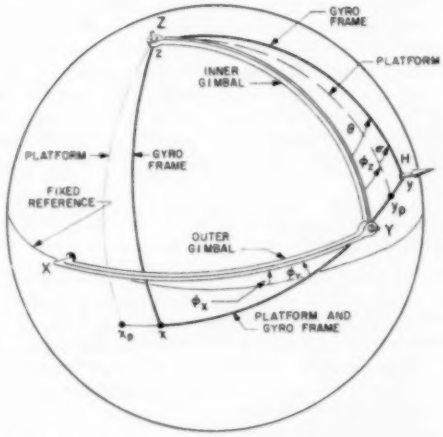

Fig. 2 "Unit sphere" picture of platform geometry

An important cause of gyro drift is kinematic rectification, by the gyro, of oscillatory motions of the platform on which it is mounted. Such motions are the common result of oscillatory disturbing torques produced by airframe vibration. Once the mechanism of rectification is understood quantitatively, the vibration climate of the platform can be controlled to reduce gyro drift from this cause to an acceptably low level.

The model for the present discussion is the unrestrained, single-degree-of-freedom gyro[4] in Fig. 1, serving as angular reference for the X-axis of the stable platform on which it is mounted. An electrical pick-off measures precession of the gyro with respect to the platform, σ, furnishing a signal which is used by a servo system to control the attitude ϕ_X of the platform by applying

---

[1] Based on work performed by members of the research staff at Autonetics, a Division of North American Aviation, Inc., Downey, Calif. The effect was first recognized at Autonetics by T. E. Curtis in 1953, and the basic theory was developed by Curtis and W. R. Evans in 1954.

[2] Associate Professor of Mechanical Engineering, Massachusetts Institute of Technology. Formerly, Research Specialist, Autonetics, a Division of North American Aviation, Inc.

[3] "Inertial Navigation," by J. M. Slater and D. B. Duncan, *Aeronautical Engineering Review*, vol. 15, no. 1, 1956, pp. 49–52, 57.

Contributed by the Applied Mechanics Division and presented at the Annual Meeting, New York, N. Y., December 1–6, 1957, of THE AMERICAN SOCIETY OF MECHANICAL ENGINEERS.

Discussion of this paper should be addressed to the Secretary, ASME, 29 West 39th Street, New York, N. Y., and will be accepted until October 10, 1958, for publication at a later date. Discussion received after the closing date will be returned.

NOTE: Statements and opinions advanced in papers are to be understood as individual expressions of their authors and not those of the Society. Manuscript received by ASME Applied Mechanics Division, April 29, 1957. Paper No. 57—A-72.

[4] A similar phenomenon in free gyros is discussed in "Nutation of a Free Gyro Subjected to an Impulse," by B. T. Plymale and R. Goodstein, JOURNAL OF APPLIED MECHANICS, TRANS. ASME, vol. 77, 1955, pp. 365–366.

torques to the outer gimbal. The mathematics is simplified by considering a gyro without damping. (The results are easily extended to account for damping.)

Gyro Dynamics

A gimbal system is shown in Fig. 1, not only to make clear the relation between the gyroscope and the platform it is controlling, but also to furnish a co-ordinate system for defining the orientation of the gyro and platform, the gimbal angles ϕ_X, ϕ_Y, and ϕ_Z, and the gyro pick-off angle σ being measurable quantities.

A "unit sphere" picture of the system is shown in Fig. 2. The center of the sphere is the center of the gyro. The axes of the gyro frame, x, y, z, pierce the sphere to form a rigid octant indicated by the single solid lines in Fig. 2. The platform axes x_p, y_p, z form another rigid octant shown dotted. (Axes z and Z are always coincident, Fig. 1.) The gimbals which connect the platform to the fixed reference also are shown, the outer gimbal pivoting within fixed reference axis X, and the platform pivoting within the Z-axis of the inner gimbal. The two gimbals are pivoted together at point Y.

In practice, the angles shown in Fig. 2 are never as large as 1 deg. Therefore tacit advantage is taken of small-angle approximations in the development which follows.

The important relation for a sensing gyroscope is the balance of torques about its output axis (Z-axis in Figs. 1 and 2). Let the angular velocity of the gyro frame be $\vec{\Omega}$, having components Ω_x, Ω_y, and Ω_z along the orthogonal axes fixed to the gyro frame. The angular momentum H of the gyro wheel is considered to be very large compared to the momentum of the frame. If the output-axis bearings are considered frictionless, the only torques felt by the gyro frame are the z-component of the gyroscopic torque $H\Omega_z$ and the inertial reaction $I_z\dot{\Omega}_z$ (where I_z is the moment of inertia of the gyro about its output axis), so that the balance of torques is

$$I_z\dot{\Omega}_z + H\Omega_z = 0 \qquad [1]$$

Rectification Mechanism

The drift rate of the system of Fig. 1 is most easily measured in terms of the average rates of rotation of the gimbals, i.e., in terms of $\dot{\phi}_X$, $\dot{\phi}_Y$, and $\dot{\phi}_Z$. The platform servo system is attempting to maintain pick-off angle σ at null by torquing the outer gimbal; it succeeds to the extent that $\dot{\sigma}$ is prevented from having an average value. From Fig. 2, σ is the difference between displacements of the gyro and platform

$$\sigma = \theta - \phi_Z \qquad [2]$$

Rectification comes about because, in the presence of sinusoidal motion ϕ_X, the gyro, with its momentum vector H, is precessing back and forth past gimbal axis Y in Figs. 1 and 2, so that the angular velocity Ω_z of the gyro frame is made up not only of gimbal velocity $\dot{\phi}_X$, but also of a component $\theta\dot{\phi}_Y$, of the angular velocity about the Y-axis, with the result that the gyroscopic torque $H\Omega_z$ in Equation [1] contains not only the principal term $H\dot{\phi}_X$ but also a "cross-torque" component $H(\theta\dot{\phi}_Y)$. The output-axis angular acceleration is approximately $\dot{\Omega}_z \cong \ddot{\theta}$ so that the balance of torques, Equation [1], becomes

$$I_z\ddot{\theta} + H\dot{\phi}_X + H\theta\dot{\phi}_Y \cong 0 \qquad [3]$$

The third term in Equation [3] can be shown to have an average value when $\dot{\phi}_X$ and $\dot{\phi}_Y$ are in-phase, sinusoidal motions. The average value of the first term, $I_z\ddot{\theta}$, turns out to be negligibly small (Appendix) so that the average value of $H\theta\dot{\phi}_Y$ must be opposed by an average value of $H\dot{\phi}_X$—and hence by an average gimbal drift rate $\dot{\phi}_X$—to maintain the balance of torques

$$-(H\dot{\phi}_X)_{avg} \cong (H\theta\dot{\phi}_Y)_{avg} \qquad [4]$$

Production of cross torque having an average value is demonstrated in Fig. 3. The two gimbals are oscillating sinusoidally and in phase, Fig. 3(a), and the gyro is responding essentially to the principal gyroscopic torque $H\dot{\phi}_X$

$$\ddot{\theta} \cong -\frac{H}{I_z}\dot{\phi}_X$$

or

$$\theta \cong \frac{H}{I_z\omega^2}\dot{\phi}_X$$

with ω the frequency of oscillation, Fig. 3(b).

Cross torque $H\theta\dot{\phi}_Y$ contains the product of two sine waves, and is therefore a sine-squared wave, Fig. 3(c), which has the average value

$$(T_c)_{avg} = \frac{1}{2}H\theta_{peak}\dot{\phi}_{Ypeak}$$

If $\dot{\phi}_Y$ had been 90 deg out of phase with $\dot{\phi}_X$ in Fig. 3, the cross torque would have had zero average value. Thus for an arbitrary phase between $\dot{\phi}_Y$ and θ, only the in-phase component produces torque having an average component:

$$(T_c)_{avg} = \frac{1}{2}H\theta_{peak}\dot{\phi}_{Ypeak}\cos(\angle\theta - \angle\dot{\phi}_Y)$$

which, by Equation [4], results in a drift rate

$$(\dot{\phi}_X)_{avg} = \frac{1}{2}\theta_{peak}\dot{\phi}_{Ypeak}\cos(\angle\theta - \angle\dot{\phi}_Y) \qquad [5]$$

Equation [5] is based on a situation which is entirely general (for small angles). It is therefore the general formula for rectification drift of an unrestrained, undamped, single-axis gyro.

Special Cases

The kinematic aspects of the mechanism of rectification can be studied by plotting motions on the unit sphere. Two special cases are especially instructive and easy to visualize; in the first, the platform is made to follow the inner gimbal, and in the second, the gyro frame. In the first case, the servo produces a steady gimbal drift in response to a false gyro signal caused by cross torque. In the second case, the servo fails to correct a gimbal drift produced by "gimbal walk" because the gyro fails to report it.

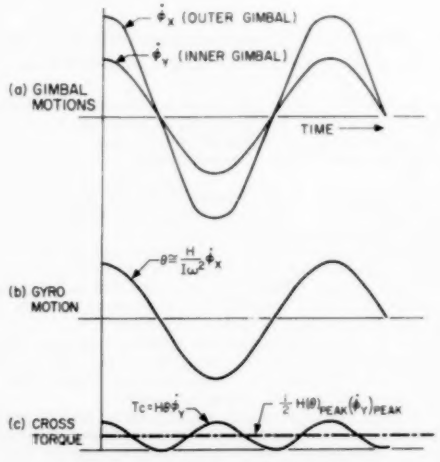

Fig. 3 Rectification of cross torque

Cross Torque. The motions of Fig. 3 are illustrated in Fig. 4 for the special case that ϕ_Z is 0 (i.e., the platform is clamped to the inner gimbal in Fig. 1). For this case, the gimbal motions of Fig. 3 simply cause the platform to rock about some point R as illustrated in Fig. 4. For this case, also, $\sigma = \theta$ (from Equation [2]), and Equation [3] becomes

$$I_s\ddot{\sigma} + H\dot{\phi}_X + H\theta\dot{\phi}_Y = 0$$

in which the average value of the first term is maintained dead zero by the servo. Therefore the servo also must provide the counter torque for $H\theta\dot{\phi}_Y$ by instigating the small steady drift $(\dot{\phi}_X)_{avg}$ required by Equation [5].

Gimbal Walk. Another special case is encountered in the study of rectification drift which emphasizes the subtleness of the phenomenon. This is the case of gimbal drift with a nulled pick-off ($\sigma = 0$), which is accomplished through superposition of just the right motion ϕ_Z upon the ϕ_X and ϕ_Y motions of Fig. 3. Specifically, ϕ_Z is caused to be exactly equal to (and in phase with) θ, Fig. 3(b), so that the platform and gyro move in unison in Fig. 1, and $\sigma = 0$, by Equation [2].

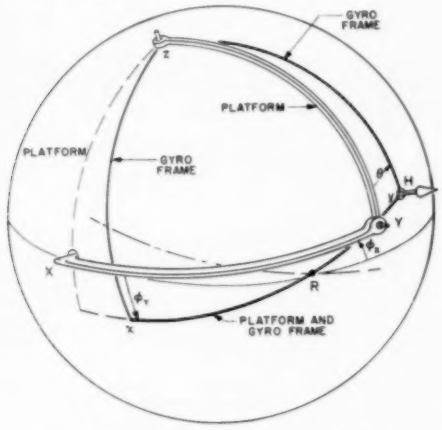

Fig. 4 Cross-torque motions with $\phi_z = 0$

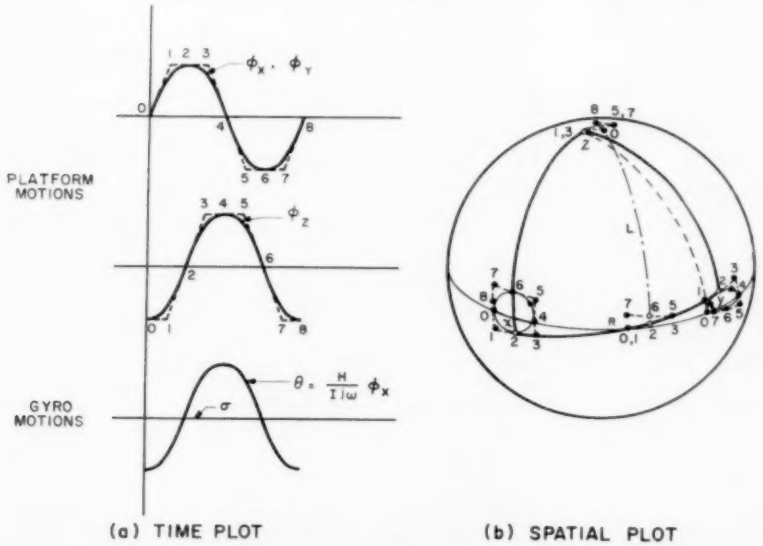

Fig. 5 Gimbal walk

The sequence of motions can be followed by considering, first, asymptotic approximations to the sinusoidal traces of Fig. 3. These are shown in Fig. 5(a). Thus at time 0, $\phi_Z = \theta$ has a negative value, and ϕ_X and ϕ_Y are zero, so that the octant sits in position O on the unit sphere. During time interval 0–1, ϕ_X and ϕ_Y change, but ϕ_Z does not, so that the octant rotates about point R. During interval 1–2–3, ϕ_X and ϕ_Y do not change, but there is a change in ϕ_Z so that the line x-y on the unit sphere slides along itself, point z remaining fixed. During interval 3–4–5, line x-y rotates about point R again, and during interval 5–6–7–8, it slides and rotates back to approximately its initial position. The squares described by the x and y-axes during this cycle do not quite close, however, because point R and point z are seen to have moved up along line L.

For the actual sinusoidal motion the x and y-axes form circles which do not quite close, and points R and z describe sine waves on the surface of the unit sphere, so that for successive cycles points R and z walk back and forth, always progressing along line L. Thus the platform has a steady drift rate which was not reported by the gyro—because its pick-off was always nulled—and was therefore unopposed by the servo.

In a sense, the special examples of Figs. 4 and 5 may be considered complementary, the first being a case of the gyro reporting a drift rate when none existed, and the second a case of the gyro failing to report a drift rate that did exist.

In both cases, however—and in general—the source of drift is the cross torque of Equation [3], and the rate of drift is given by Equation [5].

Experimental Verification

The arrangement of Fig. 1 has been duplicated carefully in the laboratory. Large oscillatory torques were applied to the gimbals so that the platform experienced substantial, sinusoidal motions.[5] Absolute platform angles ϕ_X, ϕ_Y, and ϕ_Z, were measured with precision optics and converted to electric signals to drive recording pens, alongside a pen recording gyro-pick-off angle σ.

With the gyro controlling platform attitude, ϕ_X, the "DC" component in the record of ϕ_X motion revealed the gyro drift rate directly.

Numerous combinations of sinusoidal platform motions were produced at several frequencies and relative phase angles. In each case, the expected drift rate was calculated by Equation [5] and compared with the measured drift rate, with the results shown in Fig. 6.

The drift produced with the gyro pick-off maintained at null ($\sigma = 0$), verifies explicitly the gimbal-walk analysis.

Remedial Measures

It is emphasized again that the special-test drift rates shown in Fig. 6 are very large, by operational standards, (a) because with proper installation disturbing torques on the stable element (even in high-speed aircraft) will be much smaller than those used in the tests, and (b) because major statistical cancellations accompany random disturbances.

[5] For convenience, much larger torques were used than any typical platform would see in normal use, so that the drift from rectification could be easily distinguished from drift due to other causes.

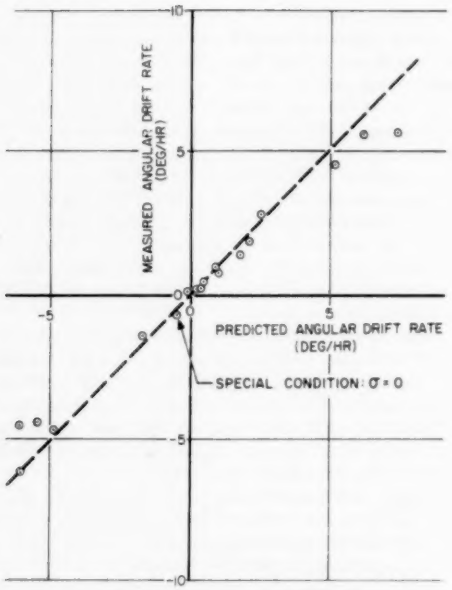

Fig. 6 Laboratory demonstration, using large oscillations

With the rectification phenomenon understood—and once the magnitudes of disturbing influences in the operational environment have been established—the stable platform, shock mount, and attendant equipment can be designed properly to limit drift from this cause to a level compatible with system tolerances.[6]

APPENDIX

Rigorous Derivation of Kinematic Drift

Let $\mathbf{H}$ be the total angular momentum of the gyro—wheel-plus-frame—in Fig. 1. This vector has the components

$$\mathbf{H} = \bar{1}_x I_x \Omega_x + \bar{1}_y (I_y \Omega_y + H) + \bar{1}_z I_z \Omega_z \quad [6]$$

in which H is the spin momentum of the wheel, I_x, I_y, and I_z are the moments of inertia of the wheel-plus-frame about each axis, and Ω_x, Ω_y, Ω_z are the components of the angular velocity of the gyro frame

$$\vec{\Omega} = \bar{1}_x \Omega_x + \bar{1}_y \Omega_y + \bar{1}_z \Omega_z \quad [7]$$

Newton's law for the wheel-plus-frame is

$$\left(\frac{d\mathbf{H}}{dt}\right)_{\text{inertial reference}} = \mathbf{M}$$

or, considering the gyro frame as a frame of reference

$$\left(\frac{d\mathbf{H}}{dt}\right)_{\text{wrt frame}} + \vec{\Omega} \times \mathbf{H} = \mathbf{M} \quad [8]$$

The z-components of the quantities in Equation [8] can be treated separately

$$\left(\frac{d\mathbf{H}}{dt}\right)_z + (\vec{\Omega} \times \mathbf{H})_z = 0$$

or, using Expressions [6] and [7],

$$I_z \dot{\Omega}_z - (I_x \Omega_x)\Omega_y + \Omega_x (I_y \Omega_y + H) = 0 \quad [9]$$

To study drift rates, it is necessary to relate the motions of the gyros to a fixed reference; e.g., via gimbal (Euler) angles defined in Figs. 1 and 2. Gyro motion is related to gimbal motions by the expression

$$\vec{\Omega} = \bar{1}_X \dot{\phi}_X + \bar{1}_Y \dot{\phi}_Y + \bar{1}_Z \dot{\theta} \quad [10]$$

from which the components of $\vec{\Omega}$ are obtained from the dot products

$$\left.\begin{aligned} \Omega_x &= \bar{1}_x \cdot \vec{\Omega} = \dot{\phi}_X + \theta\dot{\phi}_Y \\ \Omega_y &= \bar{1}_y \cdot \vec{\Omega} = \dot{\phi}_Y - \theta\dot{\phi}_X \\ \Omega_z &= \bar{1}_z \cdot \vec{\Omega} = \dot{\theta} + \phi_Y\dot{\phi}_X \end{aligned}\right\} \quad [11]$$

All angles—θ, ϕ_X, ϕ_Y, and ϕ_Z—are assumed to be very small. (Note again that x, y, and z are orthogonal gyro frame axes, while X, Y, and Z are gimbal axes, z and Z being always coincident.) When these are substituted into Equation [9], the gyro equation is obtained completely in terms of Euler angles

$$I_z \frac{d}{dt}(\dot{\theta} + \phi_Y\dot{\phi}_X) - I_x(\dot{\phi}_X + \theta\dot{\phi}_Y)(\dot{\phi}_Y - \theta\dot{\phi}_X) + I_y(\dot{\phi}_Y - \theta\dot{\phi}_X)(\dot{\phi}_X + \theta\dot{\phi}_Y) + H(\dot{\phi}_X + \theta\dot{\phi}_Y) = 0 \quad [12]$$

The term $\dot{\theta}$ is broken into its components by Equation [2], and the other terms in Equation [12] are grouped to give

$$I_z\ddot{\sigma} - (I_x - I_y)(\dot{\phi}_X + \theta\dot{\phi}_Y)(\dot{\phi}_Y - \theta\dot{\phi}_X) + H(\dot{\phi}_X + \theta\dot{\phi}_Y) + I_z \frac{d}{dt}(\dot{\phi}_Z + \phi_Y\dot{\phi}_X) = 0 \quad [13]$$

Finally, steady (nonoscillatory) motions are studied by integrating Equation [13] to give

$$I_z\dot{\sigma} - (I_x - I_y)\int(\dot{\phi}_X + \theta\dot{\phi}_Y)(\dot{\phi}_Y - \theta\dot{\phi}_X)dt + H\int(\dot{\phi}_X + \theta\dot{\phi}_Y)dt + I_z(\dot{\phi}_Z + \phi_Y\dot{\phi}_X) + C = 0 \quad [14]$$

in which C is the constant of integration.

It is now necessary to consider the terms in Equation [14] individually to determine the drift situation.

The first term, $I_z\dot{\sigma}$, cannot have a steady component because the servo will prevent any steady drift of the pick-off.

The second term

$$(I_x - I_y)\int(\dot{\phi}_X + \theta\dot{\phi}_Y)(\dot{\phi}_Y - \theta\dot{\phi}_X)dt$$

contains the product of small quantities and the difference between two nearly equal inertias, and will be small relative to the third term, which contains H. (H being greater—approximately by the wheel speed—than either I.) The terms $I_z(\dot{\phi}_Z + \phi_Y\dot{\phi}_X)$ and C may be small constant values of the same order as the component $(\dot{\phi}_X + \theta\dot{\phi}_Y)$ in the third term; however, the latter is integrated, so that after a time it would grow to an arbitrarily large value with respect to the other terms.

It is therefore concluded that the term $(\dot{\phi}_X + \theta\dot{\phi}_Y)$ must be exactly 0 in order for equation [14] to be satisfied. Thus it is, that if the quantity $\theta\dot{\phi}_Y$ has a steady component, the platform rate $\dot{\phi}_X$ must have an equal steady component, as given by Equation [5].

[6] "Stable Platforms for High-Performance Aircraft," by R. H. Cannon, Jr., and D. P. Chandler, Annual Summer Meeting of Institute of Aeronautical Sciences, June 19, 1957.

Co-Ordinates Which Uncouple the Equations of Motion of Damped Linear Dynamic Systems[1]

By K. A. FOSS,[2] CAMBRIDGE, MASS.

Orthogonality relations between the eigenvectors of damped linear dynamic systems with lumped parameters are derived; and from these relations co-ordinates are found in terms of which uncoupled equations of motion can be written. Methods are developed for determining transient stresses in terms of these co-ordinates. The present treatment is extended to systems involving transient damping and to continuous systems.

Introduction

THE EQUATIONS of motion of a damped linear dynamic system with lumped parameters can be written in matrix notation as

$$[m_{ij}]\{\ddot{q}_j\} + [r_{ij}]\{\dot{q}_j\} + [k_{ij}]\{q_j\} = \{f_i(t)\} \quad \ldots\ldots [1]$$

The classical method of solving these equations is to find the normal modes of oscillation of the homogeneous equation

$$[m_{ij}]\{\ddot{q}_j\} + [k_{ij}]\{q_j\} = \{0\} \quad \ldots\ldots [2]$$

and from these modes to determine a set of normal co-ordinates in terms of which there is no inertial or elastic coupling between the equations of motion. However, unless the matrix $[r]$ happens to be proportional to either $[m]$ or $[k]$, velocity coupling still exists, and the chief object of using normal co-ordinates is defeated except when the coupling terms are small and can be neglected.

The purpose of the present paper is to derive orthogonality relations between the homogeneous solutions of Equation [1], and from these relations to develop a set of co-ordinates in terms of which completely uncoupled equations of motion can be written.

Homogeneous Solutions

Equation [1] can be written in reduced[3] form as

$$[R]\{\dot{Z}\} + [K]\{Z\} = \{F(t)\} \quad \ldots\ldots [3]$$

where

$$[R] = \begin{bmatrix} [0] & [m] \\ [m] & [r] \end{bmatrix}, \qquad [K] = \begin{bmatrix} -[m] & [0] \\ [0] & [k] \end{bmatrix}$$

$$\{Z\} = \begin{bmatrix} \{\dot{q}\} \\ \{q\} \end{bmatrix}, \qquad \{F(t)\} = \begin{bmatrix} \{0\} \\ \{f(t)\} \end{bmatrix}$$

To obtain the homogeneous solution of Equation [3], let

$$\{Z(t)\} = e^{\alpha t}\{\Phi\} \quad \ldots\ldots [4]$$

This gives

$$\alpha[R]\{\Phi\} + [K]\{\Phi\} = \{0\} \quad \ldots\ldots [5]$$

Equation [5] may be manipulated into a form more amenable to matrix iteration, such as

$$[U]\{\Phi\} = \frac{1}{\alpha}\{\Phi\} \quad \ldots\ldots [6]$$

where

$$[U] = -[K]^{-1}[R] = \begin{bmatrix} [0] & [I] \\ -[c][m] & -[c][r] \end{bmatrix}$$

and where

$$[c] = [k]^{-1}$$

The matrix $[c]$ is a set of flexibility influence coefficients.

The solution of Equation [5] or [6] will yield $2N$ eigenvalues and eigenvectors

$$\alpha_n \quad \text{and} \quad \{\Phi^{(n)}\} = \begin{bmatrix} \alpha_n\{\phi^{(n)}\} \\ \{\phi^{(n)}\} \end{bmatrix}, \quad n = 1, 2, \ldots, 2N$$

where N is the number of degrees of freedom. For a stable system each α_n is either real and negative or complex with a negative real part. The complex roots occur as complex conjugate pairs with corresponding complex conjugate modal columns. A relatively simple method of iterating Equation [6] for complex eigenvalues and eigenvectors is described by Frazer, Duncan, and Collar.[3]

If the matrices $[m]$, $[r]$, and $[k]$ are symmetric, the matrices $[R]$ and $[K]$ are symmetric, and Equation [5] can be written in either of the two ways

$$\alpha_n[R]\{\Phi^{(n)}\} + [K]\{\Phi^{(n)}\} = \{0\} \quad \ldots\ldots [7]$$

and

$$\alpha_m\{\Phi^{(m)}\}^T[R] + \{\Phi^{(m)}\}^T[K] = \{0\}^T \quad \ldots\ldots [8]$$

where the superscript T denotes a transposed matrix. The premultiplication of Equation [7] by $\{\Phi^{(m)}\}^T$ and the postmultiplication of Equation [8] by $\{\Phi^{(n)}\}$ yields

$$\alpha_n\{\Phi^{(m)}\}^T[R]\{\Phi^{(n)}\} + \{\Phi^{(m)}\}^T[K]\{\Phi^{(n)}\} = 0 \quad \ldots\ldots [9]$$

and

$$\alpha_m\{\Phi^{(m)}\}^T[R]\{\Phi^{(n)}\} + \{\Phi^{(m)}\}^T[K]\{\Phi^{(n)}\} = 0 \quad \ldots\ldots [10]$$

When Equation [10] is subtracted from Equation [9], one obtains

$$(\alpha_n - \alpha_m)\{\Phi^{(m)}\}^T[R]\{\Phi^{(n)}\} = 0 \quad \ldots\ldots [11]$$

Thus unless $\alpha_m = \alpha_n$, the orthogonality relations are

[1] The results presented in this paper were obtained in the course of research sponsored by the Office of Naval Research, under Contract N5ori-07833, with the Massachusetts Institute of Technology.

[2] Research Engineer, Aeroelastic and Structures Research Laboratory, Massachusetts Institute of Technology.

[3] "Elementary Matrices," by R. A. Frazer, W. J. Duncan, and A. R. Collar, Cambridge University Press, London, England, 1946, p. 327.

Contributed by the Applied Mechanics Division and presented at the Annual Meeting, New York, N. Y., December 1–6, 1957, of THE AMERICAN SOCIETY OF MECHANICAL ENGINEERS.

Discussion of this paper should be addressed to the Secretary, ASME, 29 West 39th Street, New York, N. Y., and will be accepted until October 10, 1958, for publication at a later date. Discussion received after the closing date will be returned.

NOTE: Statements and opinions advanced in papers are to be understood as individual expressions of their authors and not those of the Society. Manuscript received by ASME Applied Mechanics Division, May 24, 1957. Paper No. 57—A-86.

$$\{\Phi^{(m)}\}^T[R]\{\Phi^{(n)}\} = 0, \quad \text{when } m \neq n \ldots\ldots [12]$$

and

$$\{\Phi^{(m)}\}^T[K]\{\Phi^{(n)}\} = 0, \quad \text{when } m \neq n \ldots\ldots [13]$$

Equation [12] can be used to construct "sweeping matrices" when one iterates Equation [6]. In fact, if there are "rigid body" modes present ($\alpha_n = 0$), these modes must be eliminated from Equation [5] to make Equation [6] nonsingular.

Nonhomogeneous Solutions

Nonhomogeneous solutions of Equations [1] or [3] can be obtained by expanding $\{Z\}$ into a modal series; i.e., by letting

$$\{Z\} = \sum_n \{\Phi^{(n)}\}\xi_n(t) \ldots\ldots [14]$$

which is equivalent to Lagrange's method of variation of parameters (sometimes called the method of variation of constants). In terms of the new co-ordinates $\xi_n(t)$, Equation [3] becomes

$$\sum_n [R]\{\Phi^{(n)}\}\ddot{\xi}_n + \sum_n [K]\{\Phi^{(n)}\}\xi_n = \{F(t)\} \ldots. [15]$$

Premultiplication of Equation [15] by $\{\Phi^{(m)}\}^T$ gives

$$\sum_n \{\Phi^{(m)}\}^T[R]\{\Phi^{(n)}\}\ddot{\xi}_n + \sum_n \{\Phi^{(m)}\}^T[K]\{\Phi^{(n)}\}\xi_n = \{\Phi^{(m)}\}^T\{F(t)\} \ldots\ldots [16]$$

The orthogonality relations, Equations [12] and [13], simplify Equation [16] to

$$R_n\ddot{\xi}_n - \alpha_n R_n \xi_n = F_n(t) \ldots\ldots [17]$$

where

$$R_n = \{\Phi^{(n)}\}^T[R]\{\Phi^{(n)}\} = 2\alpha_n\{\phi^{(n)}\}^T[m]\{\phi^{(n)}\} + \{\phi^{(n)}\}^T[r]\{\phi^{(n)}\}$$

and

$$F_n(t) = \{\Phi^{(n)}\}^T\{F(t)\} = \{\phi^{(n)}\}^T\{f(t)\}$$

From the orthogonality relations it also can be shown that

$$\{F(t)\} = \sum_n \frac{F_n(t)}{R_n}[R]\{\Phi^{(n)}\} \ldots\ldots [18]$$

and

$$\{f(t)\} = \sum_n \frac{F_n(t)}{R_n}[\alpha_n[m] + [r]]\{\phi^{(n)}\} \ldots\ldots [19]$$

also that

$$\sum_n \frac{F_n(t)}{R_n}[m]\{\phi^{(n)}\} = \{0\} \ldots\ldots [20]$$

and

$$\sum_n \frac{F_n(t)}{R_n}\{\phi^{(n)}\} = \{0\} \ldots\ldots [21]$$

For zero initial conditions, the solution of Equation [17] is

$$\xi_n = \frac{1}{R_n}\int_0^t e^{\alpha_n(t-\tau)}F_n(\tau)d\tau \ldots\ldots [22]$$

and

$$\dot{\xi}_n = \frac{F_n(t)}{R_n} + \frac{\alpha_n}{R_n}\int_0^t e^{\alpha_n(t-\tau)}F_n(\tau)d\tau \ldots\ldots [23]$$

Thus the nonhomogeneous solution of Equation [1] is

$$\{q_i\} = \sum_n \frac{1}{R_n}\{\phi_i^{(n)}\}\int_0^t e^{\alpha_n(t-\tau)}F_n(\tau)d\tau \ldots\ldots [24]$$

and

$$\{\dot{q}_i\} = \sum_n \frac{\alpha_n}{R_n}\{\phi_i^{(n)}\}\int_0^t e^{\alpha_n(t-\tau)}F_n(\tau)d\tau \ldots\ldots [25]$$

If α_k and α_{k+1} are complex conjugate roots, the corresponding two terms of Equation [24] are

$$\sum_{n=k}^{k+1}\frac{1}{R_n}\{\phi_i^{(n)}\}\int_0^t e^{\alpha_n(t-\tau)}F_n(\tau)d\tau = \frac{2}{|R_k|}\int_0^t e^{-\zeta_k(t-\tau)}|F_k(\tau)|\{|\phi_i^{(k)}|\cos[\omega_k(t-\tau) - \theta_R + \theta_F + \theta_i]\}d\tau \ldots\ldots [26]$$

where

$$\alpha_k = -\zeta_k + i\omega_k$$
$$R_k = |R_k|e^{i\theta_R}$$
$$F_k(t) = |F_k(t)|e^{i\theta_F}$$
$$\{\phi_i^{(k)}\} = \{|\phi_i^{(k)}|e^{i\theta_i}\}$$

Dynamic Stresses

Two methods for determining the transient stresses in terms of the normal co-ordinates of a structure have been summarized by Bisplinghoff, Isakson, and Pian.[4] These two methods are commonly called the "mode-displacement method" and the "mode-acceleration method." Two analogous methods can be derived in terms of the co-ordinates of the present paper.

If Equation [1] represents the equations of motion of a flexible structure, a stress at point i in the structure is

$$\sigma_i = [s_i^{(i)}][k_{ij}]\{q_j(t)\} \ldots\ldots [27]$$

where $[s_i^{(i)}]$ is a row matrix which sums up the elastic forces to give the total stress σ_i. For the first method, substitute

$$\{q_j(t)\} = \sum_n \{\phi_j^{(n)}\}\xi_n(t) \ldots\ldots [28]$$

into Equation [27], which yields

$$\sigma_i = \sum_n^* A_n^{(i)}\xi_n(t) \ldots\ldots [29]$$

where

$$A_n^{(i)} = [s^{(i)}][k]\{\phi^{(n)}\} = -\alpha_n^2[s^{(i)}][m]\{\phi^{(n)}\} - \alpha_n[s^{(i)}][r]\{\phi^{(n)}\}$$

and where the starred summation symbol indicates that rigid-body modes are not included. Equation [29] is analogous to the mode-displacement method.

For the second method, Equation [17] can be rearranged as

$$\xi_n = \frac{F_n(t)}{-\alpha_n R_n} + \frac{\dot{\xi}_n}{\alpha_n} \ldots\ldots [30]$$

The substitution of this into Equation [29] gives

$$\sigma_i = \sigma_{i(\text{static})} + \sum_n^* \frac{A_n^{(i)}}{\alpha_n}\dot{\xi}_n \ldots\ldots [31]$$

[4] "Methods in Transient Stress Analysis," by R. L. Bisplinghoff, G. Isakson, and T. H. H. Pian, *Journal of the Aeronautical Sciences*, vol. 17, 1950, p. 259.

where

$$\sigma_{i(\text{static})} = \sum_{n}^{*} \frac{A_n^{(i)} F_n(t)}{-\alpha_n R_n}$$

Equation [31] is analogous to the mode-acceleration method, and in this case it might be called the "mode-velocity method."

From Equation [19]

$$\{f(t)\} = \sum_{n}^{**} \frac{F_n(t)}{R_n} [r]\{\phi^{(n)}\} - \sum_{n}^{*} \frac{F_n(t)}{\alpha_n R_n} [k]\{\phi^{(n)}\} \quad [32]$$

where the double asterisk indicates that only rigid-body modes are included in the summation. Therefore

$$[s^{(i)}]\{f(t)\} = \sum_{n}^{**} \ddot{\xi}_n [s^{(i)}][r]\{\phi^{(n)}\} + \sum_{n}^{*} \frac{A_n^{(i)} F_n(t)}{-\alpha_n R_n} \quad [33]$$

and so

$$\sigma_{i(\text{static})} = [s^{(i)}]\{f(t)\} - \sum_{n}^{**} \ddot{\xi}_n s[^{(i)}][r]\{\phi^{(n)}\} \quad [34]$$

Thus through the use of Equation [31], the stress due to the applied forces can be accounted for exactly even when a limited number of vibration modes are used.

Transient Damping

Many problems in aeroelasticity require that the velocity in Equation [1] be replaced by a convolution integral containing the Wagner function; i.e., a single-degree-of-freedom equation of the same type as Equation [1] would become

$$m\ddot{q} + r\int_0^t \dot{q}(\tau)\phi(t-\tau)d\tau + kq = f(t) \quad [35]$$

where $\phi(t)$ is the Wagner function which accounts for unsteady flow effects. It can be shown by means of the Laplace transform that, if the usual exponential approximation of the Wagner function is used, Equation [35] is equivalent to a fourth-order differential equation of the type

$$a\dddot{q} + b\ddot{q} + c\dot{q} + dq + eq = g(t) \quad [36]$$

Thus Equation [1] becomes

$$[a_{ij}]\{\dddot{q}_j\} + [b_{ij}]\{\ddot{q}_j\} + [c_{ij}]\{\dot{q}_j\} + [d_{ij}]\{\dot{q}_j\} + [e_{ij}]\{q_j\} = \{g_i(t)\} \quad [37]$$

This also can be expressed in reduced form as

$$[R]\{\dot{Z}\} + [K]\{Z\} = \{F(t)\} \quad [38]$$

where now

$$[R] = \begin{bmatrix} [0] & [0] & [0] & [a] \\ [0] & [0] & [a] & [b] \\ [0] & [a] & [b] & [c] \\ [a] & [b] & [c] & [d] \end{bmatrix}$$

$$[K] = \begin{bmatrix} [0] & [0] & -[a] & [0] \\ [0] & -[a] & -[b] & [0] \\ -[a] & -[b] & -[c] & [0] \\ [0] & [0] & [0] & [e] \end{bmatrix}$$

$$\{Z\} = \begin{bmatrix} \{\dddot{q}\} \\ \{\ddot{q}\} \\ \{\dot{q}\} \\ \{q\} \end{bmatrix} \qquad \{F(t)\} = \begin{bmatrix} \{0\} \\ \{0\} \\ \{0\} \\ \{g(t)\} \end{bmatrix}$$

Continuous Systems

Orthogonality relations for continuous systems can be obtained in a manner analogous to that for lumped-parameter systems. Consider, for example, the damped motion of a simple beam. The equation of motion is

$$m(y)\ddot{z}(y,t) + r(y)\dot{z}(y,t) + \int_{y_0}^{y_1} k(y,\eta)z(\eta,t)d\eta = f(y,t) \quad [39]$$

where $k(y, \eta)$ is a stiffness influence function.[5] This equation can be written in reduced form as

$$\left.\begin{aligned} m(y)\dot{z}(y,t) - m(y)\zeta(y,t) &= 0 \\ m(y)\dot{\zeta}(y,t) + r(y)\dot{z}(y,t) + \int_{y_0}^{y_1} k(y,\eta)z(\eta,t)d\eta &= f(y,t) \end{aligned}\right\} \quad [40]$$

where

$$\zeta(y,t) = \dot{z}(y,t)$$

To obtain the homogeneous solution of Equations [39] or [40], let

$$z(y,t) = \phi(y)e^{\alpha t} \quad \text{and} \quad \zeta(y,t) = \beta(y)e^{\alpha t}$$

Equation [40] becomes

$$\left.\begin{aligned} \alpha m(y)\phi(y) - m(y)\beta(y) &= 0 \\ \alpha m(y)\beta(y) + \alpha r(y)\phi(y) + \int_{y_0}^{y_1} k(y,\eta)\phi(\eta)d\eta &= 0 \end{aligned}\right\} \quad [41]$$

The solution of Equations [41] would yield an infinite number of eigenvalues and eigenfunctions

$$\alpha_n \quad \text{and} \quad \beta_n(y) = \alpha_n\phi_n(y), \quad n = 1, 2, \ldots, \infty$$

This solution is not proposed as a method for computing the eigenfunctions but is convenient for deriving their orthogonality relations.

For the nth mode Equations [41] become

$$\left.\begin{aligned} \alpha_n m(y)\phi_n(y) - m(y)\beta_n(y) &= 0 \\ \alpha_n m(y)\beta_n(y) + \alpha_n r(y)\phi_n(y) + \int_{y_0}^{y_1} k(y,\eta)\phi_n(\eta)d\eta &= 0 \end{aligned}\right\} \quad [42]$$

If the first of Equations [42] is multiplied by $\beta_m(y)$ and the second by $\phi_m(y)$, and if the resulting equations are added together and integrated, the following equation is obtained

$$\alpha_n \int_{y_0}^{y_1} [m(y)\phi_n(y)\beta_m(y) + r(y)\phi_n(y)\phi_m(y) + m(y)\beta_n(y)\phi_m(y)]dy + \int_{y_0}^{y_1} \left[\int_{y_0}^{y_1} k(y,\eta)\phi_n(\eta)\phi_m(y)d\eta - m(y)\beta_n(y)\beta_m(y)\right] dy = 0 \quad [43]$$

In Equation [43] the subscripts m and n may be interchanged to give

$$\alpha_m \int_{y_0}^{y_1} [m(y)\phi_m(y)\beta_n(y) + r(y)\phi_m(y)\phi_n(y) + m(y)\beta_m(y)\phi_n(y)]dy + \int_{y_0}^{y_1} \left[\int_{y_0}^{y_1} k(y,\eta)\phi_m(\eta)\phi_n(y)d\eta - m(y)\beta_m(y)\beta_n(y)\right] dy = 0 \quad [44]$$

[5] "Aeroelasticity," by R. L. Bisplinghoff, H. Ashley, and R. L. Halfman, Addison-Wesley Publishing Company, Inc., Cambridge, Mass., 1955, p. 26.

When Equation [44] is subtracted from Equation [43], one obtains

$$(\alpha_n - \alpha_m)\int_{y_0}^{y_1} [m(y)\phi_n(y)\beta_m(y) + r(y)\phi_n(y)\phi_m(y) + m(y)\beta_n(y)\phi_m(y)]\,dy = 0 \quad \ldots\ldots [45]$$

because $k(y, \eta)$ is a symmetrical kernel. Thus the orthogonality relations are

$$\int_{y_0}^{y_1} [m(y)\phi_n(y)\beta_m(y) + r(y)\phi_n(y)\phi_m(y) + m(y)\beta_n(y)\phi_m(y)]dy = 0, \quad \text{when} \quad m \neq n \quad \ldots\ldots [46]$$

and

$$\int_{y_0}^{y_1} \left[\int_{y_0}^{y_1} k(y, \eta)\phi_n(\eta)\phi_m(y)d\eta - m(y)\beta_n(y)\beta_m(y)\right] dy = 0, \quad \text{when} \quad m \neq n \quad \ldots\ldots [47]$$

Through these results, uncoupled equations of motion simillar to Equation [17] can be derived for this continuous system.

Acknowledgment

The author wishes to thank Prof. T. H. H. Pian for suggestions which made the derivations more straightforward and concise. The manuscript of this paper was typed by Miss Iris G. Ellis.

Some Shock Spectra Characteristics and Uses

By Y. C. FUNG[1] and M. V. BARTON,[2] LOS ANGELES, CALIF.

A shock spectrum is a plot showing the peak response of a linear variable-frequency oscillator (of single degree of freedom) to a specific shock wave, as a function of the frequency of the oscillator. Such a spectrum may be measured, for example, by multifrequency reed gages and is sometimes used as a basis either for specifying the shock wave or for computing the response of a multi-degree-of-freedom structure to such a shock. In this paper these applications of the shock spectrum are discussed. In particular, it is shown that, if the fundamental frequency (f_1, cps) of the structure is sufficiently high, a close approximation of the peak response of a multi-degree-of-freedom system can be obtained by the algebraic sum (not the sum of absolute values) of the peak responses of the individual degrees of freedom. Numerical results for a uniform cantilever beam subjected to a shock load uniformly distributed over its span show that the high-frequency requirement is satisfied if $2f_1t_m \geq 1$, where t_m(sec) is the rise time of the pulse.

Introduction

A SHOCK spectrum of a suddenly applied force represents the peak response of a single-degree-of-freedom spring-mass-dashpot system as a function of the frequency of the system (1–4).[3] Such spectra are relatively easy to obtain by means of reed gages or other instruments (4, 5) under conditions of blast waves, collisions of vehicles, or landing impacts for which the applied shock forces are difficult to measure.

It was an important discovery by Shapiro and Hudson (4, 6) that there exist certain general properties of the shock spectrum for a single pulse which are insensitive to certain details of the impact history. On the other hand, it is well known (2, 5, 8) that multiple-pulse shocks such as those of earthquakes, train collisions, and ground motion due to blast waves yield complicated shock spectra which are very sensitive to the amount of damping. Only the single-pulse type of shocks will be discussed in this paper.

How can the shock spectra be used to estimate the shock response of complicated structures such as buildings, electronic equipment packages, or airframes? One of the earliest answers was given by Biot (1) in connection with engineering seismology, in which he disposed of the multi-degree-of-freedom response problem by the superposition of the absolute values of the maximum responses of each mode. Housner (2) showed, by statistical studies of strong-motion earthquakes, that this type of superposition of modes is not overconservative in engineering seismology. The same reasoning was applied by Biot and Bisplinghoff (3) to the more or less single-pulse-type shocks of the aircraft landing, with results that were too conservative (7, 9). Much effort has been spent on improving the accuracy of estimating the response of multi-degree systems, and alternative procedures have been suggested (6, 10, 13).

The purpose of this paper is (*a*) to indicate for single-pulse-type shocks some of the properties of the shock spectrum which can be stated in general form; (*b*) to extend Shapiro and Hudson's work to show that with proper normalization certain properties of the shock spectra are insensitive to certain details of the shock history; (*c*) to assess the practical use of such spectra to determine the response of multi-degree-of-freedom systems.

Shock Spectra for Shocks of Single-Pulse Type

Let $aF(t)$ be a more or less rapidly applied force, or shock, Fig. 1, and let the force act on a single-degree-of-freedom, linear spring-mass-dashpot system. If q is the displacement of the mass of the system, the equation for the motion is

$$\ddot{q} + 2\epsilon\omega\dot{q} + \omega^2 q = \frac{aF(t)}{m} \quad \ldots\ldots\ldots\ldots [1]$$

where ϵ is the ratio of actual damping to the critical damping of the oscillator, ω is the natural frequency of the oscillator, and m is the mass. The solution of this equation for the case of small damping, $\epsilon \ll 1$, and for a system initially at rest, so that $q(0) = \dot{q}(0) = 0$, is

$$q = \frac{1}{m\omega}\int_0^t aF(\tau)e^{-\epsilon\omega(t-\tau)} \sin \omega(t-\tau)d\tau \ldots\ldots [2]$$

Other parameters being fixed, the response q is a function of t and ω. Of particular interest is the maximum value of q which is given by

$$q_{\max}(\omega) = \max_{0<t}\left\{\frac{1}{m\omega}\int_0^t aF(\tau)e^{-\epsilon\omega(t-\tau)} \sin \omega(t-\tau)d\tau\right\} \ldots [3]$$

Then $q_{\max}$ is a function of ω and is defined as the shock spectrum of the given shock $aF(t)$ or, more specifically, the positive-displacement spectrum.

Similarly, $q_{\min}(\omega)$ may be called the negative displacement spectrum, $\dot{q}_{\max}(\omega)$ a positive velocity spectrum, $\ddot{q}_{\max}(\omega)$ a positive acceleration spectrum, and so forth.

For impact forces of the single-pulse type, Fig. 1, the characteristics of importance are the rise time t_m during which the force rises monotonically to a peak value of a, the duration of the pulse t_0, and the general shape of the curve. We shall express the pulse in the dimensionless form $F(t)$, for which

$$F(t) = 0 \quad \text{for } t \leq 0 \quad \text{and } t \geq t_0$$

$$\geq 0 \quad \text{for} \quad t \text{ in } (0, t_0)$$

$$\text{Max } F(t) = F(t_m) = 1$$

---

[1] Associate Professor, California Institute of Technology, and Consultant, The Ramo-Wooldridge Corporation.

[2] Manager, Engineering Mechanics Department, The Ramo-Wooldridge Corporation. Mem. ASME.

[3] Numbers in parentheses refer to the Bibliography at the end of the paper.

Presented at the West Coast Conference of the Applied Mechanics Division, Los Angeles, Calif., September 8–10, 1958, of THE AMERICAN SOCIETY OF MECHANICAL ENGINEERS.

Discussion of this paper should be addressed to the Secretary, ASME, 29 West 39th Street, New York, N. Y., and will be accepted until October 10, 1958, for publication at a later date. Discussion received after the closing date will be returned.

NOTE: Statements and opinions advanced in papers are to be understood as individual expressions of their authors and not those of the Society. Manuscript received by ASME, Applied Mechanics Division, October 11, 1957. Paper No. 58—APM-5.

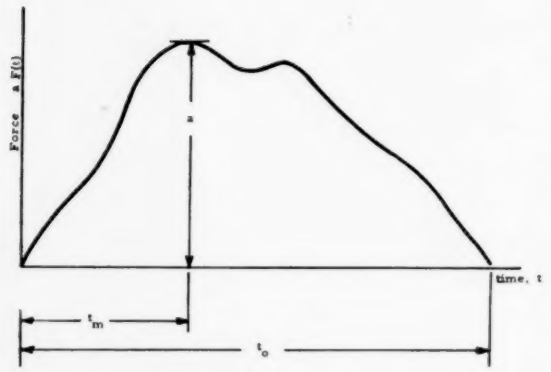

Fig. 1 An impact force-time history, or simply, a pulse, showing definitions of t_m, t_0

The response of a simple oscillator to such a pulse, Equation [2], is characterized by the following dimensionless parameters

$$2ft_m = \frac{\omega t_m}{\pi} = \frac{\text{rise time of pulse}}{\text{half period of oscillator}} \quad \ldots\ldots [4]$$

$$\frac{q(t)}{q_0} = \frac{m\omega^2 q(t)}{a} = \frac{\text{transient displacement response}}{\text{maximum static displacement}} \quad \ldots [5]$$

where $f = \omega/2\pi$ is the frequency of the oscillation in cycles per second, and

$$q_0 = \frac{a}{m\omega^2} \quad \ldots\ldots [6]$$

represents the static displacement of the mass under the peak applied load a, which will be assumed positive.

The dimensionless form of Equation [3] in which the extreme values of q_{max}/q_0 are given as a function of $\omega t_m/\pi$ is called the "positive dynamic amplification factor." Similarly, q_{min}/q_0 is called the "negative dynamic amplification factor." Fig. 2 shows the amplification spectra (solid curves) for two pulses. Note that the spectra start at the origin, rise gradually as $\omega t_m/\pi$ increases, reach maxima, then slope downward with more or less constant slope over a range of frequencies; they finally rise again, form a few ripples, and converge to unity. The negative spectra, although not shown here, behave similarly, except that for large values of $\omega t_m/\pi$ they converge to zero. The effect of a small damping on positive spectra is not large.

Also of interest is the ratio

$$\frac{t_p}{t_m} = \frac{\text{time at which peak response } q_{max} \text{ is reached}}{\text{rise time of pulse}}$$

which is also shown (dotted curves) in Fig. 2 for the two pulses. It is apparent that t_p/t_m is large for small values of ω and converges to unity as ω becomes large so that it does not deviate too much from unity for $\omega t_m/\pi > 2$. In other words, the peak response time corresponds approximately to the rise time when the rise time is long compared with the oscillation period.

Various characteristics of the amplification spectra have been determined mathematically and presented in (13). These characteristics are summarized later for a better understanding of the nature of the spectra and for practical applications. Many of these characteristics are well known; however, it is believed that properties (D), (F), (H), (I) are new. Unless otherwise stated, zero damping is assumed.

(A) For ω sufficiently small, the amplification factor is given

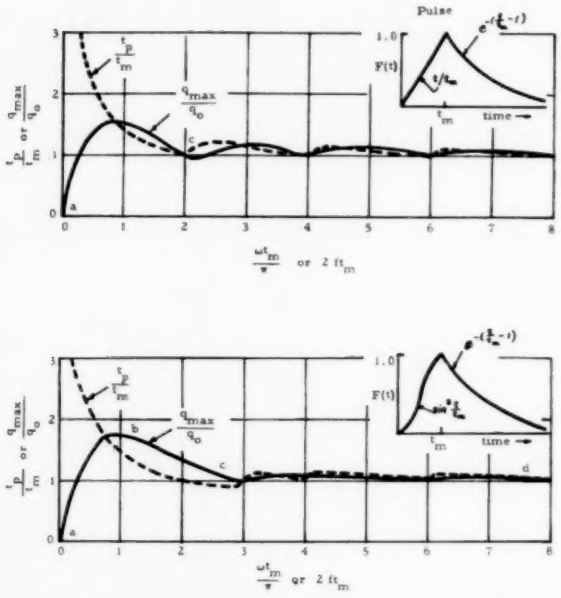

Fig. 2 Ratio of t_p to t_m, and of q_{max} to q_0, where t_p = time to peak response, t_m = rise time of pulse, q_{max} = peak dynamic response, q_0 = static response

by ω times the absolute value of the complex Fourier transform of $F(\tau)$

$$\frac{q_{max}}{q_0} = -\frac{q_{min}}{q_0} = \omega\left|\int_0^\infty F(\tau)e^{i\omega\tau}d\tau\right|, \quad \left(\frac{\omega t_m}{\pi} < \alpha\right) \ldots [7]$$

For a trapezoidal pulse, the number $\alpha = 1/2$.

(B) If $\omega \to 0$, the time t_p at which the response peak is reached approaches $\pi/2\omega$

$$t_p \to \frac{\pi}{2\omega} \quad \text{as} \quad \omega \to 0 \ldots\ldots [8]$$

(C) The slope of the spectrum at the origin ($\omega = 0$) is equal to the total impulse multiplied by the numerical factor π/t_m

$$\frac{d}{d(\omega t_m/\pi)}\left(\frac{q_{max}}{q_0}\right)_{\omega=0} = \frac{\pi}{t_m}\int_0^{t_0} F(\tau)d\tau$$

or

$$\frac{d}{d\omega}\left(\frac{q_{max}}{q_0}\right)_{\omega=0} = \int_0^{t_0} F(\tau)d\tau \ldots\ldots [9]$$

(D) Near the origin ($\omega = 0$), the curvature of the spectrum vanishes. A power-series expansion of the spectrum near the origin is

$$\frac{q_{max}}{q_0} = \mu_0\omega + \frac{1}{2}\left(\frac{\mu_1^2}{\mu_0} - \mu_2\right)\omega^3 + \frac{1}{24}\left(\mu_4 - 4\frac{\mu_1\mu_3}{\mu_0} + 6\frac{\mu_1^2\mu_2}{\mu_0^2} - 3\frac{\mu_1^4}{\mu_0^3}\right)\omega^5 + \ldots\ldots [10]$$

where

$$\mu_k \equiv \int_0^\infty \tau^k F(\tau)d\tau, \quad (k = 0, 1, 2, \ldots) \ldots\ldots [11]$$

is the kth "moment" of the pulse about the origin. If the damping does not vanish, the power-series expansion reads

$$\frac{q_{max}}{q_0} = e^{-\epsilon\frac{\pi}{2}}\left\{\mu_0\omega + \left[\frac{\mu_1^2}{2\mu_0} - \frac{\mu_2}{2} + \epsilon^2\left(\frac{1}{2} - \mu_2 + \frac{1}{2}\frac{\mu_1^2}{\mu_0}\right)\right]\omega^3 + \left[\left(\frac{\epsilon}{6} - \frac{\epsilon^2}{2} - \frac{\epsilon^3}{3}\right)\mu_2 + (\epsilon + \epsilon^3)\frac{\mu_1\mu_2}{\mu_0} + \left(-\frac{7}{6}\epsilon + \frac{1}{3}\epsilon^3\right)\frac{\mu_1^3}{\mu_0^2}\right]\omega^4 + \ldots\right\} \quad [12]$$

These expansions have a bearing on the question of inverting the integral Equation [3]. They show that the μ's are related to the successive derivatives of the shock spectrum at the origin but that the number of these equations is insufficient to determine all the μ's. Hence an inversion cannot be obtained by defining a shock spectrum as a Taylor's series about the origin.

(E) At large values of ω the response approaches a static one

$$\left.\begin{aligned}\lim_{\omega\to\infty}\frac{q(t)}{q_0} &= F(t)\\ \lim_{\omega\to\infty}\frac{q_{max}}{q_0} &= 1\\ \lim_{\omega\to\infty}\frac{q_{min}}{q_0} &= 0\end{aligned}\right\} \quad [13]$$

(F) An asymptotic expansion for the response $q(t)/q_0$ for large values of ω is

$$\frac{q(t)}{q_0} = F(t) - \frac{1}{\omega}\sin\omega t\,\dot{F}(0) + \frac{1}{\omega^2}[(\cos\omega t - 1)\ddot{F}(0) - tF^{(3)}(\theta t)] + \frac{1}{\omega^3}\sin\omega t\,F^{(3)}(\theta t), \quad (0 \le \theta \le 1) \quad [14]$$

If $F(t)$ can be approximated by a polynomial of degree n, then the indeterminate factor θ can be removed.

$$\frac{q(t)}{q_0} = F(t) - \frac{1}{\omega}\sin\omega t\,\dot{F}(0) + \frac{1}{\omega^2}\left[(\cos\omega t - 1)\ddot{F}(0) - \sum_{r=1}^{n-2}\frac{t^r}{r!}F^{(r+2)}(0)\right] + \frac{1}{\omega^3}\sin\omega t\,F^{(3)}(0) + \ldots \quad [15]$$

Hence it is clear that q/q_0 converges to $F(t)$ when $\omega \to \infty$, but the exact form depends on the higher derivatives of $F(t)$ at $t = 0$.

(G) The time t_p at which the response peak is reached approaches the rise time t_m as ω becomes large

$$t_p \to t_m \quad \text{when} \quad \frac{\omega t_m}{\pi} > b \quad [16]$$

The number b depends on the particular pulse, but is of order 2.

(H) For larger values of ω

$$\frac{q_{max}}{q_0} \cong 1 - \frac{\dot{F}(0)}{\omega}\sin\omega t_m + 0\left(\frac{1}{\omega^2}\right) \quad [17]$$

which shows that the wavy curve of the spectrum which converges to 1 as ω increases has a "period"

$$\Delta\omega t_m \cong 2\pi \quad [18]$$

This expression can be used to estimate t_m from an experimentally determined spectrum.

(I) For a given frequency ω_1, the time t_p at which the first peak of the response is reached [at which $\dot{q}(t)$ vanishes for the first time] is governed by the equation

$$\tan\omega_1 t_p = -\frac{\int_0^{t_p} F(\tau)\cos\omega_1\tau d\tau}{\int_0^{t_p} F(\tau)\sin\omega_1\tau d\tau} \quad [19]$$

This time t_p is also the time at which q_{max} is reached for at least the following types of the rising curve of the pulse: A straight line, a half sine, a versed sine, or an exponential curve, or the theoretical and experimental landplane and seaplane landing impact-load curves (6). The corresponding amplification factor, written as u_1, is

$$u_1 = \frac{q_{max}(\omega_1)}{q_0} = \omega_1\int_0^{t_p} F(\tau)\sin\omega_1(t_p - \tau)d\tau \quad [20]$$

The slope of the positive amplification spectrum at ω_1 is

$$\left(\frac{du}{d\omega}\right)_{\omega_1} = \frac{u_1}{\omega_1} - \omega_1\int_0^{t_p}\tau F(\tau)\cos\omega_1(t_p - \tau)d\tau \quad [21]$$

The curvature at ω_1 is

$$\left(\frac{d^2u}{d\omega^2}\right)_{\omega_1} = -\frac{2}{\omega_1}\left[\left(\frac{du}{d\omega}\right)_{\omega_1} - \frac{u_1}{\omega_1}\right] - \omega_1\int_0^{t_p} F(\tau)(t_p - \tau)^2\sin\omega_1(t_p - \tau)d\tau + \frac{\omega_1^2}{1 - u_1}\left[\int_0^{t_p} F(\tau)(t_p - \tau)\sin\omega_1(t_p - \tau)d\tau\right]^2 \quad [22]$$

The formulas given in the last item (I) are of considerable interest in determining the spectrum in the intermediate-frequency range. One particular instance is of special significance; namely, the case in which $t_p = t_m$, i.e., the point at which the positive peaks of the response and the pulse are attained at exactly the same time. At this point the slope of the amplification spectrum depends only on the rising part of the pulse, and is completely independent of the falling curve. This point belongs to the portion of the spectrum where the curve is fairly straight and the negative slope is large (see Fig. 7, reference 4). Specific examples are given in (13). Here the slope of the positive spectrum

$$d\left(\frac{q_{max}}{q_0}\right)\Big/ d\left(\frac{\omega t_m}{\pi}\right)$$

is of order $-1/2$.

By means of Equation [22] it can be shown that a suggestion in reference (4) that the largest negative slope is reached in the case $t_p = t_m$ is not necessarily true.

Note that the case $u_1 = 1$ corresponds in general to a discontinuous t_p versus $\omega t_m/\pi$ curve, and the expression for curvature may not necessarily hold.

Finally, the effect of small damping should be mentioned. In the intermediate-frequency range, the effect of ϵ on q_{max}/q_0 is small, but the effect on q_{min}/q_0 is large. The ratio of the leading-edge slope of q_{min}/q_0 to that of q_{max}/q_0 is equal to $e^{-2\pi\epsilon}$; i.e., approximately $1 - 2\pi\epsilon$. In the low and high-frequency ranges ($\omega t_m/\pi < 1/2$ or $\omega t_m/\pi > 3$), the effect of damping is sensitive to the pulse shape, and an increase in ϵ does not necessarily result in a reduction of the amplification factor.

Use of Shock Spectrum

The problem of the practical application of a shock spectrum

to determine something about the response of a complex structure is of considerable interest. It is convenient to express the characteristics of the structure in terms of the undamped principal modes which we will denote by

$$\phi_1(x, y, z), \quad \phi_2(x, y, z), \ldots, \phi_n(x, y, z)$$

which corresponds to circular frequencies $\omega_1, \omega_2, \ldots, \omega_n$, respectively (arranged in the order of ascending absolute values). The displacement, $w(x, y, z, t)$ at a point (x, y, z) of the structure, which will be assumed linear and elastic, can be expressed as

$$w(x, y, z, t) = \sum_{n=1}^{\infty} q_n(t)\phi_n(x, y, z) \ldots\ldots [23]$$

Assuming that positive damping exists and corresponds to a dissipation function that is a quadratic form in the generalized velocities of the same character as the kinetic-energy expression, the expansion of Equation [23] converges for all $t > 0$ and the Lagrange equations for the motion have the same form as Equation [1]

$$\ddot{q}_n + 2\epsilon_n\omega_n\dot{q}_n + \omega_n^2 q_n = \frac{Q_n(t)}{m_n}, \quad (n = 1, 2, \ldots) \ldots [24]$$

where

$$Q_n(t) = \int F(x, y, z, t)\phi_n(x, y, z)dv \ldots\ldots [25]$$

$$m_n = \int \phi_n^2(x, y, z)dm \ldots\ldots [26]$$

$Q_n(t)$ is the generalized force and m_n is the generalized mass in the nth degree of freedom; $F(x, y, z, t)$ is the external force density; dv is an element of structure volume, and dm is a mass element. The integrals are to be taken over the entire structure.

The shock-response problem for multi-degree-of-freedom systems can thus be solved formally. However, the determination of w from Equation [23] is very laborious. Also, in many cases the details of the forcing functions may not be known.

Often, in engineering design problems, only the maximum values of the elastic displacements or their derivatives are required. If the shock spectrum for the applied force is known, then something is known about the maximum values of the generalized displacements, $q_{max}(\omega)$, and one hopes to be able to say something about the maximum values of the displacement $\{w(x, y, z)\}_{max}$ from this information.

Biot (1) states an obvious upper bound

$$|w|_{max} \leq \sum_n |q_{n(max)}(\omega_n)||\phi_n(x, y, z)| \ldots\ldots [27]$$

which gives reasonable results for systems subjected to earthquake-type shocks, but may greatly overestimate the response of structures subjected to the single-pulse-type shock when the parameter $2 ft_m$ is sufficiently large.

It was pointed out previously that when the parameter $\omega t_m/\pi$, or $2 ft_m$, Equation [4], is sufficiently large, the response of an oscillator is such that the peak response is reached at about the same time as that of the pulse. In application to a multi-degree-of-freedom system, therefore, one may consider that all the degrees respond in unison; that is, all degrees reach the peak at the same time, provided that $\omega_n t_m/\pi$ are sufficiently large. Hence it is expected that, under the stated condition, a good estimate of the peak response is

$$\max_{t \geq 0} w(x, y, z, t) \doteq \sum_{n=1}^{N} q_{n(0)}(\omega_n)\left(\frac{q_{n(max)}(\omega_n)}{q_{n(0)}(\omega_n)}\right)\phi_n(x, y, z) \ldots [28]$$

We shall show that, in the case of a cantilever beam, the required condition is satisfied if

$$\frac{\omega_1 t_m}{\pi} \geq 1 \quad (\text{i.e., } 2ft_m \geq 1) \ldots\ldots [29]$$

where ω_1 is the circular frequency of the lowest mode. The Condition [29] is sufficient to insure a good approximation of the bending moment and shear in the beam derived from $w(x)$ by differentiation, to within a few per cent of the true values, throughout the entire beam.

Equation [28] is convenient to apply. $q_{n(0)}(\omega_n)$ is the static deflection of the nth degree of freedom. $q_{n(max)}(\omega_n)/q_{n(0)}(\omega_n)$ is given by the amplification spectrum, which, fortunately, is rather insensitive to the exact history of the pulse.

The applicability of Condition [29], however, cannot be established in complete generality. It is nevertheless believed, through a consideration of the spacing of the successive natural frequencies, that Condition [29] holds for general beams or plates under torsion and bending loads. For structures of which the fundamental frequency and the first few overtones are closer than the usual spacing of those of beams and plates, it may be necessary to redetermine a constant (instead of 1) in the right-hand side of Condition [29] in order to qualify Equation [28] as a good approximation.

The numerical data from which the Condition [29] is derived refer to a uniform cantilever beam subjected to an impact force distributed uniformly over its span. Let $\phi_n(x)$ be the normal modes, and ω_n the corresponding frequencies of the beam. Let $P(x)F(t)$ be the external disturbing force, $F(t)$ being of the type of a single pulse considered in the foregoing. Let

$$s_n = \int_0^l P(x)\phi_n(x)dx \ldots\ldots [30]$$

$$m_n = \int \phi_n^2(x)dm$$

= generalized mass corresponding to $\phi_n(x)$

The displacement at x may be written

$$w(x, t) \doteq \sum_{n=1}^{N} \phi_n(x)q_n(t)\frac{s_n}{|s_n|} \ldots\ldots [31]$$

where

$$\ddot{q}_n + 2\epsilon\omega_n\dot{q}_n + \omega_n^2 q_n = \frac{|s_n|}{m_n} F(t) \ldots\ldots [32]$$

The bending moment at x is then

$$M(x, t) = \sum_{n=1}^{N} M_n(x)q_n(t)\frac{s_n}{|s_n|} \ldots\ldots [33]$$

The shear at x is

$$S(x, t) = \sum_{n=1}^{N} S_n(x)q_n(t)\frac{s_n}{|s_n|} \ldots\ldots [34]$$

$M_n(x)$, $S_n(x)$ are, respectively, the moment and shear at x corresponding to $\phi_n(x)$. For a uniform cantilever beam of length l and clamped at $x = 0$, $\phi_n(x)$ is tabulated in (14). Using the notations of (14) we also have, if $P(x) = 1$

$$\left.\begin{aligned} s_n &= \int_0^l \phi_n(x)dx = \frac{2\alpha_n}{\beta_n} \\ m_n &= \int \rho\phi_n^2(x)dx = 1 \\ \frac{\omega_n}{\omega_1} &= \frac{\beta_n^2}{\beta_1^2} \end{aligned}\right\} \ldots\ldots [35]$$

$$M_n(x) = \frac{\omega_n^2}{\beta_n^2}\,\phi''(x)$$
$$S_n(x) = -\frac{\omega_n^2}{\beta_n}\,\phi'''(x) \quad \Big| \quad \text{(cont.)} \qquad \ldots\ldots\ldots [35]$$

α_n, β_n, ϕ_n, ϕ_n'', and ϕ_n''' are tabulated in (14). Two pulse shapes are considered

(A) $f(t) = t/t_m$ for $0 \le t \le t_m$

$$= \exp\left[-\left(\frac{t}{t_m} - 1\right)\right] \quad \text{for} \quad t \ge t_m \ldots\ldots [36]$$

(B) $f(t) = \sin^2\left(\frac{t}{t_m}\right) = \frac{1}{2}\left(1 - \cos\frac{\pi t}{t_m}\right)$ for $0 \le t \le t_m$

$$= \exp\left[-\left(\frac{t}{t_m} - 1\right)\right] \quad \text{for} \quad t \ge t_m \ldots\ldots [37]$$

The selection of these two pulses is based on a previous study which showed considerable difference in the amplification spectra owing to the presence or absence of a point of inflection on the rising part of the pulse. Fig. 2 shows the amplification spectra of these pulses, and the ratio t_p/t_m.

To compare the exact results with the approximations embodied in Approximations [27] and [28], respectively, the following quantities were computed

$$w^*(x) = \sum_{n=1}^{5} |\phi_n(x)| q_{n(\max)} \ldots\ldots [38]$$

$$w^{**}(x) = \sum_{n=1}^{5} \phi_n(x) \frac{\delta_n}{|\delta_n|} q_{n(\max)} \ldots\ldots [39]$$

$$M^*(x) = \sum_{n=1}^{5} |M_n(x)| q_{n(\max)} \ldots\ldots [40]$$

$$M^{**}(x) = \sum_{n=1}^{5} M_n(x) \frac{\delta_n}{|\delta_n|} q_{n(\max)} \ldots\ldots [41]$$

$$S^*(x) = \sum_{n=1}^{5} |S_n(x)| q_{n(\max)} \ldots\ldots [42]$$

$$S^{**}(x) = \sum_{n=1}^{5} S_n(x) \frac{\delta_n}{|\delta_n|} q_{n(\max)} \ldots\ldots [43]$$

The following ratios were then determined

$$\frac{w(x)_{\max}}{w^*(x)}, \quad \frac{w(x)_{\max}}{w^{**}(x)}$$

$$\frac{M(x)_{\max}}{M^*(x)}, \quad \frac{M(x)_{\max}}{M^{**}(x)}$$

$$\frac{S(x)_{\max}}{S^*(x)}, \quad \frac{S(x)_{\max}}{S^{**}(x)}$$

Five modes were taken. $q_{n(\max)}$ are the positive peak values of the response q_n as given by Equation [32]. $w(x)_{\max}$, $M(x)_{\max}$, and so on, are the peak values of w, M, and so on, at specified values of x/l (0, 0.2, 0.4, 0.6, 0.8, 1.0), calculated by a digital computer.

The results of $w(x)_{\max}/w^*(x)$ show that w^* is a good approximation; the maximum overestimation along the entire beam is less than 10 per cent for $0.25 < 2f_1 t_m < 4$. On the other hand, Fig. 3 shows that M^* overestimates the maximum bending moment considerably, near the free end, although the most important portion, the root bending moment, is well approximated.

Figs. 4 to 7 show the maximum and minimum of the ratios w/w^{**}, M/M^{**}, S/S^{**} across the entire beam. It is seen that, for $2f_1 t_m > 1$, the double-starred values approximate the exact values within a few per cent, thus verifying our Condition [29]. It is also seen that the approximation deteriorates rapidly as $2f_1 t_m$ be-

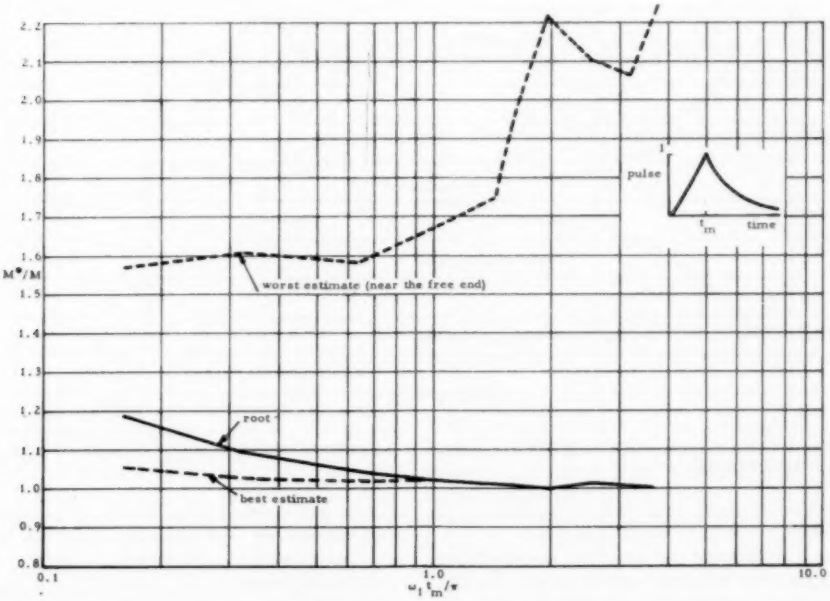

Fig. 3 Ratio M^*/M over beam. M is peak bending moment, M^* is approximation given by Equation [40]. Pulse A.

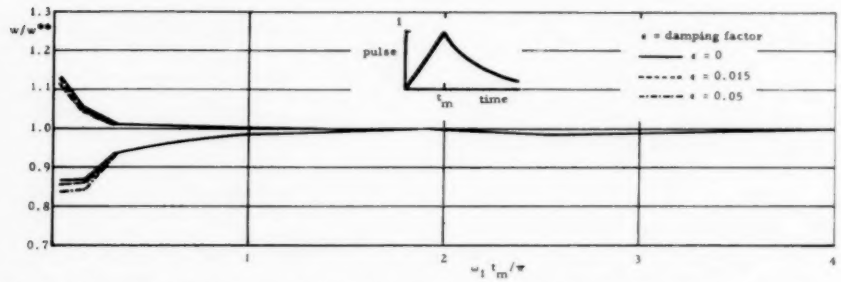

Fig. 4 Extreme values of ratio w/w^{**} over beam. w is maximum value of deflection, w^{**} is approximation given by Equation [39]. Pulse A.

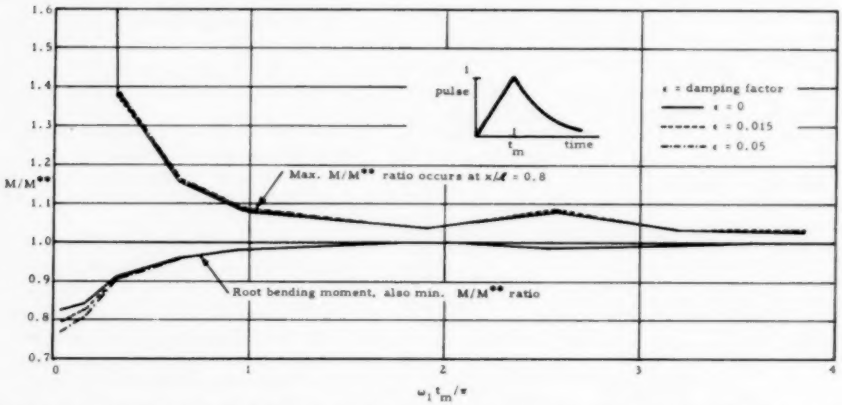

Fig. 5 Extreme values of ratio M/M^{**} over beam. M is maximum value of bending moment, M^{**} is approximation given by Equation [41]. Pulse A.

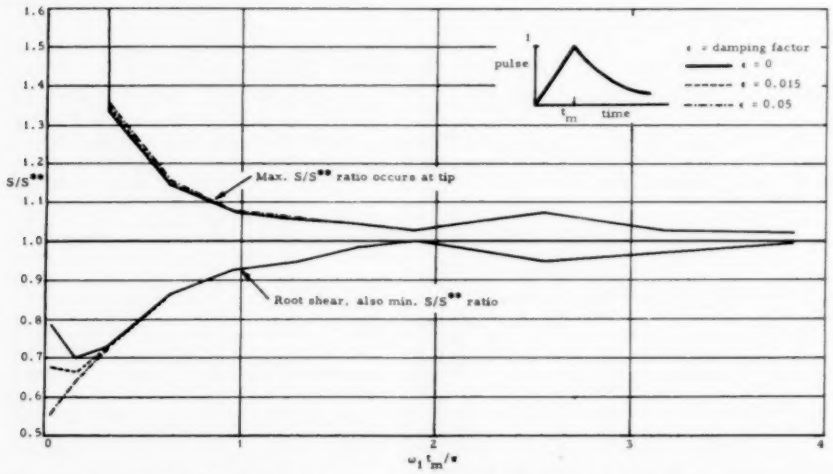

Fig. 6 Extreme values of ratio S/S^{**} over beam. S is maximum value of shear, S^{**} is approximation given by Equation [43]. Pulse A.

comes small. The effect of the damping factor ϵ (assumed to be the same for all modes), is seen to be small, Figs. 4 to 6.

So far, Approximations [27] and [28] have been examined over the entire beam on the basis of ratios to exact values. To give some idea about the actual variation of the deflection, moment, and shear, we plot the root bending moment, the root shear, and the tip deflection versus $\omega_1 t_m/\pi$ in Figs. 8 and 9. Here two cases must be distinguished: Fig. 8 refers to a fixed beam ($\omega_1 = .1$), hence the abscissa reads the variation of rise time; Fig. 9 refers to a fixed shock ($t_m = \pi$), hence the abscissa reads the varying fundamental frequency (stiffness) of the beam. The difference is evident from Approximation [28], for, although $q_{n(\max)}/q_{n(0)}$ is a function of $\omega_1 t_m$, $q_{n(0)}$ itself is inversely proportinal to ω_1^2. Fig. 8 shows that the root moment and shear are reasonably estimated

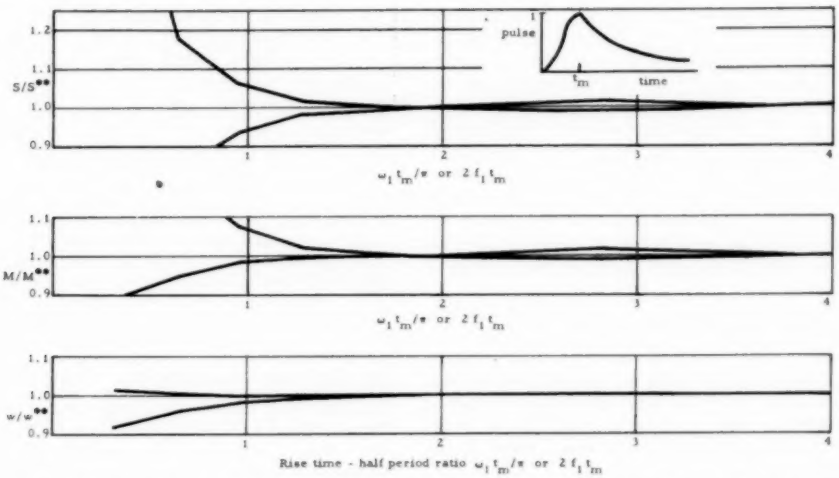

Fig. 7 Extreme values of S/S^{**}, M/M^{**}, w/w^{**} over beam. S, M, w are exact values of maximum response at any station. S^{**}, and so on, are approximations by Equations [43], [41], [39]. Damping factor $\epsilon = 0$. Pulse B.

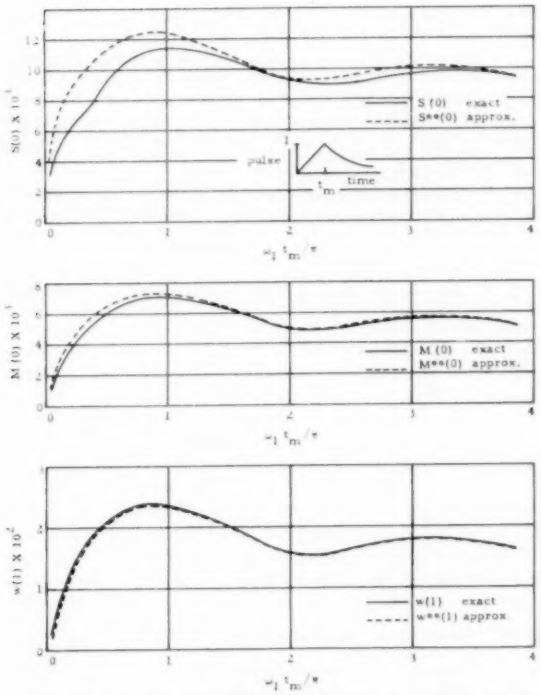

Fig. 8 Tip deflection, root bending moment, and root shear, in a cantilever beam whose fundamental frequency is $\omega_1 = 1$ rad per sec. Pulse rise time, t_m, varies. Mass of beam = 1. Pulse A.

by approximations of the type [28] for $\omega_1 t_m/\pi < 1$ as well. The tip-deflection estimation appears excellent over the entire $\omega_1 t_m/\pi$ range.

One must remark, finally, that if $\omega_1 t_m/\pi$ is very small so that the pulse acts like a pure impulse, the exact analysis of the structural response is fairly simple. For, if I_n is the total impulse that acts in the nth mode

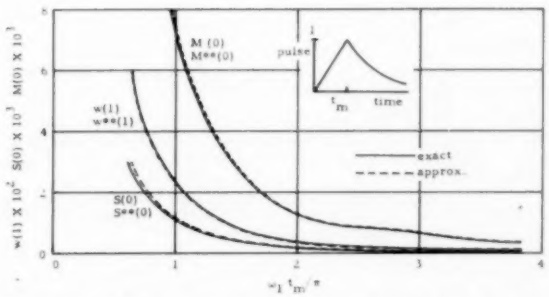

Fig. 9 Tip deflection, root bending moment, and root shear for cantilever beams of different fundamental frequency, ω_1. Fixed pulse rise time, $t_m = \pi$. Mass of beam = 1. Pulse A.

$$I_n = \int_0^t \int_0^l aF(x, t)\phi_n(x)dxdt \quad \ldots\ldots [44]$$

then

$$q_n(t) = \frac{I_n}{m_n\omega_n} e^{-\epsilon n\omega_n t} \sin \omega_n t \quad \ldots\ldots [45]$$

whence

$$w(x, t) = \Sigma q_n(t)\phi_n(x) \quad \ldots\ldots [46]$$

and other responses (stresses, and so forth) can be relatively easily derived.

Conclusions

With respect to shocks of the earthquake type, it seems that a statistical average of the spectrum offers a reasonable basis for engineering design, and that the representation of the maximum response of a multi-degree-of-freedom structure by the sum of the absolute values of the maximum response of individual degrees of freedom is adequate.

For a shock of the single-pulse type, the most important parameter characterizing the amplification spectrum is the ratio of rise time of pulse, t_m, to the half period of the oscillator; i.e., $\omega t_m/\pi$, or $2ft_m$. From an experimentally determined amplifica-

tion spectrum, the total impulse, the rise time, and the peak value of the pulse can be determined; but the complete determination of the pulse history appears to be impossible. In applying the amplification spectrum to the calculation of the maximum response of a multi-degree-of-freedom system, the upper bound derived by a simple summation of the absolute values of the peak responses of all degrees of freedom tends to be overconservative. If the fundamental (the lowest) frequency (ω_1 rad per sec or f_1 cps) of the structure is sufficiently high, say $\omega_1 t_m/\pi = 2f_1 t_m > 1$, a close approximation of the peak response of a multi-degree-of-freedom system can be obtained by the algebraic sum of the peak responses of the individual degrees of freedom.

The amplification spectrum is rather insensitive to the details of the exact history of the pulse. Hence in specifying a pulse form for engineering design purposes, there is little point in specifying the exact manner the pulse varies with time; in particular, the time history after the peak value of the pulse is reached is unimportant. Only the total impulse, the rise time, and when greater accuracy is desired, the time history of the rising curve, need be specified.

Acknowledgment

The help of Dr. John A. Brooks and the Digital Computing Center of R-W GMRD on the numerical analysis is gratefully acknowledged.

Bibliography

1 "A Mechanical Analyzer for the Prediction of Earthquake Stresses," by M. A. Biot, *Bulletin Seismological Society of America*, vol. 31, 1941, pp. 143–149.

2 "Spectrum Intensities of Strong-Motion Earthquakes," by G. W. Housner, Proceedings of the Symposium on Earthquake and Blast Effects in Structures, University of California, Los Angeles, Calif., 1952.

3 "Dynamic Loads in Airplane Structures During Landing," by M. A. Biot and R. L. Bisplinghoff, Wartime Report No. W-92 (A.R.R. 4H10), October, 1944.

4 "The Measurement of Acceleration Pulses With the Multi-frequency Reed Gage," by H. Shapiro and D. E. Hudson, JOURNAL OF APPLIED MECHANICS, TRANS. ASME, vol. 75, 1953, pp. 422–426.

5 "Railroad Switching Shock," by W. H. Cross and M. McWhirter, Sandia Corp., 1952.

6 "On the Dynamic Amplification Spectra of Landing Impacts," by Y. C. Fung, Report submitted to Bureau of Aeronautics, on Contract Noas 53-348-c, by Aer Inc., Pasadena, Calif., December, 1953.

7 "Studies of Transient Streases in an Airplane Model Wing During Drop Test," by O. N. Leal, R. L. Bisplinghoff, and T. H. H. Pian, *Proceedings of the Society for Experimental Stress Analysis*, vol. 6, 1948, p. 115.

8 "Spectrum Analysis of Strong-Motion Earthquakes," by G. W. Housner, R. R. Martel, and J. L. Alford, *Bulletin Seismological Society of America*, vol. 43, 1953, pp. 97–119.

9 "Experimental Verification of Theory of Landing Impact," by W. Ramberg and A. R. McPherson, National Bureau of Standards, *Journal of Research*, vol. 41, 1948, pp. 509–520.

10 "The Analysis of Dynamic Stresses in Aircraft Structures During Landing as Nonstationary Random Processes," by Y. C. Fung, JOURNAL OF APPLIED MECHANICS, TRANS. ASME, vol. 77, 1955, pp. 449–457.

11 "A Comparative Study of Pulse and Step-Type Loads on a Simple Vibratory System," by L. S. Jacobsen and R. S. Ayre, Vibration Research Laboratory, Stanford University, Report to Navy, Contract N6-ori-154 (NR-035-033), 1952.

12 "Effect of Impact on Simple Elastic Structures," by J. M. Frankland, David Taylor Model Basin, Report No. 481, 1942.

13 "Some Characteristics and Uses of Shock Spectra," by Y. C. Fung and M. V. Barton, Report No. AM 6-14, GM-TR-82, Engineering Mechanics Section, The Ramo-Wooldridge Corporation, Inglewood, Calif., October, 1956.

14 "Tables of Characteristic Functions Representing Normal Modes of Vibration of a Beam," by D. Young and R. P. Felgar, The University of Texas, Publication No. 4913, July, 1949.

15 "Analytical and Experimental Studies on Dynamic Loads in Airplane Structures During Landing," by T. H. H. Pian, *Journal of the Aeronautical Sciences*, vol. 17, December, 1950, pp. 765–774.

16 "A Mechanical Analyzer for Computing Transient Stresses in Airplane Structures," by R. L. Bisplinghoff, T. H. H. Pian, and L. I. Levy, JOURNAL OF APPLIED MECHANICS, TRANS. ASME, vol. 72, 1950, pp. 310–314.

17 "The Analysis of Strong-Motion Earthquake Records With the Electric Analog Computer," by G. W Housner and G. D. McCann, *Bulletin Seismological Society of America*, vol. 39, 1949, pp. 47–56.

18 "A Response Spectrum Analyzer for Transient Loading Studies," by T. Caughey and D. E. Hudson, *Proceedings of the Society for Experimental Stress Analysis*, vol. 13, 1955, pp. 199–206.

Coupled Vibrations of Thin-Walled Beams of Open Cross Section

By J. M. GERE[1] and Y. K. LIN[2]

The determination of coupled frequencies of free vibration for beams of nonsymmetric, open cross section is discussed in this paper. Beams with various end conditions, including simple supports, fixed ends and a cantilever, are considered. Results of both exact and approximate analyses are presented. For practical use, a simple approximate formula for determining frequencies of vibration for beams with any end conditions is given. The accuracy of the approximate formula is shown by comparison with results obtained by the exact method. The exact calculations were carried out on an IBM 605 Card Programmed Calculator.

1 Introduction

IF A BEAM of nonsymmetrical cross section is caused to vibrate freely, the resulting vibration is composed of both bending and torsion. These coupled bending and torsional vibrations occur whenever the shear center and the centroid of the cross section do not coincide.

In the most general situation, bending vibrations in two perpendicular directions are coupled with torsional vibrations. This case is called "triple coupling" and is illustrated by the nonsymmetrical channel section shown in Fig. 1(*a*). Point *O* represents the shear center and point *C* the centroid. The y and z-axes are through the shear center and parallel to the principal centroidal axes η and ζ. The figure shows the channel in its equilibrium position. Bending vibrations in the y and z-directions are coupled with torsional vibrations, measured by the angle of rotation ϕ.

When the beam cross section has an axis of symmetry, one of the bending vibrations is independent of the other vibrations. This results in "double coupling" between the other bending vibrations and the torsional vibrations, illustrated by the channel section shown in Fig. 1(*b*). Bending vibrations in the y-direction are coupled with torsional vibrations, whereas vibrations in the z-direction occur independently.

Finally, the simplest case arises when the shear center and centroid coincide, such as for an I-beam with two axes of symmetry, Fig. 1(*c*). The two bending vibrations and the torsional vibrations occur independently of one another.

In this paper, the differential equations for triple coupling are derived, following the development given by Timoshenko for double coupling.[3] The solution of these equations by an exact method is described, and the frequency equation for the case of simple supports is given. For other end conditions, the Rayleigh-Ritz method is used to derive an equation from which approximate values of frequencies may be found.

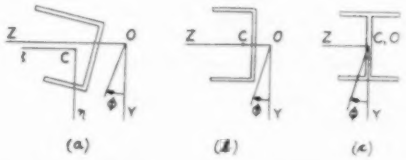

Fig. 1 Cross sections of beams typifying three cases of vibration

For double coupling, the results of determining the frequencies of vibration by the exact method are given for various end conditions of the beam, including simple supports, fixed ends, and a cantilever. A useful and simplified approximate method of determining frequencies for any end condition is also presented.

2 Equations of Coupled Vibrations

The equations of triple coupling may be derived by using d'Alembert's principle and substituting inertia forces into the equations of static equilibrium. Consider first a beam of arbitrary cross section, Fig. 2, where the y and z-axes are taken through the shear center *O* and parallel to the principal centroidal axes η and ζ. The equations for bending and nonuniform torsion under static loads are

$$EI_\zeta \frac{d^4v}{dx^4} = w_y, \quad EI_\eta \frac{d^4w}{dx^4} = w_z,$$

$$GC \frac{d^2\phi}{dx^2} - EC_w \frac{d^4\phi}{dx^4} = -w_t \quad \ldots\ldots [1]$$

where the following notation is used

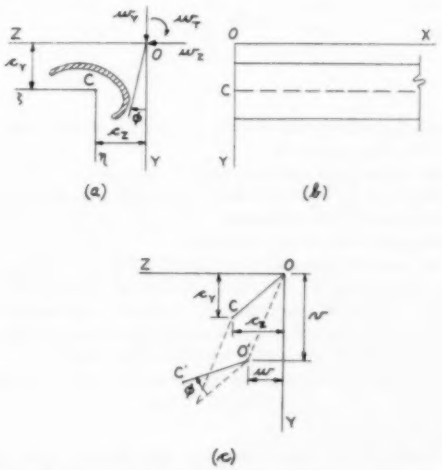

Fig. 2 Thin-walled beam of arbitrary cross section

[1] Associate Professor of Civil Engineering, Stanford University, Stanford, Calif.

[2] Stress Engineer, Vertol Aircraft Corporation, Morton, Pa.

[3] "Vibration Problems in Engineering," by S. P. Timoshenko, third edition in collaboration with D. H. Young, D. Van Nostrand Company, New York, N. Y., 1955, p. 407.

Contributed by the Applied Mechanics Division and presented at the Annual Meeting, New York, N. Y., December 1–6, 1957, of The American Society of Mechanical Engineers.

Discussion of this paper should be addressed to the Secretary, ASME, 29 West 39th Street, New York, N. Y., and will be accepted until October 10, 1958, for publication at a later date. Discussion received after the closing date will be returned.

Note: Statements and opinions advanced in papers are to be understood as individual expressions of their authors and not those of the Society. Manuscript received by ASME Applied Mechanics Division, April 11, 1957. Paper No. 57—A-26.

v, w = deflections of shear center in y and z-directions, respectively
ϕ = angle of rotation of cross section
w_y, w_z = intensities of distributed load acting along shear-center axis
w_t = intensity of distributed torque acting along shear-center axis
I_η, I_ζ = principal centroidal moments of inertia
C = torsion constant
C_w = warping constant
E = modulus of elasticity
G = modulus of elasticity in shear

When the beam vibrates, the inertia forces of translation in the y and z-directions are

$$-mA\,\frac{\partial^2}{\partial t^2}\,(v - \phi c_z),\quad -mA\,\frac{\partial^2}{\partial t^2}\,(w + \phi c_y)$$

as may be seen from Fig. 2(c). In the foregoing expressions, the following additional notation is used:

m = mass density of material of bar
A = cross-sectional area
t = time
c_y, c_z = co-ordinates of centroid C

Noting that the inertia forces of translation act through the centroid C, Fig. 2(a), and must be transferred to the shear center O in order to use Equations [1], it can be seen that the total inertia torque is

$$-mI_p\,\frac{\partial^2\phi}{\partial t^2} + mA\,\frac{\partial^2}{\partial t^2}\,(v - \phi c_z)c_z - mA\,\frac{\partial^2}{\partial t^2}\,(w + \phi c_y)c_y$$

where I_p is the polar moment of inertia of the cross section about the centroid C.

Substituting the inertia forces into Equations [1], three simultaneous differential equations of triple coupling are obtained

$$EI_\zeta\,\frac{\partial^4 v}{\partial x^4} + mA\,\frac{\partial^2 v}{\partial t^2} - mAc_z\,\frac{\partial^2\phi}{\partial t^2} = 0 \qquad [2]$$

$$EI_\eta\,\frac{\partial^4 w}{\partial x^4} + mA\,\frac{\partial^2 w}{\partial t^2} + mAc_y\,\frac{\partial^2\phi}{\partial t^2} = 0 \qquad [3]$$

$$EC_w\,\frac{\partial^4\phi}{\partial x^4} - GC\,\frac{\partial^2\phi}{\partial x^2} - mAc_z\,\frac{\partial^2 v}{\partial t^2} + mAc_y\,\frac{\partial^2 w}{\partial t^2} + mI_0\,\frac{\partial^2\phi}{\partial t^2} = 0 \qquad [4]$$

in which I_0 is the polar moment of inertia of the cross section about the shear center O.

If the z-axis is an axis of symmetry, Fig. 1(b), so that $c_y = 0$, then Equation [3] is independent and represents uncoupled bending vibrations in the z-direction.[4] Equations [2] and [4] reduce to the equations for double coupling.[5]

If the beam has two axes of symmetry, Fig. 1(c), then $c_y = c_z = 0$ and Equations [2], [3], and [4] become independent of one another. The first two equations represent uncoupled bending vibrations in the y and z-directions and the last equation reduces to the equation of uncoupled torsional vibrations.[6]

Solution of Equations. The equations for triple coupling were solved by taking the displacements v, w, and ϕ in the product form $X(x)T(t)$, where X is a normal function giving the shape of the mode of vibration. Substitution into Equations [2], [3], and [4] then yields three simultaneous ordinary differential equations for the normal functions, and also gives

$$T = A_n \cos p_n t + B_n \sin p_n t$$

where p_n is the radian frequency of vibration.

The three coupled equations for the normal functions were reduced to three independent equations by a procedure analogous to the solution of simultaneous algebraic equations. The result is an ordinary differential equation of 12th order for each normal function. These latter equations were solved by taking a solution in the exponential form De^{rz}, which leads to an auxiliary algebraic equation of 12th degree in r. Thus the expressions for the normal functions contain 12 arbitrary constants of integration as well as the values of r found from the auxiliary equation. The values of r depend on the radian frequency of vibration p_n, inasmuch as p_n also appears in the auxiliary equation. Thus there are 13 unknown quantities to be determined. Application of the boundary conditions at the ends of the beam makes it possible to determine 11 of the constants of integration in terms of the 12th, and also to obtain a frequency equation for p_n. There are two boundary conditions on v, w, and ϕ at each end of the bar, making a total of 12 conditions.[7] One of the constants of integration, representing the amplitude of the vibration, remains arbitrary.

The procedure for solving the equations of double coupling is similar to that just outlined, except that there are 8 constants of integration, instead of 12, appearing in the general solution and 8 boundary conditions for each beam. This general method of solution[8] was used to obtain values of frequencies for double coupling for beams with fixed ends, one end fixed and the other simply supported, and for cantilever beams. Because of the extremely lengthy computations, and since the solution must be by trial and error (assuming a value of frequency p_n at the beginning and then revising as necessary), it was found desirable to program the calculations on an IBM 605 Card Programmed Calculator. The results are presented in section 4.

For a simply supported beam it is possible to show[9, 10] that the normal functions are sine functions for both triple and double coupling, and hence the solution is greatly simplified. The result is a quadratic equation for the two frequencies of double coupling and a cubic equation giving the three frequencies of triple coupling, given in later sections.

3 Solution by Rayleigh-Ritz Method

The Rayleigh-Ritz method[11] may be used to determine approximate values for frequencies of coupled vibrations, and offers the advantage of much simpler calculations than the exact method. The method is based upon the principle of conservation of the total energy of the system. For a beam undergoing coupled vibrations, the strain energy U and kinetic energy T of the beam are

[4] Footnote 3, p. 325.
[5] Ibid., p. 409.
[6] "Torsional Vibrations of Beams of Thin-Walled Open Section," by J. M. Gere, JOURNAL OF APPLIED MECHANICS, TRANS. ASME, vol. 76, 1954, p. 381.
[7] The boundary conditions for bending are given in footnote 3, p. 331, et seq., and the boundary conditions for torsion are discussed in footnote 6.
[8] A more complete discussion of the solution of the differential equations for both triple and double coupling, for any end conditions, is given in footnote 9.
[9] "Bending and Torsional Vibrations of Thin-Walled Bars of Open Cross Section," by J. M. Gere, dissertation, Stanford University, Stanford, Calif., 1954.
[10] "Free Vibrations of Straight Bars With Thin-Walled and Open Cross Section" (German), by K. Federhofer, Sitzungsberichte der Wiener Akademie der Wissenschaften, *Math.-Natur. Klasse*, vol. 156, IIa, 1947, p. 393.
[11] See, for example, footnote 3, pp. 380–385.

$$U = \frac{EI_\xi}{2}\int_0^l \left(\frac{\partial^2 v}{\partial x^2}\right)^2 dx + \frac{EI_\eta}{2}\int_0^l \left(\frac{\partial^2 w}{\partial x^2}\right)^2 dx + \frac{EC_w}{2}\int_0^l \left(\frac{\partial^2 \phi}{\partial x^2}\right)^2 dx + \frac{GC}{2}\int_0^l \left(\frac{\partial \phi}{\partial x}\right)^2 dx \quad [5]$$

$$T = \frac{mA}{2}\int_0^l \left[\frac{\partial(v - \phi c_x)}{\partial t}\right]^2 dx + \frac{mA}{2}\int_0^l \left[\frac{\partial(w + \phi c_y)}{\partial t}\right]^2 dx + \frac{mI_p}{2}\int_0^l \left(\frac{\partial \phi}{\partial t}\right)^2 dx \quad [6]$$

After rearrangement of terms, Equation [6] may be written in the form

$$T = \frac{mA}{2}\left[\int_0^l \left(\frac{\partial v}{\partial t}\right)^2 dx + \int_0^l \left(\frac{\partial w}{\partial t}\right)^2 dx - 2c_x\int_0^l \frac{\partial v}{\partial t}\frac{\partial \phi}{\partial t}\,dx + 2c_y\int_0^l \frac{\partial w}{\partial t}\frac{\partial \phi}{\partial t}\,dx\right] + \frac{mI_0}{2}\int_0^l \left(\frac{\partial \phi}{\partial t}\right)^2 dx \quad [7]$$

If the origin for time is taken at the instant the beam is in the static equilibrium position, we may write

$$\left.\begin{aligned} v &= v_0 X_y \sin p_n t \\ w &= w_0 X_x \sin p_n t \\ \phi &= \phi_0 X_\phi \sin p_n t \end{aligned}\right\} \quad [8]$$

where v_0, w_0, ϕ_0 represent amplitudes of vibration, and X_y, X_x, X_ϕ are functions of x only giving the mode shapes of the vibrations. Substitution of Equations [8] into Equations [5] and [7] gives

$$U = \frac{1}{2}\left[v_0^2 EI_\xi \int_0^l \left(\frac{d^2 X_y}{dx^2}\right)^2 dx + w_0^2 EI_\eta \int_0^l \left(\frac{d^2 X_x}{dx^2}\right)^2 dx + \phi_0^2 EC_w \int_0^l \left(\frac{d^2 X_\phi}{dx^2}\right)^2 dx + \phi_0^2 GC\int_0^l \left(\frac{dX_\phi}{dx}\right)^2 dx\right]\sin^2 p_n t \quad [9]$$

$$T = \frac{p_n^2}{2}\left[v_0^2 mA\int_0 X_y^2 dx + w_0^2 mA\int_0^l X_x^2 dx - 2v_0\phi_0 mAc_x\int_0^l X_y X_\phi dx + 2w_0\phi_0 mAc_y\int_0^l X_x X_\phi dx + \phi_0^2 mI_0\int_0^l X_\phi^2 dx\right]\cos^2 p_n t \quad [10]$$

or, more concisely $$U = \frac{1}{2}N\sin^2 p_n t \quad [11]$$

$$T = \frac{p_n^2}{2}M\cos^2 p_n t \quad [12]$$

where N and M represent the terms in brackets.

Equating the maximum strain energy and the maximum kinetic energy, we obtain the relation

$$p_n^2 = \frac{N}{M} \quad [13]$$

Equation [13] contains the amplitudes v_0, w_0, and ϕ_0, for which the optimum values are those resulting in a minimum value of p_n (or p_n^2). This condition is fulfilled when

$$\frac{\partial p_n^2}{\partial v_0} = 0, \quad \frac{\partial p_n^2}{\partial w_0} = 0, \quad \frac{\partial p_n^2}{\partial \phi_0} = 0 \quad [14]$$

Application of Equations [14] to Equation [13] gives

$$\left.\begin{aligned} \frac{\partial N}{\partial v_0} - p_n^2\frac{\partial M}{\partial v_0} &= 0 \\ \frac{\partial N}{\partial w_0} - p_n^2\frac{\partial M}{\partial w_0} &= 0 \\ \frac{\partial N}{\partial \phi_0} - p_n^2\frac{\partial M}{\partial \phi_0} &= 0 \end{aligned}\right\} \quad [15]$$

Equations [15] constitute a set of linear simultaneous equations for v_0, w_0, ϕ_0 with a trivial solution $v_0 = w_0 = \phi_0 = 0$. For the amplitudes to have values other than zero, the determinant formed by their coefficients in the simultaneous equations must be equal to zero. This gives the following frequency equation

$$\begin{vmatrix} \left[EI_\xi\int_0^l \left(\frac{d^2X_y}{dx^2}\right)^2 dx - p_n^2 mA\int_0^l X_y^2 dx\right] & 0 & \left[p_n^2 mAc_x\int_0^l X_y X_\phi dx\right] \\ 0 & \left[EI_\eta\int_0^l \left(\frac{d^2X_x}{dx^2}\right)^2 dx - p_n^2 mA\int_0^l X_x^2 dx\right] & \left[-p_n^2 mAc_y\int_0^l X_x X_\phi dx\right] \\ \left[p_n^2 mAc_x\int_0^l X_y X_\phi dx\right] & \left[-p_n^2 mAc_y\int_0^l X_x X_\phi dx\right] & \left[EC_w\int_0^l \left(\frac{d^2X_\phi}{dx^2}\right)^2 dx + GC\int_0^l \left(\frac{dX_\phi}{dx}\right)^2 dx - p_n^2 mI_0\int_0^l X_\phi^2 dx\right] \end{vmatrix} = 0 \quad [16]$$

If the exact expressions for the mode shapes X_y, X_z, X_ϕ are substituted into Equation [16], then the resulting solution for p_n^2 also will be exact. Usually the exact mode shapes are not known, but substitution into Equation [16] of assumed mode shapes (satisfying the boundary conditions) will yield an approximate solution for the frequency.

For the special case of uncoupled vibrations ($c_y = c_z = 0$) Equation [16] results in three values of frequency

$$\left.\begin{aligned} p_y^2 &= \frac{EI_\zeta \int_0^l \left(\frac{d^2X_y}{dx^2}\right)^2 dx}{mA \int_0^l X_y^2 dx} \\ p_z^2 &= \frac{EI_\eta \int_0^l \left(\frac{d^2X_z}{dx^2}\right)^2 dx}{mA \int_0^l X_z^2 dx} \\ p_\phi^2 &= \frac{EC_w \int_0^l \left(\frac{d^2X_\phi}{dx^2}\right)^2 dx + GC \int_0^l \left(\frac{dX_\phi}{dx}\right)^2 dx}{mI_0 \int_0^l X_\phi^2 dx} \end{aligned}\right\} \quad \ldots [17]$$

where p_y, p_z, and p_ϕ represent uncoupled frequencies in the y, z, and ϕ-directions, respectively, for any particular end conditions of the beam.

The effect of coupling is to alter both frequencies and mode shapes. However, changes in mode shapes are minor because the same boundary conditions still apply. Therefore in the Rayleigh-Ritz method we may use the uncoupled mode shapes as approximations for coupled mode shapes, and Equations [17] represent approximate relations between uncoupled frequencies and coupled mode shapes. Substituting Equations [17] into Equation [16], expanding the determinant and simplifying, the frequency equation for triple coupling becomes

$$\begin{aligned} &\left(\frac{p_n^2}{p_y^2}\right)^3 \left(1 - \alpha \frac{Ac_z^2}{I_0} - \beta \frac{Ac_y^2}{I_0}\right) \\ &- \left(\frac{p_n^2}{p_y^2}\right)^2 \left[\left(\frac{p_z^2}{p_y^2}\right)\left(1 - \alpha \frac{Ac_z^2}{I_0}\right) + 1 - \beta \frac{Ac_y^2}{I_0} + \frac{p_\phi^2}{p_y^2}\right] \\ &+ \frac{p_n^2}{p_y^2}\left(\frac{p_z^2}{p_y^2} + \frac{p_\phi^2}{p_y^2} + \frac{p_z^2}{p_y^2}\frac{p_\phi^2}{p_y^2}\right) - \frac{p_z^2}{p_y^2}\frac{p_\phi^2}{p_y^2} = 0 \ldots\ldots [18] \end{aligned}$$

where

$$\alpha = \frac{\left[\int_0^l X_y X_\phi dx\right]^2}{\int_0^l X_y^2 dx \int_0^l X_\phi^2 dx} \quad \ldots\ldots [19]$$

$$\beta = \frac{\left[\int_0^l X_z X_\phi dx\right]^2}{\int_0^l X_z^2 dx \int_0^l X_\phi^2 dx} \quad \ldots\ldots [20]$$

For double coupling, Fig. 1(b), vibrations in the z-direction are independent. Substituting $c_y = 0$ in Equation [18], and also dividing by $(p_n^2/p_y^2) - (p_z^2/p_y^2)$, we obtain

$$\left(\frac{p_n^2}{p_y^2}\right)^2 \left(1 - \alpha \frac{Ac_z^2}{I_0}\right) - \frac{p_n^2}{p_y^2}\left(1 + \frac{p_\phi^2}{p_y^2}\right) + \frac{p_\phi^2}{p_y^2} = 0 \ldots [21]$$

Equation [21] is the frequency equation for double coupling.

In the case of simply supported beams, $\alpha = \beta = 1$, since the three mode shapes are identical

$$X_y = X_z = X_\phi = \sin \frac{n\pi x}{l}$$

For other end conditions both α and β are less than unity (Schwarz's theorem of inequality) yet very close to unity. This can be seen by substituting approximate mode functions into Equations [19] and [20]. For most practical purposes, using $\alpha = \beta = 1$ is sufficiently accurate for any end conditions, as shown in the next section.

4 Results for Double Coupling

Simply Supported Beam. The equation for the coupled frequencies may be derived by the exact method described in section 2, or found from Equation [21] of the Rayleigh-Ritz method by substituting $\alpha = 1$ into that equation. The resulting equation (given by Timoshenko,[2] p. 410) is

$$\frac{I_p}{I_0}\left(\frac{p_n^2}{p_y^2}\right)^2 - \left(1 + \frac{p_\phi^2}{p_y^2}\right)\frac{p_n^2}{p_y^2} + \frac{p_\phi^2}{p_y^2} = 0 \ldots [22]$$

The symbols p_y and p_ϕ in this equation represent the uncoupled bending and torsional frequencies for simple supports. These frequencies are

$$p_y = \frac{n^2\pi^2}{l^2}\left(\frac{EI_\zeta}{mA}\right)^{1/2}, \quad p_\phi = \frac{n\pi}{l^2}\left(\frac{n^2\pi^2 EC_w + l^2GC}{mI_0}\right)^{1/2} \ldots [23]$$

and are constants for any given beam. The coupled frequencies given by Equation [22] are plotted in Fig. 3. The lower coupled frequency is always less than the uncoupled frequencies p_y and p_ϕ, and the upper frequency is always greater.

Other End Conditions. Frequencies of vibration for the first mode were found by the exact method of section 2 for fixed-end beams, cantilever beams, and beams with one end fixed, the other simply supported (fixed-simple). Values were found for[12] $I_0/I_p = 1.6$ and 2.4 and the results are shown in Figs. 4(a) and (b). The corresponding curves for simple supports (from Fig. 3) are repeated in Fig. 4 for comparison. Each of the calculated curves in Fig. 4(a) exhibits a "hump" in the region where the transition is made from predominantly bending vibration to predominantly torsional vibration. For the lower frequency, Fig. 4(b), the curves for the different end conditions are indistinguishable.

[12] The value 1.6 corresponds to an equal-legged angle section.

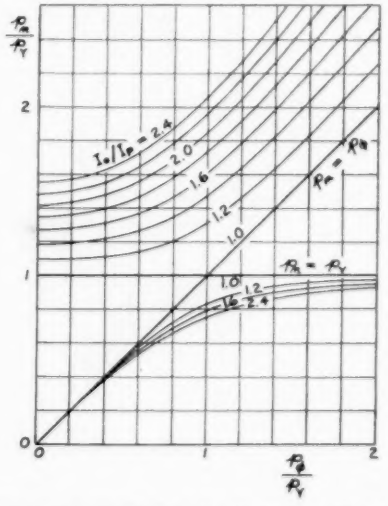

Fig. 3 Frequencies of vibration for double coupling for simply supported beam

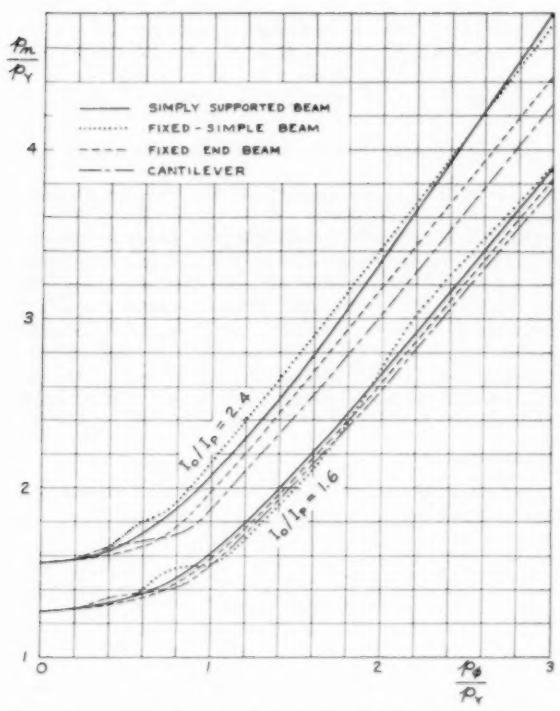

Fig. 4(*a*) Frequencies of vibration for double coupling—upper frequency, first mode

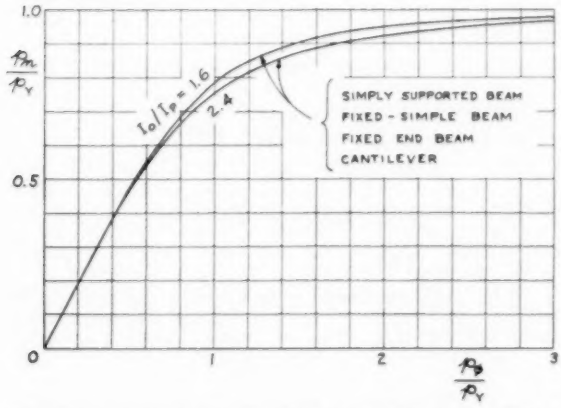

Fig. 4(*b*) Frequencies of vibration for double coupling—lower frequency, first mode

The uncoupled frequencies of vibration p_y and p_ϕ, as used in plotting Fig. 4, have different values for each end condition. The uncoupled bending frequencies (see footnote 3, p. 336, et seq.) may be written in the form

$$p_y = k \frac{\pi^2}{l^2} \left(\frac{EI_\zeta}{mA} \right)^{1/2} \quad \ldots\ldots\ldots\ldots\ldots [24]$$

where k is a constant depending on the end conditions. For the first mode, the value of k for a simply supported beam is 1; for fixed ends, $k = 2.267$; for a cantilever, $k = 0.3562$; for a fixed-simple beam, $k = 1.562$. The uncoupled torsional frequencies p_ϕ for any end conditions are obtained from the equations and graphs given in footnote 6.

It is seen from Figs. 4(*a*) and (*b*) that the relation of the coupled to the uncoupled frequencies is nearly the same for all end conditions. The values of p_n/p_y for the lower frequency, which is usually the frequency of most practical interest, differ by less than 1 per cent between the various end conditions. This close agreement holds for values of p_ϕ/p_y less than 5, which was the limit of the computations. For the upper frequency the differences are larger, especially for the higher values of p_ϕ/p_y, as indicated in Fig. 4(*a*). Thus within this accuracy, the frequency equation for a simply supported beam, Equation [22], also may be used for other end conditions. Inasmuch as an exact determination of frequency is an extremely laborious process for end conditions other than simple supports, the use of the approximate procedure results in considerable saving of effort. In using the approximate method, and when referring to Fig. 4, it must be kept in mind that p_y and p_ϕ are the uncoupled frequencies corresponding to the particular boundary conditions being considered.

5 Results for Triple Coupling

Simply Supported Beam. The equation for the coupled frequencies is

$$\frac{I_p}{I_0}\left(\frac{p_n^2}{p_y^2}\right)^3 - \left[1 - \frac{Ac_y^2}{I_0} + \frac{p_x^2}{p_y^2}\left(1 - \frac{Ac_x^2}{I_0}\right) + \frac{p_\phi^2}{p_y^2}\right]\left(\frac{p_n^2}{p_y^2}\right)^2 + \left[\frac{p_x^2}{p_y^2} + \frac{p_\phi^2}{p_y^2} + \frac{p_x^2}{p_y^2}\frac{p_\phi^2}{p_y^2}\right]\frac{p_n^2}{p_y^2} - \frac{p_x^2}{p_y^2}\frac{p_\phi^2}{p_y^2} = 0 \quad \ldots\ldots [25]$$

where p_y, p_x, and p_ϕ are the uncoupled frequencies for a simply supported beam. The frequencies p_y and p_ϕ are given by Equations [23] and in addition

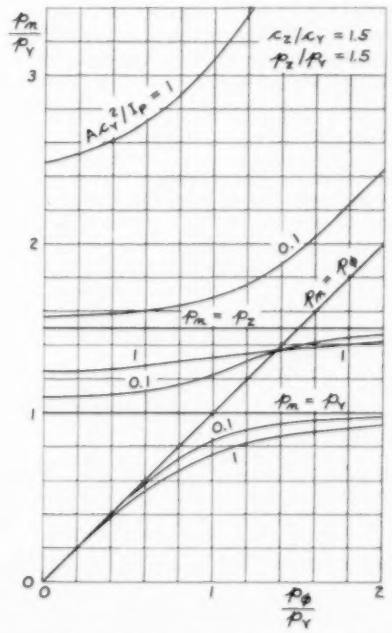

Fig. 5 Frequencies of vibration for triple coupling for simply supported beam

$$p_s = \frac{n^2\pi^2}{l^2}\left(\frac{EI_\eta}{mA}\right)^{1/2} \quad \text{[26]}$$

Equation [25] may be obtained from the exact analysis described in section 2 or by substituting $\alpha = \beta = 1$ into Equation [18]. The equation gives three values of frequency for each mode. One frequency is always higher than any of the uncoupled frequencies and one is always lower. The third frequency is intermediate between the uncoupled frequencies. A graph of the coupled frequencies, showing their relation to the uncoupled frequencies, is presented in Fig. 5, for particular values of the ratios c_s/c_y and p_s/p_y. Similar plots may be made for other values of these parameters.

Each of the three frequencies for a given mode corresponds to a particular pattern of vibration. For example, in Fig. 6 are shown the three vibration patterns (first mode) for a $6 \times 3 \times {}^1/_2$ angle section supported as a simple beam on a span of 6 ft. The first figure gives the vibration pattern for the lowest frequency, the second figure is for the next higher value, and the third figure corresponds to the highest frequency. The frequencies were determined from Equation [25] and the relative amplitudes[13] of

[13] The displacements shown in Fig. 6 are greatly enlarged relative to the size of the angle section.

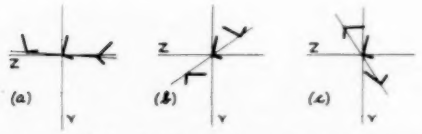

Fig. 6 Typical vibration patterns for angle section

vibration in the y, z, and ϕ-directions were found by the exact method described in section 2.

Other End Conditions. The coefficients α and β in Equation [18] for triple coupling, derived by the Rayleigh-Ritz method, are very nearly unity for end conditions other than simple supports. This indicates that Equation [25], derived for simple supports, is reasonably accurate for other end conditions in a manner analogous to the situation for double coupling. In using this approximation, it must be recalled that p_y, p_z, and p_ϕ are uncoupled frequencies for the particular boundary conditions under consideration.

Acknowledgment

The authors are grateful to the National Science Foundation for sponsoring this work.

Some Solutions of the Timoshenko Beam Equation for Short Pulse-Type Loading[1]

By H. J. PLASS, JR.,[2] AUSTIN, TEXAS

A collection of solutions to the Timoshenko beam equation is presented. Various types of support conditions and impact conditions are included. In every case the impact is assumed to be a pulse in the form of a half-sine wave. The results were found numerically, using the method of characteristics, except for one case, which was done in addition by the Laplace transform method, for check purposes. Agreement with experiment is good except for a pulse of duration comparable to the time required for the bending-type wave to travel a distance of one diameter. Discussion is included of the differences among the various cases studied.

Nomenclature

THE following nomenclature is used in the paper:

$a = \dfrac{2}{k(C-1)}$

A = dimensionless cross-section area = area/h^2

$b = \dfrac{1}{k\sqrt{C}}$

$c_0 = (E/\rho)^{1/2}$ = bar velocity

$c_Q = (K'G/\rho)^{1/2}$ = modified shear-wave velocity

$C = c_0^2/c_Q^2$

E = modulus of elasticity

G = shear modulus

h = diameter

H = const

k = dimensionless section radius of gyration = radius of gyration/h

K' = a correction factor = $\dfrac{\text{average shear stress in section}}{\text{maximum shear stress in section}}$

$\mathfrak{M} = \left(\dfrac{1+C}{2}\right)^{1/2}$

M = dimensionless moment = moment/(Eh^3)

$\mathfrak{N} = \dfrac{C-1}{C+1}$

Q = dimensionless shear force = shear force/(Eh^2)

r = integration variable

$R = [r^2 + \mathfrak{N}^2(a^2 - r^2)]^{1/2}$

$S = \mathfrak{M}\sqrt{r}[\mathfrak{N}(a^2 + r^2)^{1/2} - r]^{1/2}$

$S_0 = (S)_{r=\pi/\tau}$

t = dimensionless time = $\dfrac{\text{time}}{h/c_0}$

$T = \mathfrak{M}\sqrt{r}[\mathfrak{N}(a^2 + r^2)^{1/2} + r]^{1/2}$

$T_0 = (T)_{r=\pi/\tau}$

v^* = dimensionless transverse velocity of element = velocity/c_0

w = dimensionless transverse displacement = displacement/h

x = dimensionless axial co-ordinate = axial distance/h

$\zeta = \left[\dfrac{r(R+r)}{2}\right]^{1/2}$

ρ = density

τ = dimensionless duration of applied pulse = duration/(h/c_0)

ϕ = variable of integration

$\psi = \left[\dfrac{r(R-r)}{2}\right]^{1/2}$

ω = dimensionless angular velocity of section = angular velocity/(c_0/h)

Introduction

There has been considerable literature on the solutions to the Timoshenko bending equation for beams (1–5)[3] subject to sudden loads. This paper presents a collection of results obtained by means of the method of characteristics.

In order to assess the accuracy of the solutions obtained by the method of characteristics, one case is worked out by the Laplace transform technique described in (3) and is compared with the same case worked out by characteristics. In addition, in several cases results are compared with experimental results of Ripperger (6) and are found to be in good agreement, except when the pulses are exceedingly short.

General Theory

The equation known as the Timoshenko equation is usually presented as a single fourth-order partial differential equation in one variable, say, moment. It is more convenient, especially in using the method of characteristics, to substitute for the Timoshenko equation four first-order equations. They are as follows (in dimensionless form)

$$\left.\begin{aligned}
&\frac{\partial M}{\partial x} - Q = Ak^2\frac{\partial \omega}{\partial t} \quad \text{(rotatory motion)}\\
&\frac{\partial Q}{\partial x} = A\frac{\partial v}{\partial t} \quad \text{(transverse motion)}\\
&\frac{\partial M}{\partial t} = Ak^2\frac{\partial \omega}{\partial x} \quad \text{(time derivative of moment-curvature relation)}\\
&C\frac{\partial Q}{\partial t} = A\left(\frac{\partial v}{\partial x} + \omega\right) \quad \text{(time derivative of shear-deformation relation)}
\end{aligned}\right\} \quad \ldots [1]$$

---

[1] The material in this paper was obtained as a result of research supported by the U.S. Navy Bureau of Ordnance, under Contract NOrd-16498 with The University of Texas, Defense Research Laboratory, Austin, Texas.

Associate Professor of Engineering Mechanics, and Research Engineer, Defense Research Laboratory, The University of Texas. Mem. ASME.

Presented at the West Coast Conference of the Applied Mechanics Division, Los Angeles, Calif., September 8–10, 1958, of THE AMERICAN SOCIETY OF MECHANICAL ENGINEERS.

Discussion of this paper should be addressed to the Secretary, ASME, 29 West 39th Street, New York, N. Y., and will be accepted until October 10, 1958, for publication at a later date. Discussion received after the closing date will be returned.

NOTE: Statements and opinions advanced in papers are to be understood as individual expressions of their authors and not those of the Society. Manuscript received by ASME Applied Mechanics Division, May 17, 1957. Paper No. 58—APM-3.

[2] Numbers in parentheses refer to the Bibliography at the end of the paper.

Elimination of all but one variable, say M, results in the usual form of the Timoshenko equation (in dimensionless form)

$$k^2 \frac{\partial^4 M}{\partial x^4} + \frac{\partial^2 M}{\partial t^2} - k^2(1 + C) \frac{\partial^4 M}{\partial x^2 \partial t^2} + k^2 C \frac{\partial^4 M}{\partial t^4} = 0 \quad [2]$$

The initial conditions associated with Equations [1] are those for the bar initially at rest

$$M(x, 0) = \omega(x, 0) = Q(x, 0) = v(x, 0) = 0 \quad [3a]$$

A variety of boundary conditions is assumed, which correspond to different types of end impact. These will be discussed later in the paper. One particular case is solved by Laplace transform and by characteristics. The boundary conditions assumed for this case are those corresponding to a sinusoidal moment applied to a simply supported end

$$\left.\begin{aligned} M(0, t) &= H \sin \frac{\pi t}{\tau}, \quad t \geq 0 \\ M(0, t) &= 0, \qquad\quad t \leq 0 \\ v(0, t) &= 0 \end{aligned}\right\} \quad [3b]$$

By using the Laplace transform technique described in (3), it can be shown that

For $t \geq \sqrt{C}\, x$

$$M(x, t) = \frac{H}{2}\left\{1 - \frac{\frac{\pi}{\tau}}{\left[a^2 + \left(\frac{\pi}{\tau}\right)^2\right]^{1/2}}\right\} \left[-\sin T_0 x \cos \frac{\pi t}{\tau} + \cos T_0 x \sin \frac{\pi t}{\tau}\right] + \frac{H}{2}\left\{1 + \frac{\frac{\pi}{\tau}}{\left[a^2 + \left(\frac{\pi}{\tau}\right)^2\right]^{1/2}}\right\} \left[-\sin S_0 x \cos \frac{\pi t}{\tau} + \cos S_0 x \sin \frac{\pi t}{\tau}\right] - \frac{H}{\tau} \int_0^b \left[1 + \frac{r}{(a^2 + r^2)^{1/2}}\right] \frac{1}{\left(\frac{\pi}{\tau}\right)^2 - r^2} \cos rt \sinh Sx \, dr$$

$$\text{if } \frac{\pi}{\tau} > b \quad [4]$$

For $x \leq t \leq \sqrt{C}\, x$

$$M(x, t) = \frac{H}{2}\left\{1 + \frac{\frac{\pi}{\tau}}{\left[a^2 + \left(\frac{\pi}{\tau}\right)^2\right]^{1/2}}\right\} \left[-\sin S_0 x \cos \frac{\pi t}{\tau} + \cos S_0 x \sin \frac{\pi t}{\tau}\right] - \frac{H}{\tau} \int_0^a \frac{1}{r^2 + \left(\frac{\pi}{\tau}\right)^2} \left[\frac{r}{(a^2 - r^2)^{1/2}} \cos \mathfrak{M}\psi x \sinh (\mathfrak{M}\zeta x - rt) + \sin \mathfrak{M}\psi x \cosh (\mathfrak{M}\zeta x - rt)\right] dr - \frac{H}{\tau} \int_0^b \left[1 + \frac{r}{(a^2 + r^2)^{1/2}}\right] \frac{1}{\left(\frac{\pi}{\tau}\right)^2 - r^2} \cos rt \sinh Sx \, dr \quad \text{if } \frac{\pi}{\tau} > b \quad [5]$$

Similar manipulation for the case $\pi/\tau < b$ leads to:

For $t \geq \sqrt{C}\, x$

$$M(x, t) = \frac{H}{2}\left\{1 - \frac{\frac{\pi}{\tau}}{\left[a^2 + \left(\frac{\pi}{\tau}\right)^2\right]^{1/2}}\right\} \left[-\sin T_0 x \cos \frac{\pi t}{\tau} + \cos T_0 x \sin \frac{\pi t}{\tau}\right] + \frac{H}{2}\left\{1 + \frac{\frac{\pi}{\tau}}{\left[a^2 + \left(\frac{\pi}{\tau}\right)^2\right]^{1/2}}\right\} \cosh S_0 x \sin \frac{\pi t}{\tau} - \frac{H}{\tau} \int_0^b \left[1 + \frac{r}{(a^2 + r^2)^{1/2}}\right] \frac{1}{\left(\frac{\pi}{\tau}\right)^2 - r^2} \cos rt \sinh Sx \, dr$$

$$\text{if } \frac{\pi}{\tau} < b \quad [6]$$

For $x \leq t \geq \sqrt{C}\, x$

$$M(x, t) = \frac{H}{2}\left\{1 + \frac{\frac{\pi}{\tau}}{\left[a^2 + \left(\frac{\pi}{\tau}\right)^2\right]^{1/2}}\right\} \cosh S_0 x \sin \frac{\pi t}{\tau} - \frac{H}{\tau} \int_0^a \frac{1}{r^2 + \left(\frac{\pi}{\tau}\right)^2} \left[\frac{r}{(a^2 - r^2)^{1/2}} \cos \mathfrak{M}\psi x \sinh (\mathfrak{M}\zeta x - rt) + \sin \mathfrak{M}\psi x \cosh (\mathfrak{M}\zeta x - rt)\right] dr - \frac{H}{\tau} \int_0^b \left[1 + \frac{r}{(a^2 + r^2)^{1/2}}\right] \frac{1}{\left(\frac{\pi}{\tau}\right)^2 - r^2} \cos rt \sinh Sx \, dr$$

$$\text{if } \frac{\pi}{\tau} < b \quad [7]$$

The evaluation of the integrals in the foregoing equations was done numerically, after removing the singularities at 0, a, or b. The details of this integration process are given in a report by Plass and Steyer (7).

For purposes of computation the following quantities were selected:

Assumed Constants

Diameter of bar = 0.516 in., material steel [similar to one used experimentally by Ripperger (6)]

$E = 30 \times 10^6$ psi
$\nu = 0.30$
$\rho = 7.187 \times 10^{-4}$ lb-sec^2/in.^{4}
$K' = 3/4$
$C = 4$
$H = 1$
$\tau = 2.4$

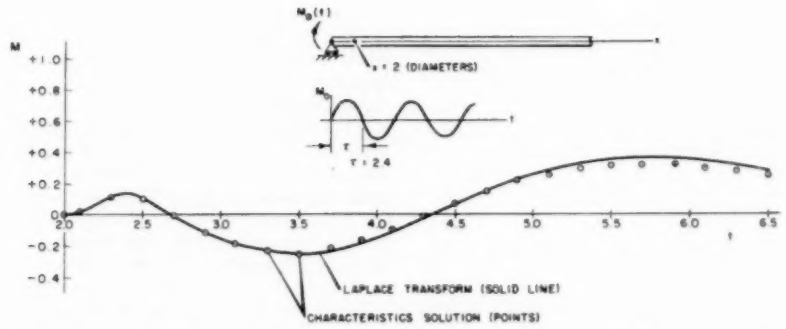

Fig. 1 Comparison of results compiled for $x = 2$ from Laplace transform and characteristics; M and t are dimensionless

Derived Constants

$$\mathfrak{M} = 1.58115, \quad \mathfrak{N} = 0.60000, \quad a = 2.66667, \quad b = 2.00000$$
$$S_0 = 1.23789, \quad T_0 = 3.20577$$

In Fig. 1 are shown the results for the foregoing computation for $x = 2.0$, $t = 2.0, 2.5, 3.0, 3.5, 4, \ldots, 12$. These results are on the curve labeled "Laplace transform." In the same figure is shown another curve which is obtained from the solution of the same example by the method of characteristics (curve labeled "Characteristics Solution"). This method of solution will now be discussed.

Solution by Method of Characteristics

A rather complete discussion of the method of characteristics as applied to the Timoshenko beam equation is given by Leonard and Budiansky (8). The characteristics for Equations [1] are curves satisfying the following four differential equations

$$\left.\begin{aligned} dt &= dx \\ dt &= -dx \\ dt &= \sqrt{C}\,dx \\ dt &= -\sqrt{C}\,dx \end{aligned}\right\} \quad \ldots\ldots\ldots\ldots\ldots [8]$$

In reference (8) it was assumed that the velocity-square ratio C is unity; that is, the modified shear-wave velocity c_Q was assumed to be equal to the bending-wave velocity c_b. In the present paper this restriction is removed. When these relations are used, together with the four first-order equations, Equations [1], it can be shown that

$$\left.\begin{aligned} dM - Ak^2 d\omega &= Q dt, && \text{along } dt = dx \\ dM + Ak^2 d\omega &= -Q dt, && \text{along } dt = -dx \\ dQ - \frac{A}{\sqrt{C}}\,dv &= \frac{A}{C}\,\omega dt, && \text{along } dt = \sqrt{C}\,dx \\ dQ + \frac{A}{\sqrt{C}}\,dv &= \frac{A}{C}\,\omega dt, && \text{along } dt = -\sqrt{C}\,dx \end{aligned}\right\} \quad \ldots [9]$$

These equations are solved numerically for M, ω, Q, v by writing them as difference equations for corner points of an element bounded by two sets of characteristics of the bending-wave family, $dt = \pm dx$, Fig. 2.

Within this element are two members of the modified shear-wave family $dt = \pm\sqrt{C}\,dx$. The difference equations, obtained directly from the differential equations, Equations [9], are as follows

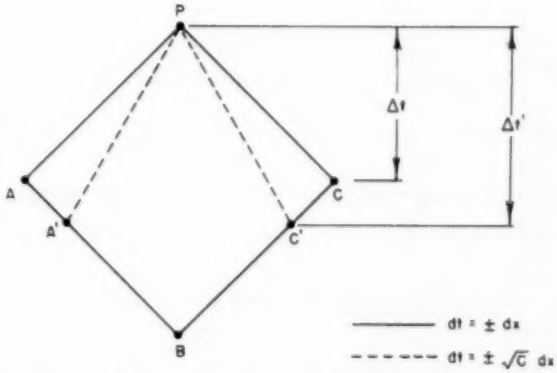

Fig. 2 Element used in numerical computation by method of characteristics

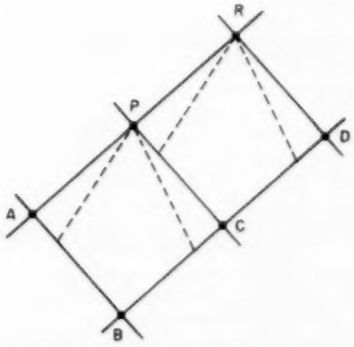

Fig. 3 Two consecutive elements

$$\left.\begin{aligned} (M_P - M_A) - Ak^2(\omega_P - \omega_A) &= \frac{Q_P + Q_A}{2}\,\Delta t \\ (M_P - M_C) + Ak^2(\omega_P - \omega_C) &= -\frac{Q_P + Q_C}{2}\,\Delta t \\ (Q_P - Q_{A'}) - \frac{A}{\sqrt{C}}(v_P - v_{A'}) &= \frac{A}{C}\,\frac{\omega_P + \omega_{A'}}{2}\,\Delta t' \\ (Q_P - Q_{C'}) + \frac{A}{\sqrt{C}}(v_P - v_{C'}) &= \frac{A}{C}\,\frac{\omega_P + \omega_{C'}}{2}\,\Delta t' \end{aligned}\right\} \quad \ldots [10]$$

In the foregoing

$$\left.\begin{aligned} \Delta t' &= \frac{2\sqrt{C}}{1+\sqrt{C}}\,\Delta t \\ Q_{A'} &= Q_B + \frac{2}{1+\sqrt{C}}\,(Q_A - Q_B) \\ Q_{C'} &= Q_B + \frac{2}{1+\sqrt{C}}\,(Q_C - Q_B) \end{aligned}\right\} \quad \ldots\ldots [11]$$

etc., for $v_{A'}$, $v_{C'}$, $\omega_{A'}$, $\omega_{C'}$

Equations [10] are solved simultaneously for M_P, ω_P, Q_P, v_P in terms of values, previously calculated at A, B, C of the element. In Fig. 3 is shown a strip composed of elements similar to the one just discussed. If the values are known also at D, then they can be found for R, after having obtained the values at P, and so on.

Since new values depend upon previously determined values, there has to be a starting point somewhere. In the problems solved in this paper, the end of the bar, $x = 0$, is subject to various types of impacts in the form of continued sine waves, or single half-sine waves. In fact, the cases for the single half-sine wave are all solved by superposing solutions for the continued sine wave for starting times differing by one-half period. In all cases, the values of M, ω, Q, and v along the leading wave front $t = x$, are assumed to be zero. Along the t-axis, i.e., the end of the bar $x = 0$, two of the four variables are specified, depending upon the kind of support and the kind of impact supplied. The remaining two variables along the t-axis are computed by means of the two difference equations associated with the right half of the element of Fig. 2.

The results are shown in Figs. 4 through 14. Figs. 4 and 5 are

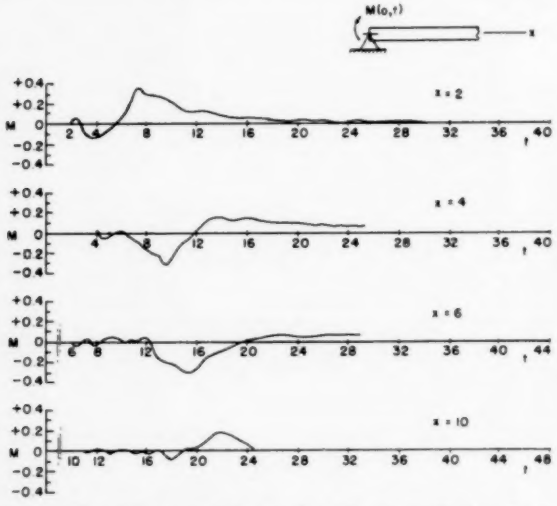

Fig. 4 $M - t$ curves at various stations along bar with pinned end, resulting from half-sine moment impact. $\tau = 4.8$, $C = 4$.

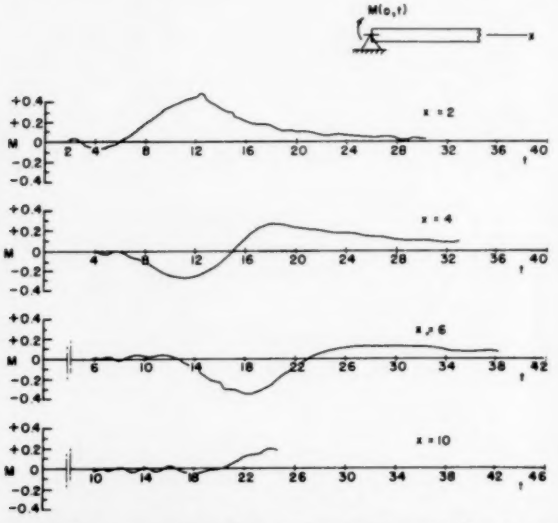

Fig. 5 $M - t$ curves at various stations along bar with pinned end, resulting from half-sine moment impact. $\tau = 10$, $C = 4$.

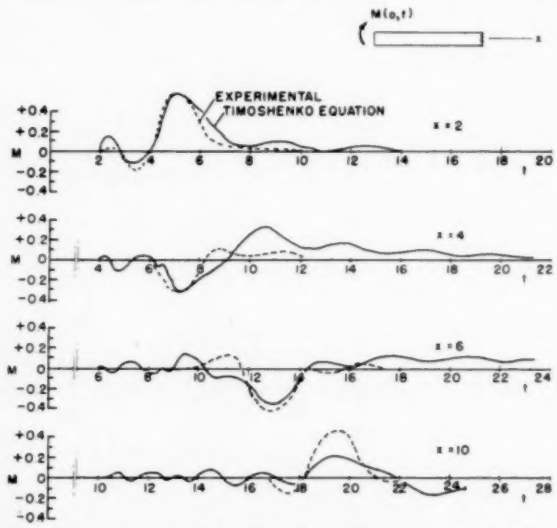

Fig. 6 $M - t$ curves at various stations along bar with unsupported end, resulting from half-sine moment impact. $\tau = 2.4$, $C = 4$.

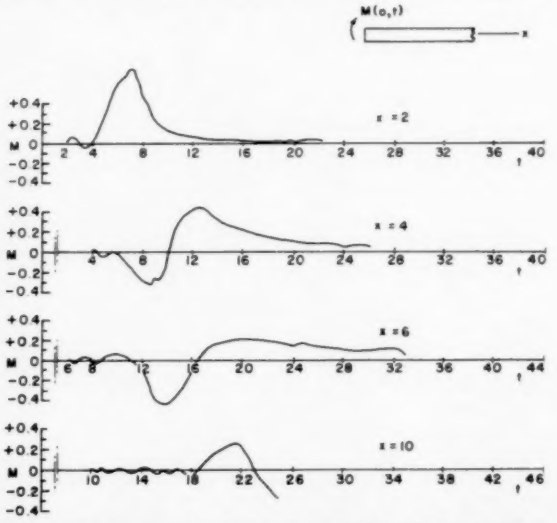

Fig. 7 $M - t$ curves at various stations along bar with unsupported end, resulting from half-sine moment impact. $\tau = 4.8$, $C = 4$.

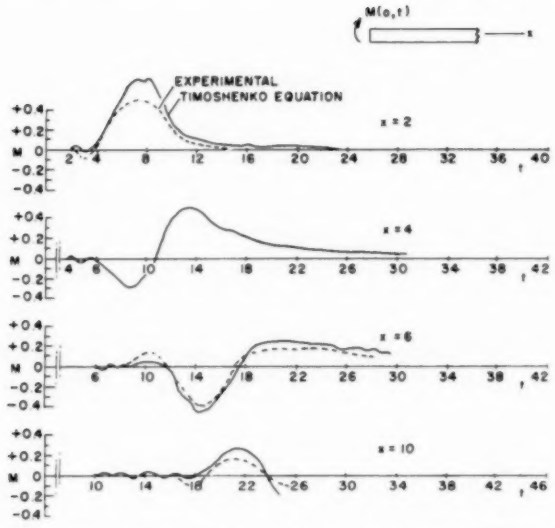

Fig. 8 $M - t$ curves at various stations along bar with unsupported end, resulting from half-sine moment impact. $\tau = 6.0$, $C = 4$.

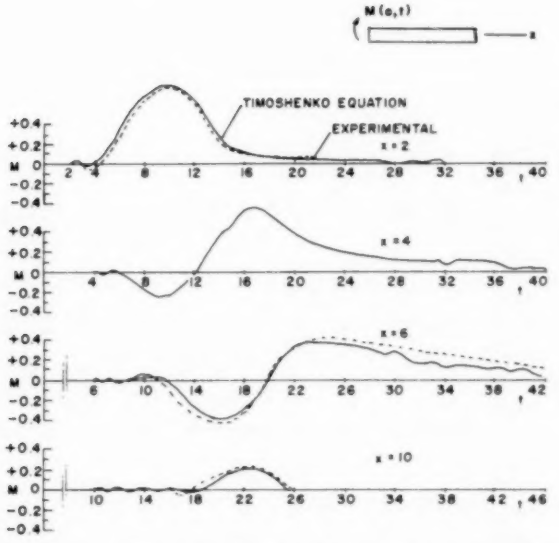

Fig. 9 $M - t$ curves at various stations along bar with unsupported end, resulting from half-sine moment impact. $\tau = 10.0$, $C = 4$.

$M - t$ curves at various stations for pin-ended beams subjected to moment pulses. Figs. 6, 7, 8, and 9 are similar curves for unsupported beams subjected to an end-moment pulse. Experimental results of Ripperger (6) are included in Figs. 6, 8, and 9. Fig. 10 shows one set of moment-time relations for a half-sine shear impact on the unsupported end of a semi-infinite beam. The effects of prescribing transverse or angular end-section velocity are shown in Figs. 11, 12, and 13.

Solutions for a different value of C, $C = 3$, were carried out. One set of results is shown in Fig. 14. A lower value of C is equivalent to a relatively larger value of c_Q with respect to c_0.

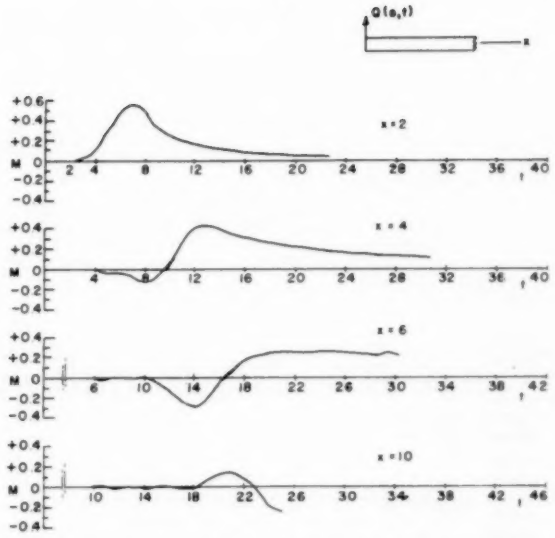

Fig. 10 $M - t$ curves at various stations along bar, resulting from transverse shear force half-sine impact. $\tau = 4.8$, $C = 4$.

General Conclusions

(*a*) *Comparison With Experiment.* The experimental results of Ripperger (6) for moment impacts having timewise variations very nearly in the form of a half-sine wave are selected for comparison with theoretical results. The moments in every case were generated by means of the eccentric impact of a small steel ball on the end of the rod. The longitudinal wave, also generated by such an impact, was eliminated from the strain measurements by connecting diametrically opposed strain gages properly. For such a connection only the bending-wave strains are recorded. In Figs. 6, 8, and 9 are shown some strain records converted to dimensionless moment records by means of multiplication by proper constants. It is seen upon examining these figures that, except for the shortest pulse, the agreement between the theoretical (Timoshenko equation) results and the experimental results is quite good. The theoretical results are those for $C = 4$; that is, for the bending velocity c_0 equal to twice the modified shear velocity c_Q. This is the nearest value to that for circular steel rods, according to Timoshenko's assumptions. Hence the bulk of the calculations were made with $C = 4$. A reduction of the value of C, with fixed $c_0 = (E/\rho)^{1/2}$, is thus equivalent to an increase in the modified shear velocity c_Q. Such a change would result in somewhat the same form for the moment-time curves at the various stations, but a more rapid propagation of that portion of the energy which is primarily in the shear mode of transmission. The experimental data agree, so far as time relationship is concerned, most closely with the theoretical results for $C = 4$. On comparing the curves of Fig. 6 ($C = 4$, $\tau = 2.4$) with those of Fig. 14 ($C = 3$, $\tau = 2.4$) it is seen that the large peaks for $C = 3$ occur earlier in time than those for $C = 4$, as anticipated. The fact that experimental results are predicted as accurately as they are by the Timoshenko theory for $C = 4$ is encouraging. Because of the frequently good agreement, it can be said with a fair degree of confidence that the results presented in the other figures in which experimental data are not presented are reliable. For impact loads, the Timoshenko theory is quite satisfactory, provided that the duration of the impact exceeds the time required for a bending wave (velocity = c_0) to travel a distance equal to the bar diameter.

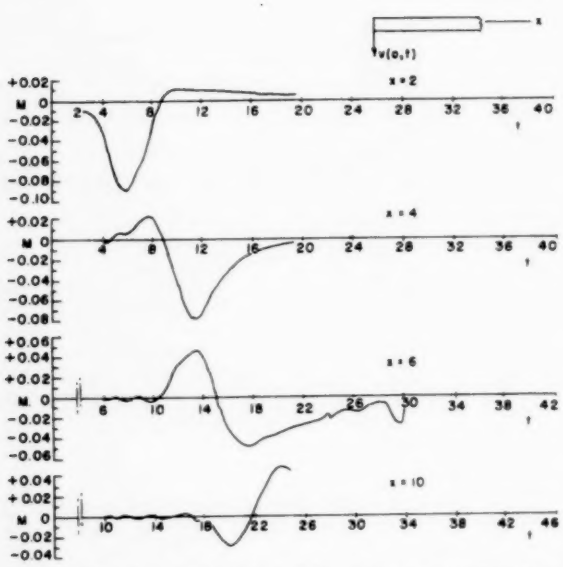

Fig. 11 $M - t$ curves at various stations along bar, resulting from transverse velocity half-sine impact. $\tau = 4.8$, $C = 4$.

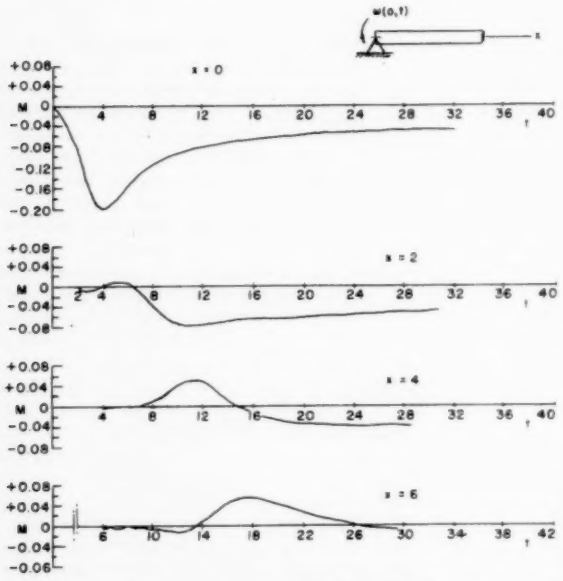

Fig. 12 $M - t$ curves at various stations along bar, resulting from angular velocity half-sine impact, end simply supported. $\tau = 4.8$, $C = 4$.

(*b*) *Comparison of Theoretical Results (Timoshenko Equation) for Similar Impacts but Different Methods of Support.* The moment-time relations at various stations resulting from half-sine moment impacts are shown in Figs. 4 and 5, and Figs. 6 through 9. The curves for Figs. 4 and 5 are those resulting from assuming the end to be simply supported, while those of Figs. 6 through 9 are for an unsupported end. Certain similarities as well as differences are noted in comparing figures for impacts of equal duration; e.g., Figs. 4 and 7. When the impact end is simply supported, the moments do not build up anywhere to values as large

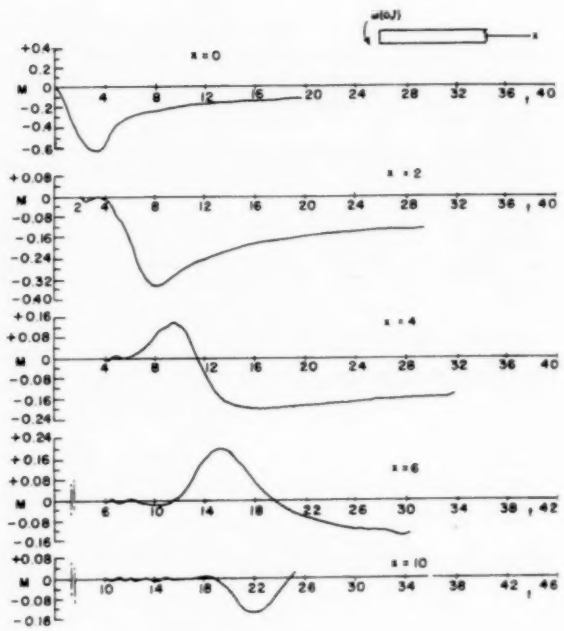

Fig. 13 $M - t$ curves at various stations along bar, resulting from angular velocity half-sine impact, end unsupported. $\tau = 4.8$, $C = 4$.

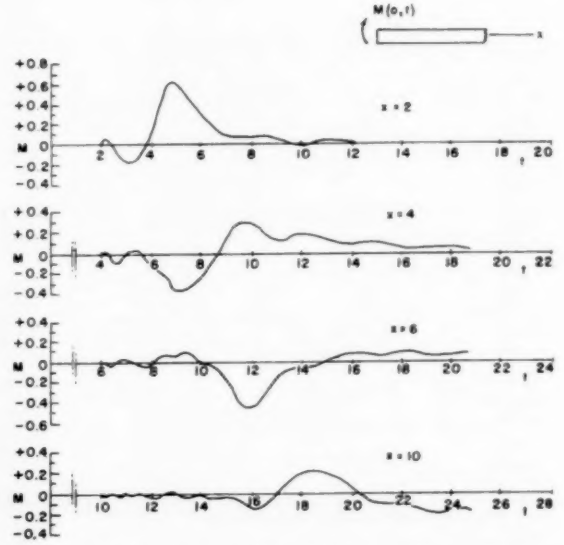

Fig. 14 $M - t$ curves at various stations along bar, resulting from moment half-sine impact, end unsupported. $\tau = 2.4$, $C = 3$.

as those occurring when the impact end is unsupported. During the earliest stages of the development of the $M - t$ wave there are, however, only small differences. It is also noticed that for the simply supported end the largest peaks occur later in time than for the unsupported end. This seems to indicate that large shear waves are formed more slowly when the end is supported.

(*c*) *Comparison of Theoretical Results (Timoshenko Equation) for Similar Types of Support but Different Types of Impact.* On

comparing Fig. 7 with Fig. 13 for unsupported beams with moment and angular velocity half-sine impacts, it is seen that the main difference between the $M - t$ trace at the station under study is in the amount of spreading out of the wave. For moment impacts the $M - t$ curve is less dispersed than for angular-velocity impacts. It also should be pointed out that the two sets of curves have opposite polarity, since the definition of positive ω and positive M are opposite for the section on which they are assumed to act.

Similar comparisons for Fig. 10 with Fig. 11 for unsupported beams with end shear force and end transverse velocity half-sine impacts, yield similar results. The transverse velocity impact in this case is the lesser dispersed of the two.

For simply supported bars, differences between results of moment and angular velocity impacts can be seen by comparing Figs. 4 and 12. Similar conclusions are obtained to those for unsupported bars. The dispersion for moment impacts is not as great as that for angular velocity impacts.

Bibliography

1 "The Propagation of Waves in the Transverse Vibrations of Bars and Plates," by Ya. S. Uflyand (in Russian), *Prikladnaya Matematika i Mekhanika*, vol. 12, 1948, pp. 287–300.

2 "Propagation of Elastic Impact in Beams in Bending," by M. Goland, P. D. Wickersham, and M. A. Dengler, JOURNAL OF APPLIED MECHANICS, TRANS. ASME, vol. 77, 1955, pp. 1–7.

3 "Flexural Waves in Beams According to the More Exact Theory of Bending," by J. Miklowitz, U.S. Naval Ordnance Test Station, Report NOTS 741 NAVORD 2049, 1953.

4 "Some Solutions of the Timoshenko Beam Equations," by B. A. Boley and C. C. Chao, JOURNAL OF APLLIED MECHANICS, TRANS. ASME, vol. 77, 1955, pp. 579–586.

5 "Flexural Waves in Beams," by E. E. Zajac, dissertation, Stanford University, Stanford, Calif., 1954.

6 "Measurements of Short Bending Wave Pulses in Steel Bars," by E. A. Ripperger, Defense Research Laboratory, The University of Texas, Report DRL-367, CM-838, 1955.

7 "Studies on Longitudinal and Bending Waves in Long Elastic Rods," by H. J. Plass, Jr., and C. C. Steyer, Defense Research Laboratory, The University of Texas, Report DRL-376, CM-860, 1956.

8 "On Traveling Waves in Beams," by R. W. Leonard and B. Budiansky, National Advisory Committee for Aeronautics, Technical Note 2874, 1953.

Nonaxial Bending of Ring Plates of Varying Thickness

By H. D. CONWAY,[1] ITHACA, N. Y.

A solution is given to the problem of the bending of circular ring plates of varying thickness which are subjected at their outer and inner edges to any system of forces and moments. The thickness is assumed to be proportional to any power of the radius, this having the effect of making the solution tractable. Numerical results are given for a plate, clamped at its inner, free at its outer, edge and subjected to a normal concentrated load on its outer edge. The constant-thickness version of this problem was first solved by Reissner.[2]

Introduction

THE problem of the nonaxially symmetrical bending of circular plates of constant thickness has received a great deal of attention in the literature because of its considerable practical and academic interest. On the other hand, solutions to the corresponding problems of varying thickness are rare because of their inherent difficulty. However, the problem of a circular disk of variable thickness simply supported or clamped around the rim and bent by a couple applied to a rigid central core has recently been solved by Baclig and the author,[3] the plate thickness being proportional to any power of the radius. This solution is now extended to include any ring plate bent by systems of couples and normal forces on its edges, the thickness variation being as before.

Theory

With the usual assumptions and nomenclature of small-deflection plate theory, the equations for the bending moments M_r and M_θ and torque $M_{r\theta}$ are, respectively

$$\left.\begin{aligned} M_r &= -D\left[\frac{\partial^2 w}{\partial r^2} + \nu\left(\frac{1}{r}\frac{\partial w}{\partial r} + \frac{1}{r^2}\frac{\partial^2 w}{\partial \theta^2}\right)\right] \\ M_\theta &= -D\left[\frac{1}{r}\frac{\partial w}{\partial r} + \frac{1}{r^2}\frac{\partial^2 w}{\partial \theta^2} + \nu\frac{\partial^2 w}{\partial r^2}\right] \\ M_{r\theta} &= D(1-\nu)\frac{\partial}{\partial r}\left(\frac{1}{r}\frac{\partial w}{\partial \theta}\right) \end{aligned}\right\} \quad \ldots [1]$$

The equations of equilibrium are

$$\frac{\partial M_r}{\partial r} - \frac{1}{r}\frac{\partial M_{r\theta}}{\partial \theta} + \frac{1}{r}(M_r - M_\theta) - Q_r = 0$$

$$\frac{1}{r}\frac{\partial M_\theta}{\partial \theta} - \frac{\partial M_{r\theta}}{\partial r} - \frac{2}{r}M_{r\theta} - Q_\theta = 0$$

$$\frac{\partial}{\partial r}(rQ_r) + \frac{\partial Q_\theta}{\partial \theta} + qr = 0$$

from which we obtain

$$\frac{\partial}{\partial r}(2M_r - M_\theta) - 2\frac{\partial^2 M_{r\theta}}{\partial r \partial \theta} + r\frac{\partial^2 M_r}{\partial r^2} + \frac{1}{r}\frac{\partial^2 M_\theta}{\partial \theta^2} - \frac{2}{r}\frac{\partial M_{r\theta}}{\partial \theta} = -qr \ldots [2]$$

Substituting from Equation [1] and assuming the flexural rigidity D is a function only of r, gives

$$D\left[\frac{\partial^4 w}{\partial r^4} + \frac{2}{r}\frac{\partial^3 w}{\partial r^3} - \frac{1}{r^2}\frac{\partial^2 w}{\partial r^2} + \frac{1}{r^3}\frac{\partial w}{\partial r} + \frac{2}{r^2}\frac{\partial^4 w}{\partial r^2 \partial \theta^2} - \frac{2}{r^3}\frac{\partial^3 w}{\partial r \partial \theta^2} + \frac{4}{r^4}\frac{\partial^2 w}{\partial \theta^2} + \frac{1}{r^4}\frac{\partial^4 w}{\partial \theta^4}\right] + \frac{dD}{dr}\left[2\frac{\partial^3 w}{\partial r^3} + \frac{(2+\nu)}{r}\frac{\partial^2 w}{\partial r^2} - \frac{1}{r^2}\frac{\partial w}{\partial r} + \frac{2}{r^2}\frac{\partial^3 w}{\partial r \partial \theta^2} - \frac{3}{r^3}\frac{\partial^2 w}{\partial \theta^2}\right] + \frac{d^2 D}{dr^2}\left[\frac{\partial^2 w}{\partial r^2} + \frac{\nu}{r}\frac{\partial w}{\partial r} + \frac{\nu}{r^2}\frac{\partial^2 w}{\partial \theta^2}\right] = q \ldots [3]$$

For a ring plate subjected to any system of forces and moments on its inner and outer edges, we may write the deflection in the form

$$w = R_0 + \sum_1^m R(r)\cos m\theta + \sum_1^m S(r)\sin m\theta \ldots\ldots [4]$$

where R_0, R, and S are functions only of r.

Consider, for example, the cosine term. After substitution in Equation [3] we obtain, writing $q = 0$

$$D\left[R^{iv} + \frac{2}{r}R''' - \frac{1}{r^2}R'' + \frac{1}{r^3}R' - \frac{2m^2}{r^2}R'' + \frac{2m^2}{r^3}R' - \frac{4m^2}{r^4}R + \frac{m^4}{r^4}R\right] + \frac{dD}{dr}\left[2R''' + \frac{(2+\nu)}{r}R'' - \frac{1}{r^2}R' - \frac{2m^2}{r^2}R' + \frac{3m^2}{r^3}R\right] + \frac{d^2 D}{dr^2}\left[R'' + \frac{\nu}{r}R' - \frac{\nu m^2}{r^2}R\right] = 0 \ldots [5]$$

where the superscripts denote differentiation with respect to r.

It will now be observed that this equation is homogeneous if the thickness of the disk is proportional to some power of the radius and the flexural rigidity written as $D = D_0(r/a)^{-n}$. Because such a plate would either have zero or infinite thickness at the center according as to whether n is negative or positive, it is assumed that we are dealing with ring plates. Thus we write

$$D = D_0\left(\frac{r}{a}\right)^{-n}; \quad \frac{dD}{dr} = \frac{-nD}{r}; \quad \frac{d^2 D}{dr^2} = \frac{n(n+1)D}{r^2} \ldots [6]$$

and obtain

---

[1] Professor of Mechanics, Cornell University.

[2] "Über die Unsymmetrische Biegung dünner Kreisringplatte," by H. Reissner, *Ingenieur-Archiv*, vol. 1, 1929, p. 72.

[3] "Asymmetrical Bending of a Cylindrically Aeolotropic Tapered Disk," by E. S. Baclig and H. D. Conway, JOURNAL OF APPLIED MECHANICS, Trans. ASME, vol. 78, 1956, pp. 11–14.

Contributed by the Applied Mechanics Division and presented at the Annual Meeting, New York, N. Y., December 1–6, 1957, of THE AMERICAN SOCIETY OF MECHANICAL ENGINEERS.

Discussion of this paper should be addressed to the Secretary, ASME, 29 West 39th Street, New York, N. Y., and will be accepted until October 10, 1958, for publication at a later date. Discussion received after the closing date will be returned.

NOTE: Statements and opinions advanced in papers are to be understood as individual expressions of their authors and not those of the Society. Manuscript received by ASME Applied Mechanics Division, May 24, 1957. Paper No. 57—A-92.

$$r^4R^{iv} + 2(1-n)r^3R''' + [n(n+1) - n(2+\nu) - 2m^2 - 1]r^2R'' + [1 + 2m^2 + n + 2m^2n + \nu n(n+1)]rR' + [m^4 - 4m^2 - 3m^2n - \nu m^2n(n+1)]R = 0 \quad [7]$$

By the transformation $z = \log r$, this becomes

$$\frac{d^4R}{dz^4} - 2(n+2)\frac{d^3R}{dz^3} + [(n+2)^2 + n(1-\nu) - 2m^2]\frac{d^2R}{dz^2} + (n+2)[2m^2 - n(1-\nu)]\frac{dR}{dz} + m^2[m^2 - 1 - (3+\nu n)(n+1)]R = 0 \quad [8]$$

and, for solutions of the form $R = e^{\lambda z}$, the characteristic equation is the quartic

$$\lambda^4 - 2\lambda^3(n+2) + \lambda^2[(n+2)^2 + n(1-\nu) - 2m^2] + \lambda(n+2)[2m^2 - n(1-\nu)] + m^2[m^2 - 1 - (3+\nu n)(n+1)] = 0 \quad [9]$$

To find the roots of the characteristic equation, we write the latter in the form

$$(\lambda + \alpha_1 + \beta_1)(\lambda + \alpha_1 - \beta_1)(\lambda + \alpha_2 + \beta_2)(\lambda + \alpha_2 - \beta_2) = 0 \quad [10]$$

which gives after multiplication

$$\lambda^4 + 2\lambda^3(\alpha_1 + \alpha_2) + \lambda^2(\alpha_1^2 - \beta_1^2 + \alpha_2^2 - \beta_2^2 + 4\alpha_1\alpha_2) + \lambda[2\alpha_1(\alpha_2^2 - \beta_2^2) + 2\alpha_2(\alpha_1^2 - \beta_1^2)] + (\alpha_1^2 - \beta_1^2)(\alpha_2^2 - \beta_2^2) = 0 \quad [11]$$

Comparing with Equation [9], we see that

$$\alpha_1 + \alpha_2 = -(n+2)$$

and hence

$$\lambda^4 - 2\lambda^3(n+2) + \lambda^2[(n+2)^2 - \beta_1^2 - \beta_2^2 + 2\alpha_1\alpha_2] + \lambda[-2\alpha_1\alpha_2(n+2) - 2\alpha_1\beta_2^2 - 2\alpha_2\beta_1^2] + (\alpha_1^2 - \beta_1^2)(\alpha_2^2 - \beta_2^2) = 0 \quad [12]$$

Comparing the coefficients of λ^2 and λ in Equations [12] with the corresponding ones of Equation [9] we find, after some simplifications, that

$$\alpha_1 = \alpha_2 = -\frac{1}{2}(n+2) \quad [13]$$

and Equation [12] becomes

$$\lambda^4 - 2\lambda^3(n+2) + \lambda^2\left[(n+2)^2 + \frac{1}{2}(n+2)^2 - \beta_1^2 - \beta_2^2\right] + \lambda(n+2)\left[-\frac{1}{2}(n+2)^2 + \beta_1^2 + \beta_2^2\right] + \left[\frac{1}{4}(n+2)^2 - \beta_1^2\right]\left[\frac{1}{4}(n+2)^2 - \beta_2^2\right] = 0 \quad [14]$$

Thus the equations for finding β_1 and β_2, and hence, with Equation [13], the roots of the characteristic equation, are

$$\beta_1^2 + \beta_2^2 = \frac{1}{2}(n+2)^2 - n(1-\nu) + 2m^2; \quad \left[\frac{1}{4}(n+2)^2 - \beta_1^2\right]\left[\frac{1}{4}(n+2)^2 - \beta_2^2\right] = m^2[m - 1 - (3+\nu n)(n+1)] \quad [15]$$

or in forms more suited for computation

$$\beta_1^2 + \beta_2^2 = \frac{1}{2}(n+2)^2 - n(1-\nu) + 2m^2$$

$$(\beta_1^2 - \beta_2^2)^2 = n^2(1-\nu)^2 + 4m^2n(2 + 2\nu + \nu n) + 16m^2 \quad [16]$$

A simple and interesting solution of the characteristic equation occurs when $n = -2$ and hence $D = D_0(r/a)^2$. The coefficients of λ^3 and λ then disappear, and we have a quadratic in λ^2

$$\lambda^4 - 2\lambda^2(m^2 + 1 - \nu) + m^2(3 - 2\nu + m^2 - 1) = 0 \quad [17]$$

The roots of this equation are

$$\lambda = \pm m, \pm(m^2 + 2 - 2\nu)^{1/2} \quad [18]$$

For the constant-thickness case, $n = 0$ and the roots are

$$\lambda = \pm m, -2 \pm m \quad [19]$$

The deflected form of the plate will be given by the series

$$w = \sum_{m=1}^{m=\infty}(Ar^{\lambda_1} + Br^{\lambda_2} + Cr^{\lambda_3} + Dr^{\lambda_4})\cos m\theta \quad [20]$$

where the λ are the roots of the characteristic equation, these roots being determined as shown from Equations [13] and [16]. A similar result may be obtained for the sine series in Equation [4]. Axisymmetrical loading may be treated by writing $m = 0$ in the cosine expansion.

Finally, to obtain the solution to a particular problem, the loadings around the inner and outer edges of the ring plate are expanded in Fourier series, and the constants A, B, C, and D found from the boundary conditions. It will be observed that the λ are functions of m, an integer, and n, the plate-thickness constant, and hence the λ and consequently A, B, C, and D must be found separately for each value of m.

Example

As a numerical example, we consider the hollow circular disk the thickness of which varies according to the equation $D = D_0(a/r)$, that is, $n = 1$, clamped rigidly at its inner radius b, free at its outer radius a, and carrying a single normal concentrated load P at its outer edge. We assume a radius ratio a/b of 4. The constant-thickness version of this problem was first discussed by H. Reissner.[2]

Expanding the loading in a Fourier series, the boundary conditions at the outer radius $r = a$ are

$$Q_r - \frac{1}{r}\frac{\partial M_{r\theta}}{\partial\theta} = -D_0\frac{\partial}{\partial r}(\nabla w) - \frac{(1-\nu)}{r}\frac{\partial}{\partial\theta}\left[D\left(\frac{1}{r}\frac{\partial^2 w}{\partial r\partial\theta} - \frac{1}{r^2}\frac{\partial w}{\partial\theta}\right)\right]_{r=a} = \frac{P}{\pi a}\left(\frac{1}{2} + \sum_1^\infty \cos m\theta\right)$$

$$\frac{\partial^2 w}{\partial r^2} + \nu\left(\frac{1}{r}\frac{\partial w}{\partial r} + \frac{1}{r^2}\frac{\partial^2 w}{\partial\theta^2}\right) = 0 \quad [21]$$

D_0 being the flexural rigidity at the outer radius and the angle θ being measured from a radius through the load P. At the

inner radius $r = b$

$$w = \frac{\partial w}{\partial r} = 0 \quad \text{[22]}$$

From Equation [20] these give

$$Ab^{\lambda_1} + Bb^{\lambda_2} + Cb^{\lambda_3} + Db^{\lambda_4} = 0$$

$$A\lambda_1 b^{\lambda_1} + B\lambda_2 b^{\lambda_2} + C\lambda_3 b^{\lambda_3} + D\lambda_4 b^{\lambda_4} = 0$$

$$A[\lambda_1(\lambda_1 - 1) + \nu\lambda_1 - \nu m^2]a^{\lambda_1} + B[\lambda_2(\lambda_2 - 1) + \nu\lambda_2 - \nu m^2]a^{\lambda_2}$$
$$+ C[\lambda_3(\lambda_3 - 1) + \nu\lambda_3 - \nu m^2]a^{\lambda_3} + D[\lambda_4(\lambda_4 - 1)$$
$$+ \nu\lambda_4 - \nu m^2]a^{\lambda_4} = 0$$

$$A[(\lambda_1 - 2)(\lambda_1^2 - m^2) + (1 - \nu)m^2(1 - \lambda_1)]a^{\lambda_1}$$
$$+ B[(\lambda_2 - 2)(\lambda_2^2 - m^2) + (1 - \nu)m^2(1 - \lambda_2)]a^{\lambda_2}$$
$$+ C[(\lambda_3 - 2)(\lambda_3^2 - m^2) + (1 - \nu)m^2(1 - \lambda_3)]a^{\lambda_3}$$
$$+ D[(\lambda_4 - 2)(\lambda_4^2 - m^2) + (1 - \nu)m^2(1 - \lambda_4)]a^{\lambda_4}$$
$$= -\frac{Pa^2}{\pi D_0} \quad \text{[23]}$$

which enable A, B, C, and D to be found for each value of m.

Assuming Poisson's ratio $\nu = 0.3$, we have from Equations [13] and [16]

$$\alpha_1 = \alpha_2 = -\frac{1}{2}(n + 2) = -1.5$$

$$\beta_1^2 + \beta_2^2 = 3.8 + 2m^2$$

$$(\beta_1^2 - \beta_2^2)^2 = 0.49 + 27.6m^2$$

from which we determine

$m = 1$	$\lambda_1 = -0.856$	$\lambda_2 = 3.856$
$m = 2$	$\lambda_1 = -1.842$	$\lambda_2 = 4.842$
$m = 3$	$\lambda_1 = -2.835$	$\lambda_2 = 5.835$
$m = 4$	$\lambda_1 = -3.833$	$\lambda_2 = 6.833$
$m = 5$	$\lambda_1 = -4.828$	$\lambda_2 = 7.828$

$m = 1$	$\lambda_3 = 1.000$	$\lambda_4 = 2.000$
$m = 2$	$\lambda_3 = 0.703$	$\lambda_4 = 2.297$
$m = 3$	$\lambda_3 = -0.236$	$\lambda_4 = 3.236$
$m = 4$	$\lambda_3 = -1.218$	$\lambda_4 = 4.218$
$m = 5$	$\lambda_3 = -2.210$	$\lambda_4 = 5.210$

Noting that $a/b = 4$, the roots of the simultaneous Equations [23] are determined for each of the foregoing values of m (and consequently λ) and hence the deflected form of the plate is determined.

For the deflection under the load, we thus find

Axial symmetrical load $\frac{P}{2\pi a}$	$0.01280\ Pa^2/D_0$
$m = 1$	$0.02900\ Pa^2/D_0$
$m = 2$	$0.02059\ Pa^2/D_0$
$m = 3$	$0.00947\ Pa^2/D_0$
$m = 4$	$0.00421\ Pa^2/D_0$
$m = 5$	$0.00221\ Pa^2/D_0$

and it appears that the maximum deflection at the load is given approximately by

$$w_{max} = 0.08\frac{Pa^2}{D_0}$$

Values of

$$M_r = -D\left(\frac{\partial^2 w}{\partial r^2} + \frac{\nu}{r}\frac{\partial w}{\partial r} + \frac{\nu}{r^2}\frac{\partial^2 w}{\partial \theta^2}\right)$$

$$M_\theta = -D\left(\nu\frac{\partial^2 w}{\partial r^2} + \frac{1}{r}\frac{\partial w}{\partial r} + \frac{1}{r^2}\frac{\partial^2 w}{\partial \theta^2}\right)$$

also were investigated for $\theta = 0$ and various radii, and it was found that the greatest stress is radial and occurs at the inner clamped edge. It is given by

$$\sigma_{r_{max}} = 10.50\frac{P}{H^2}$$

where H is the thickness at the clamped edge. Reissner[3] found, for the corresponding plate of constant thickness

$$\sigma_{r_{max}} = 7.90\frac{P}{H^2}$$

On the Transverse Vibrations of Rectangular Orthotropic Plates

By N. J. HUFFINGTON, JR.,[1] AND W. H. HOPPMANN II[2]

Frequency equations and modal eigenfunctions have been determined for the flexural vibrations of rectangular plates of orthotropic material, for those cases which may be treated by the method of M. Lévy (1)[3]. In addition, for a broader class of boundary-value problems, an orthogonality criterion for the eigenfunctions has been established and relations for the kinetic and potential energies derived. The value of these energy functions in dealing with forced vibrations is demonstrated.

Nomenclature

The following nomenclature is used in the paper:

D = flexural rigidity of isotropic plate

$D_x = \dfrac{E_x h^3}{12(1 - \nu_{xy}\nu_{yx})}$

$D_y = \dfrac{E_y h^3}{12(1 - \nu_{xy}\nu_{yx})}$

$D_{xy} = \dfrac{G_{xy} h^3}{12}$

$D_1 = \dfrac{\nu_{xy} E_y h^3}{12(1 - \nu_{xy}\nu_{yx})}$

} rigidity constants of orthotropic plate

E = Young's modulus of isotropic material

E_x, E_y = Young's moduli of orthotropic material

G = shear modulus of isotropic material

G_{xy} = shear modulus of orthotropic material

$H = D_1 + 2D_{xy}$

M_n = bending moment acting normal to boundary

$M_x = -\left(D_x \dfrac{\partial^2 w}{\partial x^2} + D_1 \dfrac{\partial^2 w}{\partial y^2}\right)$

$M_y = -\left(D_y \dfrac{\partial^2 w}{\partial y^2} + D_1 \dfrac{\partial^2 w}{\partial x^2}\right)$

} bending moments

$M_{xy} = -M_{yx} = 2D_{xy} \dfrac{\partial^2 w}{\partial x \partial y}$ twisting moments

$\bar{M}_{xmn} = -\left(D_x \dfrac{\partial^2 U_{mn}}{\partial x^2} + D_1 \dfrac{\partial^2 U_{mn}}{\partial y^2}\right)$

$\bar{M}_{ymn} = -\left(D_y \dfrac{\partial^2 U_{mn}}{\partial y^2} + D_1 \dfrac{\partial^2 U_{mn}}{\partial x^2}\right)$

P = applied transverse pressure

Q_{mn} = generalized force

$R = 4D_{xy} \dfrac{\partial^2 w}{\partial x \partial y}\Big|_{\text{corner}}$ corner reaction

$\bar{R}_{mn} = 4D_{xy} \dfrac{\partial^2 U_{mn}}{\partial x \partial y}$

T = kinetic energy

U_{mn} = plate eigenfunction

V = potential energy

V_n = Kirchhoff shear reaction at boundary

$V_x = -\left[D_x \dfrac{\partial^3 w}{\partial x^3} + (D_1 + 4D_{xy}) \dfrac{\partial^3 w}{\partial x \partial y^2}\right]$

$V_y = -\left[D_y \dfrac{\partial^3 w}{\partial y^3} + (D_1 + 4D_{xy}) \dfrac{\partial^3 w}{\partial x^2 \partial y}\right]$

} shear reactions

$\bar{V}_{xmn} = -\left[D_x \dfrac{\partial^3 U_{mn}}{\partial x^3} + (D_1 + 4D_{xy}) \dfrac{\partial^3 U_{mn}}{\partial x \partial y^2}\right]$

$\bar{V}_{ymn} = -\left[D_y \dfrac{\partial^3 U_{mn}}{\partial y^3} + (D_1 + 4D_{xy}) \dfrac{\partial^3 U_{mn}}{\partial x^2 \partial y}\right]$

Y_{mn} = trace of U_{mn} on plane x = const

a, b = plate widths in x and y-directions, respectively

h = plate thickness

K_1, K_2, K_3, K_4 = compliance coefficients of elastic support

p_{mn} = circular frequency

q_{mn} = generalized co-ordinate

r = b/a aspect ratio

t = time

w = displacement of plate in z-direction

x, y, z = rectangular co-ordinates

$\gamma_{mn} = D_y \phi_{mn}^2 - m^2\pi^2 D_1$

γ_{xy} = shearing strain

$\delta_{mn} = D_y \psi_{mn}^2 + m^2\pi^2 D_1$

ϵ_x, ϵ_y = dilatational strains

ν = Poisson's ratio of isotropic material

ν_{xy}, ν_{yx} = Poisson's ratios of orthotropic material

ρ = mass density of plate material

σ_x, σ_y = normal stresses

τ = auxiliary time variable

τ_{xy} = shearing stress

ϕ_{mn}, ψ_{mn} = frequency numbers

Introduction

The literature contains many analyses of specific boundary-value problems in small-deflection, thin-plate theory for which the transverse vibrations have been investigated.[4] Exact solutions were obtained in a few cases, but the majority of these problems were dealt with by approximate methods. These investigations were, for the most part,[5] concerned with plates of isotropic

[1] Professor of Applied Mechanics, Virginia Polytechnic Institute, Blacksburg, Va. Assoc. Mem. ASME.

[2] Associate Professor of Mechanical Engineering, The Johns Hopkins University, Baltimore, Md. Mem. ASME.

[3] Numbers in parentheses refer to the Bibliography at the end of the paper.

Contributed by the Applied Mechanics Division and presented at the Annual Meeting, New York, N. Y., December 1–6, 1957, of THE AMERICAN SOCIETY OF MECHANICAL ENGINEERS.

Discussion of this paper should be addressed to the Secretary, ASME, 29 West 39th Street, New York, N. Y., and will be accepted until October 10, 1958, for publication at a later date. Discussion received after the closing date will be returned.

NOTE: Statements and opinions advanced in papers are to be understood as individual expressions of their authors and not those of the Society. Manuscript received by ASME Applied Mechanics Division, May 29, 1957. Paper No. 57—A-85.

[4] No attempt will be made to give a complete listing of such references; however, the paper by Warburton (2) provides a fairly extensive bibliography on the subject.

[5] Certain exceptions being the papers by Hearmon (3), Kanazawa and Kawai (4), and Hoppmann, Huffington, and Magness (5), which deal with the flexural vibrations of orthotropic plates.

material. In the present paper, the flexural vibrations of rectangular plates of rectangularly orthotropic material are studied for a class of boundary-value problems for which solutions of classical type may be obtained. Only the transverse inertia forces will be considered, the effects of rotatory inertia and shear deformation being neglected. The reduction of the solutions possible in the special case of an isotropic material is indicated in the Appendix.

The results detailed herein should be of value in vibration analysis of plates of wood, plywood, plastics, and of orthogonally stiffened plates (5) to the extent that rotatory inertia effects do not become excessive.

Statement of problems

An orthotropic material, possessing three planes of elastic symmetry at a point, has nine independent elastic constants. Only four of these constants occur in the flexure theory of thin plates, for which the strain-stress relations may be written

$$\left.\begin{aligned} \epsilon_x &= \frac{1}{E_x}\sigma_x - \frac{\nu_{yx}}{E_y}\sigma_y \\ \epsilon_y &= -\frac{\nu_{xy}}{E_x}\sigma_x + \frac{1}{E_y}\sigma_y \\ \gamma_{xy} &= \frac{1}{G_{xy}}\tau_{xy} \end{aligned}\right\} \quad \ldots\ldots\ldots\ldots [1]$$

provided that the x, y-axes coincide with the symmetry axes of the orthotropic material. Since the matrix of elastic coefficients must be symmetric, there exists the further relation

$$\frac{\nu_{xy}}{E_x} = \frac{\nu_{yx}}{E_y} \quad \ldots\ldots\ldots\ldots\ldots\ldots [2]$$

which reduces the number of independent elastic constants to four.

With the customary assumptions that the strains are proportional to the distance from the neutral surface and that the curvatures are small, one may derive the differential equation of motion for the transversely vibrating plate of homogeneous orthotropic material

$$D_x\frac{\partial^4 w}{\partial x^4} + 2H\frac{\partial^4 w}{\partial x^2\partial y^2} + D_y\frac{\partial^4 w}{\partial y^4} + \rho h\frac{\partial^2 w}{\partial t^2} = P(x, y, t) \quad \ldots [3]$$

The symbols employed, plus the definitions of various quantities significant in plate theory (e.g., bending and twisting moments, shear reactions, concentrated corner reactions), are fully listed in the Nomenclature. In order to obtain reasonably tractable boundary conditions, attention will be restricted to cases where the symmetry axes of the material are orthogonal to the plate boundaries. The usually considered limiting cases for physical boundaries may be expressed as follows

$$\text{Simply supported edge} \left\{\begin{aligned} w &= 0 \\ M_n &= 0 \end{aligned}\right\} \text{ on boundary}$$

$$\text{Fixed edge} \left\{\begin{aligned} w &= 0 \\ \frac{\partial w}{\partial n} &= 0 \end{aligned}\right\} \text{ on boundary}$$

$$\text{Free edge} \left\{\begin{aligned} M_n &= 0 \\ V_n &= 0 \end{aligned}\right\} \text{ on boundary}$$

where n is the direction of the normal at the boundary, which may be either the x or y-direction for the cases to be considered.

Free vibrations

No difficulty is encountered in effecting a separation of space and time-dependent variables for the homogeneous form of Equation [3]. Letting

$$w = \sum_m \sum_n U_{mn}(x, y)q_{mn}(t) \quad \ldots\ldots\ldots\ldots [4]$$

it develops that q_{mn} is a harmonic function of time with circular frequency p_{mn} and that U_{mn} must satisfy the equation

$$D_x\frac{\partial^4 U_{mn}}{\partial x^4} + 2H\frac{\partial^4 U_{mn}}{\partial x^2\partial y^2} + D_y\frac{\partial^4 U_{mn}}{\partial y^4} = \rho h p_{mn}^2 U_{mn} \quad \ldots [5]$$

A further separation of U_{mn} as a product of a function of x and a function of y is not generally possible; however, M. Lévy (1) in connection with the static flexure probem has noted that the assumption

$$w = \sum_m \sin\frac{m\pi x}{a} Y_m(y) \qquad (m \text{ an integer})$$

effects a separation of variables for plates having two opposite edges simply supported. Applying the Lévy method, i.e., assuming

$$U_{mn}(x, y) = \sin\frac{m\pi x}{a} Y_m(y) \quad \ldots\ldots\ldots\ldots [6]$$

and substituting this into Equation [5] leads one to the following ordinary differential equation for Y_m

$$\frac{d^4 Y_m}{dy^4} - 2\frac{m^2\pi^2}{a^2}\frac{H}{D_y}\frac{d^2 Y_m}{dy^2} + \left(\frac{m^4\pi^4}{a^4}\frac{D_x}{D_y} - \frac{\rho h p_{mn}^2}{D_y}\right) Y_m = 0 \quad \ldots\ldots [7]$$

The general solution of Equation [7] is

$$\left.\begin{aligned} Y_m = {} & C_{1m}\cosh\frac{\phi_{mn}y}{a} + C_{2m}\sinh\frac{\phi_{mn}y}{a} \\ & + C_{3m}\cos\frac{\psi_{mn}y}{a} + C_{4m}\sin\frac{\psi_{mn}y}{a} \end{aligned}\right\} \quad \ldots [8]$$

where

$$\left.\begin{aligned} \phi_{mn} &= \frac{m\pi}{\sqrt{D_y}}\left[\left(H^2 - D_xD_y + \frac{\rho h D_y a^4 p_{mn}^2}{m^4\pi^4}\right)^{1/2} + H\right]^{1/2} \\ \psi_{mn} &= \frac{m\pi}{\sqrt{D_y}}\left[\left(H^2 - D_xD_y + \frac{\rho h D_y a^4 p_{mn}^2}{m^4\pi^4}\right)^{1/2} - H\right]^{1/2} \end{aligned}\right\}$$

For homogeneous boundary conditions of the type discussed in the preceding section, only the ratios of the constants C_{im} are determinate, the fourth boundary condition leading to the frequency equation. The roots of this equation are the eigenvalues ϕ_{mn}, ψ_{mn} for which the solution is valid. These two sets of eigenvalues are not independent, but are related by the equation

$$\phi_{mn}^2 - \psi_{mn}^2 = 2m^2\pi^2\frac{H}{D_y} \quad \ldots\ldots\ldots\ldots [9]$$

It will be seen that, for each value of m, there is an infinite number of roots of the frequency equation. These roots are numbered in ascending order: $n = 1, 2, 3, \ldots$. For each ϕ_{mn} there is a corresponding eigenfunction $U_{mn} = \sin(m\pi x/a)Y_m$, which constitutes a normal mode of vibration of the plate. The complete solution is obtained by superposition of all the normal modes; i.e.

$$w = \sum_m \sum_n \sin\frac{m\pi x}{a} Y_m(y)\,(A_{mn}\cos p_{mn}t + B_{mn}\sin p_{mn}t). \quad [10]$$

where the arbitrary constants A_{mn}, B_{mn} may be evaluated to satisfy the initial conditions. The circular frequency p_{mn} is re-

lated to the roots ϕ_{mn} of the frequency equation by

$$p_{mn} = \frac{(D_y\phi_{mn}^4 - 2m^2\pi^2H\phi_{mn}^2 + m^4\pi^4D_x)^{1/2}}{a^2\sqrt{(\rho h)}} \quad \ldots\ldots [11]$$

Six particular cases have been investigated, involving plates with combinations of simply supported, fixed, and free edges which have solutions of the form of Equation [10] (see Fig. 1). The frequency equations and the function Y_{mn} for these cases will now be presented. Case I, for which the solution is well known (3), is included for completeness.

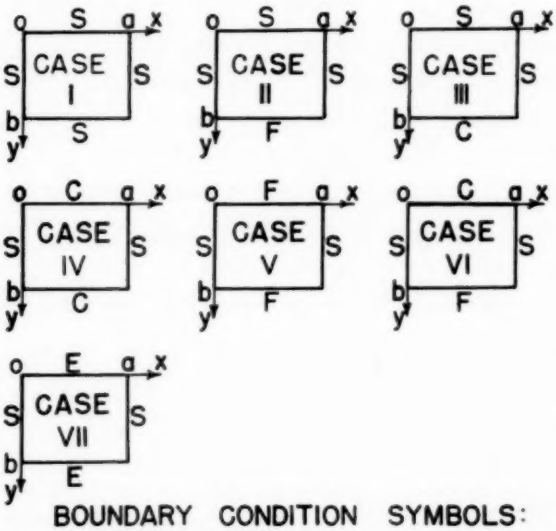

Fig. 1 Boundary-condition cases investigated

Case I. Plate simply supported on all four boundaries. The frequency equation has the simple form

$$\sin \psi_{mn}r = 0$$

the roots of which are

$$\psi_{mn} = \frac{n\pi}{r} = \frac{n\pi a}{b}, \quad n = 1, 2, 3, \ldots$$

Therefore

$$p_{mn} = \pi^2\left(\frac{m^4}{a^4}D_x + 2\frac{m^2n^2}{a^2b^2}H + \frac{n^4}{b^4}D_y\right)^{1/2}$$

and

$$Y_{mn} = \sin\frac{n\pi y}{b}$$

Case II. Plate simply supported on three edges, free on fourth. The frequency equation is

$$\frac{\tan \psi_{mn}r}{\tanh \phi_{mn}r} = \frac{\psi_{mn}\gamma_{mn}^2}{\phi_{mn}\delta_{mn}^2}$$

and

$$Y_{mn} = \frac{\sinh\frac{\phi_{mn}y}{a}}{\sinh \phi_{mn}r} + \frac{\gamma_{mn}\sin\frac{\psi_{mn}y}{a}}{\delta_{mn}\sin \psi_{mn}r}$$

Case III. Plate simply supported on three edges, clamped on fourth. The frequency equation is

$$\frac{\tan \psi_{mn}r}{\tanh \phi_{mn}r} = \frac{\psi_{mn}}{\phi_{mn}}$$

and

$$Y_{mn} = \frac{\sinh\frac{\phi_{mn}y}{a}}{\sinh \phi_{mn}r} - \frac{\sin\frac{\psi_{mn}y}{a}}{\sin \psi_{mn}r}$$

Case IV. Plate simply supported on two opposite edges, clamped on other two. The frequency equation is

$$m^2\pi^2\frac{H}{D_y}\sinh \phi_{mn}r \sin \psi_{mn}r + \phi_{mn}\psi_{mn}(1 - \cosh \phi_{mn}r \cos \psi_{mn}r) = 0$$

and

$$Y_{mn} = \frac{\cosh\frac{\phi_{mn}y}{a} - \cos\frac{\psi_{mn}y}{a}}{\cosh \phi_{mn}r - \cos \psi_{mn}r} - \frac{\psi_{mn}\sinh\frac{\phi_{mn}y}{a} - \phi_{mn}\sin\frac{\psi_{mn}y}{a}}{\psi_{mn}\sinh \phi_{mn}r - \phi_{mn}\sin \psi_{mn}r}$$

Case V. Plate simply supported on two opposite edges, free on other two. The frequency equation is

$$(\psi_{mn}^2\gamma_{mn}^4 - \phi_{mn}^2\delta_{mn}^4)\sinh \phi_{mn}r \sin \psi_{mn}r + 2\phi_{mn}\psi_{mn}\gamma_{mn}^2\delta_{mn}^2(\cosh \phi_{mn}r \cos \psi_{mn}r - 1) = 0$$

and

$$Y_{mn} = \frac{\delta_{mn}\cosh\frac{\phi_{mn}y}{a} + \gamma_{mn}\cos\frac{\psi_{mn}y}{a}}{\gamma_{mn}\delta_{mn}(\cosh \phi_{mn}r - \cos \psi_{mn}r)} - \frac{\psi_{mn}\gamma_{mn}\sinh\frac{\phi_{mn}y}{a} + \phi_{mn}\delta_{mn}\sin\frac{\psi_{mn}y}{a}}{\psi_{mn}\gamma_{mn}^2\sinh \phi_{mn}r - \phi_{mn}\delta_{mn}^2\sin \psi_{mn}r}$$

Case VI. Plate simply supported on two opposite edges, clamped on third edge, and free on fourth. The frequency equation is

$$(\psi_{mn}^2\gamma_{mn}^2 - \phi_{mn}^2\delta_{mn}^2)\sinh \phi_{mn}r \sin \psi_{mn}r + \phi_{mn}\psi_{mn}[(\gamma_{mn}^2 + \delta_{mn}^2)\cosh \phi_{mn}r \cos \psi_{mn}r + 2\gamma_{mn}\delta_{mn}] = 0$$

and

$$Y_{mn} = \frac{\cosh\frac{\phi_{mn}y}{a} - \cos\frac{\psi_{mn}y}{a}}{\gamma_{mn}\cosh \phi_{mn}r + \delta_{mn}\cos \psi_{mn}r} - \frac{\psi_{mn}\sinh\frac{\phi_{mn}y}{a} - \phi_{mn}\sin\frac{\psi_{mn}y}{a}}{\psi_{mn}\gamma_{mn}\sinh \phi_{mn}r + \phi_{mn}\delta_{mn}\sin \psi_{mn}r}$$

In addition to the preceding boundary-value problems, the more general problem of a plate with two opposite boundaries elastically supported has been investigated. If the support is linearly elastic with respect to both transverse displacement and slope of the boundary normal, the boundary conditions may be expressed as

$$\left.\begin{aligned} V_y\Big|_{y=0} &= K_1 w\Big|_{y=0} & V_y\Big|_{y=b} &= -K_3 w\Big|_{y=b} \\ M_y\Big|_{y=0} &= -K_2\frac{\partial w}{\partial y}\Big|_{y=0} & M_y\Big|_{y=b} &= K_4\frac{\partial w}{\partial y}\Big|_{y=b} \\ (K_1, K_2, K_3, K_4 \geq 0) & & & \end{aligned}\right\} \quad \ldots [12]$$

The application of these boundary conditions in conjunction with Equation [8] leads to the results which follow.

Case VII. Plate simply supported on two opposite edges, and elastically supported on other two. The frequency equation is

$$\begin{aligned}
&[\psi_{mn}^2\gamma_{mn}^2(\gamma_{mn}^2 - K_1K_2a^4) - \phi_{mn}^2\delta_{mn}^2(\delta_{mn}^2 - K_1K_2a^4) + K_2K_4a^4\{\phi_{mn}^2(\delta_{mn}^2 - K_1K_2a^4) - \psi_{mn}^2(\gamma_{mn}^2 - K_1K_2a^4)\} \\
&\quad + a^2(\gamma_{mn} + \delta_{mn})^2(K_2K_4\phi_{mn}^2\psi_{mn}^2 - K_1K_3a^4)]\sinh\phi_{mn}r\sin\psi_{mn}r + \phi_{mn}\psi_{mn}[2\gamma_{mn}^2\delta_{mn}^2 - K_1K_2a^4(\gamma_{mn}^2 + \delta_{mn}^2) \\
&\quad - K_2K_4a^4(\delta_{mn}^2 + \gamma_{mn}^2 - 2K_1K_2a^4) - a^4(K_1K_4 + K_2K_3)(\gamma_{mn} + \delta_{mn})^2]\cosh\phi_{mn}r\cos\psi_{mn}r \\
&\quad + a\psi_{mn}(\gamma_{mn} + \delta_{mn})[-K_1a^2\gamma_{mn}^2 + K_2\phi_{mn}^2\delta_{mn}^2 - K_2a^2(\gamma_{mn}^2 - K_1K_2a^4) + K_4\phi_{mn}^2(\delta_{mn}^2 - K_1K_2a^4) \\
&\quad + K_2K_4a^4(K_1a^2 - K_2\phi_{mn}^2)]\sinh\phi_{mn}r\cos\psi_{mn}r + a\phi_{mn}(\gamma_{mn} + \delta_{mn})[K_1a^2\delta_{mn}^2 + K_2\psi_{mn}^2\gamma_{mn}^2 + K_2a^2(\delta_{mn}^2 - K_1K_2a^4) \\
&\quad + K_4\psi_{mn}^2(\gamma_{mn}^2 - K_1K_2a^4) - K_2K_4a^4(K_1a^2 + K_2\psi_{mn}^2)]\cosh\phi_{mn}r\sin\psi_{mn}r - 2\phi_{mn}\psi_{mn}(\gamma_{mn}\delta_{mn} + K_1K_2a^4)(\gamma_{mn}\delta_{mn} + K_2K_4a^4) = 0
\end{aligned}$$

and

$$\begin{aligned}
Y_{mn} &= [\psi_{mn}(\gamma_{mn}\delta_{mn} + K_1K_2a^4)(\gamma_{mn}\sinh\phi_{mn}r + K_4a\phi_{mn}\cosh\phi_{mn}r) - \phi_{mn}(\delta_{mn}^2 - K_1K_2a^4)(\delta_{mn}\sin\psi_{mn}r - K_4a\psi_{mn}\cos\psi_{mn}r) \\
&\quad + K_2a\phi_{mn}\psi_{mn}(\gamma_{mn} + \delta_{mn})(\delta_{mn}\cos\psi_{mn}r + K_4a\psi_{mn}\sin\psi_{mn}r)]\cosh\frac{\phi_{mn}y}{a} + [\psi_{mn}(\gamma_{mn}^2 - K_1K_2a^4)(\gamma_{mn}\sinh\phi_{mn}r + K_4a\phi_{mn}\cosh\phi_{mn}r) \\
&\quad + K_2a\phi_{mn}\psi_{mn}(\gamma_{mn} + \delta_{mn})(\gamma_{mn}\cosh\phi_{mn}r + K_4a\phi_{mn}\sinh\phi_{mn}r) - \phi_{mn}(\gamma_{mn}\delta_{mn} + K_1K_2a^4)(\delta_{mn}\sin\psi_{mn}r - K_4a\psi_{mn}\cos\psi_{mn}r)]\cos\frac{\psi_{mn}y}{a} \\
&\quad + [-\psi_{mn}(\gamma_{mn}\delta_{mn} + K_1K_2a^4)(\gamma_{mn}\cosh\phi_{mn}r + K_4a\phi_{mn}\sinh\phi_{mn}r) + \psi_{mn}(\gamma_{mn}^2 - K_1K_2a^4)(\delta_{mn}\cos\psi_{mn}r + K_4a\psi_{mn}\sin\psi_{mn}r) \\
&\quad + K_1a^2(\gamma_{mn} + \delta_{mn})(\delta_{mn}\sin\psi_{mn}r - K_4a\psi_{mn}\cos\psi_{mn}r)]\sinh\frac{\phi_{mn}y}{a} + [K_1a^2(\gamma_{mn} + \delta_{mn})(\gamma_{mn}\sinh\phi_{mn}r + K_4a\phi_{mn}\cosh\phi_{mn}r) \\
&\quad - \phi_{mn}(\delta_{mn}^2 - K_1K_2a^4)(\gamma_{mn}\cosh\phi_{mn}r + K_4a\phi_{mn}\sinh\phi_{mn}r) + \phi_{mn}(\gamma_{mn}\delta_{mn} + K_1K_2a^4)(\delta_{mn}\cos\psi_{mn}r + K_4a\psi_{mn}\sin\psi_{mn}r)]\sin\frac{\psi_{mn}y}{a}
\end{aligned}$$

The frequency equations and eigenfunctions for the first six cases may be deduced from those of Case VII by assigning the proper limiting values (0 or ∞) to the constants K_1, K_2, K_3, and K_4. In addition, other solutions for boundary-value problems involving the less physically significant "guided" boundary, expressible analytically as

$$\frac{\partial w}{\partial y}\Big|_{y=y_b} = 0, \qquad V_y\Big|_{y=y_b} = 0$$

may be deduced from the results for Case VII.

The treatment of a specific vibration problem involving any of the foregoing boundary-value cases necessitates the determination of the eigenvalues ϕ_{mn}, ψ_{mn} of the appropriate frequency equation. By consideration of the geometrical properties of the functions occurring therein and the use of available detailed tables of the transcendental functions (6, 7), one may find the lower eigenvalues without excessive labor. The higher eigenvalues, if needed, may be determined from explicit asymptotic relations, deducible from the frequency equations by virtue of the properties of the hyperbolic functions of large argument and other order of magnitude considerations (8, 9).

The existence of real roots for each frequency equation has been ascertained for a particular set of values of the parameters r, D_{xy}/D_y, D_1/D_y. Since a complete set of eigenvalues is associated with every assignable value of each of these parameters, no attempt has been made to provide tables of frequency roots. Such an extensive project would be facilitated by use of high-speed digital computing equipment.

Orthogonality properties

Since both free and forced-vibration calculations are greatly simplified when orthogonal eigenfunctions are employed, it is desirable to establish a criterion for the occurrence of such eigenfunctions as determined by the boundary conditions. The plate eigenfunctions U_{mn} comprise an orthogonal set provided that

$$\int_0^a\int_0^b U_{mn}U_{ij}dxdy = 0 \qquad \text{for } mn \neq ij$$

Consider Equation [5] and the corresponding equation satisfied by the ij^{th} function. By multiplying the former by U_{ij} and the latter by U_{mn}, taking the difference and integrating the result over the area of the plate, one obtains an expression involving the desired integral. Successive integrations by parts result in the following relation

$$\begin{aligned}
&\int_0^a\int_0^b U_{mn}U_{ij}dxdy \\
&= \frac{1}{\rho h(p_{ij}^2 - p_{mn}^2)}\Bigg[\int_0^a\Bigg\{\left(D_y\frac{\partial^2U_{mn}}{\partial y^2} + D_1\frac{\partial^2U_{mn}}{\partial x^2}\right)\frac{\partial U_{ij}}{\partial y} \\
&\quad - \left(D_y\frac{\partial^2U_{ij}}{\partial y^2} + D_1\frac{\partial^2U_{ij}}{\partial x^2}\right)\frac{\partial U_{mn}}{\partial y} \\
&\quad + \left(D_y\frac{\partial^3U_{ij}}{\partial y^3} + (D_1 + 4D_{xy})\frac{\partial^3U_{ij}}{\partial x^2\partial y}\right)U_{mn} \\
&\quad - \left(D_y\frac{\partial^3U_{mn}}{\partial y^3} + (D_1 + 4D_{xy})\frac{\partial^3U_{mn}}{\partial x^2\partial y}\right)U_{ij}\Bigg\}_0^b dx \\
&\quad + \int_0^b\Bigg\{\left(D_x\frac{\partial^2U_{mn}}{\partial x^2} + D_1\frac{\partial^2U_{mn}}{\partial y^2}\right)\frac{\partial U_{ij}}{\partial x} \\
&\quad - \left(D_x\frac{\partial^2U_{ij}}{\partial x^2} + D_1\frac{\partial^2U_{ij}}{\partial y^2}\right)\frac{\partial U_{mn}}{\partial x}
\end{aligned}$$

$$+\left(D_x\frac{\partial^3 U_{ij}}{\partial x^3}+(D_1+4D_{xy})\frac{\partial^3 U_{ij}}{\partial x\partial y^2}\right)U_{mn}$$

$$-\left(D_x\frac{\partial^3 U_{mn}}{\partial x^3}+(D_1+4D_{xy})\frac{\partial^3 U_{mn}}{\partial x\,\partial y^2}\right)U_{ij}\Big\}_0^a dy$$

$$-4D_{xy}\left\{U_{mn}\frac{\partial^2 U_{ij}}{\partial x\,\partial y}-U_{ij}\frac{\partial^2 U_{mn}}{\partial x\partial y}\right\}_{0,0}^{a,b}\Bigg]\quad\ldots\ldots[13]$$

The terms in Equation [13] have been grouped for identification of their correspondence with the geometric and natural boundary conditions of classical thin-plate theory. Introducing the symbol $\bar{M}_{xmn}$ defined by the relation

$$M_x=-\sum_m\sum_n\left(D_x\frac{\partial^2 U_{mn}}{\partial x^2}+D_1\frac{\partial^2 U_{mn}}{\partial y^2}\right)q_{mn}$$

$$=\sum_m\sum_n\bar{M}_{xmn}q_{mn}$$

and quantities $\bar{M}_{ymn}$, $\bar{V}_{xmn}$, $\bar{V}_{ymn}$, $\bar{R}_{mn}$ defined in a similar manner, Equation [13] may be rewritten as

$$\int_0^a\int_0^b U_{mn}U_{ij}dxdy=\frac{1}{\rho h(p_{mn}^2-p_{ij}^2)}\Bigg[\int_0^a\Big\{\bar{M}_{ymn}\frac{\partial U_{ij}}{\partial y}$$

$$-\bar{M}_{yij}\frac{\partial U_{mn}}{\partial y}+\bar{V}_{yij}U_{mn}-\bar{V}_{ymn}U_{ij}\Big\}_0^b dx$$

$$+\int_0^b\Big\{\bar{M}_{xmn}\frac{\partial U_{ij}}{\partial x}-\bar{M}_{xij}\frac{\partial U_{mn}}{\partial x}+\bar{V}_{xij}U_{mn}-\bar{V}_{xmn}U_{ij}\Big\}_0^a dy$$

$$+\Big\{\bar{R}_{ij}U_{mn}-\bar{R}_{mn}U_{ij}\Big\}_{0,0}^{a,b}\Bigg]\quad\ldots\ldots[14]$$

From this relation it is clear that the eigenfunctions of a plate having any combination of simply supported, fixed, free, or guided boundaries will be orthogonal. The elastically supported boundary may be included in this listing provided that the concentrated corner reactions are zero or directly proportional to the corner displacements. This result may be established easily by use of the boundary conditions of Equation [12] in conjunction with Equation [14].

Energy functions

In the analysis of forced vibrations by the Lagrangian method (10) it is necessary to express the kinetic and potential energies of the vibrating system as functions of the generalized velocities and displacements, respectively. Starting with the basic definition and introducing Equation [4], the kinetic energy assumes the form

$$T=\frac{\rho h}{2}\int_0^a\int_0^b\left(\frac{\partial w}{\partial t}\right)^2dxdy$$

$$=\frac{\rho h}{2}\int_0^a\int_0^b\left(\sum_m\sum_n U_{mn}\dot{q}_{mn}\right)^2dxdy$$

$$=\frac{\rho h}{2}\int_0^a\int_0^b\sum_m\sum_n\sum_i\sum_j U_{mn}U_{ij}\dot{q}_{mn}\dot{q}_{ij}\,dxdy$$

$$=\frac{\rho h}{2}\sum_m\sum_n\dot{q}_{mn}^2\int_0^a\int_0^b U_{mn}^2\,dxdy$$

$$+\frac{\rho h}{2}\sum_m\sum_n\sum_{i^*}\sum_{j^*}\dot{q}_{mn}\dot{q}_{ij}\int_0^a\int_0^b U_{mn}U_{ij}\,dxdy\quad\ldots[15]$$

where i^*, j^* imply that terms for which $ij=mn$ are excluded. Since the latter term vanishes for orthogonal eigenfunctions, the kinetic-energy function for plates having the boundary conditions discussed in the preceding section reduces to

$$T=\frac{\rho ha^2}{2}\sum_m\sum_n k_{mn}\dot{q}_{mn}^2$$

where

$$k_{mn}=\frac{1}{a^2}\int_0^a\int_0^b U_{mn}^2dxdy\qquad\ldots\ldots[16]$$

The potential energy (of strain) for a rectangular orthotropic plate expressed in terms of the displacement function is given (11) by the relation

$$V=\frac{1}{2}\int_0^a\int_0^b\left[D_x\left(\frac{\partial^2 w}{\partial x^2}\right)^2+2D_1\frac{\partial^2 w}{\partial x^2}\frac{\partial^2 w}{\partial y^2}\right.$$

$$\left.+D_y\left(\frac{\partial^2 w}{\partial y^2}\right)^2+4D_{xy}\left(\frac{\partial^2 w}{\partial x\partial y}\right)^2\right]dxdy\quad\ldots\ldots[17]$$

Substituting for w from Equation [4] and separating the terms proportional, respectively, to the squares and to the products of the generalized co-ordinates, Equation [17] becomes

$$V=\frac{1}{2}\sum_m\sum_n q_{mn}^2\int_0^a\int_0^b\left[D_x\left(\frac{\partial^2 U_{mn}}{\partial x^2}\right)^2\right.$$

$$+2D_1\frac{\partial^2 U_{mn}}{\partial x^2}\frac{\partial^2 U_{mn}}{\partial y^2}+D_y\left(\frac{\partial^2 U_{mn}}{\partial y^2}\right)^2+4D_{xy}\left(\frac{\partial^2 U_{mn}}{\partial x\partial y}\right)^2\Bigg]dxdy$$

$$+\frac{1}{2}\sum_m\sum_n\sum_{i^*}\sum_{j^*}q_{mn}q_{ij}\int_0^a\int_0^b\left[D_x\frac{\partial^2 U_{mn}}{\partial x^2}\frac{\partial^2 U_{ij}}{\partial x^2}\right.$$

$$+D_1\left(\frac{\partial^2 U_{mn}}{\partial x^2}\frac{\partial^2 U_{ij}}{\partial y^2}+\frac{\partial^2 U_{mn}}{\partial y^2}\frac{\partial^2 U_{ij}}{\partial x^2}\right)+D_y\frac{\partial^2 U_{mn}}{\partial y^2}\frac{\partial^2 U_{ij}}{\partial y^2}$$

$$\left.+4D_{xy}\frac{\partial^2 U_{mn}}{\partial x\partial y}\frac{\partial^2 U_{ij}}{\partial x\partial y}\right]dxdy\quad\ldots\ldots[18]$$

It is desired to replace the double integrals appearing in this expression by fully or partially integrated terms, to be evaluated at the boundaries, which may be grouped in the manner discussed in connection with Equation [13]. This may be accomplished by substituting for individual terms in the integrands expressions obtained by use of Equation [5]. For example, to evaluate the first term appearing in the quadruple summation, operate on Equation [5] with

$$D_x\frac{\partial^2 U_{ij}}{\partial x^2}\frac{\partial^2}{\partial x^2}$$

and on the corresponding equation for U_{ij} with

$$D_x\frac{\partial^2 U_{mn}}{\partial x^2}\frac{\partial^2}{\partial x^2}$$

take the difference, and integrate over the area of the plate. After two partial integrations one obtains

$$\int_0^a\int_0^b D_x\frac{\partial^2 U_{mn}}{\partial x^2}\frac{\partial^2 U_{ij}}{\partial x^2}\,dxdy=\frac{1}{p_{ij}^2-p_{mn}^2}\int_0^b$$

$$D_x\Big\{p_{ij}^2\left(\frac{\partial^2 U_{mn}}{\partial x^2}\frac{\partial U_{ij}}{\partial x}-\frac{\partial^2 U_{mn}}{\partial x^2}U_{ij}\right)$$

$$-p_{mn}^2\left(\frac{\partial^2 U_{ij}}{\partial x^2}\frac{\partial U_{mn}}{\partial x}-\frac{\partial^2 U_{ij}}{\partial x^2}U_{mn}\right)\Big\}_0^a dy$$

$$+\frac{1}{\rho h(p_{ij}^2-p_{mn}^2)}\int_0^a\int_0^b D_x\left(\frac{\partial^4 U_{mn}}{\partial x^4}\nabla_0^4 U_{ij}-\frac{\partial^4 U_{ij}}{\partial x^4}\nabla_0^4 U_{mn}\right)dxdy$$

where it has been convenient to employ the "orthotropic biharmonic operator"

$$\nabla_0^4 = D_x\frac{\partial^4}{\partial x^4}+2H\frac{\partial^4}{\partial x^2\partial y^2}+D_y\frac{\partial^4}{\partial y^4}$$

In an analogous manner, the other terms occurring in Equation [18] may be evaluated. When these quantities are collected and certain further partial integrations performed, the result takes the form

$$\begin{aligned}V=\frac{1}{2}\sum_m\sum_n q_{mn}^2\Bigg[&\rho h p_{mn}^2\int_0^a\int_0^b U_{mn}^2\,dxdy\\&+\int_0^a\left\{\bar{V}_{ymn}U_{mn}-\bar{M}_{ymn}\frac{\partial U_{mn}}{\partial y}\right\}_0^b dx\\&+\int_0^b\left\{\bar{V}_{xmn}U_{mn}-\bar{M}_{xmn}\frac{\partial U_{mn}}{\partial x}\right\}_0^a dy+\left\{\bar{R}_{mn}U_{mn}\right\}_{0,0}^{a,b}\Bigg]\\+\frac{1}{2}\sum_m\sum_n\sum_{i\neq}\sum_{j\neq}\frac{q_{mn}q_{ij}}{p_{mn}^2-p_{ij}^2}\Bigg[&\int_0^a\left\{p_{ij}^2\left(\bar{M}_{ymn}\frac{\partial U_{ij}}{\partial y}-\bar{V}_{ymn}U_{ij}\right)-p_{mn}^2\left(\bar{M}_{yij}\frac{\partial U_{mn}}{\partial y}-\bar{V}_{yij}U_{mn}\right)\right\}_0^b dx\\&+\int_0^b\left\{p_{ij}^2\left(\bar{M}_{xmn}\frac{\partial U_{ij}}{\partial x}-\bar{V}_{xmn}U_{ij}\right)-p_{mn}^2\left(\bar{M}_{xij}\frac{\partial U_{mn}}{\partial x}-\bar{V}_{xij}U_{mn}\right)\right\}_0^a dy\\&+\left\{p_{mn}^2\bar{R}_{ij}U_{mn}-p_{ij}^2\bar{R}_{mn}U_{ij}\right\}_{0,0}^{a,b}\Bigg]\end{aligned}\quad\ldots\ldots[19]$$

It is obvious that a great simplification of this expression occurs for plates with any combination of simply supported, fixed, free, or guided boundaries. For all these cases

$$V=\frac{\rho h a^2}{2}\sum_m\sum_n k_{mn}p_{mn}^2q_{mn}^2\quad\ldots\ldots[20]$$

In the case of the elastically supported plate, many additional terms remain after the application of the boundary conditions. However, these energy terms will be found to correspond to just the negative of the energy stored in the elastic foundation. Consequently, if V is used to denote the potential energy of the system, rather than that of the plate alone, Equation [20] is valid for this case as well. Reference to Equations [16] and [20] indicates that, for a plate having any of the boundary conditions discussed in this paper, the functions U_{mn} (which satisfy the boundary conditions and Equation [5]) pair off with generalized co-ordinates q_{mn} which are the normal co-ordinates of the system.

Forced vibrations

The forced vibrations of rectangular orthotropic plates, governed by Equation [3], may be readily investigated by the Lagrangian method with the aid of the energy functions. In general, the energy functions obtained by use of Equations [13], [15], and [19] will not necessarily be expressed in terms of normal co-ordinates. The use of the Lagrangian method will provide $m \times n$ ordinary differential equations which individually may contain terms in all the generalized co-ordinates and which must be solved simultaneously. Approximate solutions for such problems may be obtained by iteration procedures.

Restricting attention to those boundary conditions for which it has been shown that the energy functions may be expressed in terms of normal co-ordinates, the kinetic and potential energies are given by the simple relations of Equations [16] and [20]. The substitution of these energy functions into Lagrange's equations leads to $m \times n$ independent differential equations of the form

$$\ddot{q}_{mn}+p_{mn}^2q_{mn}=\frac{Q_{mn}}{\rho h a^2 k_{mn}}\quad\ldots\ldots[21]$$

where the generalized force has the value

$$Q_{mn}(t)=\int_0^a\int_0^b P(x,y,t)U_{mn}(x,y)dxdy\quad\ldots\ldots[22]$$

The formal solution of Equation [21] is easily obtained; when this is substituted in Equation [4], the displacement function w is found to be

$$\begin{aligned}w(x,y,t)=\frac{1}{a^2}\sum_{m=1}^{\infty}\sum_{n=1}^{\infty}\frac{U_{mn}(x,y)}{k_{mn}p_{mn}}\Bigg[&\frac{1}{\rho h}\int_0^t Q_{mn}(\tau)\\&\sin p_{mn}(t-\tau)d\tau+p_{mn}\cos p_{mn}t\int_0^a\int_0^b w(x,y,0)U_{mn}dxdy\\&+\sin p_{mn}t\int_0^a\int_0^b\dot{w}(x,y,0)U_{mn}dxdy\Bigg]\end{aligned}\quad\ldots\ldots[23]$$

where $w(x, y, 0)$, $\dot{w}(x, y, 0)$ are the initial conditions specified at $t = 0$ and the load $P(x, y, t)$ acts for $t \geqq 0$. Other quantities of interest in design, e.g., stresses, shear forces, and reactions, may be determined readily once the displacement function is known.

Summary

The free transverse vibrations of thin rectangular orthotropic and isotropic plates have been investigated for a variety of boundary combinations, all of which had the characteristic that two opposite boundaries were simply supported. The method introduced by M. Lévy for treating static problems has been exploited to obtain frequency equations and mode shapes for these boundary-value problems. Frequency numbers have been determined for special cases but no tabulations are provided, since this would require a more ambitious computing program than is presently contemplated.

It should be noted that the results presented in the discussion of orthogonality properties and energy functions are not restricted to the class of problems which may be treated by the Lévy method, but apply whenever the separation of variables represented by Equation [4] is possible. The relations expressed by Equations [13], [15], and [19] serve a dual purpose. They indicate great simplifications which are possible for many boundary combinations, even permitting deductions regarding the form of the energy functions for many boundary-value problems for which solutions have not been found. Also, these relations may be used in analyses where the boundary conditions lead to non-orthogonal eigenfunctions.

Although only the formal aspects of the forced-vibration problem are presented in this paper, the reader will find in references (8) and (9) examples of the application of such analysis to dynamical problems involving the blast loading of plates.

Acknowledgments

The authors gratefully acknowledge the support for this investigation provided by the Operations Research Office of The Johns

Hopkins University and by the Virginia Engineering Experiment Station. The authors also wish to thank Mr. Kuang-Liu Cheng, graduate student in Applied Mechanics at Virginia Polytechnic Institute, for his assistance in certain numerical computations.

Bibliography

1 "Sur l'équilibre élastique d'une plaque rectangulaire," by M. Lévy, *Comptes Rendus*, vol. 129, 1899, pp. 535–539.

2 "The Vibration of Rectangular Plates," by G. B. Warburton, Proceedings of The Institution of Mechanical Engineers, vol. 168, no. 12, 1954, pp. 371–384.

3 "The Fundamental Frequency of Vibration of Rectangular Wood and Plywood Plates," by R. F. S. Hearmon, Proceedings of the Physical Society of London, vol. 58, 1946, pp. 78–92.

4 "On the Lateral Vibration of Anisotropic Rectangular Plates (Studied by the Integral Equation)," by T. Kanazawa and T. Kawai, Proceedings of Second Japan National Congress for Applied Mechanics, 1952, pp. 333–338.

5 "A Study of Orthogonally Stiffened Plates," by W. H. Hoppmann II, N. J. Huffington, Jr., and L. S. Magness, JOURNAL OF APPLIED MECHANICS, TRANS. ASME, vol. 78, 1956, pp. 343–350.

6 "Tables of Circular and Hyperbolic Sines and Cosines for Radian Arguments," National Bureau of Standards, Applied Mathematics Series, No. 36.

7 "Table of Hyperbolic Sines and Cosines — $x = 2$ to $x = 10$," National Bureau of Standards, Applied Mathematics Series, No. 45.

8 "Blast Loading of Walls," by N. J. Huffington, Jr., and W. H. Hoppmann II, Technical Memorandum ORO-T-199, Operations Research Office, The Johns Hopkins University, Baltimore, Md., January, 1953.

9 "Blast Loading of Orthotropic Plates," by N. J. Huffington, Jr., and W. H. Hoppmann II, Technical Memorandum ORO-T-239, Operations Research Office, The Johns Hopkins University, Baltimore, Md., January, 1954.

10 "Vibration Problems in Engineering," by S. Timoshenko, D. Van Nostrand Company, Inc., New York, N. Y., second edition, 1937.

11 "Zur Elastizitätstheorie der anorthotropen Platten," by M. T. Huber, Timoshenko 60th Anniversary Volume, The Macmillan Company, New York, N. Y., 1938, pp. 89–92.

12 "Die Eigenwertprobleme für die elastische rechteckige Platte," by S. Iguchi, *Memoirs of the Faculty of Engineering*, Hokkaido Imperial University, vol. 4, 1938, pp. 305–372.

13 "On the Lateral Vibration of a Rectangular Plate Clamped at Four Edges," by K. Sezawa, Report of the Aeronautical Research Institute, Tokyo Imperial University, Tokyo, Japan, No. 70, 1931.

14 "On the Bending and Vibration of Rectangular Plates," by H. Kato, *Journal of the Society of Naval Architects* (Japan), vol. 50, 1932, pp. 209–230.

15 "Bemerkung zu dem Problem der transversalen Schwingungen rechteckiger Platten," by W. Voigt, Nachrichten, Göttingen, Germany, 1893, pp. 225–230.

16 "Ein einfacher Fall der transversalen Schwingung einer rechteckigen elastischen Platte," by C. Zeissig, *Annalen der Physik*, Wiedemann, Leipzig, vol. 64, 1898, pp. 360–397.

APPENDIX

The foregoing results for plates of rectangularly orthotropic material necessarily apply to the special case of the isotropic material. Particularization to the isotropic case may be accomplished by replacing the orthotropic constants by their corresponding isotropic values as listed

$$E_x, E_y \to E \qquad \nu_{xy}, \nu_{yx} \to \nu \qquad G_{xy} \to G = \frac{E}{2(1+\nu)}$$

$$D_x, D_y, H \to D = \frac{Eh^3}{12(1-\nu^2)} \qquad D_1 \to \nu D \qquad D_{xy} \to \frac{(1-\nu)}{2} D$$

The frequency equations and mode shapes for isotropic plates with boundary conditions of Cases I–VI have been listed previously (8). Certain of these results may be compared with data from other sources. Iguchi (12) has calculated frequencies for several modes of Case III, and Warburton (2) has derived a transcendental frequency equation which may be shown to agree with the solution of this paper reduced to the isotropic case. Frequencies corresponding to Case IV have been studied by Sezawa (13), Kato (14), and Iguchi (12). Voigt (15) derived a frequency equation corresponding to Case V, and Zeissig (16) determined a number of frequencies and mode shapes for this case. In addition, Warburton (2) has determined approximate frequency relations for isotropic plates having a wide selection of boundary conditions by use of the Rayleigh method.

Contact Stresses Under Combined Pressure and Twist[1]

By M. HETÉNYI[2] and P. H. MCDONALD, JR.[3]

An analytical solution is presented for the case when an elastic sphere is pressed against an elastic half-space and twisted until complete slip occurs. Formulas are derived for the stress and displacement components, their evaluation is illustrated by numerical examples, and comparisons are made with the results of photoelastic tests. These tests also furnished an experimental verification of the assumption that the tangential-surface traction is proportional at every point to the normal pressure within the sliding-contact area, the proportionality constant being the coefficient of friction.

Analytical Solution

The deformation and relative motion of spheres subjected to combined pressure and twist have been the subject of several papers by R. D. Mindlin and his associates (1).[4] It has been found that, as the magnitude of the applied torque is increased, there is a widening annular band of slip occurring within the boundary of the contact area, leading to a nonlinear torque-twist relation which has interesting consequences. Though it has been surmised for some time that the state of stress due to such combined loading was likely to be severe, since tests of this type lead to a rapid destruction and failure of material at the contacting surfaces (2), no solution of the corresponding stress problem has been attained thus far. The object of this paper is to present such a solution for the limiting case when the applied torque is large enough to cause slippage over the entire contact area. In the analytical solution it will be assumed that, at any point within the contact area, the tangential surface traction resulting from the applied torque will be proportional to the normal pressure produced at that point according to the Hertzian theory, the factor of proportionality being the coefficient of friction f between the contacting surfaces. In the latter part of the paper, it will be shown that photoelastic measurements corroborate the existence of this proportionality, which has been a basic assumption in all previous analytical work dealing with relative sliding between contacting surfaces (1).

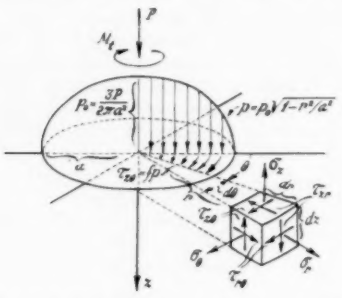

Fig. 1 Leading and stress components in a cylindrical co-ordinate system

Thus the problem can be formulated as that of a semi-infinite solid, loaded on its plane surface by a so-called "hemispherical" distribution of Hertzian normal pressure, $p = -(\sigma_z)_{z=0}$, and a similarly distributed surface shear loading $(\tau_{z\theta})_{z=0} = fp$, as shown in Fig. 1. The cylindrical system of co-ordinates r, θ, and z, which will be used in the analysis, is also indicated in the same figure, together with the positive directions of the corresponding stress components. The displacement components acting in the positive direction of r, θ, and z will be denoted by u, v, and w, respectively.

It has been shown (3) that it is possible to derive a solution for this simultaneous pressure and twist problem by means of the theory of potentials. However, it is easily seen that, in this combined contact problem, the effects of pressure and twist are independent of each other; namely, owing to its axial symmetry, the normal pressure by itself will produce no circumferential displacement, $v = 0$. On the other hand, as shown by J. H. Michell (4), this same v will be the only nonvanishing displacement component when the rotationally symmetrical surface-shear loading is applied. Thus there will be no "coupling" between the two types of action. Since, for the normal loading alone, the stress components already have been given by A. E. H. Love (5), at this place, for the sake of brevity, only the second part of the solution will be discussed; namely, that due to the surface-shear loading. Having, in this case, $u = 0$ and $w = 0$, there will be only two nonvanishing stress components, $\tau_{r\theta}$ and $\tau_{z\theta}$. The equilibrium conditions can thus be stated by one equation

$$\frac{\partial \tau_{r\theta}}{\partial r} + \frac{\partial \tau_{z\theta}}{\partial z} + \frac{2}{r}\tau_{r\theta} = 0 \qquad [a]$$

Expressing these stress components in terms of the displacement v

$$\tau_{r\theta} = \mu\left(\frac{\partial v}{\partial r} - \frac{v}{r}\right) \quad \text{and} \quad \tau_{z\theta} = \mu\frac{\partial v}{\partial z} \qquad [b]$$

where μ denotes the modulus of elasticity in shear. By substitution into the foregoing equilibrium equation we get

$$\frac{\partial^2 v}{\partial r^2} + \frac{1}{r}\frac{\partial v}{\partial r} - \frac{v}{r^2} + \frac{\partial^2 v}{\partial z^2} = 0 \qquad [c]$$

---

[1] The content of this paper was first presented at the Ninth International Congress of Applied Mechanics in Brussels, Belgium, September, 1956. The results were obtained in the course of an investigation conducted for the Office of Naval Research, under Contract N7onr-45009.

[2] Walter P. Murphy Professor of Engineering Science, The Technological Institute, Northwestern University, Evanston, Ill. Mem. ASME.

[3] Research Professor of Mechanical Engineering, North Carolina State College, Raleigh, N. C.; formerly, Cabell Research Fellow at The Technological Institute of Northwestern University, Evanston, Ill.

[4] Numbers in parentheses refer to the Bibliography at the end of the paper.

Contributed by the Applied Mechanics Division and presented at the Annual Meeting, New York, N. Y., December 1–6, 1957, of The American Society of Mechanical Engineers.

Discussion of this paper should be addressed to the Secretary, ASME, 29 West 39th Street, New York, N. Y., and will be accepted until October 10, 1958, for publication at a later date. Discussion received after the closing date will be returned.

Note: Statements and opinions advanced in papers are to be understood as individual expressions of their authors and not those of the Society. Manuscript received by ASME Applied Mechanics Division, July 3, 1957. Paper No. 57—A-95.

Now, since we are dealing with an infinite solid, it is reasonable to assume that the dependence of v on the co-ordinate z will be of the nature of $v \approx e^{-zt}$, where t may be any parameter. This will make possible finite displacement and stress values at $z = 0$, which will vanish as $z \to \infty$. With this substitution, Equation [c] will reduce to an ordinary differential equation in r, which is satisfied by Bessel function of the first order $J_1(rt)$. Writing now the solution of Equation [c] in terms of dimensionless variables z/a and r/a, where a is the radius of the contact area, we have

$$v = Ae^{-\frac{z}{a}t} J_1\left(\frac{r}{a}t\right) \quad \ldots\ldots [d]$$

Since this expression provides a solution at any arbitrary choice of the parameter t, it is clear that the same expression multiplied by any function $f(t)$ also will be a solution. Generalizing this, we may write

$$v = A\int_0^\infty e^{-\frac{z}{a}t} J_1\left(\frac{r}{a}t\right) f(t)dt \quad \ldots\ldots [e]$$

The problem is reduced now to finding a form for $f(t)$ which will fulfill the prescribed boundary conditions; namely, that at $z = 0$

$$\left.\begin{aligned} \tau_{z\theta} &= fp_0[1 - (r/a)^2]^{1/2}, \quad \text{for} \quad r/a \le 1 \\ \text{and} \qquad & \\ \tau_{z\theta} &= 0, \qquad\qquad\quad \text{for} \quad r/a > 1 \end{aligned}\right\} \quad \ldots\ldots [f]$$

We find that these conditions are satisfied by taking

$$f(t) = (1/t)J_1^2(t/2), \quad \text{and} \quad A = fp_0\pi a/2\mu$$

The solution for v is, therefore

$$v = \frac{fp_0\pi a}{2\mu}\int_0^\infty e^{-\frac{z}{a}t} J_1\left(\frac{r}{a}t\right) J_1^2\left(\frac{1}{2}t\right)\frac{1}{t}\,dt \quad \ldots [1]$$

which, on substitution into Equations [b], defines the stress components as

$$\tau_{r\theta} = -fp_0\frac{\pi}{2}\int_0^\infty e^{-\frac{z}{a}t} J_2\left(\frac{r}{a}t\right) J_1^2\left(\frac{1}{2}t\right)dt \quad \ldots [2]$$

and

$$\tau_{z\theta} = fp_0\frac{\pi}{2}\int_0^\infty e^{-\frac{z}{a}t} J_1\left(\frac{r}{a}t\right) J_1^2\left(\frac{1}{2}t\right)dt \quad \ldots [3]$$

The formulas in Equations [1], [2], and [3] constitute the complete solution for the torque loading. Adding these to the formulas of Love (5), and using Lamé's elastic constants, λ and μ, which, in terms of Young's modulus of elasticity E and Poisson's ratio ν, are

$$\lambda = \frac{E\nu}{(1+\nu)(1-2\nu)}, \quad \mu = \frac{E}{2(1+\nu)}$$

the complete set of stress components, for the combined problem of pressure and twist, is obtained as

$$\sigma_r = p_0\left\{\frac{1-2\nu}{3}\frac{a^2}{r^2}\left[1 - \left(\frac{z}{\sqrt{s_0}}\right)^3\right] + (1+\nu)\frac{z}{a}\tan^{-1}\frac{a}{\sqrt{s_0}} + (1-\nu)\frac{z\sqrt{s_0}}{a^2+s_0} - 2\frac{z}{\sqrt{s_0}} + \frac{a^2z^2}{s_0^2+a^2z^2}\frac{z}{\sqrt{s_0}}\right\} \quad \ldots\ldots [4a]$$

$$\sigma_\theta = p_0\left\{-\frac{1-2\nu}{3}\frac{a^2}{r^2}\left[1 - \left(\frac{z}{\sqrt{s_0}}\right)^3\right] + (1+\nu)\frac{z}{a}\tan^{-1}\frac{a}{\sqrt{s_0}} - (1-\nu)\frac{z\sqrt{s_0}}{a^2+s_0} - 2\nu\frac{z}{\sqrt{s_0}}\right\} \quad \ldots\ldots [4b]$$

$$\sigma_z = -p_0\frac{a^2z^2}{s_0^2+a^2z^2}\frac{z}{\sqrt{s_0}} \quad \ldots\ldots [4c]$$

$$\tau_{rz} = -p_0\frac{a^2r^2\sqrt{s_0}}{(s_0^2+a^2z^2)(a^2+s_0)} \quad \ldots\ldots [4d]$$

$$\tau_{r\theta} = -fp_0\frac{\pi}{2}\int_0^\infty e^{-\frac{z}{a}t} J_2\left(\frac{r}{a}t\right) J_1^2\left(\frac{1}{2}t\right)dt \quad \ldots\ldots [4e]$$

$$\tau_{z\theta} = fp_0\frac{\pi}{2}\int_0^\infty e^{-\frac{z}{a}t} J_1\left(\frac{r}{a}t\right) J_1^2\left(\frac{1}{2}t\right)dt \quad \ldots\ldots [4f]$$

In the foregoing equations s_0 denotes the non-negative root of the equation

$$\left.\begin{aligned} &\frac{z^2}{s_0} + \frac{r^2}{a^2+s_0} - 1 = 0 \\ \text{that is} \qquad & \\ &s_0 = \frac{1}{2}(r^2+z^2-a^2) \pm \frac{1}{2}[(r^2+z^2-a^2)+4a^2z^2]^{1/2} \end{aligned}\right\} \quad \ldots [g]$$

Since

$$\frac{z}{\sqrt{s_0}} = [1 - (r^2/a^2+s_0)]^{1/2}$$

in the limiting case, when $z = 0$, we have

$$\left.\begin{aligned} s_0 &= 0, \qquad \text{for} \quad r/a \le 1 \\ \text{and} \qquad & \\ s_0 &= r^2 - a^2, \quad \text{for} \quad r/a > 1 \end{aligned}\right\} \quad \ldots\ldots [h]$$

Thus we get from Equations [4a] to [4f] the following formulas for surface stresses

$$(\sigma_r)_{z=0} \begin{cases} = p_0\left\{\frac{1-2\nu}{3}\frac{a^2}{r^2}\left[1 - \left(1 - \frac{r^2}{a^2}\right)^{3/2}\right] - \left(1 - \frac{r^2}{a^2}\right)^{1/2}\right\}, & \text{for} \quad \frac{r}{a} \le 1 \\ = p_0\frac{1-2\nu}{3}\frac{a^2}{r^2}, & \text{for} \quad \frac{r}{a} > 1 \end{cases} \quad \ldots\ldots [5a]$$

$$(\sigma_\theta)_{z=0} \begin{cases} = -p_0\left\{\frac{1-2\nu}{3}\frac{a^2}{r^2}\left[1 - \left(1 - \frac{r^2}{a^2}\right)^{3/2}\right] + 2\nu\left(1 - \frac{r^2}{a^2}\right)^{1/2}\right\}, & \text{for} \quad \frac{r}{a} \le 1 \\ = -p_0\frac{1-2\nu}{3}\frac{a^2}{r^2}, & \text{for} \quad \frac{r}{a} > 1 \end{cases} \quad \ldots\ldots [5b]$$

$$(\sigma_z)_{z=0} \begin{cases} = -p_0\left(1 - \frac{r^2}{a^2}\right)^{1/2}, \\ = 0, \end{cases} \qquad (\tau_{z\theta})_{z=0} \begin{cases} = fp_0\left(1 - \frac{r^2}{a^2}\right)^{1/2}, & \text{for } \frac{r}{a} \leq 1 \\ = 0, & \text{for } \frac{r}{a} > 1 \end{cases} \quad \ldots [5c] \text{ and } \ldots [5f]$$

$$(\tau_{rz})_{z=0} = 0 \quad \ldots [5d]$$

$$(\tau_{r\theta})_{z=0} = -fp_0 \frac{\pi}{2} \int_0^\infty J_2\left(\frac{r}{a}t\right) J_1^2\left(\frac{1}{2}t\right) dt \quad \ldots [5e]$$

The fact that, for $z = 0$, Equation [4f] reduces to the form given in Equation [5f], can be proved by means of a formula by Sonine, given in G. N. Watson's treatise (6). Though we find from Equation [5f] that $(\tau_{z\theta})_{z=0} \to fp_0$ as $r \to 0$, from the original Equation [4f] it is clear that $(\tau_{z\theta})_{z=0}$ has to vanish when r actually becomes zero. Therefore at $r = 0$ there is a singularity, a "hole"

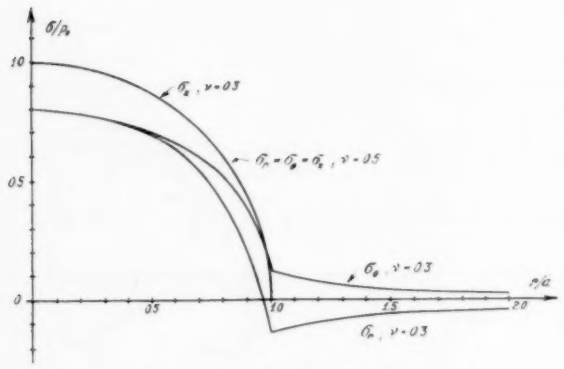

Fig. 2 Normal stresses at surface

in the surface-shear loading. This is, of course, a physical requirement because of the rotational symmetry of the loading, but it is satisfying to see that the mathematics employed is capable of expressing this particular feature in the solution. A similar singularity occurs also in the integral for $\tau_{r\theta}$ in Equation [4e]. The evaluation of this will be discussed in detail later on, when comparisons are made with photoelastic test results.

With reference to Equations [5a] and [5b], we find that

$$\frac{a^2}{r^2}\left[1 - \left(1 - \frac{r^2}{a^2}\right)^{3/2}\right] \to \frac{3}{2} \quad \text{as} \quad r \to 0$$

Consequently, for $z = 0$, and $r = 0$, we have

$$\sigma_r = \sigma_\theta = -p_0 \frac{1 + 2\nu}{2}$$

A graphical representation of the surface stresses σ_r, σ_θ, and σ_z, as calculated from Equations [5a] to [5c] is shown in Fig. 2. It is to be noted that for Poisson's ratio $\nu = 1/2$ there is a state of hydrostatic compression, $\sigma_r = \sigma_\theta = \sigma_z = -p$, at every point within the contact area, which will be found very helpful later on in the interpretation of photoelastic data.

The displacement components u, v, and w, due to the combined pressure and twist, are as follows

$$u = -\frac{p_0 a}{12}\left\{\frac{1}{\lambda + \mu}\left[2\frac{a}{r} + 3\frac{rz}{a^2}\left(\frac{a}{\sqrt{s_0}} - \tan^{-1}\frac{a}{\sqrt{s_0}}\right) - \frac{a}{r}\frac{z}{\sqrt{s_0}}\left(3 - \frac{z^2}{s_0}\right)\right] - \frac{3}{\mu}\frac{rz}{a^2}\left(\tan^{-1}\frac{a}{\sqrt{s_0}} - \frac{a\sqrt{s_0}}{a^2 + s_0}\right)\right\} \quad \ldots [6a]$$

$$v = \frac{fp_0\pi a}{2\mu}\int_0^\infty e^{-\frac{z}{a}t} J_1\left(\frac{r}{a}t\right) J_1^2\left(\frac{1}{2}t\right)\frac{1}{t}\,dt \quad \ldots [6b]$$

$$w = \frac{p_0 a}{4\mu}\left\{\frac{\lambda + 2\mu}{\lambda + \mu}\left[\left(1 - \frac{1}{2}\frac{r^2}{a^2} + \frac{z^2}{a^2}\right)\tan^{-1}\frac{a}{\sqrt{s_0}} + \frac{1}{2}\frac{r^2}{a^2}\frac{a\sqrt{s_0}}{a^2 + s_0} - \frac{z^2}{a^2}\frac{a}{\sqrt{s_0}}\right] + 2\frac{z^2}{a^2}\left(\frac{a}{\sqrt{s_0}} - \tan^{-1}\frac{a}{\sqrt{s_0}}\right)\right\} \quad \ldots [6c]$$

The foregoing expressions for u and w had not been actually given by Love (5). However, there are enough fundamental data in his paper from which these formulas may be reconstructed with relative ease.

At the surface, $z = 0$, the foregoing displacements become

$$(u)_{z=0} \begin{cases} = -\frac{p_0 a^2}{2r(\lambda + \mu)}\left\{1 - \left(1 - \frac{r^2}{a^2}\right)^{3/2}\right\} & \text{for } \frac{r}{a} \leq 1 \ldots \\ = -\frac{p_0 a^2}{2r(\lambda + \mu)}, & \text{for } \frac{r}{a} > 1 \ldots \end{cases} \quad \ldots [7a]$$

$$(v)_{z=0} = \frac{fp_0\pi a}{2\mu}\int_0^\infty J_1\left(\frac{r}{a}t\right) J_1^2\left(\frac{1}{2}t\right)\frac{1}{t}\,dt \quad \ldots [7b]$$

$$(w)_{z=0} \begin{cases} = \frac{p_0\pi a}{8\mu}\frac{\lambda + 2\mu}{\lambda + \mu}\left(1 - \frac{1}{2}\frac{r^2}{a^2}\right), & \text{for } \frac{r}{a} \leq 1 \ldots \\ = \frac{p_0 a}{4\mu}\frac{\lambda + 2\mu}{\lambda + \mu}\left[\left(1 - \frac{1}{2}\frac{r^2}{a^2}\right)\tan^{-1}\frac{a}{(r^2 - a^2)^{1/2}} + \frac{1}{2}\left(\frac{r^2}{a^2} - 1\right)^{1/2}\right], & \text{for } \frac{r}{a} > 1 \ldots \end{cases} \quad \ldots [7c]$$

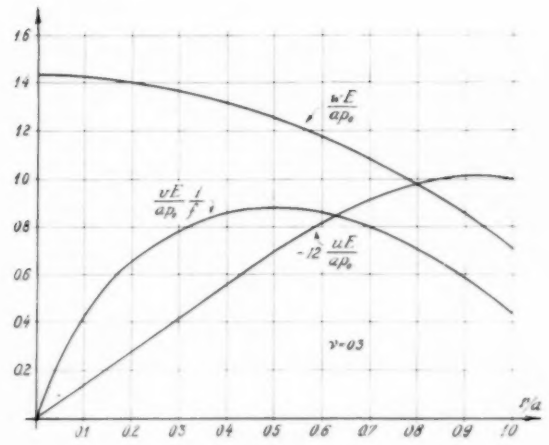

Fig. 3 Displacement components at surface

The variation of these displacement components within the contact area is shown in Fig. 3, for Poisson's ratio $\nu = 0.3$. It is seen from Equation [7*a*] that for $\nu = 1/2$, that is, $\lambda = \infty$, the radial displacement u becomes zero everywhere on the surface.

Photoelastic Tests

The foregoing analytical work was complemented by a series of photoelastic tests, using Fosterite models and the three-dimensional "stress-freezing" technique.

In each test the model consisted of a pair of solid Fosterite cylinders, one of which had a flat end and the other a spherical end of 6 in. radius. The two were mounted, in contact, in a specially designed loading frame. This frame prevented the upper cylinder from rotating, while it provided complete freedom as regards vertical displacement. The lower cylinder, on the other hand, was mounted on a circular platform, resting on a single ball bearing in a conical recess. This arrangement eliminated any possibility of a sidewise shift from the common axis of the two cylinders when the torque was applied to the circular platform. The entire frame was placed in an electric oven for the tests, with cables leading to the outside for the operation of the torque-loading.

The testing procedure consisted of first weighting the assembled cylinders with a vertical load of $P = 12$ lb, then closing the oven, and slowly raising the temperature to the annealing level of 90 C. At this temperature the torque was introduced. Its magnitude was to be as near as possible to the maximum torque value, in order to simulate the condition assumed in the analytical solution, without actually causing total slip. To assure this, a series of preliminary tests was made to determine the coefficient of friction between freshly machined and carefully degreased Fosterite surfaces at the annealing temperature, which gave an average value of $f = 0.564$. On this basis it was possible to make several tests in which the applied torque was about 95 per cent of the total slip torque. The radius of the contact area in each of these tests was $a = 0.368$ in., corresponding to the values of $P = 12$ lb, $r = 6$ in., and $E = 1620$ psi, $\nu = 1/2$, as the elastic constants of Fosterite at the elevated temperature.

After the completion of the annealing cycle under constant vertical and torque loadings, the model was removed and its frozen stress pattern analyzed. As a rule, slices were taken out for this purpose only from the flat-ended cylinder, while its counterpart was used over again, after it was strain-free annealed and its spherical surface remachined.

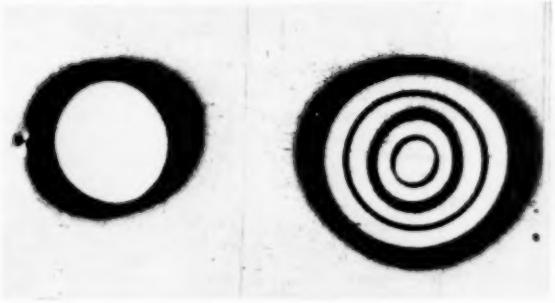

(*a*) (*b*)

Fig. 4 Photoelastic patterns in a 1/8 in-thick surface layer. (*a*) Normal load alone; (*b*) normal load, plus an estimated 88 per cent of total-slip torque.

A qualitative picture, illustrating the difference in the stress pattern caused by the torque loading, is shown in Fig. 4. The view on the left was taken of a top slice of a model loaded only by a normal force, while the one on the right was subjected to a combined normal and torque loading. Each slice was 1/8 in. thick, and they were obtained in some of the early tests in this series. It soon became apparent, however, that within a depth of 1/8 in. from the surface, that is, nearly one third of the radius of the contact area, there is such rapid change in the state of stress that slices of such thickness are unsuitable for quantitative photoelastic measurements at normal incidence. After several trials it was found necessary to reduce the thickness of this top slice to 0.012 in. At this thickness the photoelastic pattern became, of course, hardly visible, and the results had to be derived from point-by-point retardation measurements. This was done with a Leitz compensator and a Soleil plate, which combination was found to have a limited range but a remarkable sensitivity. The minimum reading, corresponding to a 1/2-deg rotation of the Soleil plate, was about 2 mμ of relative retardation, the total range being ± 120 mμ in white light. This minimum reading is equivalent to about one third of 1 per cent of one isochromatic line. During the measurement the slice was mounted on a microscope slide and was advanced by 1 mm along the radius between two successive readings. Since the radius of contact area $a = 0.368$ in. $= 9.09$ mm, nine points were obtained within its range.

The results of these measurements are shown in Fig. 5, together with the corresponding values of $\tau_{r\theta}$ at $z = 0$ as calculated from Equation [5*e*]. Since the integral in this formula turned out to be by far the most difficult to evaluate, and since it is of importance in another applied mechanics problem, its numerical values are given in detail in Table 1. It is seen that while the value of this integral approaches $1/\pi$ as $r \to 0$, according to

Table 1 Values of the definite integral in Equation [5*e*] for $\tau_{r\theta}$ at $z = 0$

r/a	$\int_0^\infty J_2\left(\frac{r}{a}t\right) J_1^2\left(\frac{1}{2}t\right) dt$	r/a	$\int_0^\infty J_2\left(\frac{r}{a}t\right) J_1^2\left(\frac{1}{2}t\right) dt$
0.1	0.32226	1.1	0.21891
0.2	0.33087	1.2	0.14966
0.3	0.34245	1.3	0.10981
0.4	0.35618	1.4	0.08391
0.5	0.37158	1.5	0.06596
0.6	0.38830	1.6	0.05299
0.7	0.40610	1.7	0.04331
0.8	0.42481	1.8	0.03591
0.9	0.44428	1.9	0.03014
1.0	0.46440	2.0	0.02557

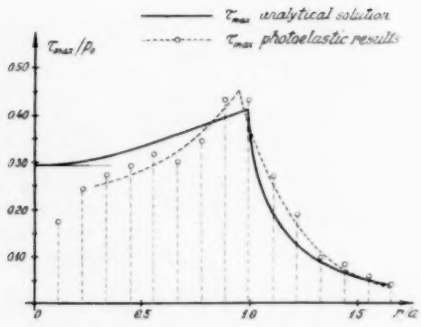

Fig. 5 Comparison between analytical and experimental values of $\tau_{max} = \tau_{r\theta}$ at surface

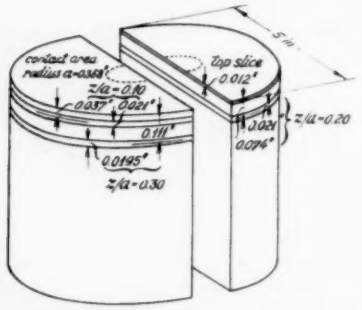

Fig. 6 Position of slices used in determination of τ_{max} in horizontal planes at depths $z/a = 0$, 0.1, 0.2, and 0.3

Equation [5e] it has to vanish at $r = 0$. Therefore it represents the same type of singularity that has been found earlier in connection with the expression for $\tau_{z\theta}$ at $z = 0$. Having noted the rapid change of stress within a depth equivalent to one third of the contact radius, it was decided to make similar comparisons as that in Fig. 5 for $z = 0$, at small intervals corresponding to $z/a = 0.1$, 0.2, and 0.3. In order to obtain the respective slices from a single test, they had to be taken out of the same Fosterite cylinder in a staggered way as shown in Fig. 6. The middle planes of these slices were at 0.037, 0.074, and 0.111 in. from the surface, and their respective thicknesses were 0.021, 0.021, and 0.0195 in. The relative retardation measurements on these slices gave, of course, the τ_{max}-values in the corresponding horizontal planes. However, below the surface these are no longer the same as the $\tau_{r\theta}$-values, because now there will be a difference between the normal stresses, even for $\nu = 1/2$. For sake of comparison, the σ_r and σ_θ-values were calculated for these points from Equations [4a] and [4b], the corresponding distribution of $\tau_{r\theta}$ from Equation [4c], and from these the maximum shearing-stress values were derived as

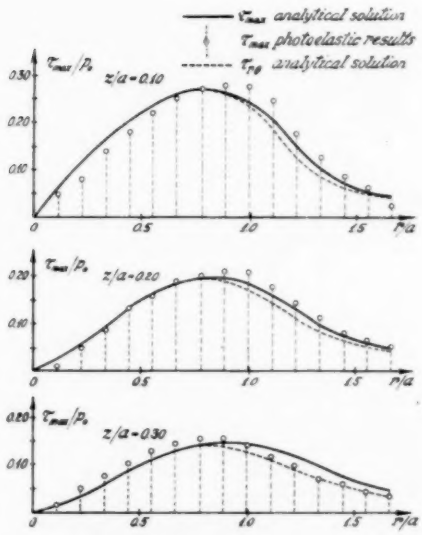

Fig. 7 Comparison between analytical and experimental values of τ_{max} in horizontal planes at depths $z/a = 0.1$, 0.2, and 0.3

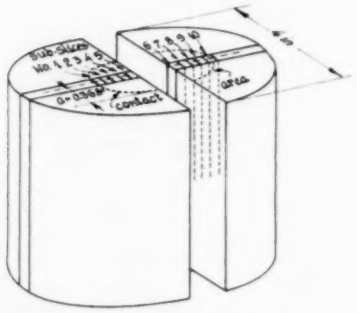

Fig. 8 Position of subslices used in determination of $\tau_{r\theta}$ at surface

$$\tau_{max} = \left[\left(\frac{\sigma_r - \sigma_\theta}{2}\right)^2 + \tau_{r\theta}^2\right]^{1/2}$$

The stress components used in this calculation are tabulated in Table 2 and the results shown in Fig. 7. It is seen that the correction due to normal stress differences is noticeable only around the edge of the contact area.

The most interesting feature of these photoelastic tests was, undoubtedly, that they provided a means for the determination of the actual surface-shear load distribution occurring within the contact area. This was achieved by making retardation measurements on minute circumferential slices, taken out of the model

Table 2 Stress components in horizontal planes at depths $z/a = 0.1$, 0.2, and 0.3

	$z/a = 0.1$				$z/a = 0.2$				$z/a = 0.3$			
r/a	σ_r/p_0	σ_θ/p_0	$\tau_{r\theta}/p_0$	τ_{max}/p_0	σ_r/p_0	σ_θ/p_0	$\tau_{r\theta}/p_0$	τ_{max}/p_0	σ_r/p_0	σ_θ/p_0	$\tau_{r\theta}/p_0$	τ_{max}/p_0
0	0.7843	0.7843	0	0	0.6072	0.6072	0	0	0.4656	0.4656	0	0
0.1	0.7841	0.7794	0.0502	0.0502	0.6035	0.6028	—	—	0.4623	0.4617	—	—
0.2	0.7630	0.7643	0.1142	0.1142	0.5906	0.5893	0.0526	0.0526	0.4531	0.4501	0.0284	0.0284
0.3	0.7400	0.7395	0.1604	0.1604	0.5701	0.5665	—	—	0.4375	0.4306	—	—
0.5	0.6567	0.6550	0.2206	0.2206	0.5038	0.4913	0.1454	0.1454	0.3905	0.3675	0.1003	0.1011
0.8	0.4365	0.4102	0.2710	0.2714	0.3569	0.2923	0.1924	0.1952	0.3065	0.2163	0.1371	0.1440
1.0	0.2672	0.1345	0.2346	0.2438	0.2814	0.1245	0.1683	0.1856	0.2676	0.1070	0.1242	0.1480
1.2	0.1164	0.0236	0.1235	0.1320	0.1796	0.0375	0.1083	0.1295	0.2010	0.0423	0.0894	0.1196
1.5	0.0433	0.0047	0.0573	0.0602	0.0799	0.0087	0.0542	0.0649	0.1060	0.0117	0.0494	0.0682

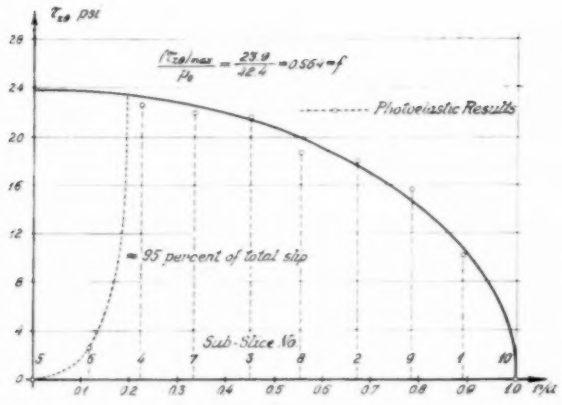
$\tau_{z\theta}$ psi
$\frac{(\tau_{z\theta})_{max}}{p_0} = \frac{23.9}{42.4} = 0.564 = f$
Photoelastic Results
≈ 95 percent of total slip
Sub-Slice No
5 6 4 7 3 8 2 9 1 10
0 4 8 12 16 20 24 28
.01 .02 .03 .04 .05 .06 .07 .08 .09 .10 r/a

Fig. 9 Distribution of $\tau_{z\theta}$ at surface

at various radial distances. In order to provide a sufficient number of points within the contact area for the distribution curve, these subslices were taken out in a staggered arrangement from a central radial slice, 5 subslices from each half of the cylinder, as shown in Fig. 8. During measurement they were viewed at normal incidence, that is radially, and the retardation readings were taken along the z-axis, starting from the bottom and ending at the surface. At any point along these lines the measured birefringence was proportional to the τ_{max}-value in the plane of the subslice. Below the surface the τ_{max}-values were the resultants of the $\tau_{z\theta}$-stresses and the corresponding differences in the σ_θ and σ_z stress components. At $z = 0$, however, the state of hydrostatic compression due to the normal stresses causing no stress birefringence, the relative retardation is a direct measure of $\tau_{z\theta} = \tau_{max}$. By plotting curves of these readings and taking their intersection with the boundary, the $\tau_{z\theta}$-values could be very well defined at the top end of each of the ten subslices. The results are plotted in Fig. 9 and show that the experimental points accurately describe the Hertzian ellipse, with the friction coefficient as a proportionality factor. To the best of the authors' knowledge, this was the first instance when the load distribution actually could be measured within the contact area of a three-dimensional elastic solid.

Bibliography

1(*a*) "Compliance of Elastic Bodies in Contact," by R. D. Mindlin, JOURNAL OF APPLIED MECHANICS, TRANS. ASME, vol. 71, 1949, pp. 259–268.

(*b*) "The Torsion of Elastic Spheres in Contact," by J. L. Lubkin, JOURNAL OF APPLIED MECHANICS, TRANS. ASME, vol. 73, 1951, pp. 183–187.

(*c*) "Contact of Elastic Spheres Under an Oscillating Torsional Couple," by H. Deresiewicz, JOURNAL OF APPLIED MECHANICS, TRANS. ASME, vol. 76, 1954, pp. 52–56.

2(*a*) "An Investigation of the Fretting Corrosion of Closely Fitting Surfaces," by G. A. Tomlinson, P. L. Thorpe, and H. J. Gough, Proceedings of The Institution of Mechanical Engineers, London, England, vol. 141, 1939, pp. 223–249.

(*b*) "Investigation on the Effects of Surface-Shear Loading," by M. Hetényi, Interim Report, Office of Naval Research, Contract N7onr-45009, July, 1952, pp. 1–86.

3 "Analysis of Contact Stresses Under Combined Pressure and Twist," by P. H. McDonald, Jr., Doctoral dissertation, Northwestern University, Evanston, Ill., February, 1953.

4(*a*) "Theory of Elasticity," by S. Timoshenko and J. N. Goodier, second edition, McGraw-Hill Book Company, Inc., New York, N. Y., 1951, p. 307.

(*b*) "A Treatise on the Mathematical Theory of Elasticity," by A. E. H. Love, fourth edition, Dover Publications, New York, N. Y., 1944, p. 325.

5 "The Stress Produced in a Semi-Infinite Solid by Pressure on Part of the Boundary," by A. E. H. Love, Philosophical Transactions of the Royal Society of London, series A, vol. 228, 1929, pp. 377–420.

6 "A Treatise on the Theory of Bessel Functions," by G. N. Watson, second edition, Cambridge University Press, 1945, p. 411, Equation 3.

Stress-Strain Relations for a Simple Model of a Granular Medium[1]

By H. DERESIEWICZ,[2] NEW YORK, N. Y.

A granular assemblage is represented by a model consisting of like spheres in contact arranged in a simple cubic lattice. Based on consideration of local contact forces and concomitant deformations, incremental stress-strain relations are derived and subsequently integrated, for certain types of loading, to yield total stress-strain relations. The integration is carried out for both a loading and an unloading process. A criterion of failure for the model is set up and the theory applied to a regimen of loading which gives rise to a plane state of stress.

Introduction

In a recent paper Mindlin (1)[3] summarized some of the difficulties encountered and some of the results obtained in the course of development of a mathematical theory of small deformations of granular media. The medium is assumed to be composed of discrete, isotropic, elastic granules in direct contact under local forces which, in general, vary in magnitude and in direction. The consideration of the effects of this variation serves to distinguish the present theory from several others (2) in which only normal components of the contact forces were taken into account. The great complexity of the problem arises from the fact that the relations connecting the individual contact forces and deformations are nonlinear and, in addition, depend on the history of loading. To simplify matters, the investigation, for the present, has been confined to an idealized medium consisting of regular arrays of like spheres.

The face-centered cubic arrangement, one of the packings of greatest density, has served as the starting point of the study. Duffy and Mindlin (3) derived the incremental stress-strain relations for this structure on the supposition that an initial state of isotropic stress existed before the incremental loading was imposed. These differential relations, in which the elastic coefficients are combinations of the various local normal and tangential stiffnesses, suffice to describe the small vibrations of such a medium when it is under relatively high initial stress. However, in order to investigate phenomena arising at levels of stress of the order of magnitude of the initial stress, it is necessary to employ total, or integrated, stress-strain relations. Unfortunately, to obtain such a set of relations for the face-centered cubic array, a statically indeterminate structure, one is faced with the formidable problem of solving a set of simultaneous, nonlinear, integrodifferential equations.

The present paper is concerned with a derivation of incremental stress-strain relations, and their subsequent integration, for another kind of lattice of like spheres; namely, the simple cubic array. When under initial isotropic pressure this assemblage is statically determinate, so that the loading history does not enter into the calculation of the contact forces (although it does affect the value of the local tangential compliances). Consequently, for "homothetic" loading,[4] the system of simultaneous integrodifferential equations, which arises in the process of integrating the incremental stress-strain relations, reduces to a set of tractable quadratures. In this manner, total stress-strain relations are obtained both for homothetic loading to an arbitrary stress level and for subsequent homothetic unloading from that level. In addition, a criterion of failure for the structure is propounded, based on conditions for gross sliding of two contiguous spheres. Finally, the theory is illustrated for a simple load variation which gives rise to a two-dimensional state of stress.

We may note that the usefulness of the study of the mechanical behavior of face-centered cubic and simple cubic arrays of like spherical particles is due not only to the fact that each structure represents an approximation, though a rather rough one, to a granular medium, but that experimental verification of the theory would offer additional evidence in favor of the solutions of the equations of elasticity for the problem of contact of a pair of spheres compressed by oblique forces (4). Moreover, as suggested by Smith, Foote, and Busang (5), the internal configuration of a granular mass may be approximated by a mixture of zones composed of face-centered cubic and simple cubic arrays in a proportion yielding the observed porosity of the material; in such a model the average number of contacts per sphere is found to correspond fairly closely to observed values.

Incremental Stress-Strain Relations

Consider an array of like spheres in contact whose centers form a simple cubic lattice, as illustrated in Fig. 1. Since each sphere is thereby placed in contact with six other spheres, this arrangement gives rise to a total of eighteen rectangular components of contact forces per sphere, of which six are normal and twelve are tangential components. But, with the assumption of a homogeneous state of stress, the forces on diametrically opposed contact surfaces are equal and oppositely directed, leaving only nine independent force components (three normal, six tangential).

It is simple to relate the nine unknown contact forces to the applied incremental forces acting on a unit volume of the medium. Consideration of the equilibrium of a sphere and any portion thereof shows that the components of the incremental contact forces, dN_{ij}, are equal to the corresponding components of the incremental applied forces, dP_{ij}; i.e., $dN_{ij} = dP_{ij}$, $i, j = 1, 2, 3$. For $i = j$, dN_{ij} denotes a normal component and, for $i \neq j$, dN_{ij} denotes a tangential component.

We define the incremental stress components, $d\sigma_{ij}$, as the ratios of the corresponding incremental forces to the area of a face of the cube. Thus

[1] This investigation was supported by the Office of Naval Research under Contract Nonr-266(09) with Columbia University.

[2] Associate Professor of Mechanical Engineering, Columbia University. Assoc. Mem. ASME.

[3] Numbers in parentheses refer to the Bibliography at the end of the paper.

Contributed by the Applied Mechanics Division and presented at the Annual Meeting, New York, N. Y., December 1–6, 1957, of The American Society of Mechanical Engineers.

Discussion of this paper should be addressed to the Secretary, ASME, 29 West 39th Street, New York, N. Y., and will be accepted until October 10, 1958, for publication at a later date. Discussion received after the closing date will be returned.

Note: Statements and opinions advanced in papers are to be understood as individual expressions of their authors and not those of the Society. Manuscript received by ASME Applied Mechanics Division, May 16, 1957. Paper No. 57—A-90.

[4] At any two load levels the stress quadrics are similar and similarly oriented; this type of loading is sometimes referred to as "radial" since, in stress space, the loading path is represented by a straight line through the origin.

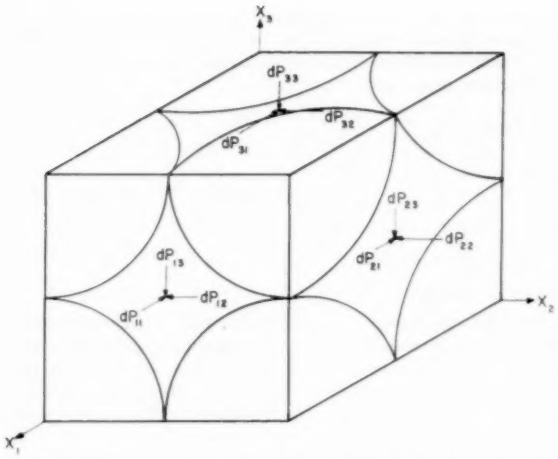

Fig. 1 Elementary cube of a simple cubic array of like spheres subjected to incremental forces

$$d\sigma_{ij} = dP_{ij}/4R^2$$

where R is the radius of a sphere. The relative incremental displacements of the spheres are obtained by multiplying the contact forces by the corresponding compliances. From these displacements the deformation of the unit block resulting from the application of an incremental stress can be found. Owing to the nonlinearity of the tangential force-displacement relations, particular care must be exercised in computing the displacements parallel to the co-ordinate axes. Thus components along the co-ordinate axes must be found of the displacements due to, and in the direction of, the resultant tangential force on each contact rather than considering the displacements resulting from the components along the co-ordinate axes of the resultant tangential force. On proceeding in this manner, the relations connecting components of incremental strain and stress are found to be

$$\left.\begin{aligned} d\epsilon_{ii} &= 2RC_i d\sigma_{ii} \\ d\epsilon_{ij} &= R[(S_i\sigma_{ij}/\tau_{jk})d\tau_{jk} \\ &\quad + (S_j\sigma_{ji}/\tau_{ik})d\tau_{ik}],\ i \neq j \neq k = 1, 2, 3 \end{aligned}\right\} \quad \ldots [1]$$

where τ_{jk}, for example, denotes the resultant shear stress on a plane whose normal is parallel to the x_i-direction; i.e.

$$\tau_{jk} = (\sigma_{ij}^2 + \sigma_{ik}^2)^{1/2}$$

The C_i and S_i represent, respectively, the normal and tangential compliances of a pair of spheres in contact. The subscript in each of these symbols indicates the normal component of the contact force. In addition, in the S_i, the subscript serves to identify the resultant tangential force on the contact; e.g., the tangential force which corresponds to S_i is $(N_{ij}^2 + N_{ik}^2)^{1/2}$. It should be noted that the conditions of geometric compatibility are identically satisfied.

For two spheres, each of radius R, shear modulus μ and Poisson's ratio ν, compressed by a normal force N, the contact radius a, and the normal approach α, are given by the Hertz theory (6)

$$a = \left[\frac{3(1-\nu)RN}{8\mu}\right]^{1/3} \quad \ldots [2]$$

$$\alpha = 2\left[\frac{3(1-\nu)N}{8\mu R^{1/2}}\right]^{2/3} \quad \ldots [3]$$

From Equations [2] and [3] the normal compliance of the contact is found to be

$$C = d\alpha/dN = (1-\nu)/2\mu a \quad \ldots [4]$$

this expression being valid no matter what the loading history of the spheres.

The situation with the tangential compliances is considerably different. These are dependent on the past history of normal and tangential forces, on the relative rate and sense of their variation, and on the sense of the current loading as compared to the sense of the loading immediately preceding (4). Consequently, it is necessary to specify in advance the type of loading occurring in each particular case. We shall discuss the following loading program: The entire medium is subjected to an initial isotropic pressure, $4R\sigma_0$, giving rise to normal contact forces of magnitude N_0. Additional loading is applied in such a manner that, on each contact surface, the normal component of the force increases and the relative rate of (resultant) tangential with respect to the normal loading is constant and greater than the coefficient of friction, f. Thus the additional force on each contact acts at constant obliquity to the contact normal; its line of action is assumed to remain in the same plane. The tangential compliance per contact for such a loading history is[5]

$$S_i = \frac{2-\nu}{4\mu a_i}\left[\theta_i + (1-\theta_i)\left(1 - \frac{L_i}{1+\theta_i L_i}\right)^{-1/3}\right] \quad \ldots [5]$$

where

$$\theta_i = f/\beta_i, \quad \beta_i = d[(N_{ij}^2 + N_{ik}^2)^{1/2}]/dN_{ii},$$

$$L_i = (N_{ij}^2 + N_{ik}^2)^{1/2}/fN_0$$

Loading to Finite Stress Levels

In view of the loading conditions specified in the preceding section, we must restrict the applied stresses so that they form homothetic quadrics. That is, we postulate that the stresses obey the relations

$$d\sigma_{ij}/d\sigma_{11} = \lambda_{ij}\ \text{(constant)},\ i, j = 1, 2, 3 \quad \ldots [6]$$

Under these circumstances, the compliances, Equations [4] and [5], may be written

$$C_i = \frac{1-\nu}{2\mu a_i} = \frac{1-\nu}{2\mu a_0}\left(1 + \frac{\sigma_{ii}}{\sigma_0}\right)^{-1/3} \quad \ldots [7]$$

$$S_i = \frac{2-\nu}{4\mu a_0}\left(1 + \frac{\lambda_{ii}\sigma_{ij}}{\lambda_{ij}\sigma_0}\right)^{-1/3}\left[\frac{f\lambda_{ii}}{\lambda_{jk}} + \left(1 - \frac{f\lambda_{ii}}{\lambda_{jk}}\right)\left(1 - \frac{\lambda_{jk}\sigma_{ij}/\lambda_{ij}f\sigma_0}{1 + \lambda_{ii}\sigma_{ij}/\lambda_{ij}\sigma_0}\right)^{-1/3}\right] \quad \ldots [8]$$

where, e.g., $\lambda_{jk} = (\lambda_{ij}^2 + \lambda_{ik}^2)^{1/2}$, and a_0 denotes the contact radius due to the initial pressure.

As a result of Equations [6], the second set of Equations [1] reads

$$d\epsilon_{ij} = R(S_i + S_j)d\sigma_{ij} \quad \ldots [9]$$

To obtain finite stress-strain relations, we substitute Equation [7] in the first set of Equations [1] and expressions of the type given by Equation [8] in [9]; integrating between the desired levels (from zero at the initial state to the final values), we find

$$\left.\begin{aligned} \epsilon_{ii} &= \frac{3(1-\nu)R\sigma_0}{2\mu a_0}\left[\left(1 + \frac{\sigma_{ii}}{\sigma_0}\right)^{2/3} - 1\right] \\ \epsilon_{ij} &= \frac{3f(2-\nu)R\sigma_0}{8\mu a_0}\left\{\frac{\sigma_{ij}}{\tau_{jk}}\left(1 + \frac{\sigma_{ii}}{\sigma_0}\right)^{2/3} \times \right. \end{aligned}\right\} \quad \ldots [10]\ (cont.)$$

[5] Equation [82] of (4).

$$\left[1-\left(1-\frac{\tau_{jk}}{f(\sigma_0+\sigma_{ii})}\right)^{2/3}\right]+\frac{\sigma_{ji}}{\tau_{ik}}\times$$
$$\left(1+\frac{\sigma_{jj}}{\sigma_0}\right)^{2/3}\left[1-\left(1-\frac{\tau_{ik}}{f(\sigma_0+\sigma_{jj})}\right)^{2/3}\right]\Bigg\}\Bigg\} \quad [10]$$

Unloading Between Finite Stress Levels

Suppose we have attained, by means of the loading process prescribed previously, a given level of (additional) stress, denoted by σ_{ij}^*. We now consider the problem of finding the stress-strain relations which are valid for a similarly conducted process of unloading; that is, the stresses σ_{ij}^*, which were reached homothetically, are now to be reduced to a lower level of homothetic stress denoted by σ_{ij}. The difference between the computations of the present and the preceding sections lies in the values of the compliances S_i and S_j in Equation [9]. In the present case, S_i is given by[6]

$$S_i=\frac{2-\nu}{4\mu a_i}\Bigg\{-\theta_i+(1+\theta_i)\times$$
$$\left[1-(1-\theta_i)\frac{L_i^*-L_i}{2(1+\theta_iL_i)}\right]^{-1/2}\Bigg\} \quad [11]$$

in which

$$L_i^*=(N_{ij}^{*2}+N_{ik}^{*2})^{1/2}/fN_0$$

Again the integration is performed without difficulty and results in

$$\frac{2\mu a_0}{3(1-\nu)R\sigma_0}(\epsilon_{ii}-\epsilon_{ii}^*)=\left(1+\frac{\sigma_{ii}}{\sigma_0}\right)^{3/2}-\left(1+\frac{\sigma_{ii}^*}{\sigma_0}\right)^{3/2}$$

$$\frac{8\mu a_0}{3f(2-\nu)R\sigma_0}(\epsilon_{ij}-\epsilon_{ij}^*)=$$
$$-\frac{\sigma_{ij}^*}{\tau_{jk}^*}\left(1+\frac{\sigma_{ii}^*}{\sigma_0}\right)^{3/2}+\frac{\sigma_{ij}}{\tau_{jk}}\left(1+\frac{\sigma_{ii}}{\sigma_0}\right)^{3/2}\times$$
$$\Bigg\{-1+2\left[1-\left(1-\frac{f\sigma_{ii}}{\tau_{jk}}\right)\frac{\tau_{jk}^*-\tau_{jk}}{2f(\sigma_0+\sigma_{ii})}\right]^{3/2}\Bigg\}$$
$$+\text{ terms obtained by interchanging } i \text{ and } j, \text{ with } i\neq j$$

Since ϵ_{ii}^* and ϵ_{ij}^* are given by Equations [10], in which σ_{ij} is replaced by σ_{ij}^*, the expressions for the strains during unloading may be written

$$\frac{2\mu a_0}{3(1-\nu)R\sigma_0}\epsilon_{ii}=\left(1+\frac{\sigma_{ii}}{\sigma_0}\right)^{3/2}-1$$
$$\frac{8\mu a_0}{3f(2-\nu)R\sigma_0}\epsilon_{ij}=-\frac{\sigma_{ij}^*}{\tau_{jk}^*}\left(1+\frac{\sigma_{ii}^*}{\sigma_0}\right)^{3/2}\times$$
$$\left(1-\frac{\tau_{jk}^*}{f(\sigma_0+\sigma_{ii}^*)}\right)^{3/2}+\frac{\sigma_{ij}}{\tau_{jk}}\left(1+\frac{\sigma_{ii}}{\sigma_0}\right)^{3/2}\times$$
$$\Bigg\{-1+2\left[1-\left(1-\frac{f\sigma_{ii}}{\tau_{jk}}\right)\frac{\tau_{jk}^*-\tau_{jk}}{2f(\sigma_0+\sigma_{ii})}\right]^{3/2}\Bigg\}$$
$$+\text{ terms obtained by interchanging } i \text{ and } j \quad [12]$$

We note that the expression for ϵ_{ii} during unloading (the first of Equations [12]) is identical with the corresponding expression valid during loading (the first of Equations [10]). This is due to the fact that no dissipation takes place in the course of pure dilatational deformation. Consequently, as the loading is reduced to its initial level, i.e., $\sigma_{ij}=0$, the normal strains, ϵ_{ii}, vanish. On the other hand, the shear strains, ϵ_{ij}, are not removed completely when $\sigma_{ij}=0$, owing to the frictional dissipation mechanism inherent in the tangential displacements. Their value in this case is given by

$$\frac{8\mu a_0}{3f(2-\nu)R\sigma_0}\epsilon_{ij}^{(0)}=\frac{\sigma_{ij}^*}{\tau_{jk}^*}\Bigg[2\left(1+\frac{f\sigma_{ii}^*-\tau_{jk}^*}{2f\sigma_0}\right)^{3/2}$$
$$-\left(1+\frac{f\sigma_{ii}^*-\tau_{jk}^*}{f\sigma_0}\right)^{3/2}-1\Bigg]$$
$$+\text{ terms obtained by interchanging } i \text{ and } j \quad [13]$$

Criterion of Failure

We will consider our simple cubic structure to have failed when sliding occurs between any pair of contiguous spheres. The conditions for such an event to take place may be obtained from the expression for ϵ_{ij} (the second of Equations [10]). We note that, in it, each of the quantities raised to the power 2/3 must be nonnegative. This requisite goes back to consideration of the tangential load-displacement relation for a pair of spheres, and simply states that the inner radius of the slip annulus[7] is not negative. If we, further, take account of the homothetic loading program, we find that sliding will occur if the inequality

$$\tau_{jk}>f\sigma_0/(1-f\lambda_{ii}/\lambda_{jk}) \quad [14]$$

is satisfied.

Example

Consider the problem of computing the stress-strain relations appropriate to a simple cubic lattice, under initial isotropic pressure, when it is compressed in the direction of one of its face diagonals.[8]

The incremental stress-strain law, with both sets of components measured with respect to the principal axes of the cube, contains six nonzero elastic moduli (see Equations [1] and [9]), s_{ii}, $i=1, 2, \ldots, 6$. We now introduce a system of rectangular co-ordinate axes, x_1', x_2', x_3', which is obtained from the original system x_1, x_2, x_3, Fig. 1, by a rotation through an angle $\theta=45°$ about the x_3-axis. Referred to the primed axes, the (nonzero) elastic moduli are

$$\left.\begin{aligned}
s_{11}'&=(s_{11}+s_{22}+s_{66})/4=s_{22}'\\
s_{12}'&=(s_{11}+s_{22}-s_{66})/4\\
s_{16}'&=(s_{22}-s_{11})/2=s_{26}'\\
s_{33}'&=s_{33}\\
s_{44}'&=(s_{44}+s_{55})/2=s_{55}'\\
s_{45}'&=(s_{44}-s_{55})/2\\
s_{66}'&=s_{11}+s_{22}
\end{aligned}\right\} \quad [15]$$

and the relation between the original (unprimed) and rotated (primed) stress components for this case is

$$\left.\begin{aligned}
\sigma_{11}&=(\sigma_{11}'+\sigma_{22}'-2\sigma_{12}')/2\\
\sigma_{22}&=(\sigma_{11}'+\sigma_{22}'+2\sigma_{12}')/2\\
\sigma_{33}'&=\sigma_{33}\\
\sigma_{23}'&=(\sigma_{13}'+\sigma_{23}')/\sqrt{2}\\
\sigma_{13}'&=(\sigma_{13}'-\sigma_{23}')/\sqrt{2}\\
\sigma_{12}'&=(\sigma_{11}'-\sigma_{22}')/2
\end{aligned}\right\} \quad [16]$$

[6] Equation [85] of (4).

[7] Equation [5] of (4).

[8] It will appear in the sequel that this loading is homothetic.

Now, apply an incremental compressive force in the direction of one of the face diagonals, i.e., parallel to one of the rotated coordinate axes (say x_1'), and denote the corresponding incremental stress component by $d\sigma_{11}'$. Then, from Equations [16], the incremental stresses, referred to the principal axes of the cube, are

$$\left.\begin{aligned} d\sigma_{11} &= d\sigma_{22} = d\sigma_{12} = d\sigma_{11}'/2 \\ d\sigma_{13} &= d\sigma_{23} = d\sigma_{33} = 0 \end{aligned}\right\} \quad \ldots\ldots\ldots [17]$$

We see that the loading is homothetic, the λ_{ij} of Equations [6] having the values

$$\lambda_{11} = \lambda_{12} = \lambda_{22} = 1, \qquad \lambda_{13} = \lambda_{23} = \lambda_{33} = 0 \ldots [18]$$

Furthermore, since $d\sigma_{11}'$ is the only nonzero component of stress in the rotated system, the incremental stress-strain relations in the primed system become

$$\left.\begin{aligned} d\epsilon_{11}' &= s_{11}'d\sigma_{11}' & d\epsilon_{13}' &= 0 \\ d\epsilon_{22}' &= s_{12}'d\sigma_{11}' & d\epsilon_{23}' &= 0 \\ d\epsilon_{12}' &= s_{16}'d\sigma_{11}' & d\epsilon_{33}' &= 0 \end{aligned}\right\} \quad \ldots\ldots\ldots [19]$$

Inserting Equations [15] in [19], taking account of [1], [7], [8], [9], [17], and [18], and integrating, we find the finite stress-strain relations for the loading process in the primed system

$$\left.\begin{aligned} \epsilon_{11}', \epsilon_{22}' = {} & \frac{3(1-\nu)R\sigma_0}{4\mu a_0}\left[\left(1+\frac{\sigma_{11}'}{2\sigma_0}\right)^{2/3} - 1\right] \\ & \pm \frac{3f(2-\nu)R\sigma_0}{8\mu a_0}\left(1+\frac{\sigma_{11}'}{2\sigma_0}\right)^{2/3} \times \\ & \left[1 - \left(1 - \frac{\sigma_{11}'/2f\sigma_0}{1+\sigma_{11}'/2\sigma_0}\right)^{2/3}\right] \end{aligned}\right\} \quad [20]$$

$$\epsilon_{13}' = \epsilon_{12}' = \epsilon_{23}' = \epsilon_{33}' = 0$$

From [14] and [18], we see that failure will occur when

$$\sigma_{11}' = 2\sigma_{12}' > 2f\sigma_0/(1-f) \ldots\ldots\ldots [21]$$

The relation between σ_{11}' and ϵ_{11}', expressed in Equations [20] and depicted in Fig. 2 for several values of the coefficient of friction, shows clearly the nonlinear nature of the stress-strain law. It is of interest that each of the curves in Fig. 2 terminates with a horizontal slope, at which point failure occurs in the lattice.

A similar computation for the unloading process from $\sigma_{11}'^* < 2f\sigma_0/(1-f)$ yields the following relations for the nonzero strain components

$$\begin{aligned} \epsilon_{11}', \epsilon_{22}' = {} & \frac{3(1-\nu)R\sigma_0}{4\mu a_0}\left[\left(1+\frac{\sigma_{11}'}{2\sigma_0}\right)^{2/3} - 1\right] \\ & \pm \frac{3f(2-\nu)R\sigma_0}{8\mu a_0}\left(1+\frac{\sigma_{11}'^*}{2\sigma_0}\right)^{2/3}\left[1 - \frac{\sigma_{11}'^*}{f(2\sigma_0+\sigma_{11}'^*)}\right]^{2/3} \\ & + \left(1+\frac{\sigma_{11}'}{2\sigma_0}\right)^{2/3}\left[-1 + 2\left\{1 - (1-f)\frac{\sigma_{11}'^* - \sigma_{11}'}{2f(2\sigma_0+\sigma_{11}'^*)}\right\}^{2/3}\right] \end{aligned} \quad \ldots\ldots [22]$$

Equations [20] and [22] may be rewritten to furnish the more convenient forms

$$\begin{aligned} (8\mu a_0/3R\sigma_0)(\epsilon_{11}', \epsilon_{22}') = {} & [2(1-\nu) \pm f(2-\nu)](1+\sigma_{11}'/2\sigma_0)^{2/3} \\ & - 2(1-\nu) \mp f(2-\nu)[1 - (1/f-1)\sigma_{11}'/2\sigma_0]^{2/3} \end{aligned} \quad \ldots\ldots [23]$$

valid for the loading process, and

$$\begin{aligned} (8\mu a_0/3R\sigma_0)(\epsilon_{11}', \epsilon_{22}') = {} & [2(1-\nu) \mp f(2-\nu)](1+\sigma_{11}'/2\sigma_0)^{2/3} \\ & - 2(1-\nu) \mp f(2-\nu)[1 - (1/f-1)\sigma_{11}'^*/2\sigma_0]^{2/3} \\ & \pm 2f(2-\nu)[1 - (\sigma_{11}'^* - \sigma_{11}')/4f\sigma_0 \\ & + (\sigma_{11}'^* + \sigma_{11}')/4\sigma_0]^{2/3} \end{aligned} \quad \ldots\ldots [24]$$

valid for the unloading process. The relations between σ_{11}' and ϵ_{11}', given in Equations [23] and [24], are plotted in Fig. 3 for $f = 0.25$ and for various values of the loading amplitude, $\sigma_{11}'^*/2\sigma_0$. The inception of a hysteresis loop may be noted, and is due to the frictional energy dissipated in the course of the tangential displacements.

Finally, a surface of failure may be constructed for the problem discussed, but generalized by permitting an arbitrary angle of rotation θ about the x_3- axis. In this case

$$\left.\begin{aligned} \sigma_{11} &= \sigma_{11}' \cos^2\theta \\ \sigma_{22} &= \sigma_{11}' \sin^2\theta \\ \sigma_{12} &= \sigma_{11}' \sin\theta\cos\theta \end{aligned}\right\} \quad \ldots\ldots\ldots [25]$$

so that

$$\lambda_{11} = 1, \qquad \lambda_{12} = \tan\theta, \qquad \lambda_{22} = \tan^2\theta \ldots\ldots [26]$$

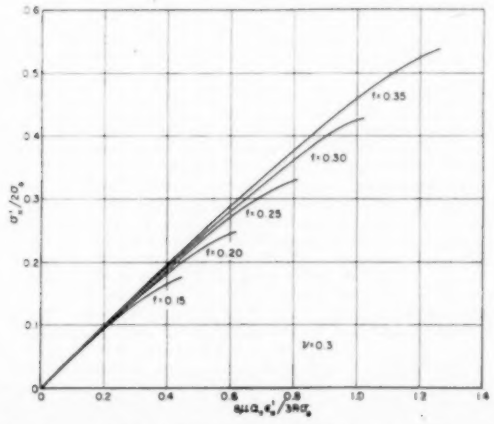

Fig. 2 Stress-strain relation for a simple cubic array of like spheres compressed in the [110] direction: loading portion of cycle

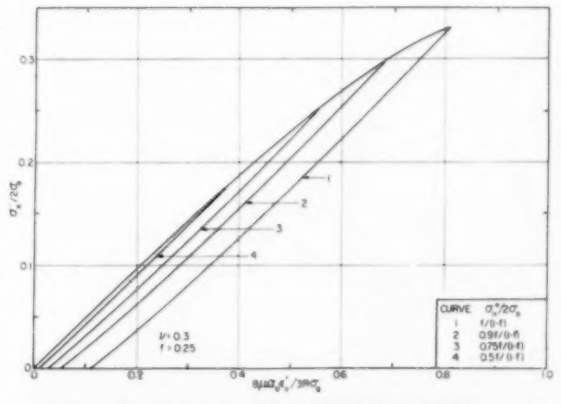

Fig. 3 Stress-strain relation for a simple cubic array of like spheres compressed in the [110] direction: loading-unloading cycle

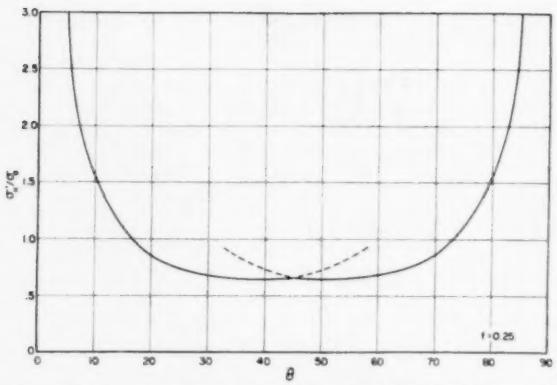

Fig. 4 Compressive stress causing failure in a simple cubic array of like spheres as a function of angle between direction of loading (in the x_1, x_2-plane) and the [100] direction

Hence, for failure to occur

$$\left.\begin{aligned} \frac{\sigma_{11}'}{\sigma_0} &\geqslant \frac{2f/\sin 2\theta}{1 - f\tan\theta} \qquad 0 \leqslant \theta \leqslant \pi/4 \\ \frac{\sigma_{11}'}{\sigma_0} &\geqslant \frac{2f/\sin 2\theta}{1 - f\cot\theta} \qquad \pi/4 \leqslant \theta \leqslant \pi/2 \end{aligned}\right\} \quad \ldots\ldots [27]$$

These equations are plotted in Fig. 4 for $f = 0.25$. The angle at which the resistance to failure (sliding) is lowest, depends on the value of the coefficient of friction and is given by the roots of

$$\tan 2\theta = \pm 1/f \quad \ldots\ldots [28]$$

The corresponding smallest stress causing failure is

$$(\sigma_{11}'/\sigma_0)_{\min} = 2f[f + (1 + f^2)^{1/2}] \quad \ldots\ldots [29]$$

Acknowledgment

The valuable advice of Prof. R. D. Mindlin of Columbia University is hereby gratefully acknowledged.

Bibliography

1 "Mechanics of Granular Media," by R. D. Mindlin, Proceedings of the Second U. S. National Congress of Applied Mechanics, Ann Arbor, Mich., 1954, pp. 13–20.

2 "Theorie der akustischen Schwingungsbreitung in gekörnten Substanzen und experimentelle Untersuchung an Kohlepulver," by G. Hara, *Elektrische Nachrichten-Technik*, vol. 12, 1935, pp. 191–200.

"Velocity of Elastic Waves in a Granular Substance," by K. Iida, *Bulletin of the Earthquake Research Institute*, Tokyo University, vol. 17, 1939, pp. 783–808.

"On the Theory of Elastic Waves in Granular Substance," by T. Takahashi and Y. Satô, *Bulletin of the Earthquake Research Institute*, Tokyo University, vol. 27, 1949, pp. 11–16; vol. 28, 1950, pp. 37–43.

"Elastic Waves Through a Packing of Spheres," by F. Gassmann, *Geophysics*, vol. 16, 1951, pp. 673–685; vol. 18, 1953, p. 268.

"A Study of the Speed of Sound in Porous Granular Media," by H. Brandt, JOURNAL OF APPLIED MECHANICS, TRANS. ASME, vol. 77, 1955, pp. 479–486.

3 "Stress-Strain Relations and Vibrations of a Granular Medium," by J. Duffy and R. D. Mindlin, JOURNAL OF APPLIED MECHANICS, TRANS. ASME, vol. 79, 1957, pp. 585–593.

4 "Elastic Spheres in Contact Under Varying Oblique Forces," by R. D. Mindlin and H. Deresiewicz, JOURNAL OF APPLIED MECHANICS, TRANS. ASME, vol. 75, 1953, pp. 327–344.

5 "Packing of Homogeneous Spheres," by W. O. Smith, P. D. Foote, and P. F. Busang, *Physical Review*, vol. 34, 1929, pp. 1271–1274.

6 "Theory of Elasticity," by S. Timoshenko and J. N. Goodier, second edition, McGraw-Hill Book Company, Inc., New York, N. Y., 1951, p. 372.

On Plane Stress Solution of an Elastic, Perfectly Plastic Wedge[1]

By P. M. NAGHDI,[2] ANN ARBOR, MICH.

With the use of Tresca's yield function and its associated flow laws, the complete solution is obtained for an isotropic elastic, perfectly plastic wedge (with an included angle $\beta < \pi/2$) subjected to a uniform traction in the state of plane stress. Unlike its corresponding plane strain solution, the state of stress in a portion of the plastic domain of the wedge is at a corner of Tresca's yield hexagon where, in general, the normal to the yield surface is not defined uniquely.

Introduction

THE elastic-plastic solution of the acute isotropic wedge (with an included angle $0 < \beta < \pi/2$) subjected to a uniform traction in the state of plane strain, has been given recently for an incompressible material employing Prandtl-Reuss stress-strain law in (1),[3] and for a compressible material with the use of Tresca's yield condition and its associated flow rules in (2). The present paper, again employing Tresca's piecewise linear loading function, is concerned with the corresponding plane stress solution of the problem treated previously (1, 2). The complete solution is obtained for an isotropic, compressible elastic, perfectly plastic wedge (with an included angle $\beta < \pi/2$)[4] in the state of plane stress[5] subjected to a uniform lateral pressure (assumed to be monotonically increasing with time) on one boundary, as shown in Fig. 1.

As noted in (2), for an incompressible elastic, perfectly plastic wedge in the state of plane strain, Mises' and Tresca's (with normal component of stress σ_z as the intermediate principal stress) yield conditions are identical and may be written as

$$\frac{1}{4}(\sigma_r - \sigma_\theta)^2 + \sigma_{r\theta}^2 - k^2 = 0 \quad \ldots\ldots [1]$$

where $\{\sigma_r, \sigma_\theta, \sigma_{r\theta}\}$ are the plane components of stress referred to cylindrical polar co-ordinates (r, θ, z) and k is the yield limit in simple shear. Furthermore, for problems of plane plastic flow of a compressible material, Tresca's yield condition is again given by Equation [1] as long as σ_z is the intermediate principal stress. While this intermediary condition on σ_z is fulfilled for a wedge in the state of plane strain, it is not necessarily fulfilled for a wedge in the state of plane stress. Indeed, as will be shown presently, for the wedge in question, a portion of the plastic domain is initially at a corner of Tresca's yield hexagon where two of the principal stresses vanish simultaneously. In this connection, it should be mentioned that singular loading functions in general, and Tresca's yield function in particular, as well as their associated flow laws have been discussed by Koiter (3), Prager (4), and Hodge (5), where other references may be found.

Before closing this section, we recall that in the state of plane stress ($\sigma_{rz} = \sigma_{\theta z} = \sigma_z = 0$), the stress-strain relations in the plastic range involving a plastic potential have the form[6]

$$\{\dot{e}_r, \dot{e}_\theta, \dot{e}_z, \dot{\epsilon}_{r\theta}\} = \frac{1}{2G}\{\dot{s}_r, \dot{s}_\theta, \dot{s}_z, \dot{\sigma}_{r\theta}\} + \frac{\partial f}{\partial\{\sigma_r, \sigma_\theta, \sigma_z, \sigma_{r\theta}\}}\dot{\lambda} \quad \ldots [2a]$$

$$\dot{s} = 3K\dot{\epsilon} \quad \ldots\ldots [2b]$$

where

$$\left.\begin{aligned} s &= \frac{1}{3}(\sigma_r + \sigma_\theta), \quad \epsilon = \frac{1}{3}(\epsilon_r + \epsilon_\theta + \epsilon_z) \\ \epsilon_r &= \epsilon_r' + \epsilon_r'', \text{ etc.}, \quad e_r = e_r' + e_r'', \text{ etc.} \end{aligned}\right\} \quad \ldots [3]$$

$\{\epsilon_r, \epsilon_\theta, \epsilon_z, \epsilon_{r\theta}\}$ are the components of strain; $\{e_r, e_\theta, e_z, \epsilon_{r\theta}\}$ are the components of strain deviation; dot denotes differentiation with respect to time; λ is a scalar function which depends on both co-ordinates and time; prime and double primes refer, respectively, to the elastic and plastic components of strain; E and ν

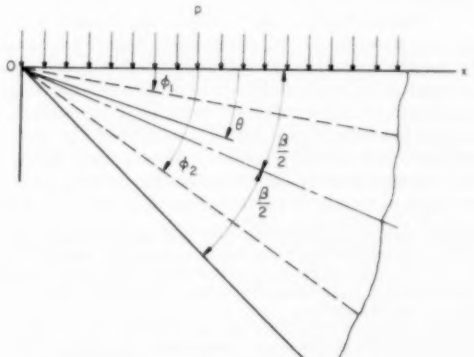

Fig. 1 Narrow wedge under a uniform lateral pressure

[1] The results presented in this paper were obtained in the course of research sponsored by the Office of Naval Research under Contract Nonr-1224(01), Project NR-064-408, with the University of Michigan.

[2] Formerly Professor of Engineering Mechanics, University of Michigan. Now, Professor of Engineering Science, University of California, Berkeley, Calif. Mem. ASME.

[3] Numbers in parentheses refer to Bibliography at end of the paper.

[4] As discussed in (1), this limitation is due to the character of the initial yield and the locus of the elastic-plastic boundary which depend on the loading as well as on the included wedge angle β.

[5] The character of the plane stress solution considered here is approximate in that the variation of the plane components of stress and displacements with axial co-ordinate z (the z-axis is taken perpendicular to the plane of the cross section in Fig. 1) is neglected.

Contributed by the Applied Mechanics Division and presented at the Annual Meeting, New York, N. Y., December 1–6, 1957, of THE AMERICAN SOCIETY OF MECHANICAL ENGINEERS.

Discussion of this paper should be addressed to the Secretary, ASME, 29 West 39th Street, New York, N. Y., and will be accepted until October 10, 1958, for publication at a later date. Discussion received after the closing date will be returned.

NOTE: Statements and opinions advanced in papers are to be understood as individual expressions of their authors and not those of the Society. Manuscript received by ASME Applied Mechanics Division, May 13, 1957. Paper No. 57—A-40.

[6] As pointed out in (1) and (2), it is not necessary to define the "stress rate" on the right-hand side of [2a] with respect to convected co-ordinates. Since the components of strain and displacements are assumed infinitesimal, at a fixed point of observation, the partial derivative of the stress with respect to time may be employed instead.

are Young's modulus and Poisson's ratio, respectively

$$G = \frac{E}{2(1+\nu)}$$

and

$$K = \frac{E}{3(1-2\nu)}$$

Fully elastic solution and initial yield

We record here for future reference the plane stress solution of the fully elastic isotropic wedge subjected to uniform tractions in the form

$$\left.\begin{aligned} Gu_r &= r[N(b + d\theta) + P(\theta)] \\ Gu_\theta &= r[Ld \log r + Q(\theta)] \end{aligned}\right\} \quad \ldots\ldots\ldots [4a]$$

where u_r and u_θ are the radial and tangential displacements, respectively

$$\left.\begin{aligned} P(\theta) &= -(a \cos 2\theta + c \sin 2\theta) \\ Q(\theta) &= (a \sin 2\theta - c \cos 2\theta) \end{aligned}\right\} \quad \ldots\ldots\ldots [4b]$$

the constants N and L are

$$N = \frac{1-\nu}{1+\nu}, \quad L = -\frac{2}{1+\nu} \quad \ldots\ldots\ldots [4c]$$

the coefficients a, b, c, and d are the same as those employed in (1), and the nonvanishing stresses which, with the aid of Hooke's law may be deduced from Equation [4], are identical with the corresponding components of an incompressible material[7] and are given by

$$\left.\begin{aligned} \sigma_r &= 2[(b + d\theta) + P(\theta)] \\ \sigma_\theta &= 2[(b + d\theta) - P(\theta)] \\ \sigma_{r\theta} &= -d + 2Q(\theta) \end{aligned}\right\} \quad \ldots\ldots\ldots [5]$$

Denoting the plane components of the principal stresses by σ_1 and σ_2, then

$$\{\sigma_1, \sigma_2\} = \frac{\sigma_r + \sigma_\theta}{2} \pm \left[\left(\frac{\sigma_r - \sigma_\theta}{2}\right)^2 + \sigma_{r\theta}^2\right]^{1/2} \quad \ldots\ldots [6]$$

and substitution of Equation [6] with the aid of Equations [5] into Tresca's yield function

$$f = \max\left[|\sigma_1 - \sigma_2|, |\sigma_2 - \sigma_3|, |\sigma_3 - \sigma_1|\right] - 2k \quad \ldots\ldots [7]$$

reveals that, since $\sigma_3 = \sigma_z = 0$, the right-hand side of Equation [7] vanishes when $|\sigma_1 - \sigma_2| = 2k$ which is equivalent to Equation [1]. Hence as in the case of the corresponding plane strain solution of the wedge (1, 2), yielding will begin simultaneously at the outside boundaries $\theta = 0$ and $\theta = \beta$ when the lateral pressure has reached the value $p^* = 2k\,(\tan\beta - \beta)\,(\tan\beta)^{-1}$. For a pressure $p^* < p < p^{**}$ (p^{**} being the value of the lateral pressure in the fully plastic state), a portion of the wedge becomes plastic and, as in (1), subject to a subsequent verification, it will be assumed that the elastic-plastic boundaries are the planes[8] $\theta = \phi_1$ and $\theta = \phi_2$, as indicated in Fig. 1. Here we

[7] This is readily seen from the fact that in the absence of body forces the determination of the plane components of stress in the state of plane strain and plane stress (with z-variation neglected) are characterized by a biharmonic stress function which is independent of Poisson's ratio.

[8] In fact, as has been pointed out by Drucker (6), in view of the lack of dependence of the plane components of stress on the radial co-ordinate and with the aid of any symmetric loading function, this feature of the solution together with $\phi_1 + \phi_2 = \beta$ can be established without finding the solution itself.

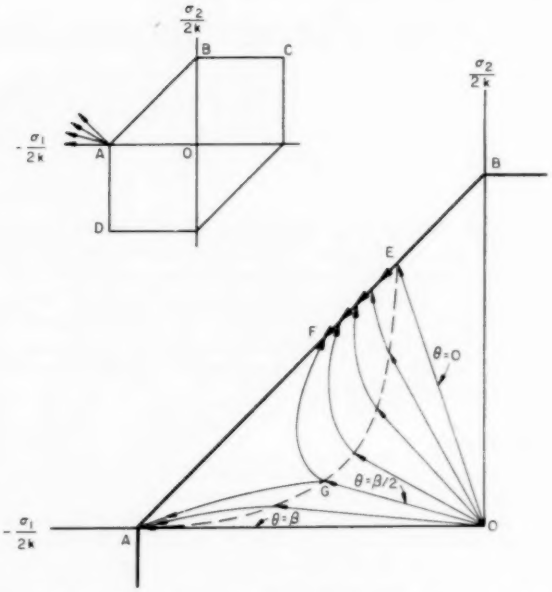

Fig. 2 Tresca's yield surface in the plane $\sigma_z = 0$, showing schematically the principal stress paths at the initiation of yield and throughout the elastic-plastic wedge

also observe that for the fully elastic wedge, the stress paths are radial and, as indicated schematically in Fig. 2, terminate on the dashed curve[9] AGE. The principal stresses at the initiation of yield are given by

$$\left.\begin{aligned} \sigma_1 &= -p^* \\ \sigma_2 &= 2k - p^* \end{aligned}\right\} \quad \text{on} \quad \theta = 0 \quad \ldots\ldots\ldots [8a]$$

and

$$\left.\begin{aligned} \sigma_1 &= -2k \\ \sigma_2 &= 0 \end{aligned}\right\} \quad \text{on} \quad \theta = \beta \quad \ldots\ldots\ldots [8b]$$

the former on segment AB of the yield hexagon, and the latter at regime A; i.e., a point of an edge of Tresca's yield hexagon where a fan of possible normals to the yield surface exists, only one of which lies in the plane[10] $\sigma_z = 0$.

Elastic-plastic solution

Since in the plastic domain the state of stress is statically determinate and assumed independent of r, it follows from the nonvanishing stress differential equations of equilibrium, Tresca's yield condition, and the boundary conditions, that the stresses in the plastic region $0 \leq \theta \leq \phi_1$ are given by

$$\left.\begin{aligned} \sigma_r &= -p + k(1 + \cos 2\theta) \\ \sigma_\theta &= -p + k(1 - \cos 2\theta) \\ \sigma_{r\theta} &= -k \sin 2\theta \end{aligned}\right\}; \quad 0 \leq \theta \leq \phi_1 \quad \ldots\ldots [9a]$$

or by Equation [6] and with reference to Fig. 2

[9] In Fig. 2, the nonradial extensions of the stress paths of the fully elastic wedge between the dashed curve AGE and segment AB refer to those appropriate for the elastic-plastic wedge.

[10] This also follows from the condition at a multiple intersection given by Hodge (5, Equation [3.15]), which for regime A of Fig. 2 yields $\dot{\epsilon}_1'' = -\dot{\lambda}$, $\dot{\epsilon}_2'' + \dot{\epsilon}_3'' = \dot{\lambda}$.

$$\left.\begin{aligned}\sigma_1 &= -p\\ \sigma_2 &= 2k - p\end{aligned}\right\};\quad 0 \le \theta \le \phi_1 \qquad [9b]$$

As seen from Equations [9b], for a given $p^* \le p \le p^{**}$ (corresponding to an elastic-plastic boundary $\theta = \phi_1$), the ratio of (σ_2/σ_1) in the region $0 \le \theta \le \phi_1$ is always negative and hence the state of stress, as shown in Fig. 2, remains on f_{AB} and moves toward F.

In the lower plastic region $\phi_2 \le \theta \le \beta$, the state of stress which on initial yielding is given by Equations [8b], with reference to Fig. 2, either moves along AB, moves along AD, or remains at regime A. If the state of stress lies on f_{AB}, then by means of the stress differential equations of equilibrium in cylindrical polar co-ordinates, Tresca's yield condition [1], as well as the appropriate boundary conditions, it can be readily shown that the nonvanishing stresses are

$$\left.\begin{aligned}\sigma_r &= -k[1 + \cos 2(\theta - \beta)]\\ \sigma_\theta &= -k[1 - \cos 2(\theta - \beta)]\\ \sigma_{r\theta} &= k \sin 2(\theta - \beta)\end{aligned}\right\};\quad \phi_2 \le \theta \le \beta \qquad [10a]$$

or by Equation [6]

$$\left.\begin{aligned}\sigma_1 &= -2k\\ \sigma_2 &= 0\end{aligned}\right\};\quad \phi_2 \le \theta \le \beta \qquad [10b]$$

To establish the possible state of stress on AD, we utilize the Lamé-Maxwell equations of equilibrium in the form given in (7)

$$\frac{\partial \sigma_1}{\partial s_1} + \frac{\sigma_1 - \sigma_2}{\rho_2} = 0, \quad \frac{\partial \sigma_2}{\partial s_2} + \frac{\sigma_1 - \sigma_2}{\rho_1} = 0 \qquad [11]$$

where s_1 and s_2 are the stress trajectories through a generic point P, and ρ_1 and ρ_2 are the corresponding radii of curvature at P. Since on f_{AD}, $\sigma_1 = -2k$ and $-2k \le \sigma_2 \le 0$, then by the first of Equations [11], either (*a*) $\sigma_2 = -2k$ or (*b*) $\rho_2 = \infty$. In case (*a*), with the aid of Equation [6], it is easily seen that the solution $\sigma_1 = \sigma_2$ implies the vanishing of all of the components of stress which do not hold on f_{AD} and hence (*a*) is false. In case (*b*), the stress trajectories s_2 must be straight lines and in view of the orthogonality of s_1 and s_2 as well as the fact that $\theta = \beta$ is a known trajectory, it follows that the family of the stress trajectories s_1 and s_2 have the pattern indicated in Fig. 3 which, by Equations [11], corresponds to the solution $\sigma_1 = -2k$, $\sigma_2 = 0$. Thus in the lower plastic region, the state of stress initially at regime A will remain there and is given by Equations [10].

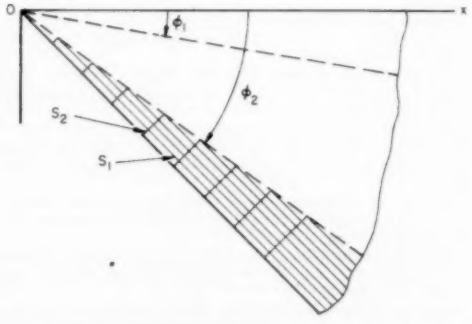

Fig. 3 Narrow wedge showing stress trajectories in lower plastic region

As in (1), the continuity of stresses at the elastic-plastic boundaries yields $\phi_1 + \phi_2 = \beta$ (or $\phi_1 = \phi$ and $\phi_2 = \beta - \phi$), as well as the functional relation between the lateral pressure p and the elastic-plastic boundary ϕ, which, since it is identical with the corresponding expression for a wedge in the state of plane strain (1, 2), will not be repeated here.

While in the upper plastic region $(0 \le \theta \le \phi)$ $\dot{\epsilon}_z'' = 0$ and the normal to f_{AB} is uniquely determined, the direction of the plastic strain-rate vector at regime A is limited to the directions included between the normals to the adjacent surfaces; and unless the normal at A to the loading surface is determined uniquely, the stress-strain relations [2*a*] are not valid in the lower plastic region.

As the thickness h, expressed in terms of the initial wedge thickness h_0 by

$$h = h_0(1 + \epsilon_z) \qquad [12]$$

does not remain constant during deformation, the Lamé-Maxwell equations of equilibrium assume the form

$$\frac{\partial(h\sigma_1)}{\partial s_1} + \frac{h(\sigma_1 - \sigma_2)}{\rho_2} = 0, \quad \frac{\partial(h\sigma_2)}{\partial s_2} + \frac{h(\sigma_1 - \sigma_2)}{\rho_1} = 0 \qquad [13]$$

which in the lower plastic region (with the state of stress at regime A and $\rho_1 = \rho_2 = \infty$) reduce to $\partial h/\partial s_1 = 0$; i.e., $h = h(s_2) = \text{const}$ on s_1. But since the family s_2, as well as s_1, intersect $\theta = (\beta - \phi)$ on which h is also constant, it follows that h, as well as ϵ_z, is constant throughout the lower plastic region.

Since the axial strain in the elastic and plastic domains is given by

$$\epsilon_z' = -\frac{\nu}{E}(\sigma_r + \sigma_\theta)$$

and

$$\epsilon_z = -\frac{\nu}{E}(\sigma_r + \sigma_\theta) + \epsilon_z''$$

respectively, the continuity requirements of h and by Equation [12] ϵ_z as well as those of the stresses at the elastic-plastic boundaries demand the vanishing of the plastic axial strain at $\theta = (\beta - \phi)$. Further, since

$$(\sigma_r + \sigma_\theta) = -2k$$

and $\epsilon_z = \text{const}$ in $(\beta - \phi) \le \theta \le \beta$, it follows that

$$\epsilon_z'' = \dot{\epsilon}_z'' = 0$$

throughout the lower plastic region. Recalling that for Tresca's yield surface, Fig. 2, the vanishing of the plastic axial-strain rate occurs only on f_{AB} and its image about the origin, then the state of stress (in $[\beta - \phi] \le \theta \le \beta$) at regime A, given by Equations [10], is on f_{AB} the normal to which is uniquely determined.

The determination of the plane components of displacement in the two plastic regions, with the aid of Equation [2*a*], and the continuity requirements for u_r and u_θ at the elastic-plastic boundaries, may now be carried out in a manner similar to that in (2), and only the final results will be given here. In the upper plastic region

$$\left.\begin{aligned}u_r &= r\{D + \cos 2\theta[A + B \log|\sec 2\theta + \tan 2\theta|]\}\\ u_\theta &= r\{-\sin 2\theta[A + B \log|\sec 2\theta + \tan 2\theta|] + B \log|\sec 2\theta| - 2B \log r + C\}\end{aligned}\right\};\quad 0 \le \theta \le \phi \qquad [14]$$

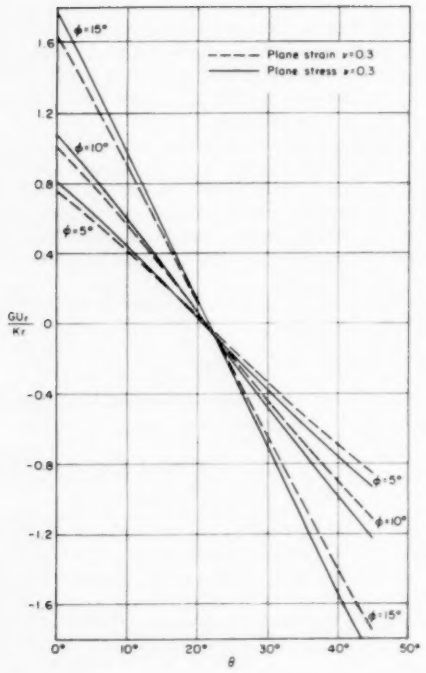

Fig. 4 Ratio of radial displacement to r (or radial strain) for plane stress and plane strain

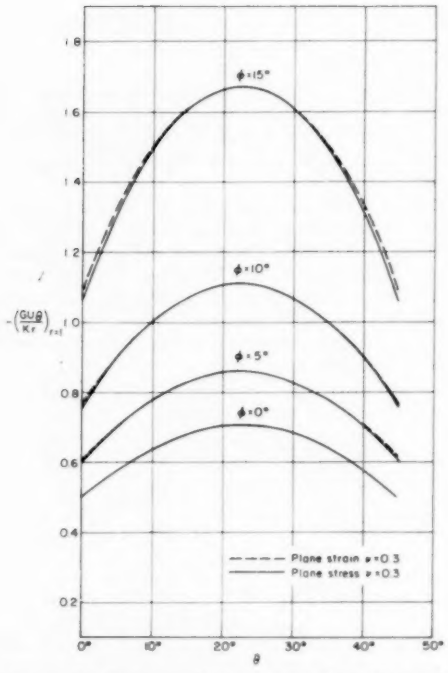

Fig. 5 Tangential displacement at $r = 1$ for plane stress and plane strain

where

$$\left.\begin{aligned} D &= \left(\frac{1-\nu}{1+\nu}\right)\frac{k-p}{2G}, \quad B = \frac{d}{(1+\nu)G} \\ A &= \frac{k}{2G} + H, \\ H &= -B\log|\sec 2\phi + \tan 2\phi| \\ C &= \frac{d}{2G}\left[1 - \frac{2}{1+\nu}\log|\sec 2\phi|\right] \end{aligned}\right\} \quad ; \quad 0 \le \theta \le \phi \qquad [15]$$

and for the lower plastic region, the displacements are of the same form as Equations [14], except that the argument θ is replaced by $(\theta - \beta)$ and the coefficient functions by

$$\left.\begin{aligned} D &= \left(\frac{1-\nu}{1+\nu}\right)\frac{-k}{2G}, \quad B = \frac{d}{(1+\nu)G} \\ A &= -\frac{k}{2G} + H, \\ H &= -B\log|\sec 2\phi| \\ C &= \frac{d}{2G}\left[1 - \frac{2}{1+\nu}\log|\sec 2\phi|\right] \end{aligned}\right\} \quad ; \quad (\beta - \phi) \le \theta \le \beta \qquad [16]$$

Conclusion

In spite of the fact that the state of stress in the lower plastic region of the wedge considered here is at a corner of Tresca's yield surface, it is interesting to note that the nonvanishing stresses as given by Equations [5], [9a], and [10a] are identical with the corresponding plane components of stress of the wedge in the state of plane strain (1, 2). The displacements u_r and u_θ given by Equations [4], [14], [15], and [16], though of the same form as the corresponding plane strain solution (2), have different coefficient functions.

Comparisons of the displacements u_r and u_θ of the present paper with those of the plane strain solution for the case $\beta = \pi/4$ are shown in Figs. 4 and 5, and numerical values of the nonvanishing stresses (since they are identical with the corresponding plane components of stress for an incompressible elastic-plastic wedge) for $\beta = \pi/4$ may be found in (1).

Finally, it may be observed that while the elastic-plastic solution for the wedge (of a compressible material using Tresca's yield function) in the state of plane strain (2) with $\nu = 1/2$ reduces to that of a wedge obeying Prandtl-Reuss stress-strain law for an incompressible material, the corresponding reduction does not hold for the wedge in the state of plane stress.

Bibliography

1 "Stresses and Displacements in an Elastic-Plastic Wedge," by P. M. Naghdi, JOURNAL OF APPLIED MECHANICS, TRANS. ASME, vol. 79, March, 1957, pp. 98–104.

2 "A Compressible Elastic, Perfectly Plastic Wedge," by D. R. Bland and P. M. Naghdi, JOURNAL OF APPLIED MECHANICS, TRANS. ASME, vol. 80, 1958, pp. 239–242.

3 "Stress-Strain Relations, Uniqueness, and Variational Theorems for Elastic-Plastic Materials With a Singular Yield Surface," by W. T. Koiter, *Quarterly of Applied Mathematics*, vol. 11, 1953, pp. 350–354.

4 "On the Use of Singular Yield Conditions and Associated Flow Rules," by W. Prager, JOURNAL OF APPLIED MECHANICS, TRANS. ASME, vol. 75, 1953, pp. 317–320.

5 "Minimum Principles of Piecewise Linear Isotropic Plasticity," by P. G. Hodge, Jr., *Journal of Rational Mechanics and Analysis*, vol. 5, 1956, pp. 917–938.

6 Discussion of reference (1), by D. C. Drucker, JOURNAL OF APPLIED MECHANICS, TRANS. ASME, vol. 79, 1957, p. 631.

7 "Photoelasticity," by M. M. Frocht, John Wiley & Sons, Inc., New York, N. Y., vol. 1, 1941.

Brief Notes*

On the recommendations of the Executive Committee of the ASME Applied Mechanics Division, it has been decided to initiate a section devoted to brief notes on technical matters in mechanics. These notes must not be longer than 750 words (about 2½ double-spaced typewritten pages, including figures) and will be subject to the usual review procedure prior to publication. After approval such notes will be published as soon as possible, normally in the next issue of the Journal. The notes should be submitted to the Technical Editors of the *Journal of Applied Mechanics*.

Effect of Tensile Plastic Deformation on Yield Condition[1]

By L. W. HU[2] and J. F. BRATT[3]

A yield condition specifies the stress state under which the incipience of plastic flow in metals is possible. Knowledge of the effects of the stress history on the yield condition is of great importance in formulating the plastic stress-strain relations for metals with strain-hardening. Early experimental studies on this subject, such as the one by Cunningham, Thomsen, and Dorn [1],[4] were essentially restricted to tests of the constant stress ratio type and gave evidence to support the concept of the isotropic expansion of yield surface. In other words, the yield surface was postulated to expand isotropically in all directions due to plastic deformation. However, in 1950, Shaw and Wycherley conducted an experiment of the variable stress ratio type and disproved the concept of isotropic expansion of yield surface [2]. Thereafter, many investigations have been conducted to study the behavior of yield surface. In 1952, Marin and Hu gave qualitative evidence to support the postulation of the yield corner by the slip-line theory of plasticity [3]. Attempts were made by them in 1954 to determine the change in shape of the yield surface due to plastic deformation [4]. In the same year, the test results of Naghdi and his associates confirmed again qualitatively the existence of the yield corner [5, 6]. Recently, Naghdi, Essenburg, and Koff reported their comprehensive torsion-tension reversed-torsion experiments on the effects of shear plastic deformation on the yield condition [7]. In the following note, a biaxial stress investigation on the effects of tensile plastic deformation on the yield condition is reported.

Tubular specimens of the dimensions given in reference [3] were made of an aluminum alloy 2S-F. The material was supplied by the Aluminum Company of America in a tubular form of 1⅝-in. OD and 1-in. ID. The specimens were annealed after machining at a temperature of 650 F for not less than 30 min in an atmosphere of helium. Grain size was measured after annealing and was found to be in the range of 0.08 to 0.09 mm for all specimens. The Brinell hardness number after annealing was found to vary from 20 to 26.

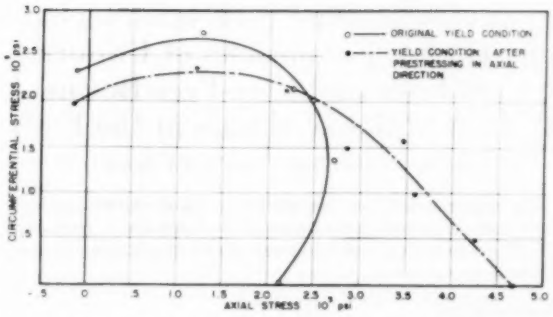

Fig. 1 Original and subsequent yield conditions

A biaxial stress state was produced in the specimen by applying the axial load and the internal pressure simultaneously in a predetermined manner. The axial load was applied through a 60,000-lb Universal Testing Machine made by Baldwin-Lima-Hamilton Corporation, and the internal pressure was generated by using a Dudgeon Hand Pump with a 2000-psi Duragauge. SR-4 strain gages of type A5-1 were employed to measure the longitudinal and circumferential strains.

In Fig. 1 each point represents the test result of one specimen. The original yield surface was determined by the stress state at which the stress-strain relation first deviated from its initial portion. The subsequent yield surface was determined in a similar manner except that the specimens were prestressed axially by a tensile stress of 4690 psi.

For the material tested, the following conclusions were drawn:

(*a*) The original yield surface is fairly in agreement with the von Mises yield condition.

(*b*) The subsequent yield surface after prestressing in tension does not expand isotropically in all directions.

(*c*) A yield corner is formed in the direction of the prestressing.

(*d*) After prestressing in the axial direction by tension, the tensile yield stress in the tangential direction is reduced considerably from its value before prestressing.

References

1 D. M. Cunningham, E. G. Thomsen, and J. E. Dorn, "Plastic Flow of Magnesium Alloy Under Biaxial Stresses," *Proceedings of the ASTM*, vol. 47, 1947, pp. 546–553.

2 F. S. Shaw and G. W. Wycherley, "Experiments on the Plasticity of Metals, the Octahedral Shear Stress Leading Criterion," Structure and Materials Note 181, Department of Supply and Development, Australia, March, 1950.

3 J. Marin and L. W. Hu, "On the Validity of Assumptions Made in Theories of Plastic Flow for Metals," Trans. ASME, vol. 75, 1953, pp. 1181–1190.

4 J. Marin and L. W. Hu, "Biaxial Plastic Stress-Strain Relations of a Mild Steel for Variable Stress Ratios," Trans. ASME, vol. 78, 1956, pp. 499–509.

5 P. M. Naghdi and J. C. Rowley, "An Experimental Study of Biaxial Stress-Strain Relations in Plasticity," *Journal of the Mechanics and Physics of Solids*, vol. 3, 1954, pp. 63–80.

6 P. M. Naghdi, J. C. Rowley, and C. W. Beadle, "Experiments Concerning the Yield Surface and the Assumption of Linearity in the Plastic Stress-Strain Relations," Journal of Applied Mechanics, vol. 22, Trans. ASME, vol. 77, 1955, pp. 416–420.

7 P. M. Naghdi, F. Essenburg, and W. Koff, "An Experimental Study of Initial and Subsequent Yield Surfaces in Plasticity," Journal of Applied Mechanics, vol. 25, Trans. ASME, vol. 80, 1958, pp. 201–209.

[1] This work was supported in part by a grant from E. I. du Pont de Nemours and Company, Inc.

[2] Associate Professor of Engineering Mechanics, The Pennsylvania State University, University Park, Pa.

[3] Formerly Instructor in Engineering Mechanics, The Pennsylvania State University, University Park, Pa. Now at Materialsprovingsanstalen, Norges Tekniske Hogskole, Trondheim, Norway.

[4] Numbers in brackets indicate References at end of paper.

* Discussion of papers in Brief Notes should be addressed to the Secretary, ASME, 29 West 39th Street, New York, N. Y., and will be accepted until October 10, 1958, for publication at a later date. Discussion received after the closing date will be returned.

Note: Statements and opinions advanced in papers are to be understood as individual expressions of their authors and not those of the Society. Manuscript received by Applied Mechanics Division, February 10, 1958.

Formulas for the Frequencies Including Higher Frequencies of Uniform Cantilever and Free-Free Beams With Additional Masses at the Ends

By JUAN HAENER,[1] WICHITA, KAN.

The approximated formulas, the derivation of which is outlined here, make it possible to determine immediately the n^{th} frequency of uniform cantilever and free-free beams with additional masses at the ends.

Nomenclature

EI = stiffness in bending
I_2 = moment of inertia of the mass M_2
l = length of the beam
M_1 = total mass of the beam
M_2 = additional mass
n = number of waves in $2l$ for the free-free beam
= number of waves in $4l$ for the cantilever beam
$a_n = \sqrt[4]{\frac{M_1\omega_n^2}{lEI}}$
ω_n = n^{th} frequency, in radians per sec

(A) The characteristic equation for the constant cross section cantilever beam with an additional mass at its free end is

$$\frac{1}{\cosh al} + \cos al = -al\,\frac{M_2}{M_1}\,(\tanh al.\cos al - \sin al) + (al)^3\,\frac{I_2}{M_1 l^2}\,(\tanh al.\cos al + \sin al) + (al)^4\,\frac{M_2 I_2}{M_1^2 l^2}\left(\frac{1}{\cosh al} - \cos al\right) \quad (1)$$

If the moment of inertia of the mass at the free end can be neglected, a simpler equation than (1) can be solved for (al). The $(al)_n$ thus derived allows us to express the frequencies by the following formula

$$\omega_n = \left[\frac{EI}{l^3 M_1}\left(\frac{R_n^4}{\frac{M_2}{M_1}\mu_n + k_n} + r_n^4\right)\right]^{1/2} \quad (2)$$

in which

n	R_n	r_n	k_n	μ_n
1	1.875	0	1	4.091
2	4.694	3.940	1.9839	21.608
$n>2$	$\pi\left(n-\frac{1}{2}\right)$	$\pi\left(n-\frac{3}{4}\right)$	$\frac{1}{1-\left(\frac{4n-3}{4n-2}\right)^4}$	$4n(n+0.6)$

(3)

The accuracy of (2) increases with increasing values of n. For $n = 3$ the error is less than $^1/_4$ per cent.

(B) The characteristic equation for the constant cross-section free-free beam with additional masses M_2 at both ends is

$$\left(\frac{M_2}{M_1}\right)^2 = \frac{1 - \cos al.\cosh al}{2(al)^2 \sin al.\sinh al} \quad (4)$$

[1] Research Specialist, Cessna Aircraft Company. Now Staff Specialist, Research and Development Engineering, Solar Aircraft Company, San Diego, Calif.

Manuscript received by ASME Applied Mechanics Division, July 17, 1957.

The solutions $(al)_n$ of (4) make it possible to derive the following formulas for the first, second, and n^{th} frequencies.

$$\omega_1 = \pi^2\left[\left(1 - \frac{5.45}{77.4\left(\frac{M_2}{M_1}\right)^2 - 1}\right)\frac{EI}{M_1 l^3}\right]^{1/2}\left(\frac{M_2}{M_1}\right)^2 > 0.08 \quad (5)$$

$$\omega_2 = \pi^2\left[\left(16 - \frac{10.86}{77.7\left(\frac{M_2}{M_1}\right)^2 + 1}\right)\frac{EI}{M_1 l^3}\right]^{1/2} \quad (6)$$

$$\omega_n = \pi^2\left[\left(n^4 - \frac{n^4 - (n-0.5)^4}{17.5n\left(\frac{M_2}{M_1}\right)^2 + 1}\right)\frac{EI}{M_1 l^3}\right]^{1/2} \qquad n>2 \quad (7)$$

The accuracy of these equations increases with increasing values of n. The value of ω_1 in (5) is about 1 per cent too large for $M_2/M_1 > 0.02$ and is good to three decimals for $0.1553 < M_2/M_1 < 1$.

When I_2 cannot be neglected, the solution of (1) for the higher frequencies can be found by determining $(al)_n$ from (2) and then plotting (1) in the range of smaller values as defined by (2).

References

Lord Rayleigh, "Theory of Sound," The Macmillan Company, London, 1877.

Richard Schulz, "Grundlagen fuer die Berechnung von Schwingungsmessgeräten," Askania-Warte, no. 43, January, 1953.

J. Haener, "Schwingungen zweier zusammengesetzter Balken," *Österreichisches Ingenieur-Archiv*, Bd. III, Heft 1, 1948.

On Particular Integrals for Toroidal Shells Subjected to Uniform Internal Pressure

By G. D. GALLETLY,[1] EMERYVILLE, CALIF.

For toroidal shells which do not include the apex $\phi = 0$, two common approximations are used to evaluate a particular integral of the relevant differential equations. These approximations, which are known to violate the compatibility relations and are chosen to satisfy only the equilibrium conditions, are:

(*a*) The transverse shear Q_ϕ and the rotation V are both set equal to zero, and the stress resultants N_ϕ and N_θ are given by their membrane values.

(*b*) Same as (*a*), except that the rotation V is given by the membrane rotation V_m.

The purpose of the present note is to point out that these approximations are not very good even when ϕ is as large as 30 degrees.[2] To illustrate the point, a constant-thickness toroidal shell under uniform internal pressure will be investigated.

Numerical Example

The toroidal shell considered is shown in Fig. 1. The pertinent dimensions are: $\lambda = a/b = 7$; $b/h = 30$; $b = 18$ in.; $\alpha = 30$

[1] Shell Development Company, Emeryville Research Center.

[2] The case when $\phi \backsimeq 0$ has been investigated by R. A. Clark ("On the Theory of Thin Elastic Toroidal Shells," *Journal of Mathematics and Physics*, vol. 29, 1950, page 146). Therein he considered approximation (*a*) and a particular integral obtained by asymptotic integration.

Manuscript received by ASME Applied Mechanics Division, November 20, 1957.

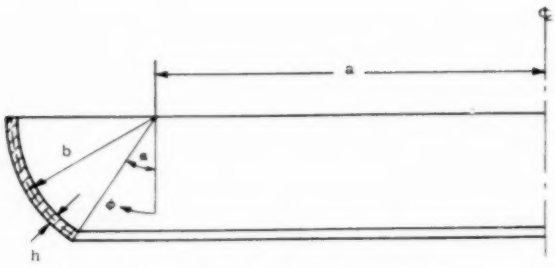

Fig. 1 Half section through toroidal shell

deg. It will be assumed that the internal pressure equals 60 psig.

When this toroidal shell is used as a transition piece on a pressure vessel, say between a cylinder and a spherical cap, edge moments and shears will be produced at the cylinder-torus and torus-spherical cap junctions. These edge loads are produced, of course, because the three shells deform by different amounts under the action of the internal pressure.

To evaluate the edge bending loads, the edge rotations and edge displacements have to be known for each shell in terms of the unknown edge moments M and shears Q, and the internal pressure p. The coefficients of M and Q are usually known as edge influence coefficients. We are not concerned with these here. Rather, we are interested in the edge rotations and displacements of the torus due to the pressure. We shall evaluate these using three approaches as follows:

(i) Using approximation (a) cited. We obtain therefore for the horizontal displacement δ and the rotation V:

$$E\delta = -\frac{p}{2}\left(\frac{b}{h}\right) b \sin\phi \left(1 + \frac{\lambda}{\sin\phi}\right)^2 \left(\frac{\lambda}{\sin\phi} + \nu - 1\right) \quad (a)$$

$$EV = 0 \quad (b) \qquad (1)$$

(ii) Using approximation (b) cited. We have then

$$E\delta = \text{See equation } 1(a) \quad (a)$$

$$EV = -\frac{p}{2}\left(\frac{b}{h}\right)\frac{\lambda \cot\phi}{\sin\phi}\left(1 + \frac{\lambda}{\sin\phi}\right)\left(\frac{2\lambda}{\sin\phi} - 1\right) \quad (b) \qquad (2)$$

(iii) The small-deflection nonhomogeneous differential equations for the bending of a torus were integrated numerically on an electronic computer. The step length used was $^1/_2$ degree.

The results of these calculations are as follows (for $\nu = 0.3$):

Table 1 Edge displacements and rotations due to pressure

		Method (i)	Method (ii)	Method (iii)
$\phi = 90°$	$EV \div 10^3$	0	0	−607.6
	$E\delta \div 10^3$	−6,532	−6,532	−4,085
$\phi = 30°$	$EV \div 10^3$	0	−8,839	−1,136
	$E\delta \div 10^3$	−24,240	−24,240	−17,255

Discussion of Results

It can be seen from the above tabulation that the numerical integration results (method (iii)) for the horizontal displacement δ are only 60 per cent of those given by the two approximate methods. The edge rotation V obtained by numerical integration is much less than the membrane rotation (method (ii)) at $\phi = 30$ deg; it is also much more uniform over the whole of the torus than the membrane rotation.

Since the numerical values of the edge displacements and rotations due to pressure affect the edge moments and shears at places where the toroidal shell joins the other types of shell in a structure, it can be seen that the three methods will give different results for the final elastic stress distribution in the torus. An example of this (where the torus is used as a portion of a torispherical shell) is given in a recent paper by the author.[3] In that case, approximation (a) gave a maximum meridional bending stress ($\sigma_\phi{}^b$) which was 25 per cent too high, and the maximum circumferential direct stress ($\sigma_\theta{}^d$) was overestimated by 10 per cent. Approximation (b) overestimated the maximum $\sigma_\phi{}^b$-stress by a factor of two, but correctly estimated the $\sigma_\theta{}^d$-stress. However, the stress distributions for both approximations were significantly different from the numerical integration results.

It has also been brought to the author's attention, by one of the reviewers, that the membrane stress resultants do not give an adequate representation of the deformations even when the cross section of the shell is a complete circle. This point is discussed by Dean.[4]

A Comparison of Methods for Analyzing Bending Effects in Toroidal Shells

By G. D. GALLETLY,[1] EMERYVILLE, CALIF.

An accurate estimate of the effects of bending loads acting on toroidal shells is, at the present time, a time-consuming problem for the designer. He is, in consequence, interested in the accuracy with which the faster approximate methods can furnish him with the information he requires.

The author recently had occasion to utilize two approximate methods in the bending analysis of a toroidal shell of revolution as well as an exact method. The purpose of this note is to present the results of these analyses in so far as they pertain to the calculation of the edge displacements and rotations.

Methods Used in the Problem

The three methods used to analyze the toroidal shell were: (a) Numerical integration of the classical differential equations on an electronic digital computer; (b) the asymptotic integration method of Clark;[2] and (c) the Geckeler-type solution recently described by Horvay, Linkous, and Born.[3]

Brief descriptions of these three methods follow:

The differential equation used in the numerical integration method was either of the complex conjugate equations given in Timoshenko.[4] This equation can be separated into two simultaneous ordinary differential equations in the real variables x and y by substituting $U = x + iy$ (U is proportional to the transverse shearing force). The linearly independent solutions of these equa-

[3] G. D. Galletly, "Torispherical Shells—A Caution to Designers," ASME Paper No. 58—PET-3.

[4] W. R. Dean, "The Distortion of a Curved Tube Due to Internal Pressure," *Philosophical Magazine*, vol. 28, 1939, p. 452.

[1] Shell Development Company, Emeryville Research Center.

[2] R. A. Clark, "On the Theory of Thin Elastic Toroidal Shells," *Journal of Mathematics and Physics*, vol. 29, 1950, pp. 146–178.

[3] G. Horvay, C. Linkous, and J. S. Born, "Analysis of Short Thin Axisymmetrical Shells Under Axisymmetric Edge Loading," Journal of Applied Mechanics, vol. 23, Trans. ASME, vol. 78, 1956, p. 68.

[4] S. Timoshenko, "Theory of Plates and Shells," McGraw-Hill Book Company, Inc., New York, N. Y., 1940, see Equation 267, page 458.

Manuscript received by ASME Applied Mechanics Division, November 20, 1957.

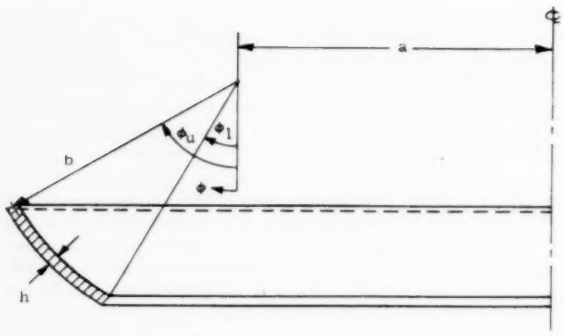

Fig. 1 Half section through toroidal shell used as an illustrative example

tions were then obtained on a digital computer using a step length of $^1/_2$ degree and the Runge-Kutta integration scheme.

Clark[2] shows that the modified Hankel functions of order one-third are very good approximations to the exact solutions if $h/b \ll 1$ and if $[12(1 - \nu^2)]^{1/2}\, b^2/ah$ is large (see Fig. 1 for notation). Both of these requirements are satisfied in the numerical example considered herein. The Hankel functions used in this method are tabulated[5] and Clark gives a table for evaluating an integral which appears in his method. This integral is

$$\omega(\phi, \lambda) = \int_0^{\phi} \left(\frac{\sin \phi}{1 + \lambda \sin \phi} \right)^{1/2} d\phi \qquad (1)$$

where

$$\lambda = \frac{b}{a}$$

By considering the bending of a tapered curved beam on an elastic foundation, Horvay, et al.[3] derived an approximate equation for short, thin, axisymmetrical shells under axisymmetrical edge loading. After some manipulation this equation can be solved in terms of exponential and trigonometric functions. For toroidal shells of constant thickness, the integral defined by equation (1) is also required in this method. The authors state that in using the method the angle ϕ should be such that $\pi/6 < \phi < 5\pi/6$, and for completely dependable results it should be within the range $\pi/4 < \phi < 3\pi/4$. The horizontal radius of the shell middle surface r should vary slowly with distance along the shell surface and h/r should be small. The example considered in the next section satisfies all of these requirements, except that the lower value of ϕ is less than $\pi/4$. It is, however, greater than $\pi/6$.

[5] "Modified Hankel Functions of Order One-Third," Annals of Harvard Computation Laboratory, vol. II, 1945.

Numerical Example

The toroidal shell considered had the following geometric characteristics:

$b = 34.625$ in. $\quad a = 230$ in. $\quad h = 1.25$ in.

$\phi_u = 73°$ $\quad \phi_l = 36°10'$

The bending loads considered in the problem were unit edge moments and unit horizontal forces applied to the lower and upper edges of the shell.

The results obtained by the three methods for the edge horizontal displacements δ and edge rotations V are tabulated hereunder.

Discussion of Results

From the results given in Table 1, and selecting the numerical integration results as the criterion of accuracy, the percentage errors of the approximate methods can be determined. It will be found that the maximum error in Clark's method is slightly less than -4 per cent while that in the HLB is $+15$ per cent. The sign of the error is negative for all the coefficients in Clark's method, but errors of both signs occur in the HLB method.

The method of Clark can thus be considered as being very good. The HLB method is certainly adequate for design purposes, especially as the 15 per cent error occurred at the lower angle of ϕ for which $\pi/6 < \phi < \pi/4$.

The HLB method is much faster than that of Clark in so far as the edge influence coefficient calculation is concerned. This is because no matrix inversion is necessary and little interpolation in tables is required. However, it should be remembered that the designer's problem does not end with the calculation of the edge influence coefficients. He is also concerned with the stress distribution throughout the shell. He would therefore like to have available the influence coefficients for the stress resultants at a few points in the interior of the shell. When this factor is taken into account, the HLB method loses much of its advantage over the Clark method.

Table 1 Edge influence coefficients obtained by the three methods

Edge Loading Condition	ϕ	$E\delta$ Num. int.	$E\delta$ Clark	$E\delta$ HLB[a]	EV Num. int.	EV Clark	EV HLB[a]
Unit moment at $\phi = 73°$	73°	1007	990	965	−134.2	−132.5	−129
	36°10′	−695.7	−680	−685	−77.99	−76.2	−82.7
Unit inward horizontal force at $\phi = 73°$	73°	−11545	−11400	−11530	1007	987	964
	36°10′	4554	4375	4600	830.1	811	893
Unit moment at $\phi = 36°10'$	73°	−792.4	−776	−853	73.95	72.6	79.0
	36°10′	834.3	820	919	138.7	137.6	160
Unit outward horizontal force at $\phi = 36°10'$	73°	−4343	−4180	−4390	664.0	646	655
	36°10′	8657	8530	8430	834.5	818	920

[a] HLB = Horvay, Linkous, and Born (footnote 3).

Effect of Magnetic Field on Forced Convection Heat Transfer in a Parallel Plate Channel

By ROBERT SIEGEL,[1] CLEVELAND, OHIO

The fully developed laminar flow of a conducting liquid between two parallel plates under the influence of a transverse magnetic field has been studied by Hartmann and Lazarus.[2] Their analytical and experimental results are conveniently summarized by Cowling.[3] It is shown in these references that the retarding force due to the fluid crossing the magnetic field lines causes the laminar velocity distribution to be more uniform across the channel, similar to that for turbulent flow without a magnetic field. If heat is being transferred, the relatively higher velocities near the wall would be expected to reduce the difference between the wall temperature and the mean fluid temperature. The temperature distribution within the fluid is also influenced by an internal heat source resulting from a current flow due to the fluid motion in the magnetic field. It is the purpose of the present paper to examine quantitatively the effect of a magnetic field on the fully developed convective heat transfer in a parallel plate channel for uniform wall heat flux.

Analysis

The configuration of the system is shown in Fig. 1. Fluid flows with a velocity v in the x-direction. At the solid boundaries

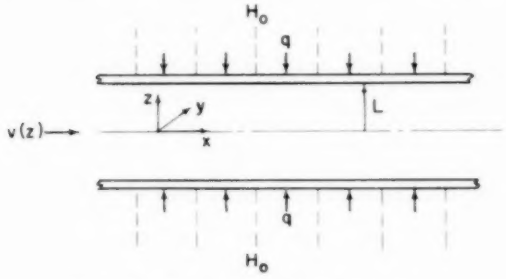

Fig. 1 Physical model and co-ordinate system

($z = \pm L$) a uniform transverse magnetic field H_0 and a uniform heat flux q are imposed. The energy equation for this situation can be written as

$$v \frac{\partial t}{\partial x} = \alpha \frac{\partial^2 t}{\partial z^2} + \frac{Q}{\rho c_p} \tag{1}$$

where α is the thermal diffusivity, ρ the fluid density, c_p the specific heat, Q the internal heat generation per unit volume, and t the fluid temperature. It has been assumed that fluid properties are constant and that viscous dissipation is negligible compared with transverse heat conduction.

The velocity v is given by Cowling as

$$v = \frac{PM}{\mu^2 \sigma H_0^2} \left[\frac{\cosh M - \cosh (Mz/L)}{\sinh M} \right] \tag{2}$$

where $M = \mu H_0 L (\sigma/\nu\rho)^{1/2}$ is a parameter which is a measure of the ratio of magnetic viscous force to ordinary viscous force. μ is the permeability, σ the electrical conductivity, and ν the kinematic viscosity of the fluid. The pressure gradient along the channel, $-\partial p/\partial x \equiv P$, can be eliminated during the analysis by introducing the integrated mean fluid velocity V,

$$V = \frac{P}{\mu^2 \sigma H_0^2} (M \coth M - 1) \tag{3}$$

The internal heat source is given by the electrical dissipation,

$$Q = j^2/\sigma \tag{4}$$

where j is the current density generated within the fluid. This current can be found from the relation $4\pi j = \partial H_x/\partial z$ where H_x is the x component of the magnetic field within the fluid. Using the results in Cowling we obtain

$$j = \frac{P}{\mu H_0} \left[\frac{M \cosh (Mz/L)}{\sinh M} - 1 \right] \tag{5}$$

If we combine Equations (2), (3), (4), and (5), and use the definition for M, Equation (1) can be put in the form

$$V \frac{[M \cosh M - M \cosh (Mz/L)]}{M \cosh M - \sinh M} \frac{\partial t}{\partial x} = \alpha \frac{\partial^2 t}{\partial z^2} + \frac{P^2 L^2}{\rho^2 c_p \nu} \left[\frac{\cosh (Mz/L)}{\sinh M} - \frac{1}{M} \right]^2 \tag{6}$$

The fully developed heat-transfer condition for a uniform wall heat flux and internal heat source independent of x is characterized by the fact that the temperature profile is similar in shape for all x and the temperature values rise in a linear fashion in the longitudinal direction. Thus a solution can be assumed of the form

$$t = Ax + G(z) \tag{7}$$

A is the temperature gradient $\partial t/\partial x$ (a constant), which in the fully developed situation is also equal to the gradient in mean temperature $\partial t_m/\partial x$. If Equation (7) is inserted into Equation (6) a second-order ordinary differential equation for G is obtained. This can be integrated twice subject to the boundary conditions

$$\left.\begin{aligned} \frac{dG}{dz} &= 0 \quad \text{at} \quad z = 0 \\ G &= 0 \quad \text{at} \quad z = \pm L \end{aligned}\right\} \tag{8}$$

where the zero in the second condition is selected arbitrarily. The result for G is

[1] Aeronautical Research Scientist, NACA Lewis Flight Propulsion Laboratory.

[2] J. Hartmann and F. Lazarus, *Kgl. Danske Videnskab. Selskab, Mat.-fys. Medd.* 15, nos. 6 and 7, 1937.

[3] T. G. Cowling, "Magnetohydrodynamics," Interscience Publishers, Inc., New York, 1957, pp. 13–17.

Manuscript received by ASME Applied Mechanics Division, February 10, 1958.

$$G = \frac{AVL^2M}{\alpha} \frac{\frac{1}{2}\left(\frac{z}{L}\right)^2 \cosh M - \frac{1}{M^2}\cosh (Mz/L) - \frac{1}{2M^2}(M^2 - 2)\cosh M}{M \cosh M - \sinh M} - \frac{P^2L^4}{\alpha\rho^2c_p\nu}\frac{1}{M^2}\left\{\frac{1}{2\sinh^2 M}\left[\frac{1}{4}\cosh (2Mz/L) + \frac{M^2}{2}\left(\frac{z}{L}\right)^2 - \frac{\cosh 2M}{4} - \frac{M^2}{2}\right] - \frac{2\cosh (Mz/L)}{M\sinh M} + \frac{2\cosh M}{M\sinh M} + \frac{1}{2}\left(\frac{z}{L}\right)^2 - \frac{1}{2}\right\} \quad (9)$$

A is found by considering the over-all heat balance for a differential length of channel, which gives

$$A = \frac{\partial t}{\partial x} = \frac{\partial t_m}{\partial x} = \frac{q + \int_0^L \frac{j^2}{\sigma}\,dz}{LV\rho c_p} \quad (10a)$$

Inserting j from Equation (5) and integrating, we find

$$A = \frac{q + \frac{P^2L^2}{\rho\nu}\left[\frac{1}{2M\sinh^2 M}\left(\frac{\sinh 2M}{2} + M\right) - \frac{1}{M^2}\right]}{LV\rho c_p} \quad (10b)$$

It is usually of most practical interest to be able to determine the wall temperature when the mean temperature of the fluid is known. To accomplish this we form the difference

$$t_w - t_m = Ax - \frac{1}{2LV}\int_{-L}^{L} tv\,dz \quad (11)$$

The integral can be evaluated using v from Equation (2) and t from Equation (7) with G and A from Equations (9) and (10b). After considerable rearrangement we have

$$t_w - t_m = \frac{qL}{k}\Phi(M) + \frac{(\mathrm{RePr})^2\nu\alpha}{8L^2c_p}\chi(M) \quad (12)$$

where

$$\Phi(M) = \frac{\left(\frac{2}{3}M^2 - 4\right)\cosh^2 M + \frac{5}{M}\cosh M \sinh M - 1}{2(M\cosh M - \sinh M)^2} \quad (12a)$$

and

$$\chi(M) = \frac{M^2}{(M\coth M - 1)^4}\left[\left(\frac{5}{4} - \frac{3}{M^2}\right)\coth M - \left(\frac{7}{4M} + \frac{19M}{12}\right)\coth^2 M + \left(\frac{M^2}{3} + \frac{5}{2}\right)\coth^3 M - \frac{M}{4}\coth^4 M + \left(2 + \frac{M^2}{3}\right)\frac{\coth M}{\sinh^2 M} - M\frac{\coth^2 M}{\sinh^2 M} - \frac{M}{2\sinh^4 M} - \frac{1}{3M} + \frac{2}{M^3}\right] \quad (12b)$$

Re is the Reynolds number, $V2L/\nu$, and Pr is the Prandtl number, $c_p\nu\rho/k$. The mean temperature at a particular x-position can be obtained by integrating Equation (10b) from the channel entrance to the location under consideration. After eliminating P with Equation (3), this yields

$$t_m - t_0 = \frac{2x}{\mathrm{RePr}}\left\{\frac{q}{k} + \frac{(\mathrm{RePr})^2\nu\alpha}{4L^2c_p}\frac{M^4}{(M\coth M - 1)^2}\left[\frac{1}{2M\sinh^2 M}\left(\frac{\sinh 2M}{2} + M\right) - \frac{1}{M^2}\right]\right\} \quad (13)$$

where t_0 is the mean temperature entering the channel. Equations (12a) and (12b) are most difficult to evaluate numerically when M is small, so, for convenience, $\Phi(M)$ and $\chi(M)$ have been plotted on Fig. 2 for M from 0 to 10.

We can compare the temperature difference, $t_w - t_m$, with that for heat transfer with no magnetic field, $(t_w - t_m)_{M=0} = 17\,qL/35\,k$, by forming the ratio

$$\frac{t_w - t_m}{(t_w - t_m)_{M=0}} = \frac{35}{17}\left[\Phi(M) + \frac{k}{qL}\frac{(\mathrm{RePr})^2\nu\alpha}{8L^2c_p}\chi(M)\right] \quad (14)$$

This ratio has no meaning when $q = 0$ because in this instance $(t_w - t_m)_{M=0}$ is zero while $(t_w - t_m)$ remains finite due to the internal heat generation resulting from imposing the magnetic field. With q sufficiently large, the second term on the right side of Equation (14) will generally be small, especially in the case of low Prandtl number liquid metals. In this case the ratio becomes approximately $35\,\Phi(M)/17$, which gives, for example, a 20 per cent reduction in temperature difference for $M = 10$.

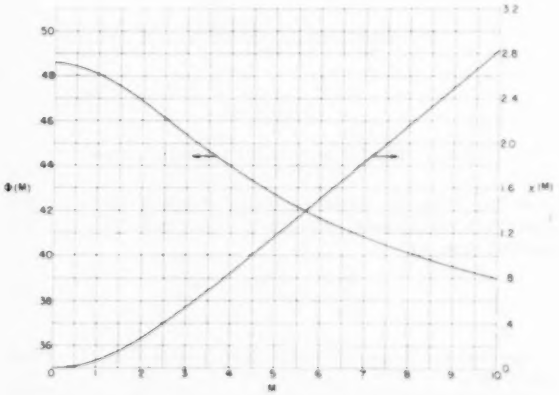

Fig. 2 Functions needed to calculate $t_w - t_m$

Discussion

Symmetrical Buckling of a Series of Uniformly Loaded Parallel Struts Supported by Spot Connections to a Long Thin Plate[1]

S. Sergev.[2] This is an interesting paper and definitely a contribution to the art. To one who may use the results of this paper, words of caution seem in order. First of all, the system shown in Fig. 1 is not an integral panel but two separate systems. The struts constitute one system and the plate another. The loaded members are the struts with the plate acting as an elastic support.

Equation [1] of the paper implies lateral loading on the plate. This precludes spot welding, riveting, or bolting the struts to the plate, because fastenings of this kind would introduce shear forces between struts and plate and change the deflection characteristics of the plate. A plate under sufficiently large compressive forces may exhibit no lateral resistance to displacement, i.e., the "spring constant" of the plate may vanish. Consequently, it would be more desirable to think of the spot connections as long links so that displacements of the struts in the y-direction are independent of the plate.

Equation [3] obviously needs resetting. With reference to Equation [21], the authors state that the left-hand side is zero when $\mu = 0$. This seems to be incorrect; anyway, μ should start with $\pi/2$. Further, it is stated that μ varies between $\pi/2$ and 4.493, the latter being "the first critical load for a strut held freely at each end and clamped at its mid-point." It appears that π is a possible solution consistent with the link connectors.

Lastly, referring to Fig. 3, it follows that when k is large the flexural rigidity of the strut is large compared to the rigidity of the plate, and the reverse. So that to obtain the buckling load for the strut when k is large, $\mu = \pi/2$, giving Euler load. The deduction here is that no matter how many fastenings there are between strut and plate, the plate is relatively too flexible to restrain the strut. At the other extreme, the plate is very stiff compared to the strut, or, what is the same, k is small. Now the number of fastenings between strut and plate must be considered, and for the lowest curve in Fig. 3, it appears $\mu = \pi$ is the conservative value and not 4.493. The former implies double-reverse and the latter triple-reverse curves for the strut axis. The buckling load on the strut with $\mu = \pi$ is about one half of the buckling load with $\mu = 4.493$. Consequently, $\mu = \pi$ should be used unless the connection at mid-length of the strut is such that zero slope can be assured. Similar argument may apply to the other curves in Fig. 3.

C. J. Thorne[3] **and H. J. Fletcher.**[3] This paper is interesting and important. The conclusions about number of rivets or spot connections should be useful. The finite sine transform is not natural to the problem but the boundary conditions are natural to the finite-cosine transform as follows:

Write Equation [1] as

$$\frac{\partial^4 w}{\partial x^4} + \frac{2\partial^4 w}{\partial x^2 \partial y^2} + \frac{\partial^4 w}{\partial y^4} = 0$$

Replace boundary condition (ii) by

$$2R(y) = D\left[\frac{\partial^3 w}{\partial x^3} + (2 - \nu)\frac{\partial^3 w}{\partial x \partial y^2}\right] \quad \text{at } x = 0$$

Define the cosine transform

$$a_n(y) = Cw(x, y) = \int_0^a w(x, y) \cos P_n x dx \quad P_n = \frac{2n\pi}{a}$$

Transforming the differential equation we obtain

$$P^4 a_n - 2P^2 a_n'' + a_n'''' = \frac{4R(y)}{D}$$

which is Equation [3]. After solving for a_n, the inverse is the series given by Equation [2]. If we had used $P_n = n\pi/a$, the transformed equation would be

$$P^4 a_n - 2P^2 a_n'' + a'''' = \frac{2R(y)}{D}\,[1 + (-1)^n]$$

This implies $a_n = 0$ if n is odd. Replacing n by $2n$ gives the same result as before.

We wish to call attention to the fact that convergence of order $1/n^3$ will only allow differentiation term by term in the open region twice. Following Stokes, as noted by the writers,[4] "proper" differentiation allows determination of derivatives of any order from values at the boundary points, if they exist. This, for example, verifies Equation [3] from Equation [2].

Author's Closure

The authors would like to thank Professor Sergev for his comments and agree that it is important to examine critically the effect of the neglect of shear forces at the connections between the plate and the struts. The neglect of shear forces does not necessarily preclude the use of riveted or bolted connections since, if the shortening of the strut under the axial load is sufficiently small, then a bolt or rivet in a slightly larger hole would provide a sliding connection that would not transmit shear. It would certainly be useful, however, to investigate the effect of shear forces upon the buckling load.

In the original paper the statement that the left-hand side of Equation [21] is zero when $\mu = 0$ should be corrected to read that the left-hand side of Equation [21] has a value of $-1/3$ when $\mu = 0$. The subsequent conclusions are not affected. As noted by Professor Sergev, his statement that μ cannot exceed π does not apply if the connection at the mid-point of the strut is such as to insure a zero slope. As implied by the title of the paper, it was supposed throughout that only symmetrical buckling could occur. The case of antisymmetrical buckling is perhaps of greater importance and could be considered in a similar manner.

The authors are grateful to Drs. Thorne and Fletcher for their interest in providing an alternative derivation of Equation [3].

---

[1] By J. L. Cutcliffe and H. S. Heaps, published in the December, 1957, issue of the JOURNAL OF APPLIED MECHANICS, TRANS. ASME, vol. 79, pp. 531–536.

[2] Professor of Engineering Mechanics, Department of Civil Engineering, University of Washington, Seattle, Wash.

[3] Code 5071, U. S. Naval Ordnance Test Station, China Lake, Calif.

[4] "Bending of Thin Rectangular Plates," by H. J. Fletcher and C. J. Thorne, Proceedings of the Second U. S. National Congress of Applied Mechanics, June 14–18, 1954.

Behavior of Cylinders With Initial Shell Deflection[1]

S. Kendrick.[2] The difference in the collapse pressures of internally and externally framed cylinders of nominally identical scantlings has only been recognized in the past 3 years and this paper is, to the writer's knowledge, the first one published in the open literature which draws attention to the fact and attempts an explanation. Several other possible explanations of this difference in strength have been suggested previously. These include, for example, the greater tendency to trip sideways of internal frames and the enhanced importance of bending stresses due to out-of-circularity with internal frames. An assessment of the relative importance of these weaknesses is very difficult since little is really understood of the mechanism of plating collapse of ring-stiffened cylinders. Most workers in the field would probably agree, however, that the initial accordion deflections due to welding, considered in this paper, are likely to be the main influencing factor.

While agreeing that these initial deflections are important on model scale, the writer cannot agree with the estimate of their importance given in this paper. A much more important phenomenon associated with axisymmetric weld distortion exists than the additional stresses under applied pressure. This is the initially stressed state which must exist to maintain the initial accordion deflection.

The additional stresses evaluated in this paper are mainly due to the exaggeration or diminution of the initial accordion deflection on applying pressure. This exaggeration in the case of an internally framed cylinder, of the dimensions chosen in the paper, is only about 15 per cent at the maximum pressure evaluated. It may be assumed, therefore, that the additional stresses evaluated by the authors are only about 15 per cent of the stresses set up by the welding producing the initial accordion deflection. The latter are by far the more important and at mid-bay are of the same sign as those evaluated in their paper.

To make this point clearer, the writer has evaluated the stresses set up by rotating the plating at the frames through an angle sufficient to cause an accordion deflection, relative to the frames at mid-bay, equal to 0.1 times the plating thickness t. The angular rotation necessary for the numerical example of the paper was 0.024 radian, and the deflection at the frames and mid-bay relative to the undeformed surface were $-0.0448t$ and $0.0552t$, respectively. The maximum circumferential stresses in the plating caused by this rotation are 32,200 psi and 24,100 psi at the frame and mid-bay, respectively. The maximum longitudinal stresses in the plating are 62,200 psi and 25,400 psi at the frame and mid-bay, respectively. The circumferential stress in the frame is 15,400 psi.

These stresses are very much greater than those evaluated in the paper and illustrate the unimportance of the latter. Applying the Hencky-von Mises criterion at the outer surface mid-bay with these initial stresses included would lead to collapse pressures far lower than are observed experimentally. This is not surprising since collapse need not occur at the onset of yielding and collapse estimates based on elastic analysis are at best semiempirical.

The initial stresses due to welding of the frames can be large on small-diameter cylinders, but usually even larger initial stresses are present due to cold-rolling the shell plating to the radius required. In many cases the sum of the various initial stresses which can be calculated is nearly equal to or even greater than the yield stress before any pressure is applied. There are good reasons for believing that these initial stresses, even when approaching yield-stress values, influence the collapse pressure by less than 20 per cent probably due to their forming a self-equilibrating system. One possible way of estimating their importance in plating collapse is to estimate their effect on the average circumferential stress in the plating. In the foregoing numerical example the mean initial circumferential stress in the plating is equal to $^1/_2$ of that in the frame (since $A/Lt = 0.5$); i.e., 7700 psi. The pressure required to produce this mean stress is 285 psi and it may be reasonable to assume that the collapse pressure is affected by this amount. This might be expected to be an underestimate of the effect on collapse pressure since the stresses at points farthest from the frames are appreciably higher than the mean stress, and the additional mean stress produced by the external pressure has been ignored. The collapse-pressure difference between internally and externally framed models of these scantlings and this degree of weld distortion would be 570 psi on this assumption. This is much higher than would be expected in practice so that even using the mean stress in the plating seems to overestimate the importance of initial stresses.

L. B. Wilson.[3] The authors have presented a very interesting paper and the reason suggested for externally framed circular cylindrical shells collapsing in general at higher pressures than similar internally framed shells is most valuable. This question has long been a matter of speculation and has been attributed to the better circularity obtainable in externally framed shells.

There are four points which the writer would like to raise in this discussion:

1 The magnitude of the maximum initial accordion deflection measured by the authors is stated to be between $^1/_8$ and $^1/_{10}$ of the plating thickness. These results could be misleading without further amplification of the size of the cylindrical shells on which these measurements were taken. Since these initial deflections are mainly due to welding they are more significant in small shells where the effect of welding is unavoidably more important. For example, in a submarine hull of typical scantlings the effect of the initial accordion deflection is probably insignificant, but it cannot be neglected in a $^1/_4$-scale or $^1/_8$-scale model. At the Naval Construction Research Establishment measurements on models indicate that the maximum initial accordion deflection is less than $^1/_{10}$ of the plating thickness for models of about $4^1/_2$–5 ft diam and scantlings similar to the example quoted in this paper. However, if smaller models of 2–3 ft diam were used, initial accordion deflections of $^1/_{10}$ to $^1/_6$ of the plating thickness are quite feasible. There is the additional point that in externally framed cylinders the welds are in tension and often tend to be made larger than in internally framed cylinders, and thus the initial accordion deflection may well be greater in externally framed shells.

2 An alternative method to that of Salerno and Pulos has been derived by the writer for solving the differential equation (Equation [7] of the paper). This method seems to have several advantages particularly when the initial accordion deflection is included.

The notation of the paper will be used for the present method, but it is convenient to measure x from midway between two frames instead of at the frame. Two forms of the initial accordion deflection are considered:

$$(a) \qquad w_i = \Delta\left(1 - \frac{4x^2}{L^2}\right) \ldots\ldots\ldots\ldots [1]$$

[1] By M. E. Lunchick and R. D. Short, Jr., published in the December, 1957, issue of the JOURNAL OF APPLIED MECHANICS, TRANS. ASME, vol. 79, pp. 559–564.

[2] Naval Construction Research Establishment, St. Leonard's Hill, Dunfermline, Scotland.

[3] Scientific Officer, Naval Construction Research Establishment, Dunfermline, Scotland.

the parabolic shape taken by the authors, and

$$(b) \qquad w_i = \frac{\Delta}{2}\left(1 + \cos\frac{2\pi x}{L}\right) \ldots\ldots\ldots [2]$$

The latter shape gives neat results for the deflections and stresses.

The differential equation and boundary conditions which are used in the paper are also used in the present analysis. Assume the solution of the differential equation as a Fourier series, then from the boundary conditions the series must be an even function; i.e., a cosine series only. The coefficients of this cosine series can be obtained by using the finite cosine transform together with the boundary conditions. The details will be omitted and only the solution given, which for the initial accordion deflection considered in Equation [1], herewith, is

$$w = \frac{\tau}{\gamma} - \left(\frac{\lambda w_f}{\pi} - \frac{2b\tau}{L}\right)\left\{\frac{1}{2\gamma} + \sum_{n=1}^{\infty}\frac{(-1)^n \cos(2n\pi x/L)}{n^4 - Kn^2 + \gamma}\right\} - \frac{4K\Delta}{\pi^2}\sum_{n=1}^{\infty}\frac{(-1)^n \cos(2n\pi x/L)}{n^4 - Kn^2 + \gamma} \ldots\ldots [3]$$

The solution when the initial accordion deflection is given by Equation [2] is

$$w = \frac{\tau}{\gamma} - \left(\frac{\lambda w_f}{\pi} - \frac{2b\tau}{L}\right)\left\{\frac{1}{2\gamma} + \sum_{n=1}^{\infty}\frac{(-1)^n \cos(2n\pi x/L)}{n^4 - Kn^2 + \gamma}\right\} + \frac{K\Delta\cos(2\pi x/L)}{2(1 - K + \gamma)} \ldots\ldots [4]$$

where

$$K = \frac{pR}{2D}\left(\frac{L}{2\pi}\right)^2$$

$$\gamma = \frac{Et}{DR^2}\left(\frac{L}{2\pi}\right)^4$$

$$\tau = \frac{p}{D}\left(1 - \frac{\mu}{2}\right)\left(\frac{L}{2\pi}\right)^4$$

$$\lambda = \frac{E(A + bt)}{DR^2}\left(\frac{L}{2\pi}\right)^2$$

and w_f is the deflection at the frame and is obtained by putting $x = L/2$ in Equations [3] and [4]. For most practical cases only a few terms in the cosine series need to be taken. The stresses and strains calculated using Equation [3] agree with those given in the paper. However, there are small differences in the longitudinal stresses and strains when Equation [4] is used, owing to the difference in shape of the initial accordion deflections.

3 The authors state that the initial accordion deflection will have more significance for those circular cylindrical shells which fail in an axisymmetric manner. Such failure tends to occur in more closely framed cylinders; that is, when the lowest shell-buckling pressure (p_m) is more than about three times the pressure at which yielding would be initiated (p_y). However, experimental evidence seems to show that the greatest differences between the collapse pressures of externally and internally framed cylinders occur in the range of p_m/p_y of 1 to 2, and as this ratio increases the differences between the two types of framing decreases.

4 Two possible practical methods are suggested to strengthen internally framed shells by removing the initial accordion deflection. The first method is to weld on the outside of the plating at the frames; this will counterbalance the welding on the inside of the plating and tend to draw the cylinder back to its original shape. The second method is to put a large internal pressure on the cylinder.

Authors' Closure

It was gratifying to read the comments of Messrs. Kendrick and Wilson of our British counterpart laboratory, as the points raised were so much in tune with our own thinking. To answer Mr. Kendrick first, we can say that we performed calculations for the collapse pressure of several internally framed cylinders taking into account three factors: initial deflection, residual stresses accompanying this deflection, and the plastic reserve strength between the inception of yielding and final collapse. The results were considered beyond the scope of the present paper and will be presented at a later date. The procedure, based on an elastic-plastic analysis, for determining the plastic reserve strength will be published shortly in the Proceedings of the Third U S. National Congress of Applied Mechanics.

We have an experimental program for studying residual stresses. We have tested two externally framed cylinders of identical geometry, one manufactured by machining the frames integral to the shell and then stress relieving, and the second fabricated by rolling flat plates to cylindrical form and welding frames to the shell. Collapse in both cases was by yielding, and the results indicated the welded cylinder to be slightly stronger than the stress-free machined cylinder. (In a similar study where failure was by shell buckling, the residual stresses were found to substantially lower the collapse pressure.) The influence of initial deflection for an externally framed welded cylinder approaches that of the perfect cylinder as in reality the deflection varies over the cylinder so that values close to zero are present. Thus for this study the influences of initial deflection and the associated residual stresses were negligible. The rolling residual stresses were present, however, but had no detrimental influence, as Mr. Kendrick has mentioned. The results of this investigation will be published soon as a David Taylor Model Basin report.

The authors must admit that the relative importance of initial deflection, as compared to the associated residual stresses, has yet to be established and ultimately will have to be resolved by a properly designed test program. We believe, however, that in many instances of internally framed cylinders the solution will not be complete unless the initial deflection is taken into account. Before concluding the discussion on residual stresses we would like to make one comment. When taking into account the residual stresses, only the circumferential membrane stresses should be used. The residual bending stresses, due to initial deflection, are self-equilibrating through the shell thickness and, like the rolling stresses, should not affect the collapse pressure. This follows from the "lower bound theorem" of limit design.

We will now comment on the four points raised by Mr. Wilson. We agree on the first point and have noted in one of our submarine reports that the size of weld in prototype would be relatively smaller than for the model of the pressure hull; hence the reduction in strength due to initial deflection for the prototype would be less than for the model.

On Mr. Wilson's second point, we can say that we obtained a solution with a shape of initial deflection as follows:

$$w_i = \Delta \sin\frac{\pi x}{L}$$

where the origin of x is at a frame. We did not assume the solution of the differential equation as a Fourier series but solved the differential equation explicitly to obtain a solution in terms of trigonometric and hyperbolic functions. Like Mr. Wilson, we compared the strains at mid-bay with those obtained by the parabolic form of initial deflection. Noting little difference, we presented the solution based on the parabolic form, as it was simpler.

On the third point, we believe that certainly in the range $p_m/p_y > 3$ the initial accordion deflection is much more important

than shell out-of-roundness. In the range $1 < p_m/p_y < 2$ we have obtained evidence that shell buckling can occur prematurely for internally framed cylinders when buckling is in the plastic range. We found the buckle lobes to be triggered by yielding of the shell induced prematurely by an initial deflection.

On the fourth point, the means cited for counteracting the detrimental influence of initial deflection have considerable merit. Preliminary experiments have been performed at the Model Basin using high internal pressure to plastically deform a cylinder to give favorable outward initial deflections. Results have indicated appreciable increases in strength (above 10 per cent).

In conclusion, we should like to add that a series of cylinders are now being tested, especially designed to study the influence of initial deflection. We expect to confirm the elastic deformations given by the theory and prove conclusively the existence of a difference in strength between internally framed and externally framed welded cylinders

Buckling of Rectangular Plates With Two Unsupported Edges[1]

C. J. Thorne.[2] It seems desirable to call attention to the solution to this problem[3] and most of those in the author's previous paper referred to. The buckling condition was not graphed, but deflections and derivatives were plotted and special stability problems discussed in illustrative examples. This solution was for edge thrust and normal loads.

Author's Closure

The author wishes to thank Professor C. J. Thorne for calling attention to the paper[3] in which, as it seems to him, the solution to this problem[1] and the solutions to problems considered in my previous papers were discussed.

After studying this paper,[3] however, I did not find the solutions to my problems nor could I derive them from the solutions considered there. This is because an unfortunate mistake has been made in the basic boundary conditions. The boundary condition (8) on p. 4 is erroneous. The authors have used boundary conditions derived by Kirchhoff from energy considerations for a plate loaded by a lateral load only. If in addition to the lateral load there are forces acting in the middle plane of the plate, as in the paper,[3] the boundary condition (8) for unsupported edge should be written in the form:

$$\frac{\partial^3 w(x, b)}{\partial y^3} + (2 - \nu)\frac{\partial^3 w(x, b)}{\partial x^2 \partial y} - \frac{N_y}{D}\frac{\partial w(x, b)}{\partial y} - \frac{N_{xy}}{D}\frac{\partial w(x, b)}{\partial x} = f_6(x) \quad \ldots\ldots(1)$$

This boundary condition was first given in my degree thesis in 1936 and later was used in several of my papers[4–10] and in papers by other authors.[11] Due to the error in the boundary condition (8) the solutions of cases III, V, and VI are wrong. Cases I, II, and IV, the solutions of which are correct, have no relation to my problems. I could not expect Professor Thorne to have seen my papers in Ukrainian and Russian[4–7] before the publication of his 1952 paper.[3] It is unfortunate, however, that he had not noted that the boundary condition for an unsupported edge as put forward in my papers in English[8,9] is different from that given in his paper[3] before his contribution to this discussion had been made.

[1] By P. Shuleshko, published in the December, 1957, issue of the JOURNAL OF APPLIED MECHANICS, TRANS. ASME, vol. 79, p. 537.

[2] Code 5071, U.S. Naval Ordnance Test Station, China Lake, Calif.

[3] "Thin Plates Under Combined Loads, I," by F. E. Maud and C. J. Thorne, Studies in Applied Mathematics, No. 7, University of Utah, April 18, 1952

References

4 P. Shuleshko, "On the Theory of Elastic Stability of Anisotropic and Nonhomogeneous Plates With Variable Thickness," *Bull. Industr. Acad. Kharkiw, Ukraine*, no. 1–2, 1940, pp. 128–144.

5 P. Shuleshko, "One Case of the Stability of a Thin Plate in Compression," *Journal of Engineers*, Moskow, 1941.

6 P. Shuleshko, "On Stability of Thin Elastic Anisotropic Plates of Variable Rigidity," *Appl. Math. and Mech., Leningrad*, vol. 6, no. 2–3, pp. 139–150. (Engineering Societies Library, New York, has this magazine.)

7 P. Shuleshko, "Stability of Thin Plates Which Have Part of the Contour Unsupported," Scientific Memoirs of the Ukrainian Technical University, Germany, vol. IV, 1948, pp. 139–174. (The Ukrainian Technical Institute, New York, has this magazine.)

8 P. Shuleshko, "Buckling of Rectangular Plates Uniformly Compressed in the Vertical Directions With Upper Edge Free," *The Journal of the Institution of Engineers, Australia*, vol. 25, 1953, p. 58.

9 P. Shuleshko, "Buckling of Rectangular Plates Uniformly Compressed in Two Perpendicular Directions With One Free Edge and Opposite Edge Elastically Restrained," JOURNAL OF APPLIED MECHANICS, vol. 23, TRANS. ASME, vol. 78, Sept., 1956, pp. 359–363.

10 P. Shuleshko, "Buckling of Rectangular Plates With One Unsupported Edge," *The Journal of the Institution of Engineers, Australia*, vol. 29, Sept., 1957, pp. 215–218.

11 Y. V. Safronov and N. V. Bankovskaya, "Solution of the Problem of Stability of Rectangular Plates by the Method of Initial Parameters," *Applied Mechanics*, vol. IV, no. 1, 1958, pp. 61–69. (Ukrainian Academy of Science Press, Kiev.)

The Effect of Lubricant Inertia in Journal-Bearing Lubrication[1]

B. Sternlicht.[2] The authors are to be commended for their contribution to this field. The following comments are offered:

1 Averaging of the inertia over the film thickness $h(x)$ suggested by Slezkin and Targ (reference 2 of the paper) and used in this solution is not a very good assumption especially at high eccentricity ratios. The method employed by Kahlert (reference 4) would yield closer agreement between theory and practice. It would be worth while if the authors would compare the two results at high eccentricity ratio.

2 The authors state: "With the Reynolds number set equal to zero, Equation [7] reduces to the familiar Reynolds equation (which neglects inertia) as we would expect. If we let P_0 be the solution to this reduced equation and H_0 be the corresponding value of H, we can write for the solution of Equation [7]. . . ." This point may be misleading to the reader, for when the Reynolds number is equal to zero, there is no velocity and we cannot generate hydrodynamic pressures. It would be worth while to clarify this statement.

3 The Sommerfeld solution, Equation [14], yields the displacement to be perpendicular to the load direction. When inertia effects are included, this is no longer so and thus the eccentricity locus differs from the Sommerfeld solution. Please comment on this point.

4 In some of our recent work we found that under the laminar-flow conditions the effect of inertia on load-carrying capacity is negligible. However, the oil flow and temperature distribution are affected significantly when inertia is considered. It would be worth while if the authors in the section, "Discussion and Conclusions," would work out an example showing the load with and without inertia effects. No comparison of the flow can be made in this paper because the authors assume infinitely long bearing without side leakage.

[1] By J. F. Osterle, Y. T. Chou, and E. A. Saibel, published in the December, 1957, issue of the JOURNAL OF APPLIED MECHANICS, TRANS. ASME, vol. 79, pp. 494–496.

[2] Bearing Analysis Engineering Specialist, Bearing and Lubricant Center, General Electric Co., Schenectady, N. Y. Mem. ASME

Information for Authors

• Manuscripts should be submitted in final form to the Technical Editors. Each manuscript must be accompanied by a statement that it has not been published elsewhere nor has it been submitted for publication elsewhere. A paper which would occupy more than five pages of the Journal may be returned to the author for abridgment.

• The author should state his business connection, the title of his position, and his mailing address. A short abstract (50 to 100 words) should be included on the first page immediately preceding the introductory paragraph of the paper.

• Three copies of the manuscript are required. One of these must be a carefully prepared printer's copy, typed in double spacing, on one side of the page only, with wide margins, on 8½ by 11-in. opaque white paper. Mimeographed manuscripts, if prepared with exceptional care, can be accepted provided they are completely edited.

• As far as possible, all mathematical expressions should be typewritten. Greek letters and other symbols not available on the typewriter should be carefully inserted in ink. Care should be taken to distinguish between capital and lowercase letters, between zero (0) and the letter (*O*), between the numeral (1) and the letter (*l*), etc. A letter representing a vector cannot be printed with an arrow above or below it. The letter should be underscored with a single wavy line, wherever it appears in the text, to designate boldface type. A list of symbols carefully marked for the use of the editor (thus: κ, Greek l.c. kappa), if it has not been included in the body of the paper, should accompany the manuscript on a separate page.

• Before preparing a manuscript the author should study printed articles in the Journal, with special attention to the form and style of mathematical expressions, tables, footnotes, references, and abstract. Numbers that identify mathematical expressions should be enclosed in parentheses. Numbers that identify references at the end of the paper should be enclosed in brackets. Care should be taken to arrange all tables and mathematical expressions in such a way that they will fit into a single column when set in type. Equations that might extend beyond the width of one column (fractions that should not be broken or long expressions enclosed in parentheses) should be rephrased to go on two or more lines within column width. Fractional powers are preferred to root signs and should always be used in more elaborate formulas. The solidus should be used instead of the horizontal line for fractions wherever possible.

• A normal paper should not exceed five pages in the Journal. It is about 6000 words or twenty to twenty-five double-spaced typewritten pages inclusive of drawings. A Brief Note should not exceed 750 words or about one column in the Journal inclusive of drawings.

• Originals and two copies of figures must accompany the manuscript. Line drawings should not be larger than 8½ × 11 inches and should be planned for reduction to column width. Lettering should be large enough to be clearly legible when the illustration is reduced. The originals of line drawings must be in India ink on white or pale blue tracing paper or tracing cloth. Photographs of equipment or test specimens must be glossy prints and should be used sparingly. Captions for figures should be typed double-spaced and included at the last page of the manuscript. The figure number and author's name should be written in the margin or on the back of each illustration.

• Titles of papers should be brief. If an adequate description of the subject requires a title which, along with the authors' names, would occupy more than one line on the cover of the Journal, a separate shorter title should be submitted.

• Authors can obtain copies of the ASME Manual MS-4, "An ASME Paper," from the Technical Editors and are urged to do so before drafting their papers in final form.

• Papers published in the Journal of Applied Mechanics must be presented at a Meeting, either in person or by title. Scheduling of papers is in the hands of the Secretary of the Applied Mechanics Division. Authors should indicate their preference in this respect to the Technical Editors when submitting a paper.

• An author is entitled to 25 preprints free of charge (in the case of two authors, 15 each; three or more authors, 10 each). Larger quantities of preprints or reprints can be ordered from Editorial Department, The American Society of Mechanical Engineers, 29 West 39th Street, New York 18, N. Y. Quotations will be sent on request.

D. C. Drucker and J. Kestin, *Technical Editors*

Please address all communications to:

Technical Editors
Journal of Applied Mechanics, ASME
Division of Engineering
Brown University
Providence 12, R. I.

TAKE

to keep posted on the latest theoretical and practical advances made by Russian scientists in mathematics, fluid dynamics, and solid-state physics.

This BIMONTHLY is an English translation of PRIKLADNAYA MATEMATIKA i MEKHANIKA which the ASME Applied Mechanics Division considers the most valuable of the Russian publications in the field of mechanical engineering.

By starting your subscription with the first number of PMM (January–February 1958, just published), you will have an opportunity to study the findings of and the theories advanced by Russian engineers on the following problems.

Spherical Pulse Waves in a Compressible Medium.

On the Solution of a Degenerate Variational Problem and the Optimum Shape of a Conic [Space] Rocket.

On Generalized Ordinary Differential Equations Possessing Discontinuous Solutions.

On a Method of Investigating the Stability of a Null-Solution in Singular Cases.

Stabilization of a System With a Salvo of Advancing Characteristics.

Supersonic Aerofoil Theory.

The Theory of Plasticity Which Takes Into Account Rotational Displacements.

On the General Equations for the Theory of Ideal Plasticity and the Theory of Cylindrical [Tubular] Shells.

On Plasticity Laws for Work-Hardening Materials.

The Influence of a Nonuniform Heating on the Stability of a Compressed Bar.

Pressure of a Cylinder Die [Punch] on an Elastic Half Space Whose Modulus of Elasticity is an Exponential Function of Depth.

Application of the Slender Body Theory to the Calculation of Aerodynamic Properties of Low Aspect Ratio Wings With Nacelles at the Tips.

Aerodynamic Characteristics of Thin Wedge-Shaped Profiles in Transonic Flows.

A Special Case of the Existence of Small Periodic Motions of Two Pendula Subjected to Uniform Rotation.

On the Property of the First Approximation System.

SUBSCRIPTION PRICE FOR THE SIX 1958 NUMBERS: $30.00 to nonmembers,
$22.50 to ASME members.

THE AMERICAN SOCIETY OF MECHANICAL ENGINEERS
29 West 39th Street New York 18, N. Y.